ISSN 1007-9327 (print)
ISSN 2219-2840 (online)

World Journal of *Gastroenterology*

World J Gastroenterol 2024 February 14; 30(6): 516-613

Published by Baishideng Publishing Group Inc

World Journal of Gastroenterology

Contents

Weekly Volume 30 Number 6 February 14, 2024

LETTER TO THE EDITOR

World Journal of Gastroenterology

Weekly Volume 30 Number 6 February 14, 2024

Contents

ABOUT COVER

Editorial Board Member of *World Journal of Gastroenterology*, Kok Yang Tan, FRCS (Ed), MBBS, Associate Professor, Chief Doctor, Senior Lecturer, Surgeon, Department of Surgery, Khoo Teck Puat Hospital, Singapore 768828, Singapore. kokyangtan@gmail.com

AIMS AND SCOPE

The primary aim of *World Journal of Gastroenterology* (*WJG*, *World J Gastroenterol*) is to provide scholars and readers from various fields of gastroenterology and hepatology with a platform to publish high-quality basic and clinical research articles and communicate their research findings online. *WJG* mainly publishes articles reporting research results and findings obtained in the field of gastroenterology and hepatology and covering a wide range of topics including gastroenterology, hepatology, gastrointestinal endoscopy, gastrointestinal surgery, gastrointestinal oncology, and pediatric gastroenterology.

INDEXING/ABSTRACTING

The *WJG* is now abstracted and indexed in Science Citation Index Expanded (SCIE), MEDLINE, PubMed, PubMed Central, Scopus, Reference Citation Analysis, China Science and Technology Journal Database, and Superstar Journals Database. The 2023 edition of Journal Citation Reports® cites the 2022 impact factor (IF) for *WJG* as 4.3; Quartile category: Q2. The *WJG*'s CiteScore for 2021 is 8.3.

RESPONSIBLE EDITORS FOR THIS ISSUE

Production Editor: *Ying-Yi Yuan*; **Production Department Director:** *Xiang Li*; **Editorial Office Director:** *Jia-Ru Fan*.

NAME OF JOURNAL

World Journal of Gastroenterology

ISSN

ISSN 1007-9327 (print) ISSN 2219-2840 (online)

LAUNCH DATE

October 1, 1995

FREQUENCY

Weekly

PUBLICATION DATE

February 14, 2024

PUBLISHING PARTNER

Shanghai Pancreatic Cancer Institute and Pancreatic Cancer Institute, Fudan University
Biliary Tract Disease Institute, Fudan University

INSTRUCTIONS TO AUTHORS

https://www.wjgnet.com/bpg/gerinfo/204

GUIDELINES FOR ETHICS DOCUMENTS

https://www.wjgnet.com/bpg/GerInfo/287

GUIDELINES FOR NON-NATIVE SPEAKERS OF ENGLISH

https://www.wjgnet.com/bpg/gerinfo/240

PUBLICATION ETHICS

https://www.wjgnet.com/bpg/GerInfo/288

PUBLICATION MISCONDUCT

https://www.wjgnet.com/bpg/gerinfo/208

POLICY OF CO-AUTHORS

https://www.wjgnet.com/bpg/GerInfo/310

ARTICLE PROCESSING CHARGE

https://www.wjgnet.com/bpg/gerinfo/242

STEPS FOR SUBMITTING MANUSCRIPTS

https://www.wjgnet.com/bpg/GerInfo/239

ONLINE SUBMISSION

https://www.f6publishing.com

PUBLISHING PARTNER's OFFICIAL WEBSITE

https://www.shca.org.cn
https://www.zs-hospital.sh.cn

World Journal of Gastroenterology

Submit a Manuscript: https://www.f6publishing.com

World J Gastroenterol 2024 February 14; 30(6): 516-522

DOI: 10.3748/wjg.v30.i6.516

ISSN 1007-9327 (print) ISSN 2219-2840 (online)

EDITORIAL

Diagnostic tools for fecal incontinence: Scoring systems are the crucial first step

Peter Liptak, Martin Duricek, Peter Banovcin

Specialty type: Gastroenterology and hepatology

Provenance and peer review: Invited article; Externally peer reviewed.

Peer-review model: Single blind

Peer-review report's scientific quality classification

Grade A (Excellent): 0
Grade B (Very good): 0
Grade C (Good): C
Grade D (Fair): 0
Grade E (Poor): 0

P-Reviewer: Iovino P, Italy

Received: October 31, 2023
Peer-review started: October 31, 2023
First decision: December 7, 2023
Revised: December 15, 2023
Accepted: January 15, 2024
Article in press: January 15, 2024
Published online: February 14, 2024

Peter Liptak, Martin Duricek, Peter Banovcin, Clinic of Internal Medicine- Gastroenterology, University Hospital in Martin, Jessenius Faculty of Medicine in Martin, Comenius University, Martin 03601, Slovakia

Corresponding author: Peter Banovcin, MD, PhD, Associate Professor, Director, Clinic of Internal Medicine- Gastroenterology, University Hospital in Martin, Jessenius Faculty of Medicine in Martin, Comenius University, Kollarova 2, Martin 03601, Slovakia. neurogastromartin@gmail.com

Abstract

The main aim of this editorial is to comment on the recent article published by Garg *et al* in the *World Journal of Gastroenterology* 2023; 29: 4593-4603. This original research presents a new scoring system for fecal incontinence. Fecal incontinence is a chronic disease with a severe impact on the quality of life of the patients. Substantial social stigmatization often leads to significant underreporting of the condition even during visits to a specialist and could lead to further mismanagement or non-existent management of the disease. An important fact is that patients are often unable to describe their condition when not asked precisely defined questions. This problem is partially resolved by scoring questionnaires. Several scoring systems are commonly used; however, each of them has their shortcomings. For example, the absence of different kinds of leakage besides flatus and stool could further lead to underscoring the incontinence severity. Therefore, there has long been a call for a more precise scoring system. The correct identification of the presence and severity of fecal incontinence is paramount for further diagnostic approach and for choosing the appropriate therapy option. This editorial describes fecal incontinence, its effect on quality of life in general and further evaluates the diagnostic approach with a particular focus on symptom scoring systems and their implications for clinical practice.

Key Words: Incontinence; Fecal; Scoring system; Questionary; Quality of life

Core Tip: The main aim of this editorial is to comment on the recent article published by Garg *et al* in the *World Journal of Gastroenterology* 2023; 29: 4593-4603. This original research present new scoring system for fecal incontinence. Fecal incontinence is a chronic disease with severe impact on quality of life of the patients. There is a long existing call for more precise scoring system than those in current use. The correct identification of presence and severity of fecal incontinence is paramount for further diagnostic approach and for choosing the appropriate therapy option.

Citation: Liptak P, Duricek M, Banovcin P. Diagnostic tools for fecal incontinence: Scoring systems are the crucial first step. *World J Gastroenterol* 2024; 30(6): 516-522
URL: https://www.wjgnet.com/1007-9327/full/v30/i6/516.htm
DOI: https://dx.doi.org/10.3748/wjg.v30.i6.516

INTRODUCTION

Fecal incontinence could be defined as the involuntary leakage of rectal content (stool, gas, mucus) through the anal canal and the inability to hold back the evacuation for a socially acceptable time. Depending on the presenting circumstances, fecal incontinence is generally classified as[1]: Passive incontinence (involuntary voiding without realizing that the stool is passing), urgent incontinence (emptying despite an active effort to retain content) and fecal soiling (leakage of stool with approximately normal continence and evacuation).

The etiopathogenesis is often multifactorial. Changed defecation patterns (chronic diarrhea, irritable bowel syndrome, (non)specific intestinal inflammation, food intolerances or constipation with subsequent paradoxical overflow incontinence) are the most common independent risk factors for fecal incontinence[1]. Another common (and important) pathophysiological factor is peripartum injury to the perineum and the sphincters (often decades before the onset of symptoms), surgical procedures in the anorectal area (hemorrhoidectomy, fistulotomy, sphincterotomy), prolapse, regular and/or traumatic anal sexual penetration or conditions after reconstructive procedures in the pelvic floor. Fecal incontinence due to gynecological trauma (traumatic vaginal birth) can occur in up to 8% of women[2]. It is important to note that symptoms often do not manifest until several years after the injury, and factors such as hormonal changes during menopause, accelerated aging of traumatically damaged sphincter muscles, or decompensation of compensatory mechanisms probably contribute to this delay[1]. In primiparous women, it is possible to prove occult or at least minimal sphincter injuries in approximately 35% of cases, while delivery using forceps, occipito-posterior position of the child, and prolonged delivery represent independent risk factors for subsequent fecal incontinence[3].

A relatively high percentage of women (13%) experience some degree of incontinence or stool urgency after their first delivery[4], and because these are mostly young women, the impact of incontinence on their quality of life is substantial [5,6].As many gastroenterologist and/or proctologist note, women who have obstetric injury related fecal incontinence do not seek medical attention immediately and continue on with their life suffering, which results in a deteriorating quality of life over time as they age[7]. Interestingly the relationship between anal sphincter defect and severity of fecal incontinence is unclear[8]. Dysfunction of the puborectalis muscle can result in complete incontinence; dysfunction of the external sphincter can lead to weakened voluntary control and thus to the so-called urgent incontinence, and a disorder of the internal sphincter is associated with a weakening of discrete fecal control, which leads to passive incontinence[1]. More pronounced propulsive axial forces in the rectal area can contribute to the development of fecal incontinence; *i.e.*, chronic diarrhea can be manifested not only by unwanted stool consistency, but due to its association with a stronger propulsive wave placing increased demands on the sphincters, it can also lead to unwanted stool leakage[1].

Based on international population studies, the prevalence of fecal incontinence ranges from 0.4%-18%[9-11]. This wide interval could be due to the specific semantic issues regarding its definition in different socio-geographical areas and from wide variety of not particularly consistent symptom questionnaires[12]. The prevalence increases with age[13]. A high prevalence occurs primarily within the elderly population; according to one study, approximately 50%-70% of patients in nursing homes suffer from incontinence[2]. Fecal incontinence can be present in both sexes and no financial or social status can be considered as a protective factor[14]. It is assumed that the incidence and prevalence of fecal incontinence is higher than the reported data due to certain social taboos associated with fecal leakage[15]. Forty-five to fifty percent (45%-50%) of patients with fecal incontinence have a severe physical or psychological disability[1]. When patients experience only mild incontinence symptoms they tend to withhold this information from their physician, and the majority of them do not consult a medical professional at all[16]. Overall, only 5% to 27% of patients seeks professional help[17]. On the other hand, studies focused on primary medical care providers report that a very low number of them screen patients for the presence of incontinence, and when they do, it is more frequently urinary than fecal[18]. An appropriate and sensitive, yet professional and precise approach when conducting a medical interview is crucial for identifying patients with fecal incontinence[18]. This is paramount for further evaluation of the disease severity and its impact on quality of life[19,20].

The impact of fecal incontinence on quality of life can range from mild social or personal discomfort to severe disruption that paralyzes almost all aspects of a patient's life[21-24]. Quality of life in patients with fecal incontinence can be measured by several different self-reporting questionnaires[25]. The most frequently used are the general Short Form (SF-36)[26], the gut-focused Gastrointestinal Quality of Life Index (GIQLI)[27], and the more specific Fecal Quality of Life Index[28].

When taking the medical history, it is necessary to distinguish isolated discharge of mucus from fecal incontinence. The soiling of underwear can also be caused by factors other than fecal incontinence, primarily lower hygiene standards, prolapsed hemorrhoids or rectal prolapse; however, for practical reasons, soiling is considered by some authors to be a manifestation of incontinence[2]. As the symptoms may vary individually over the time and there are different incontinence phenotypes, it is very important to choose the right and thorough approach during the medical interview. The need for a comprehensive scoring system suitable for clinical application in fecal incontinence has been known for a long time[29]. It is important to keep in mind that the severity scoring system does not have to inherently correlate with quality of life measurements[30].

Anorectal manometry is the method of first choice in the verification of a disturbed functional state of the sphincters. With an anorectal manometer, it is possible to measure the resting pressure of the sphincters as well as the pressure during a forceful voluntary contraction. Based on the London criteria, it is subsequently possible to classify the finding as anal hypotonia and normal contractility or anal hypotonia with hypocontractility[31]. Another complementary examination is rectal endosonography, which can be used to visualize and verify the presence of morphological changes in the internal and external sphincter or part of the puborectalis muscle and surrounding structures. In specific cases, it is possible to consider the implementation of magnetic resonance defecography or neurophysiological examination.

Fecal incontinence therapy is difficult and requires a strictly individual approach. It almost always starts conservatively, and in case of its inefficiency, an operative solution can be considered. The goal of initial conservative therapy is to optimize the stool structure, slow down intestinal motility, and minimize the average amount of stool in the rectum[1]. Conservative (pharmacological and regimen) therapy can be partially effective in patients with mild fecal incontinence [32]. In the case of failure of conservative treatment or clinically more serious fecal incontinence, it is recommended to initiate at home biofeedback training and/or professional physiotherapy[33]. As another modality, it is possible to use sacral nerve stimulation[34,35]. This is indicated in patients with incontinence caused by weakened sphincter function, without structural defects[36]. Another option is application of so-called bulking agents into the sphincters to artificially increasing their volume[33].

In patients with morphological defects of the sphincter a surgical solution is indicated, depending on the nature of the damage. This includes, for example, sphincteroplasty, or resolution of the underlying cause, such as rectovaginal fistula, rectal prolapse, and anal fistula[37]. In the case of failure of all the previously mentioned options, colostomy is indicated [33]. It is important to note that, based on the recent expert consensus[38] and the older Cochrane analysis[39], it is not possible to clearly prefer any of the above-mentioned surgical methods, and it is therefore appropriate to individually combine conservative and interventional approaches. Therefore, a properly evaluated phenotype of incontinence and medical history is crucial when tailoring the therapy for each patient individually. The cornerstone for this first step is a practical and usable scoring system. The aim of this editorial is to comment on an article recently published by Garg *et al* [40] in the *World Journal of Gastroenterology* and to compare it with previously used scoring systems, predominantly with the most commonly used Wexner and St. Mark's scores (Table 1)[41].

SCORING SYSTEMS

Pescatori Incontinence Score[42]

It is based on three degrees of incontinence severity and three types of frequency. Letters are used for the type of leakage (A for flatus/mucus, B for liquid stool, and C for solid stool) and numbers for frequency (1 for an occasional incontinence event, 2 for weekly, and 3 for daily unwished leakage); the final score range varies from 0 for full continence to 6 for daily incontinence of solid stool. It includes mucus as a type of leakage but lacks factors such as hygiene pad usage, lifestyle alteration, or urgency.

Wexner/Cleveland Clinic Florida Incontinence Score[24]

One of the most used scoring system in clinical setting[25]. It consists of 5 items regarding types of leakage (solid, liquid, gas), the necessity to wear hygiene pads, and lifestyle alterations. Every item has points assessed based on frequency (never, rarely, sometimes, usually, always). The final score ranges from 0 for full continence to 20 representing complete incontinence. It is easy to use for patients' self-reference but it does not consider leakage of mucus or urgency for the evaluation.

Vaizey/St. Mark's Incontinence Score[43]

The main points of the Vaizey/St. Mark's Incontinence Score are quite similar to the Wexner/Cleveland Clinic Incontinence score[24,43]. It is also widely used, and both Wexner and Vaizey scores provide very good inter- and intra-observer reliability[43,44]. It correlates moderately well with the patient's perception of fecal incontinence[45]. The St. Mark's Incontinence Score evaluates three main types of leakage (solid, liquid, gas) and alterations in lifestyle. All these items are graded according to the frequency of occurrence (never, rarely, sometimes, weekly, daily). Items such as need to wear a pad or plug, taking constipating medicines and urgency (lack of ability to defer defecation for 15 min) involve binary answers (yes/no). Urgency is valued two-times more than medications and/or the need to wear pad or plug (4 points *vs* 2 points). The total range varies from 0 for full continence to 24 for complete incontinence.

Fecal Incontinence Severity Index[46]

Not as widely used as the previously mentioned Wexner and St. Mark's scores, it has its strong points, namely in the

Table 1 Comparison of different fecal severity scoring systems

Scoring system	Structure	Weighted	Score range
Pescatori Incontinence Score	3 items of type, 3 items of frequency	Yes	0: Full continence; 6: Daily incontinence of solid stool
Wexner/Cleveland Clinic Florida Incontinence Score	3 items of type, 2 additional items, 5 items of frequency	No	0: Full continence; 20: Complete incontinence
St. Mark's/Vaizey Incontinence Score	3 items of type, 3 additional items, 5 items of frequency	Yes	0: Perfect continence; 24: Complete incontinence
Fecal Incontinence Severity Score	4 items of type, 6 types of frequency	Yes	Patient range: 0: least severe; 61: most severe. Surgeon range: 0: Least severe; 59: Most severe
Rapid Assessment Fecal Incontinence Score	6 items for perception, 6 items for frequency	No	Leaks: 0: For none; 10: for daily. Perception: 0: For excellent, 10: For very bad
Garg's New Severity Scale	6 items for type, 3 items for frequency	Yes	0: No incontinence; 80: Total incontinence

consideration of mucus in the score evaluation. On the other hand, this could lead to a misleading false sensation of liquid stool, as patients often are unable to differentiate between these two substances[47]. This factor could be correlated by other possible scoring items, but the Fecal Incontinence Severity Index score does not include other factors for consideration, *e.g.*, lifestyle alterations, medication usage, or urgency. Thus, its practical adoption has been limited. It could be evaluated by patients and/or by medical professionals with different point ranges. The final score ranges from 0 for least severe to 61 for most severe symptoms of fecal incontinence.

Rapid Assessment Fecal Incontinence Score[48]

This simple score was developed for the purpose of a quick assessment of fecal incontinence which can be easily used in primary care settings. Although not as comprehensive as the above-mentioned scores, we believe it is worth noticing for its simplicity and ease of use. It is oriented on patient self-evaluation and consists of 2 items. The first is patients' perceptions of their well-being according to leakage, which is evaluated by visual analog scale of 6 Levels (from very bad to excellent). Six levels are also used for the second item, which is frequency of leakage. A validation was done comparing it to the Vexner score[41] and the FIQL[30], and it shows high correlations with these two questionnaires.

The new scoring system for fecal incontinence by Garg et al[40]

The previously mentioned scoring systems have their various pitfalls, from a lack of consideration of the stress factor in all of them to not considering mucus and/or urgency in some of them. Moreover, the different leakages are weighed by the same factor in most of them.

This is why Garg and colleagues decided to develop a new questionnaire to reflect the most important issues, which would be following: proper numeric assessment of different types and severity of fecal incontinence, based primarily on patient perception of the disease along with simple usage and comprehensive accuracy.

For this evaluation patients, laypersons, and colorectal surgeons were included in the study.

In the first phase they evaluated the symptom perception in patients and laypersons. Interestingly, the exclusion criterion for patients was current presence of fecal incontinence because of the biased perception of incontinence (in terms of over quantifying symptoms). In contrast, patients who could experience incontinence due to their acute or chronic disease were included. To balance the possible extreme responses of patients, so-called laypersons were also included in the study. These were the relatives of the patients. As they closely observe but do not suffer from the condition, they could provide precise, yet emotionally unbiased answers.

In the second phase, experienced colorectal surgeons were included to provide the professional side of the evaluation of fecal incontinence and to compare this to scoring based on the responses of the patients and laypersons.

Fecal incontinence in the questionnaire is presented by 6 types or rather symptoms: urgent, stress, liquid, mucus, solid and gas. Four dimensions of quality-of-life impact (usual routine activity, anxiety/depression, self-esteem, social life) with 3 levels of severity were used. Comparing the severity perception by patients and laypersons and thereafter confronted by results from the colorectal surgeons, different weights for the types are assigned. For example, solid and liquid incontinence have assigned a weight of 8 and stress incontinence a weight of 5. This is used for multiplying the severity points, which are assessed according to three levels of frequency of leakage incident: Never, occasional (once a week or less), or common (more than once a week). Altogether, maximum points for complete incontinence are 80 and for complete bowel control (total continence) 0.

An agreement between surgeon and patient assessment of incontinence was not met. It is possible to agree with the authors' statement that patient perception and not medical professional opinion is the single most important factor, because fecal incontinence is tightly connected with individual perception of the disease.

A disputable point could be considering the type of incontinence (urge, stress) on the same level as a symptom in this questionnaire. Although it provides high added value for the evaluation of incontinence, it is possible to argue that liquid incontinence could be more connected with the stress phenotype rather than the urge phenotype and thus asymmetrically provide higher severity numbers in these cases. The type of leakage and phenotype of incontinence influence the overall quality of life in patients differently[49]. Also, this scoring system, as all previously mentioned scoring systems, does not

evaluate so-called overflow incontinence, which could be paradoxically present in some patients with constipation[1]. The overall time to fill-in the questionnaire is also not known. However, for general practice this is more of a peculiarity, and this problem could be more pronounced when performing methodically strict clinical studies. Therefore, we could say that more clinical studies are needed to comprehensively evaluate all the possible shortcomings of this new scoring system. Also, as the authors stated, the study limitation is that this new scoring system was not tested for inter- and intra-observer variability and test-retest reliability. However, they stated that this will be an objective for further study by their study group. We encourage this plan, as this will provide more relevant data for reliability and could significantly prove system's clinical application.

On the other hand, the different weighing of different symptoms/types of incontinence is a high added value and an important approach within the current problems of scoring systems.

CONCLUSION

The search for a comprehensive yet easy to use fecal incontinence severity scoring system has long been an ongoing problem. The patient perception and reporting of symptoms is the cornerstone for the correct diagnosis of this debilitating disorder. Several scoring questionnaires have been implemented thus far in clinical practice, with the Wexner and Vaizey scoring systems being the most often used. Although widely used, they, too, have their own commonly known pitfalls. The scoring system developed by Garg *et al*[40] aims to provide a more precise diagnostic tool than the forementioned ones. Although it presents a promising result, the system needs more high-quality epidemiological studies to fully evaluate its reliability and clinical utility compared to established systems.

FOOTNOTES

Author contributions: Liptak P, Duricek M and Banovcin P wrote the manuscript evenly; Liptak P coordinated the manuscript preparation; Banovcin P supervised the preparation process.

Conflict-of-interest statement: The authors have no conflicts of interest to disclose.

Country/Territory of origin: Slovakia

ORCID number: Peter Liptak 0000-0001-8257-8567; Martin Duricek 0000-0002-0754-4532; Peter Banovcin 0000-0001-6694-9364.

S-Editor: Lin C
L-Editor: A
P-Editor: Yuan YY

REFERENCES

1 **Saldana Ruiz N**, Kaiser AM. Fecal incontinence - Challenges and solutions. *World J Gastroenterol* 2017; **23**: 11-24 [PMID: 28104977 DOI: 10.3748/wjg.v23.i1.11]
2 **Rao SS**, Bharucha AE, Chiarioni G, Felt-Bersma R, Knowles C, Malcolm A, Wald A. Functional Anorectal Disorders. *Gastroenterology* 2016 [PMID: 27144630 DOI: 10.1053/j.gastro.2016.02.009]
3 **Rao SS**; American College of Gastroenterology Practice Parameters Committee. Diagnosis and management of fecal incontinence. American College of Gastroenterology Practice Parameters Committee. *Am J Gastroenterol* 2004; **99**: 1585-1604 [PMID: 15307881 DOI: 10.1111/j.1572-0241.2004.40105.x]
4 **Sultan AH**, Kamm MA, Hudson CN, Thomas JM, Bartram CI. Anal-sphincter disruption during vaginal delivery. *N Engl J Med* 1993; **329**: 1905-1911 [PMID: 8247054 DOI: 10.1056/NEJM199312233292601]
5 **Pla-Martí V**, Martín-Arévalo J, Martí-Fernández R, Moro-Valdezate D, García-Botello S, Espí-Macías A, Mínguez-Pérez M, Ruiz-Carmona MD, Roig-Vila JV. Long-term evolution of continence and quality of life after sphincteroplasty for obstetric fecal incontinence. *Ann Coloproctol* 2022; **38**: 13-19 [PMID: 32972098 DOI: 10.3393/ac.2020.09.16]
6 **Meyer I**, Blanchard CT, Markland AD, Gibson EG, Richter HE. Fecal Incontinence Symptoms and Impact in Older Versus Younger Women Seeking Care. *Dis Colon Rectum* 2019; **62**: 733-738 [PMID: 31094960 DOI: 10.1097/DCR.0000000000001353]
7 **Bartlett L**, Nowak M, Ho YH. Impact of fecal incontinence on quality of life. *World J Gastroenterol* 2009; **15**: 3276-3282 [PMID: 19598304 DOI: 10.3748/wjg.15.3276]
8 **Bjørsum-Meyer T**, Christensen P, Jakobsen MS, Baatrup G, Qvist N. Correlation of anorectal manometry measures to severity of fecal incontinence in patients with anorectal malformations - a cross-sectional study. *Sci Rep* 2020; **10**: 6016 [PMID: 32265467 DOI: 10.1038/s41598-020-62908-w]

9 **Faltin DL**, Sangalli MR, Curtin F, Morabia A, Weil A. Prevalence of anal incontinence and other anorectal symptoms in women. *Int Urogynecol J Pelvic Floor Dysfunct* 2001; **12**: 117-120; discussion 121 [PMID: 11374509 DOI: 10.1007/pl00004031]

10 **Nelson RL**. Epidemiology of fecal incontinence. *Gastroenterology* 2004; **126**: S3-S7 [PMID: 14978632 DOI: 10.1053/j.gastro.2003.10.010]

11 **Ditah I**, Devaki P, Luma HN, Ditah C, Njei B, Jaiyeoba C, Salami A, Ewelukwa O, Szarka L. Prevalence, trends, and risk factors for fecal incontinence in United States adults, 2005-2010. *Clin Gastroenterol Hepatol* 2014; **12**: 636-43.e1 [PMID: 23906873 DOI: 10.1016/j.cgh.2013.07.020]

12 **Maeda K**, Yamana T, Takao Y, Mimura T, Katsuno H, Seki M, Tsunoda A, Yoshioka K; Fecal Incontinence Guideline Preparation Committee. Japanese Practice Guidelines for Fecal Incontinence Part 1-Definition, Epidemiology, Etiology, Pathophysiology and Causes, Risk Factors, Clinical Evaluations, and Symptomatic Scores and QoL Questionnaire for Clinical Evaluations-English Version. *J Anus Rectum Colon* 2021; **5**: 52-66 [PMID: 33537501 DOI: 10.23922/jarc.2020-057]

13 **Whitehead WE**, Borrud L, Goode PS, Meikle S, Mueller ER, Tuteja A, Weidner A, Weinstein M, Ye W; Pelvic Floor Disorders Network. Fecal incontinence in US adults: epidemiology and risk factors. *Gastroenterology* 2009; **137**: 512-517, 517.e1 [PMID: 19410574 DOI: 10.1053/j.gastro.2009.04.054]

14 **Miner PB Jr**. Economic and personal impact of fecal and urinary incontinence. *Gastroenterology* 2004; **126**: S8-13 [PMID: 14978633 DOI: 10.1053/j.gastro.2003.10.056]

15 **Bharucha AE**, Dunivan G, Goode PS, Lukacz ES, Markland AD, Matthews CA, Mott L, Rogers RG, Zinsmeister AR, Whitehead WE, Rao SS, Hamilton FA. Epidemiology, pathophysiology, and classification of fecal incontinence: state of the science summary for the National Institute of Diabetes and Digestive and Kidney Diseases (NIDDK) workshop. *Am J Gastroenterol* 2015; **110**: 127-136 [PMID: 25533002 DOI: 10.1038/ajg.2014.396]

16 **Bartlett L**, Nowak M, Ho YH. Reasons for non-disclosure of faecal incontinence: a comparison between two survey methods. *Tech Coloproctol* 2007; **11**: 251-257 [PMID: 17676265 DOI: 10.1007/s10151-007-0360-z]

17 **Whitehead WE**. Diagnosing and managing fecal incontinence: if you don't ask, they won't tell. *Gastroenterology* 2005; **129**: 6 [PMID: 16012928 DOI: 10.1053/j.gastro.2005.05.043]

18 **Brown HW**, Guan W, Schmuhl NB, Smith PD, Whitehead WE, Rogers RG. If We Don't Ask, They Won't Tell: Screening for Urinary and Fecal Incontinence by Primary Care Providers. *J Am Board Fam Med* 2018; **31**: 774-782 [PMID: 30201674 DOI: 10.3122/jabfm.2018.05.180045]

19 **Cauley CE**, Savitt LR, Weinstein M, Wakamatsu MM, Kunitake H, Ricciardi R, Staller K, Bordeianou L. A Quality-of-Life Comparison of Two Fecal Incontinence Phenotypes: Isolated Fecal Incontinence Versus Concurrent Fecal Incontinence With Constipation. *Dis Colon Rectum* 2019; **62**: 63-70 [PMID: 30451749 DOI: 10.1097/DCR.0000000000001242]

20 **D'Amico F**, Wexner SD, Vaizey CJ, Gouynou C, Danese S, Peyrin-Biroulet L. Tools for fecal incontinence assessment: lessons for inflammatory bowel disease trials based on a systematic review. *United European Gastroenterol J* 2020; **8**: 886-922 [PMID: 32677555 DOI: 10.1177/2050640620943699]

21 **Brochard C**, Chambaz M, Ropert A, l'Héritier AM, Wallenhorst T, Bouguen G, Siproudhis L. Quality of life in 1870 patients with constipation and/or fecal incontinence: Constipation should not be underestimated. *Clin Res Hepatol Gastroenterol* 2019; **43**: 682-687 [PMID: 30880096 DOI: 10.1016/j.clinre.2019.02.011]

22 **Rothbarth J**, Bemelman WA, Meijerink WJ, Stiggelbout AM, Zwinderman AH, Buyze-Westerweel ME, Delemarre JB. What is the impact of fecal incontinence on quality of life? *Dis Colon Rectum* 2001; **44**: 67-71 [PMID: 11805565 DOI: 10.1007/BF02234823]

23 **Damon H**, Dumas P, Mion F. Impact of anal incontinence and chronic constipation on quality of life. *Gastroenterol Clin Biol* 2004; **28**: 16-20 [PMID: 15041805 DOI: 10.1016/s0399-8320(04)94835-x]

24 **Jorge JM**, Wexner SD. Etiology and management of fecal incontinence. *Dis Colon Rectum* 1993; **36**: 77-97 [PMID: 8416784 DOI: 10.1007/BF02050307]

25 **Hunt CW**, Cavallaro PM, Bordeianou LG. Metrics Used to Quantify Fecal Incontinence and Constipation. *Clin Colon Rectal Surg* 2021; **34**: 5-14 [PMID: 33536844 DOI: 10.1055/s-0040-1714245]

26 **Lins L**, Carvalho FM. SF-36 total score as a single measure of health-related quality of life: Scoping review. *SAGE Open Med* 2016; **4**: 2050312116671725 [PMID: 27757230 DOI: 10.1177/2050312116671725]

27 **Eypasch E**, Williams JI, Wood-Dauphinee S, Ure BM, Schmülling C, Neugebauer E, Troidl H. Gastrointestinal Quality of Life Index: development, validation and application of a new instrument. *Br J Surg* 1995; **82**: 216-222 [PMID: 7749697 DOI: 10.1002/bjs.1800820229]

28 **Rockwood TH**, Church JM, Fleshman JW, Kane RL, Mavrantonis C, Thorson AG, Wexner SD, Bliss D, Lowry AC. Fecal Incontinence Quality of Life Scale: quality of life instrument for patients with fecal incontinence. *Dis Colon Rectum* 2000; **43**: 9-16; discussion 16 [PMID: 10813117 DOI: 10.1007/BF02237236]

29 **Baxter NN**, Rothenberger DA, Lowry AC. Measuring fecal incontinence. *Dis Colon Rectum* 2003; **46**: 1591-1605 [PMID: 14668583 DOI: 10.1007/BF02660762]

30 **Rockwood TH**. Incontinence severity and QOL scales for fecal incontinence. *Gastroenterology* 2004; **126**: S106-S113 [PMID: 14978646 DOI: 10.1053/j.gastro.2003.10.057]

31 **Carrington EV**, Heinrich H, Knowles CH, Fox M, Rao S, Altomare DF, Bharucha AE, Burgell R, Chey WD, Chiarioni G, Dinning P, Emmanuel A, Farouk R, Felt-Bersma RJF, Jung KW, Lembo A, Malcolm A, Mittal RK, Mion F, Myung SJ, O'Connell PR, Pehl C, Remes-Troche JM, Reveille RM, Vaizey CJ, Vitton V, Whitehead WE, Wong RK, Scott SM; All members of the International Anorectal Physiology Working Group. The international anorectal physiology working group (IAPWG) recommendations: Standardized testing protocol and the London classification for disorders of anorectal function. *Neurogastroenterol Motil* 2020; **32**: e13679 [PMID: 31407463 DOI: 10.1111/nmo.13679]

32 **Bharucha AE**, Knowles CH, Mack I, Malcolm A, Oblizajek N, Rao S, Scott SM, Shin A, Enck P. Faecal incontinence in adults. *Nat Rev Dis Primers* 2022; **8**: 53 [PMID: 35948559 DOI: 10.1038/s41572-022-00381-7]

33 **Rao SSC**, Lee YY, Ghoshal UC. Preface. *Clin basic neurogastroenterol motil* 2020; xxvii [DOI: 10.1016/b978-0-12-813037-7.09985-4]

34 **Thaha MA**, Abukar AA, Thin NN, Ramsanahie A, Knowles CH. Sacral nerve stimulation for faecal incontinence and constipation in adults. *Cochrane Database Syst Rev* 2015; **2015**: CD004464 [PMID: 26299888 DOI: 10.1002/14651858.CD004464.pub3]

35 **Malouf AJ**, Vaizey CJ, Nicholls RJ, Kamm MA. Permanent sacral nerve stimulation for fecal incontinence. *Ann Surg* 2000; **232**: 143-148 [PMID: 10862207 DOI: 10.1097/00000658-200007000-00020]

36 **Brill SA**, Margolin DA. Sacral nerve stimulation for the treatment of fecal incontinence. *Clin Colon Rectal Surg* 2005; **18**: 38-41 [PMID: 20011338 DOI: 10.1055/s-2005-864079]

37 **Ratto C**, Donisi L, Litta F, Campennì P, Parello A. Implantation of SphinKeeper(TM): a new artificial anal sphincter. *Tech Coloproctol* 2016; **20**: 59-66 [PMID: 26658726 DOI: 10.1007/s10151-015-1396-0]

38 **Assmann SL**, Keszthelyi D, Kleijnen J, Anastasiou F, Bradshaw E, Brannigan AE, Carrington EV, Chiarioni G, Ebben LDA, Gladman MA, Maeda Y, Melenhorst J, Milito G, Muris JWM, Orhalmi J, Pohl D, Tillotson Y, Rydningen M, Svagzdys S, Vaizey CJ, Breukink SO. Guideline for the diagnosis and treatment of Faecal Incontinence-A UEG/ESCP/ESNM/ESPCG collaboration. *United European Gastroenterol J* 2022; **10**: 251-286 [PMID: 35303758 DOI: 10.1002/ueg2.12213]

39 **Brown SR**, Wadhawan H, Nelson RL. Surgery for faecal incontinence in adults. *Cochrane Database Syst Rev* 2013; **2013**: CD001757 [PMID: 23821339 DOI: 10.1002/14651858.CD001757.pub4]

40 **Garg P**, Sudol-Szopinska I, Kolodziejczak M, Bhattacharya K, Kaur G. New objective scoring system to clinically assess fecal incontinence. *World J Gastroenterol* 2023; **29**: 4593-4603 [PMID: 37621752 DOI: 10.3748/wjg.v29.i29.4593]

41 **Wexner SD**. Further validation of the Wexner Incontinence Score: A note of appreciation and gratitude. *Surgery* 2021; **170**: 53-54 [PMID: 33863582 DOI: 10.1016/j.surg.2021.02.039]

42 **Pescatori M**, Anastasio G, Bottini C, Mentasti A. New grading and scoring for anal incontinence. Evaluation of 335 patients. *Dis Colon Rectum* 1992; **35**: 482-487 [PMID: 1568401 DOI: 10.1007/BF02049407]

43 **Vaizey CJ**, Carapeti E, Cahill JA, Kamm MA. Prospective comparison of faecal incontinence grading systems. *Gut* 1999; **44**: 77-80 [PMID: 9862829 DOI: 10.1136/gut.44.1.77]

44 **Hussain ZI**, Lim M, Stojkovic S. The test-retest reliability of fecal incontinence severity and quality-of-life assessment tools. *Dis Colon Rectum* 2014; **57**: 638-644 [PMID: 24819105 DOI: 10.1097/DCR.0000000000000118]

45 **Maeda Y**, Parés D, Norton C, Vaizey CJ, Kamm MA. Does the St. Mark's incontinence score reflect patients' perceptions? A review of 390 patients. *Dis Colon Rectum* 2008; **51**: 436-442 [PMID: 18219532 DOI: 10.1007/s10350-007-9157-4]

46 **Rockwood TH**, Church JM, Fleshman JW, Kane RL, Mavrantonis C, Thorson AG, Wexner SD, Bliss D, Lowry AC. Patient and surgeon ranking of the severity of symptoms associated with fecal incontinence: the fecal incontinence severity index. *Dis Colon Rectum* 1999; **42**: 1525-1532 [PMID: 10613469 DOI: 10.1007/BF02236199]

47 **Seong MK**, Jung SI, Kim TW, Joh HK. Comparative analysis of summary scoring systems in measuring fecal incontinence. *J Korean Surg Soc* 2011; **81**: 326-331 [PMID: 22148125 DOI: 10.4174/jkss.2011.81.5.326]

48 **de la Portilla F**, Ramallo I, Maestre MV, Roig JV, Devesa M, Padillo FJ. Validation of a Novel Fecal Incontinence Scale: The Rapid Assessment Fecal Incontinence Score (RAFIS). *J Clin Gastroenterol* 2021; **55**: 141-146 [PMID: 32301835 DOI: 10.1097/MCG.0000000000001342]

49 **Hoke TP**, Meyer I, Blanchard CT, Szychowski JM, Richter HE. Characterization of symptom severity and impact on four fecal incontinence phenotypes in women presenting for evaluation. *Neurourol Urodyn* 2021; **40**: 237-244 [PMID: 33080084 DOI: 10.1002/nau.24541]

World Journal of Gastroenterology

Submit a Manuscript: https://www.f6publishing.com

World J Gastroenterol 2024 February 14; 30(6): 523-526

DOI: 10.3748/wjg.v30.i6.523

ISSN 1007-9327 (print) ISSN 2219-2840 (online)

EDITORIAL

Unmet needs in biomarkers for autoimmune pancreatitis diagnosis

Bao-Can Wang, Jian-Gao Fan

Specialty type: Gastroenterology and hepatology

Provenance and peer review: Invited article; Externally peer reviewed.

Peer-review model: Single blind

Peer-review report's scientific quality classification

Grade A (Excellent): 0
Grade B (Very good): B
Grade C (Good): 0
Grade D (Fair): 0
Grade E (Poor): 0

P-Reviewer: Day AS, New Zealand

Received: December 14, 2023
Peer-review started: December 14, 2023
First decision: December 28, 2023
Revised: January 10, 2024
Accepted: January 15, 2024
Article in press: January 15, 2024
Published online: February 14, 2024

Bao-Can Wang, Jian-Gao Fan, Department of Gastroenterology, Xinhua Hospital Affiliated to Shanghai Jiao Tong University School of Medicine, Shanghai 200092, China

Corresponding author: Jian-Gao Fan, MD, Professor, Department of Gastroenterology, Xinhua Hospital Affiliated to Shanghai Jiao Tong University School of Medicine, No. 1665 Kongjiang Road, Shanghai 200092, China. fanjiangao@xinhuamed.com.cn

Abstract

Autoimmune pancreatitis (AIP) is a rare chronic autoimmune disorder. The diagnosis of AIP mainly depends on histopathology, imaging and response to treatment. Serum immunoglobulin 4 (IgG4) is used only as collateral evidence in diagnostic criteria for AIP because of its moderate sensitivity. Serum IgG4 levels are normal in 15%-37% of type 1 AIP and most of type 2 AIP patients. In these patients, the indeterminate imaging and histopathology may lead to the difficulty in definitive diagnosis of AIP. Therefore, discovery of new biomarkers is important for AIP diagnosis. Here, we provide some views on the progression and challenges in identifying novel serological biomarkers in AIP diagnosis.

Key Words: Autoimmune pancreatitis; Immunoglobulin G4; Biomarker, Cytokine; Autoantibody

Core Tip: Serum immunoglobulin 4 is currently the only biomarker and highly specific but moderately sensitive for diagnosis of autoimmune pancreatitis (AIP). Some cytokines and antibodies have been shown potential in AIP diagnosis.

Citation: Wang BC, Fan JG. Unmet needs in biomarkers for autoimmune pancreatitis diagnosis. *World J Gastroenterol* 2024; 30(6): 523-526
URL: https://www.wjgnet.com/1007-9327/full/v30/i6/523.htm
DOI: https://dx.doi.org/10.3748/wjg.v30.i6.523

INTRODUCTION

Autoimmune pancreatitis (AIP) is referred to as non-alcoholic destructive pancreatitis and sclerosing pancreatitis. It is a chronic pancreatitis characterized by an autoimmune

inflammatory process with pancreatic swell or focal mass that responds to corticosteroid treatment. AIP was first described in 1995[1]. In 2001, elevated serum immunoglobulin 4 (IgG4) level was found as an important indicator in patients with sclerosing pancreatitis[2]. Then the International Consensus Diagnostic Criteria (ICDC) classified AIP into type 1 and type 2 in 2011[3], according to five features: Image of pancreatic parenchyma and duct, serology, other organ involvement, pancreatic histology, and response to steroid therapy. According to ICDC, more than 90% of cases are type 1 AIP, characterized by high serum IgG4 level, and IgG4-positive plasma cell infiltration in the pancreas. So, it is also known as lymphoplasmacytic sclerosing pancreatitis. Most of type 1 AIP present with the clinical signs of the systemic IgG4-related disease. Type 2 AIP is a pancreatic-specific disease, without serum IgG4 elevation, characterized by pancreatic ductal epithelium neutrophilic infiltration. So, it is also labeled as idiopathic duct-centric pancreatitis. Some of AIP patients could be diagnosed definitively, but in other patients, the clinical features including image, histopathology, IgG4 level may be not typical. Therefore, the diagnosis of AIP could not be established in all the patients using the current biomarkers[4]. New powerful biomarkers may improve the diagnosis of AIP. Some studies have shown that some cytokines and autoantibodies could be used alone or as a panel to help diagnosing AIP.

DIAGNOSTIC ROLE OF IG4 IN AIP

Many studies have shown that serum IgG4 level was elevated in AIP patients. This provides the solid data for using elevation of serum IgG4 as diagnostic biomarker for AIP in clinical practice. However, the sensitivity and specificity of IgG4 varied among these studies, which may be attributed to discrepant patient population, diagnostic criteria, race/region, and year of study before and after 2011. Among these factors, cut-off point has been studied by several researchers. In a meta-analysis of 13 studies including 594 patients, the pooled sensitivity of serum IgG4 for the diagnosis of AIP was 0.72 [95% confidence interval (CI): 0.68-0.75] when cut-off value was set at 130 to 140 mg/dL, specificity was 0.93 (95%CI: 0.92-0.95), diagnostic odds ratios was 51.37 (95%CI: 23.20-113.74), and area under the curve was 0.91 (95%CI: 0.87-0.95). When cut-off value was set at two folds of upper limit of normal level (260-280 mg/dL), the specificity increased to 0.98, while the sensitivity decreased to 43%[5]. In addition, elevated serum IgG4 level at the time of glucocorticoid cessation was an independent predictor of AIP relapse (hazard ratio: 4.511)[6]. In type 2 AIP, serum IgG4 levels are usually normal[7]. These suggested that IgG4 has poor correlation with type 2 AIP. Based on these data, serum IgG4 is a useful biomarker for diagnosing tyoe 1 AIP, but its sensitivity is not high.

In the recent issue of the *World Journal of Gastroenterology*, Zhou *et al*[8] showed that elevated serum IgG4 and IgA levels were associated with a more active immune system and higher relapse rates in AIP. Their study suggested that IgG4 could be combined with other markers to evaluate the disease activity and treatment efficacy, and monitor relapse. Even if the specificity of serum IgG4 for AIP is high, slight increase of serum IgG4 could be observed in other diseases, such as pancreatic cancer, cholangiocarcinoma, primary sclerosing cholangitis[9]. Therefore, more biomarkers are needed for AIP diagnosis. The new biomarkers may be used alone or together with IgG4.

NEW SEROLOGICAL BIOMARKERS IN AIP

Recently, great progresses have been made in understanding the abnormality of immune networks. Different types of immune cells, including dendritic cells, monocytes, T cell subgroups, B cells, were found to be involved in the pathogenesis of AIP by producing cytokines. Serum κ, λ free light chain, interleukin (IL)-5, IL-6, IL-33, soluble IL-2 receptor, interferon (IFN)-α[10-15] were significantly changed in patients with AIP. It is worth mentioning that the serum concentrations of IFN-α and IL-33 produced by dendritic cells significantly increased in the patients with active AIP, and decreased after induction of remission. The specificities of serum levels of IFN-α and IL-33 were 91.7% and 83.3%, respectively, and the sensitivity of IFN-α and IL-33 were 85.7% each. Serum levels of IFN-α and IL-33 correlated better with disease activity than that of IgG4. This study suggests that the serum concentrations of IFN-α and IL-33 have the potential to be the biomarkers for type 1 AIP diagnosis[15]. But confirmation from more studies and patients are needed.

Multiple autoantibodies secreted by plasma cells have been found in the sera of patients with AIP, such as anti-carbonic anhydrases I (anti-CA I), anti-CA II[16], anti-lactoferrin[17], antibodies against plasminogen-binding protein [18]. These studies have shown that AIP is an autoimmune-mediated disease. But the role of these autoantibodies in the diagnosis of AIP is still undetermined. Recently, three newly identified antibodies, anti-amylase α[19], anti-laminin 511 [20], and anti-prohibition[21] have shown moderate to high accuracy for AIP diagnosis in some small sample studies. Annexin A11[22] and galectin-3[23] antibodies were identified specifically in the sera of patients with AIP screened by mass spectrometry.

All these findings about autoantibodies provide the possibility for identifying the new diagnostic biomarkers for AIP. However, more studies including more patients are required to verify the sensitivity and specificity of autoantibodies as useful biomarkers for AIP.

CONCLUSION

Although there are accepted diagnostic criteria for AIP, many patients cannot be diagnosed definitively because their clinical features are not typical. Histopathology is an important examination for diagnosis. Serum IgG4 is the only

biomarker for AIP diagnosis in clinical practice, but it is only used collaterally because of its moderate sensitivity. Therefore, discovery of new biomarkers for AIP diagnosis is highly needed. The published literatures have shown that some cytokines and autoantibodies have the potential to be developed as diagnostic biomarker for AIP.

Since AIP is a rare disease, the number of cases in published papers is limited and almost all the studies were single-center retrospective study, a collaborative group can be set up in the future to collect more AIP cases for further research. Firstly, IgG4 may be combined with one more biomarker or as a panel, together with imaging, histopathology and therapy response, to classify AIP more precisely. Secondly, efforts should be made to find new autoantibodies with higher sensitivity and specificity for better diagnosing and monitoring AIP.

FOOTNOTES

Author contributions: Fan JG conceived and outlined the manuscript; Wang BC reviewed the literature, wrote and edited the manuscript; both authors have read and approved the final version to be published.

Conflict-of-interest statement: All the authors report no relevant conflicts of interest for this article.

Country/Territory of origin: China

ORCID number: Bao-Can Wang 0000-0002-6288-8100; Jian-Gao Fan 0000-0001-7443-5056.

S-Editor: Wang JJ
L-Editor: A
P-Editor: Yuan YY

REFERENCES

1 **Yoshida K**, Toki F, Takeuchi T, Watanabe S, Shiratori K, Hayashi N. Chronic pancreatitis caused by an autoimmune abnormality. Proposal of the concept of autoimmune pancreatitis. *Dig Dis Sci* 1995; **40**: 1561-1568 [PMID: 7628283 DOI: 10.1007/bf02285209]

2 **Hamano H**, Kawa S, Horiuchi A, Unno H, Furuya N, Akamatsu T, Fukushima M, Nikaido T, Nakayama K, Usuda N, Kiyosawa K. High serum IgG4 concentrations in patients with sclerosing pancreatitis. *N Engl J Med* 2001; **344**: 732-738 [PMID: 11236777 DOI: 10.1056/nejm200103083441005]

3 **Shimosegawa T**, Chari ST, Frulloni L, Kamisawa T, Kawa S, Mino-Kenudson M, Kim MH, Klöppel G, Lerch MM, Löhr M, Notohara K, Okazaki K, Schneider A, Zhang L; International Association of Pancreatology. International consensus diagnostic criteria for autoimmune pancreatitis: guidelines of the International Association of Pancreatology. *Pancreas* 2011; **40**: 352-358 [PMID: 21412117 DOI: 10.1097/MPA.0b013e3182142fd2]

4 **Umehara H**, Okazaki K, Kawa S, Takahashi H, Goto H, Matsui S, Ishizaka N, Akamizu T, Sato Y, Kawano M; Research Program for Intractable Disease by the Ministry of Health, Labor and Welfare (MHLW) Japan. The 2020 revised comprehensive diagnostic (RCD) criteria for IgG4-RD. *Mod Rheumatol* 2021; **31**: 529-533 [PMID: 33274670 DOI: 10.1080/14397595.2020.1859710]

5 **Lee SC**, Yang CH, Chang CT, Yu KH. Diagnostic Utility of Serum IgG4 in Autoimmune Pancreatitis: An Updated Comprehensive Systematic Review and Meta-analysis. *J Clin Gastroenterol* 2022; **56**: 810-817 [PMID: 34516462 DOI: 10.1097/MCG.0000000000001612]

6 **Kiyoshita Y**, Ishii Y, Serikawa M, Hanada K, Sasaki T, Fujimoto Y, Yamaguchi A, Hirao K, Noma B, Minami T, Okazaki A, Yukutake M, Mouri T, Tsuboi T, Tatsukawa Y, Nakamura S, Hirano T, Ikemoto J, Saeki S, Tamura Y, Miyamoto S, Furukawa M, Nakmura K, Yamashita Y, Iijima N, Oka S. Relapse rate and predictors of relapse after cessation of glucocorticoid maintenance therapy in type 1 autoimmune pancreatitis: a multicenter retrospective study. *BMC Gastroenterol* 2023; **23**: 295 [PMID: 37667191 DOI: 10.1186/s12876-023-02939-5]

7 **Ikeura T**, Manfredi R, Zamboni G, Negrelli R, Capelli P, Amodio A, Caliò A, Colletta G, Gabbrielli A, Benini L, Okazaki K, Vantini I, Frulloni L. Application of international consensus diagnostic criteria to an Italian series of autoimmune pancreatitis. *United European Gastroenterol J* 2013; **1**: 276-284 [PMID: 24917972 DOI: 10.1177/2050640613495196]

8 **Zhou GZ**, Zeng JQ, Wang L, Liu M, Meng K, Wang ZK, Zhang XL, Peng LH, Yan B, Pan F. Clinical characteristics and outcome of autoimmune pancreatitis based on serum immunoglobulin G4 level: A single-center, retrospective cohort study. *World J Gastroenterol* 2023; **29**: 5125-5137 [PMID: 37744294 DOI: 10.3748/wjg.v29.i35.5125]

9 **Caba O**, Diéguez-Castillo C, Martínez-Galán J, González-Cebrián I, Jiménez-Luna C. Serum biomarkers for the differentiation of autoimmune pancreatitis from pancreatic ductal adenocarcinoma. *World J Gastrointest Oncol* 2023; **15**: 268-275 [PMID: 36908319 DOI: 10.4251/wjgo.v15.i2.268]

10 **Ikemune M**, Uchida K, Tsukuda S, Ito T, Nakamaru K, Tomiyama T, Ikeura T, Naganuma M, Okazaki K. Serum free light chain assessment in type 1 autoimmune pancreatitis. *Pancreatology* 2021; **21**: 658-665 [PMID: 33741268 DOI: 10.1016/j.pan.2021.03.001]

11 **Yamamoto M**, Takano K, Kamekura R, Suzuki C, Ichimiya S, Himi T, Nakase H, Takahashi H. Stage classification of IgG4-related dacryoadenitis and sialadenitis by the serum cytokine environment. *Mod Rheumatol* 2018; **28**: 1004-1008 [PMID: 29385874 DOI: 10.1080/14397595.2018.1436029]

12 **Tsukuda S**, Ikeura T, Ito T, Nakamaru K, Masuda M, Hori Y, Ikemune M, Yanagawa M, Tanaka T, Tomiyama T, Yamaguchi T, Ando Y, Uchida K, Fukui T, Nishio A, Terasawa R, Tanigawa N, Okazaki K. Clinical implications of elevated serum interleukin-6 in IgG4-related

disease. *PLoS One* 2020; **15**: e0227479 [PMID: 31951598 DOI: 10.1371/journal.pone.0227479]

13 **Furukawa S**, Moriyama M, Miyake K, Nakashima H, Tanaka A, Maehara T, Iizuka-Koga M, Tsuboi H, Hayashida JN, Ishiguro N, Yamauchi M, Sumida T, Nakamura S. Interleukin-33 produced by M2 macrophages and other immune cells contributes to Th2 immune reaction of IgG4-related disease. *Sci Rep* 2017; **7**: 42413 [PMID: 28205524 DOI: 10.1038/srep42413]

14 **Matsubayashi H**, Uesaka K, Kanemoto H, Asakura K, Kakushima N, Tanaka M, Kimura H, Ono H. Soluble IL-2 receptor, a new marker for autoimmune pancreatitis. *Pancreas* 2012; **41**: 493-496 [PMID: 22415671 DOI: 10.1097/MPA.0b013e31823a0d4c]

15 **Minaga K**, Watanabe T, Hara A, Kamata K, Omoto S, Nakai A, Otsuka Y, Sekai I, Yoshikawa T, Yamao K, Takenaka M, Chiba Y, Kudo M. Identification of serum IFN-α and IL-33 as novel biomarkers for type 1 autoimmune pancreatitis and IgG4-related disease. *Sci Rep* 2020; **10**: 14879 [PMID: 32938972 DOI: 10.1038/s41598-020-71848-4]

16 **Kino-Ohsaki J**, Nishimori I, Morita M, Okazaki K, Yamamoto Y, Onishi S, Hollingsworth MA. Serum antibodies to carbonic anhydrase I and II in patients with idiopathic chronic pancreatitis and Sjögren's syndrome. *Gastroenterology* 1996; **110**: 1579-1586 [PMID: 8613065 DOI: 10.1053/gast.1996.v110.pm8613065]

17 **Jin CX**, Hayakawa T, Kitagawa M, Ishiguro H. Lactoferrin in chronic pancreatitis. *JOP* 2009; **10**: 237-241 [PMID: 19454813]

18 **Detlefsen S**, de Vos JD, Tanassi JT, Heegaard NHH, Fristrup C, Schaffalitzky de Muckadell OB. Value of anti-plasminogen binding peptide, anti-carbonic anhydrase II, immunoglobulin G4, and other serological markers for the differentiation of autoimmune pancreatitis and pancreatic cancer. *Medicine (Baltimore)* 2018; **97**: e11641 [PMID: 30075546 DOI: 10.1097/MD.0000000000011641]

19 **Sánchez Castañón M**, Zuliani V, Amodio A, Campagnola P, Granato A, Gabbrielli A, Benini L, López Hoyos M, Frulloni L. Role of Amylase-α2A Autoantibodies in the Diagnosis of Autoimmune Pancreatitis. *Pancreas* 2015; **44**: 1078-1082 [PMID: 26335011 DOI: 10.1097/MPA.0000000000000417]

20 **Shiokawa M**, Kodama Y, Sekiguchi K, Kuwada T, Tomono T, Kuriyama K, Yamazaki H, Morita T, Marui S, Sogabe Y, Kakiuchi N, Matsumori T, Mima A, Nishikawa Y, Ueda T, Tsuda M, Yamauchi Y, Sakuma Y, Maruno T, Uza N, Tsuruyama T, Mimori T, Seno H, Chiba T. Laminin 511 is a target antigen in autoimmune pancreatitis. *Sci Transl Med* 2018; **10** [PMID: 30089633 DOI: 10.1126/scitranslmed.aaq0997]

21 **Du H**, Shi L, Chen P, Yang W, Xun Y, Yang C, Zhao L, Zhou Y, Chen G. Prohibitin Is Involved in Patients with IgG4 Related Disease. *PLoS One* 2015; **10**: e0125331 [PMID: 25932630 DOI: 10.1371/journal.pone.0125331]

22 **Hubers LM**, Vos H, Schuurman AR, Erken R, Oude Elferink RP, Burgering B, van de Graaf SFJ, Beuers U. Annexin A11 is targeted by IgG4 and IgG1 autoantibodies in IgG4-related disease. *Gut* 2018; **67**: 728-735 [PMID: 28765476 DOI: 10.1136/gutjnl-2017-314548]

23 **Perugino CA**, AlSalem SB, Mattoo H, Della-Torre E, Mahajan V, Ganesh G, Allard-Chamard H, Wallace Z, Montesi SB, Kreuzer J, Haas W, Stone JH, Pillai S. Identification of galectin-3 as an autoantigen in patients with IgG(4)-related disease. *J Allergy Clin Immunol* 2019; **143**: 736-745.e6 [PMID: 29852256 DOI: 10.1016/j.jaci.2018.05.011]

World Journal of Gastroenterology

Submit a Manuscript: https://www.f6publishing.com

World J Gastroenterol 2024 February 14; 30(6): 527-541

DOI: 10.3748/wjg.v30.i6.527

ISSN 1007-9327 (print) ISSN 2219-2840 (online)

REVIEW

Emerging role of exosomes in ulcerative colitis: Targeting NOD-like receptor family pyrin domain containing 3 inflammasome

Xin Li, Li-Jiang Ji, Kai-Di Feng, Hua Huang, Mei-Rou Liang, Shi-Jin Cheng, Xiu-Dong Meng

Specialty type: Gastroenterology and hepatology

Provenance and peer review: Unsolicited article; Externally peer reviewed.

Peer-review model: Single blind

Peer-review report's scientific quality classification
Grade A (Excellent): 0
Grade B (Very good): B
Grade C (Good): C
Grade D (Fair): 0
Grade E (Poor): 0

P-Reviewer: Ertan A, United States; Hassan SA, United States

Received: October 22, 2023
Peer-review started: October 22, 2023
First decision: November 20, 2023
Revised: November 21, 2023
Accepted: January 9, 2024
Article in press: January 9, 2024
Published online: February 14, 2024

Xin Li, Xiu-Dong Meng, School of Basic Medicine, Guizhou University of Traditional Chinese Medicine, Guiyang 550025, Guizhou Province, China

Li-Jiang Ji, Hua Huang, Department of Anorectal Surgery, Changshu Hospital Affiliated to Nanjing University of Chinese Medicine, Changshu 215500, Jiangsu Province, China

Kai-Di Feng, Mei-Rou Liang, Shi-Jin Cheng, College of Traditional Chinese Medicine, Tianjin University of Traditional Chinese Medicine, Tianjin 301617, China

Corresponding author: Xiu-Dong Meng, PhD, Researcher, School of Basic Medicine, Guizhou University of Traditional Chinese Medicine, No. 4 Dongqing Road, Huaxi District, Guiyang 550025, Guizhou Province, China. xiudong19@163.com

Abstract

Ulcerative colitis (UC) is a chronic recurrent inflammatory bowel disease. Despite ongoing advances in our understanding of UC, its pathogenesis is yet unelucidated, underscoring the urgent need for novel treatment strategies for patients with UC. Exosomes are nanoscale membrane particles that mediate intercellular communication by carrying various bioactive molecules, such as proteins, RNAs, DNA, and metabolites. The NOD-like receptor family pyrin domain containing 3 (NLRP3) inflammasome is a cytosolic tripartite protein complex whose activation induces the maturation and secretion of proinflammatory cytokines interleukin-1β (IL-1β) and IL-18, triggering the inflammatory response to a pathogenic agent or injury. Growing evidence suggests that exosomes are new modulators of the NLRP3 inflammasome, with vital roles in the pathological process of UC. Here, recent evidence is reviewed on the role of exosomes and NLRP3 inflammasome in UC. First, the dual role of exosomes on NLRP3 inflammasome and the effect of NLRP3 inflammasome on exosome secretion are summarized. Finally, an outlook on the directions of exosome-NLRP3 inflammasome crosstalk research in the context of UC is proposed and areas of further research on this topic are highlighted.

Key Words: Ulcerative colitis; Exosomes; Inflammasome; Evidence; Therapeutics

Core Tip: Clarifying the regulatory circuits that control the abnormal immune state of the intestinal mucosa is essential for understanding ulcerative colitis (UC) pathogenesis and clinical management. The role of exosomes and NOD-like receptor family pyrin domain containing 3 (NLRP3) inflammasomes in UC has been continuously highlighted in recent years. In this review, the dual role of exosomes on NLRP3 inflammasome and the effect of NLRP3 inflammasome on exosome secretion are summarized. Furthermore, an outlook on the directions of exosome-NLRP3 inflammasome crosstalk research in the context of UC is proposed and areas of further research on this topic are highlighted.

Citation: Li X, Ji LJ, Feng KD, Huang H, Liang MR, Cheng SJ, Meng XD. Emerging role of exosomes in ulcerative colitis: Targeting NOD-like receptor family pyrin domain containing 3 inflammasome. *World J Gastroenterol* 2024; 30(6): 527-541
URL: https://www.wjgnet.com/1007-9327/full/v30/i6/527.htm
DOI: https://dx.doi.org/10.3748/wjg.v30.i6.527

INTRODUCTION

Ulcerative colitis (UC) is characterized by chronic, remitting, and recurrent mucosal inflammation[1]. Although its cause is not well understood, current evidence suggests innate and adaptive immunity play critical roles in its pathogenesis[2]. The events leading to UC involve disrupting the intestinal mucosal barrier, bringing the luminal microbial community and the mucosal immune system into direct contact[3]. Subsequently, innate immune cells, such as macrophages and dendritic cells, rapidly recognize microorganisms or their products entering the lamina propria from the intestinal lumen and transmit signals, awakening the innate defenses and the adaptive immune system[4]. A long-term feature of UC is inflammation maintained by various inflammatory mediators produced by activated immune cells, including proinflammatory cytokines and chemokines[5-8]. Another characteristic is enterocyte apoptosis sustained by several inflammatory cells, which prevents mucosal healing[2]. Considering these points, we can assume that clarifying the regulatory circuits that control the abnormal immune state of the intestinal mucosa is essential for understanding UC pathogenesis and clinical management.

The NOD-like receptor family pyrin domain containing 3 (NLRP3) inflammasome mediates the inflammatory cascade *in vivo* and is a critical regulator in inflammatory bowel disease development[9]. Its activation promotes pyroptosis and caspase-1-dependent secretion of interleukin-1β (IL-1β) and IL-18, leading to a sustained inflammatory response in the intestinal mucosa[10]. Since these two proinflammatory cytokines are present in released exosomes, one possible pathway for their unconventional secretion may occur through endosome release[11-14]. Exosomes are nanoscale membrane-derived particles that mediate intercellular communication by carrying many bioactive molecules, including proteins, RNAs, DNA, and metabolites[15,16]. They also carry out numerous functions, such as releasing cytokines and inhibiting or promoting inflammasome activation, depending on the transported molecules[17,18]. Increasing evidence suggests that crosstalk between exosomes and inflammasomes has a critical role in inflammatory diseases[19]. Therefore, systematically exploring this crosstalk in UC should have beneficial implications for the prevention and treatment.

NLRP3 INFLAMMASOME

Composition and distribution of NLRP3 inflammasome

Inflammasomes are cytosolic multiprotein complexes that initiate inflammatory cascade responses by identifying damage-associated molecular patterns (DAMPs), cellular distress signals of the host, pathogen-associated molecular patterns (PAMPs), and conserved components of infectious agents[20]. T and B lymphocytes, macrophages, antigen-presenting cells, and granulocytes all express the NLRP3 inflammasome[21]. It represents the most classical inflammasome subtype consisting of the NLRP3 receptor, apoptosis-associated speck-like protein (ASC) adapter, and caspase-1 effector proteins[22]. The NLRP3 receptor protein is composed of 3 domains: a C-terminal leucine-rich repeat domain, an N-terminal pyrin domain (PYD), and a central nucleotide-binding and oligomerization domain[23]. The ASC adapter contains several domains: 2 transactivation structural domains, the pyrin structural domain linked to the upstream NLRP3 receptor, and the caspase recruitment domain (CARD) connected to the downstream caspase-1[24,25].

Activation of NLRP3 inflammasome

The innate immune system senses exogenous (PAMPs) or endogenous (DAMPs) danger signals by recognizing them with various pattern recognition receptors, such as Toll-like receptors and NOD-like receptors. During its involvement in the inflammatory response, NLRP3 inflammasome provides a molecular model that can be stimulated by many DAMPs (aluminum adjuvants, ATP, uric acid crystals, and β-amyloid peptides) and PAMPs (microbial toxins, viral RNA, and bacterial surface components). Currently, canonical, non-canonical, and alternate routes can all activate the NLRP3 inflammasome[26] (Figure 1).

Canonical NLRP3 inflammasome activation

In most cells, canonical NLRP3 inflammasome activation involves priming and activation steps. The priming step is

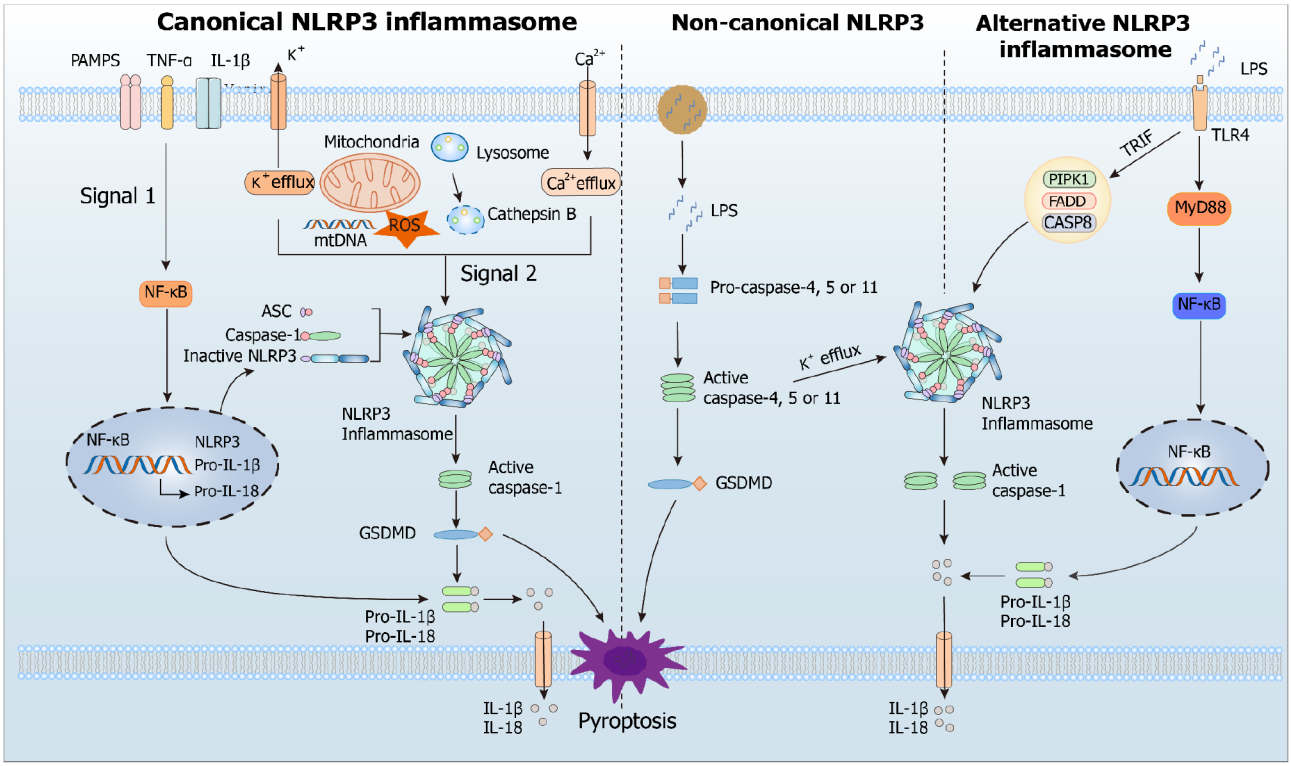

DOI: 10.3748/wjg.v30.i6.527

Figure 1 Canonical, non-canonical, and alternative modes of NOD-like receptor family pyrin domain containing 3 activation. NLRP3: NOD-like receptor family pyrin domain containing 3; PAMPs: Pathogen-associated molecular patterns; TNF-α: Tumor necrosis factor-alpha; IL-1β: Interleukin-1β; ROS: Reactive oxygen species; GSDMD: Gasdermin D; LPS: Lipopolysaccharide; ASC: Apoptosis-associated speck-like protein; IL-18: Interleukin-18.

initiated by a signal from the ligand bound to the pattern recognition receptor and promotes transcription of pro-IL-18, pro-IL-1β, and NLRP3 *via* NF-κB-dependent pathway[27-30]. The activation step leads to NLRP3 assembly and is promoted by various DAMPs or PAMPs through multiple molecular and cellular events, such as lysosomal disruption, mitochondrial DNA production, mitochondrial dysfunction, reactive oxygen species (ROS) release, and ion flux (Ca^{2+} influx and K^+/Cl^- efflux). The activated NLRP3 inflammasome induces cleavage and activation of caspase-1 *via* CARD-CARD and PYD-PYD interactions[30]. Subsequently, the activated caspase-1 recruits and cleaves the proinflammatory cytokines pro-IL-18 and pro-IL-1β, allowing their maturation and release[30]. In addition, it cleaves the pyroptotic substrate gasdermin D (GSDMD), enabling its translocation to the cell membrane, where it forms pores and triggers inflammatory programmed cell death called pyroptosis[31].

Non-canonical NLRP3 inflammasome activation

Human caspases 4 and 5, as well as murine caspase 11, are needed for non-canonical NLRP3 inflammasome activation. In this pathway, these caspases recognize and are activated by cytosolic lipopolysaccharide (LPS) from endocytosed gram-negative bacteria or, more often, their outer membrane vesicles[32]. The activated caspases catabolize GSDMD, leading to pyrolysis and promoting the release of mature IL-18 and IL-1β[33,34]. In addition to LPS, another signal called 1-palmitoyl-2-arachidonoyl-sn-glycero-3-phosphocholine (PAPC) activates the non-canonical pathway. This molecule is abundant in membranes of mammalian cells and is oxidized by ROS released from damaged or dead cells. The oxidized PAPC binds caspase-11 and caspase-4, initiating activation or inhibition of the NLRP3 inflammasome depending on the cell type[35].

Alternative NLRP3 inflammasome activation

Alternative activation of the NLRP3 inflammasome possesses cell- and species-specific characteristics[36]. For example, the TLR4-TRIF-RIPK1-FADD-CASP8 axis activates an alternative inflammasome upstream of NLRP3 in porcine and human monocytes, but this activation response is absent in murine monocytes[34,36]. Interestingly, the alternative activation lacks typical features for canonical and non-canonical activation, such as ASC speckle formation, K^+ efflux, or pyroptosis induction[34].

The role of NLRP3 inflammasome in UC

Susceptibility to UC significantly increases with single nucleotide polymorphisms rs10925019 and rs10754558 in the coding region of the NLRP3 gene[37,38]. Similarly, predisposition to inflammatory bowel disease correlates with polymorphisms affecting receptors downstream of NLRP3, including interleukin 1 receptor-like 1 and 2, interleukin 1 receptor type 1 and 2, and interleukin 18 receptor 1[39]. Disease activity of UC is associated with increased levels of

inflammasome activation markers NLRP3, caspase-1, and ASC[40,41]. A similar effect is also observed in mice with colitis, where the upregulated markers positively correlate with disease severity and pathological damage[42,43]. Conversely, mice with colitis lacking NLRP3 or caspase-1 show significantly less severe pathology compared with wild-type mice with colitis[44,45]. Furthermore, NLRP3 promotes intestinal mucosal inflammation *in vitro*[46]. These findings demonstrate that NLRP3 inflammasome activity participates in UC pathogenesis and suggest that treating the disease may rely on regulating the NLRP3 inflammasome activation or its downstream cytokine effectors.

A small-molecule inhibitor of the NLRP3 inflammasome called MCC950 significantly reduces the secretion of IL-18 and IL-1β in mice, attenuating the inflammatory cascade response evoked by NLRP3 inflammasome activation[47]. Carboxy-amidotriazole, wogonoside, or oroxylin A are other small-molecule compounds that also alleviate experimental colitis but with a mechanism that inhibits the NLRP3 inflammasome activation[48-50]. Although pharmacological inhibition of inflammasome overactivation benefits animals with UC, therapies targeting inflammasomes remain limited. Recent evidence suggests that dietary compounds or medicinal herbs reduce colonic inflammation in mice and, in some cases, even in patients with UC by targeting different inflammasome modulators to inactivate inflammasomes in the colon[51]. Thus, strategies for treating UC may involve using bioactive substances purified from food or traditional medicines to regulate inflammasome activity.

EXOSOMES

Biogenesis, biology, function, and regulation of exosomes

Exosomes are endosome-derived extracellular vesicles commonly found in body fluids, including sweat, blood, and urine, and characterized by a phospholipid bilayer, small vesicle morphology, and a diameter from 30 to 150 nm[15,16]. They mediate intercellular communication by carrying numerous biologically active molecules, such as DNA, RNAs, proteins, and metabolites, and their bioactive molecular composition depends on the cell type releasing them[15,16]. Notably, exosomes contain two classes of proteins: conserved and specific. While the make-up of specific proteins is determined by the cell type releasing the exosome and is subject to change from varying physiological conditions acting on the cell, that of the conserved proteins is constant, rendering them exosome markers. Noteworthy examples are programmed cell death 6 interacting protein, tumor susceptibility gene 10, members of the heat shock protein family HSP60, HSP70, and HSP90, and antigens CD9, CD63, CD81, and CD82[15,16]. Exosome biogenesis requires uptake, secretion, cargo sorting, and formation, achieved through the classical or direct pathways[52]. Whereas most cells utilize the classical, or exocytic, pathway of exosome biogenesis, T cells employ a direct pathway as a quick mechanism that generates exosomes directly from the plasma membrane[53] (Figure 2).

Since released exosomes contain crucial molecules for transferring information between cells, they are implicated in the cancer microenvironment[54] and the pathogenesis of various illnesses, including autoimmune[55], cardiac[56], neurological[57], and liver disorders[58]. Furthermore, because exosomes collected from sick populations have different RNA profiles than exosomes collected from healthy ones[59-61], they are potential diagnostic and therapeutic biomarkers for many diseases[62,63].

Exosomes and UC

Exosomes are thought to play an immunomodulatory function owing to their involvement in immune synapse formation and antigen presentation[64,65]. Because UC is an immune disease, and the saliva of patients with UC contains large amounts of exosomal proteins, the role of exosomes in UC is unquestionable[66-68]. Indeed, animal experiments confirm that exosomal proteins are associated with proteasomal activity and inflammatory response, suggesting that some, such as saliva-derived exosomal proteasome 20S subunit alpha 7, can be used as an ideal biomarker for UC diagnosis[68]. Other potential UC biomarkers are exosome micro RNAs, with enhanced levels in individuals with UC. For instance, elevated levels of gut-derived miR-29b in the plasma of individuals with UC not only help diagnose the disease but also an impaired cardiac function *via* miR-29b-mediated extraintestinal inhibition of vital proteins, such as brain-derived neurotrophic factor[69]. Similarly, small GTPases that regulate exosome secretion also have increased levels in UC, such as RAB27A, member RAS oncogene family and RAB27B, member RAS oncogene family. The number of RAB27A- and RAB27B-positive immune cells in the intestinal mucosa of individuals with active UC is significantly higher than that of healthy patients, indicating that exosome-mediated immune regulation is involved in the pathological process of UC[70].

Currently, the role of various sources of exosomes in UC is being widely explored (Table 1)[71-105]. Mesenchymal stem cell (MSC) therapy is a cutting-edge one for treating various diseases, due to the strong immunomodulating and immunosuppressive properties of MSCs, and stem cell-derived exosomes may have a beneficial effect on UC, according to newly available evidence[71-91]. The ameliorative effects of MSC-derived exosomes on UC are regulated in multiple ways, including inhibition of inflammatory responses, regulation of immune cell homeostasis, improvement of intestinal flora structure, and inhibition of oxidative stress, ultimately leading to repair of intestinal mucosal damage and restoration of intestinal barrier function. Similarly, dendritic cell-derived exosomes were also found to have a reparative effect on intestinal injury in UC by inhibiting pathways associated with inflammation[92-94]. In addition, it was found that encapsulating triptolide with DC cell-derived exosomes could not only reduce the toxicity of the drug, but also accurately deliver the drug to the therapeutic target to induce immunosuppression in UC mice, providing a new perspective for immunosuppressive treatment of UC[95]. However, macrophage-derived exosomes do not always provide a benefit to UC. Some exosomal molecules, such as miR-590-3p produced by M2 macrophages, reduce mucosal damage and promote epithelial cell repair in mice with colitis[96]. However, others, such as exosome miR-21a-5p produced by M1 macrophages, exacerbate UC by inhibiting E-cadherin and activating type 2 innate lymphoid cells[97].

Table 1 Sources of exosomes and their roles in ulcerative colitis

Exosomes source	Pivotal molecules	Role of the exosomes	Conclusion	Ref.
Stem cell	miR-378a-5p	Inhibiting pyroptosis through NLRP3/caspase-1 signaling	Beneficial	[71]
Stem cell	miR-539-5p	Inhibiting pyroptosis through NLRP3/caspase-1 signaling	Beneficial	[72]
Stem cell	miRNA	Suppressing pyroptosis	Beneficial	[73]
Stem cell	miR-203a-3p.2	Suppressing macrophage pyroptosis induced by caspase11/4	Beneficial	[74]
Stem cell	NA	Regulating the Treg population	Beneficial	[75]
Stem cell	NA	Modulating the gut metagenomics-metabolomics-farnesoid X receptor axis	Beneficial	[76]
Stem cell	NA	Polarizing M2b macrophages	Beneficial	[77]
Stem cell	miR-146a	Inhibiting SUMO1 expression and its binding to β-catenin	Beneficial	[78]
Stem cell	miR-216a-5p	Inducing macrophage M2 polarization by regulating the HMGB1/TLR4/NF-κB signaling pathway	Beneficial	[79]
Stem cell	NA	Regulating the Th17/Treg balance	Beneficial	[80]
Stem cell	NA	Repairing intestinal barrier *via* TSG-6	Beneficial	[81]
Stem cell	miR-125a, miR-125b	Repressing Th17 cell differentiation	Beneficial	[82]
Stem cell	NA	Limiting intestinal epithelial cells reactive oxygen species accumulation and DNA damage through HIF-1α	Beneficial	[83]
Stem cell	miR-181a	Improving gut microbiota composition, barrier function, and inflammatory status	Beneficial	[84]
Stem cell	NA	Suppressing inflammation	Beneficial	[85]
Stem cell	NA	Modulating Th1/Th17 and Treg cell responses	Beneficial	[86]
Stem cell	NA	Attenuating inflammation, oxidative stress and apoptosis	Beneficial	[87]
Stem cell	NA	Stimulating epithelial repair and decreasing epithelial apoptosis	Beneficial	[88]
Stem cell	NA	Modulating the expression of IL-7 in macrophages	Beneficial	[89]
Stem cell	NA	Downregulating intestine ferroptosis	Beneficial	[90]
Melatonin and stem cell	NA	Suppressing inflammation, oxidative stress, apoptosis, and fibrosis	Beneficial	[91]
Dendritic Cell	miR-146a	Targeting Traf6, IRAK-1, and NLRP3 in macrophages	Beneficial	[92]
Dendritic cell	NA	Preventing colon damage	Beneficial	[93]
Dendritic cell	NA	Downregulating the expression of IL-2, IFN-γ and TNF-α	Beneficial	[94]
Dendritic cell	NA	Carrying drug to dendritic cell	Beneficial	[95]
M2 macrophage	miR-590-3p	Suppressing LATS1 and activating the YAP/β-catenin signaling	Beneficial	[96]
M1 macrophage	MiR-21a-5p	Decreasing E-cadherin and subsequent ILC2 activation	Unfavorable	[97]
Intestinal	NA	Promoting wound healing	Beneficial	[98]
Visceral adipose tissue	miR-155	Promoting macrophage M1 polarization	Unfavorable	[99]
Serum	NA	Inhibiting MCP-1 and MIP-1α expression *via* NLRP12-Notch signaling pathway	Beneficial	[100]
Serum	Proteins	Implicating macrophage activation	NA	[101]
Helicobacter pylori	NA	Aggravating intestinal epithelium barrier dysfunction by facilitating Claudin-2 expression	Unfavorable	[102]
Milk	NA	Suppressing inflammation	Beneficial	[103]
Cow and human milk	miRNA-320, 375, and Let-7	Downregulating DNA methyltransferase 1 (DNMT1) and DNMT3	Beneficial	[104]
Bovine colostrum	NA	Suppressing inflammation and oxidative stress	Beneficial	[105]

NA: Not available.

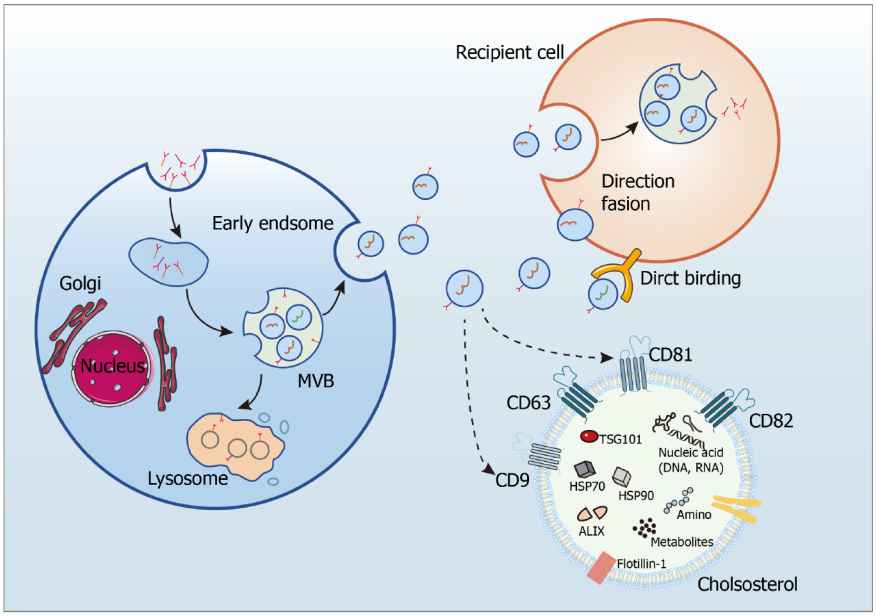

DOI: 10.3748/wjg.v30.i6.527

Figure 2 The processes of exosome biogenesis and release. MVB: Multivesicular bodies.

Furthermore, limited evidence suggests that gut-derived and serum-derived exosomes are beneficial in UC[98,100], whereas visceral adipose-derived exosomes aggravate UC[99]. Surprisingly, emerging evidence has recently suggested that human or bovine milk-derived exosomes express a favorable benefit in animals with colitis by decreasing oxidative stress and inflammation, indicating a new route for the development of therapeutic approaches for UC[103-105].

EXOSOMES AND NLRP3 INFLAMMASOME CROSSTALK

Effects of exosomes on NLRP3 inflammasome

According to recent evidence, cells utilize exosome secretion to regulate NLRP3 inflammasome activation, suppressing inflammation and promoting damage repair (Table 2)[71-73,106-147]. Since most findings originate from research on various stem cell-derived exosomes, knowledge of how they regulate the NLPR3 inflammasome activation in differentiated cells remains limited. Nonetheless, the available evidence indicates that exosomes suppress the NLRP3 inflammasome mainly by regulating the pathways upstream of NLRP3, especially TLR-related ones and those related to oxidative stress. For example, exosome release lowers ROS production, reducing ROS levels available for the NLRP3 inflammasome activation[107,112,126]. In addition, exosomes help protect mitochondria from damage induced by oxidative stress states, possibly by exosome-carried mitochondrial proteins[112]. Abundant findings also suggest that exosomes regulate the activation of NLRP3 inflammasome by directly binding to NLRP3[71,121,130,137].

We have so far learned that stem cell-derived exosomes repress the NLRP3 inflammasome activation but will see that those from other cell types, including cancer, epithelial, immune, and endothelial cells, appear to promote it (Table 2). For instance, exosomal miR-30d-5p released by polymorphonuclear neutrophils induces macrophage pyroptosis and M1 macrophage polarization *via* the NF-κB pathway, promoting sepsis-associated acute lung injury[138]. Similarly, tumor-derived exosomal tripartite motif containing 59 protein induces proteasomal degradation of abhydrolase domain containing 5 lipolytic co-activator in macrophages. Consequently, this event reprograms macrophages into cells with tumor-promoting function and activates the NLRP3 inflammasome, mediating the IL-1β release and stimulating lung cancer progression[139]. When exposed to photooxidative blue light, retinal pigment epithelium-derived exosomes exacerbate potentially harmful oxidative responses by activating the NLRP3 inflammasome[140]. In hepatic ischemia-reperfusion injury, serum exosome levels rise significantly, freely crossing the blood-brain barrier due to their small size and stimulating pyroptosis of hippocampal and cortical tissues[141]. By triggering NLRP3-dependent pyroptosis in alveolar macrophages, plasma-derived exosomes help cause lung damage brought on by pancreatitis[142]. Exosomes in patients with COVID-19 increase inflammasome activity in distant endothelial cells, enhancing immunopathogenesis of the disease[143]. In addition, plasma-derived exosomes induce pyroptosis in intestinal epithelial cells *via* NLRP3 inflammasome activation in individuals with intestinal Behçet's syndrome[144].

In summary, the above evidence suggests that exosomes play a dual role in NLRP3-mediated inflammatory response by attenuating or enhancing the inflammasome activity. The differences in how exosomes affect the inflammasome activity may depend on the cell type producing the exosomes and the specific circumstances of their release. Importantly, modulating the NLRP3 inflammasome activity by targeting exosomes is emerging as a promising strategy to combat inflammatory diseases[145-147].

Table 2 Sources of exosomes and their roles in NOD-like receptor family pyrin domain containing 3 inflammasome regulation

Exosomes source	Pivotal molecules	Role of the exosomes	Ref.
Stem cell	miR-378a-5p	Inhibiting NLRP3 inflammasome activation	[71]
Stem cell	miR-539-5p	Inhibiting NLRP3 inflammasome activation	[72]
Stem cell	NA	Inhibiting NLRP3 inflammasome activation	[73]
Stem cell	miR-17	Inhibiting NLRP3 inflammasome activation by targeting TXNIP	[106]
Stem cell	NA	Inhibiting NLRP3 inflammasome activation by down-regulating ROS levels	[107]
Stem cell	NA	Inhibiting TLR4-NLRP3-mediated pyroptosis	[108]
Plasma	NA	Inhibiting pyroptosis through the TLR4/NF-κB pathway	[109]
Stem cell	NA	Inhibiting NLRP3 inflammasome-mediated pyroptosis by promoting AMPK-dependent autophagic flux	[110]
Stem cell	circHIPK3	Inhibiting pyroptosis by down-regulating miR-421 to increase FOXO3A expression	[111]
Stem cell	miRNA Let-7	Inhibiting NLRP3 inflammasome activation by down-regulating ROS levels	[112]
Stem cell	miR-188-3p	Targeting NLRP3	[113]
Stem cell	NA	Inhibiting the tumor suppressor Rb1-mediated NLRP3 inflammasome	[114]
Stem cell	NA	Inhibiting pyroptosis through the TLR4 pathway	[115]
Cancer cells	miR-21	Repressing PTEN and BRCC3 to facilitate NLRP3 phosphorylation	[116]
Stem cell	circ_003564	Attenuating inflammasome-related pyroptosis	[117]
Stem cell	miR-100-5p	Inhibiting the FOXO3A/NLRP3 pathway	[118]
Stem cell	miR-17-5p	Suppressing TXNIP-NLRP3 inflammasome	[119]
Pericyte	circEhmt1	Upregulating NFIA levels to suppress NLRP3-mediated inflammasome formation	[120]
B cells	miR-BART15	Targeting the miR-223 binding site in the NLRP3 3′-untranslated region	[121]
Stem cell	NA	Suppressing NLRP3 inflammasome activation	[122]
Stem cell	NA	Suppressing NLRP3 inflammasome activation	[123]
Stem cell	NA	Suppressing NLRP3 inflammasome activation	[124]
Stem cell	NA	Regulating pyroptosis *via* the miR-146a-5p-TRAF6 axis	[125]
M2 macrophage	NA	Suppressing the ROS/NLRP3 pathway	[126]
Stem cell	NA	Attenuating inflammasome-related pyroptosis	[127]
Cancer cells	NA	Suppressing NLRP3 inflammasome activation	[128]
Stem cell	miR-23b	Attenuating inflammasome-related pyroptosis	[129]
Stem cell	miR-223-3p	Targeting NLRP3	[130]
Stem cell	NA	Suppressing NLRP3 inflammasome activation	[131]
Stem cell	NA	Modulating miR-126 *via* targeting HMGB1	[132]
Plasma	NA	Promoting the autophagic degradation of NLRP3	[133]
Stem cell	miR-223	Downregulating NLRP3 expression	[134]
Dendritic cell	NA	Downregulating NLRP3 expression	[135]
M2 macrophage	microRNA-148a	Inhibiting the TLR4/NF-κB/NLRP3 pathway	[136]
Salivary	miR-223-3p	Attenuating inflammasome-related pyroptosis	[137]
Neutrophils	miR-30d-5p	Upregulating NLRP3 expression through the NF-κB pathway	[138]
Cancer cells	TRIM59	Inducing the ubiquitination of ABHD5 to activate the NLRP3 inflammasome activation	[139]
Epithelium cells	NA	Upregulating the NLRP3 inflammasome	[140]
Serum	NA	Activating the NLRP3 inflammasome	[141]

Plasma	NA	Triggering NLRP3-dependent pyroptosis	[142]
Plasma	NA	Triggering NLRP3 inflammasome	[143]
Plasma	NA	Activating the NLRP3 inflammasome	[144]
Serum	NA	Inhibiting the NF-κB/NLRP3 pathway	[145]
Plasma	miRNA-223	Inhibiting NLRP3	[146]
Renal tissues	NA	Suppressing NLRP3 activation	[147]

NA: Not available.

Effects of NLRP3 inflammasome on exosomes

Some NLRP3 inflammasome activators also stimulate extracellular vesicle secretion, suggesting inflammasome activation enhances extracellular vesicle secretion[148]. After exposure to ATP, macrophages secrete exosomes carrying the major histocompatibility complex class II proteins[149]. Moreover, macrophages isolated from mice lacking the genes encoding the ASC adapter or NLRP3 cannot release these exosomes after exposure to ATP, indicating exosome release requires components of the NLRP3 complex[149]. Similarly, inflammasome activation increases exosome secretion caused by a viral infection or exposure to LPS/ATP[149]. We have seen previously that the release of mature IL-1β largely depends on the NLRP3 inflammasome activation. When synovial fibroblasts are treated with exogenous IL-1β, they show a significant increase in exosome secretion compared with the untreated control cells, implying IL-1β stimulates exosome release[150]. Although a few recent studies demonstrate that exosome secretion is induced by NLRP3 inflammasome activation, evidence supporting this claim is insufficient and requires additional confirmation[19].

Exosome-inflammasome crosstalk in UC

In inflammatory states, such as UC, MSCs have immunomodulating and homeostatic effects and may repair intestinal damage[151]. Increasing evidence indicates that MSCs maintain immunosuppressive signals through paracrine mediators instead of cell-to-cell contact and that paracrine processes predominantly mediate the therapeutic role of MSC-derived exosomes[71,152]. Although we know little about how MSC-derived exosomes suppress colonic inflammation, recent evidence suggests that crosstalk between exosomes and NLRP3 inflammasome constitutes the mechanism[71-73,92]. Thus, the roles of exosome-NLRP3 inflammasome crosstalk in inflammatory diseases are gaining much attention[19].

In mice with colitis, exosomes from human umbilical cord MSCs carrying miR-378a-5p significantly alleviate colonic inflammation and promote mucosal repair[71]. Mechanically, these exosomes inhibit the NLRP3 inflammasome activation, preventing caspase-1 cleavage and the IL-18 and IL-1β secretion and decreasing pyroptosis[71]. Similarly, exosomes from bone marrow MSCs containing miR-539-5p alleviate colitis by directly targeting the NLRP3-caspase-1 pathway to inhibit pyroptosis[72]. Moreover, hair follicle-derived MSCs inhibited pyroptosis by releasing exosomes in a paracrine manner, which ultimately exerted an alleviating effect in mice with colitis[73]. Other examples involving exosomes with small RNA cargo are dendritic cells-derived exosomes transporting miR-146a which exert a therapeutic effect by directly targeting the NLRP3-caspase-1 pathway to inhibit intestinal inflammation in mice with colitis[92] and human umbilical cord MSC-derived exosomes transferring miR-203a-3p.2 that reduce pyroptosis of macrophages caused by caspase-1 or -4[74].

Given these points, we can conclude that crosstalk between exosomes and the NLRP3 inflammasome holds promise for developing novel treatment strategies (Figure 3). Despite the scarcity of available evidence, the connection between MSC-derived exosomes with anti-inflammatory activity and the NLRP3 inflammasome offers a fresh viewpoint on using this system as a therapy for UC in the clinical setting.

CONCLUSION

Since exosomes and the NLRP3 inflammasome play vital roles in UC, they are explored as potential new targets for preventing and treating the disease, attracting considerable attention. Importantly, crosstalk between exosomes and the NLRP3 inflammasome and its emerging therapeutic benefit is gaining increasing interest in biomedicine.

Exosomes are upstream components of the NLRP3 inflammasome pathway and attenuate or enhance the NLRP3 inflammasome activation. Based on the available data, MSC-derived exosomes repress the NLRP3 inflammasome activation in receptor cells, alleviating the inflammatory response. Therefore, these exosomes are therapeutically valuable and in stark contrast to most of those derived from non-stem cells that promote the NLRP3 inflammasome activation and exacerbate tissue inflammation. Potent effectors of the crosstalk are micro RNAs that repress the NLRP3 inflammasome activation and prevent pyroptotic cell death or promote the opposite effect, depending on the cell type releasing the exosomes and the external factors triggering exosome release. However, this contrasting effect of exosomes on the NLRP3 inflammasome and the factors that decide on its direction is supported by limited evidence. Similarly, evidence is lacking about the regulatory role of the NLRP3 inflammasome activation in exosome release. Thus, although crosstalk between exosomes and the NLRP3 inflammasome undoubtedly has a central role in UC research, further studies are necessary to elucidate it.

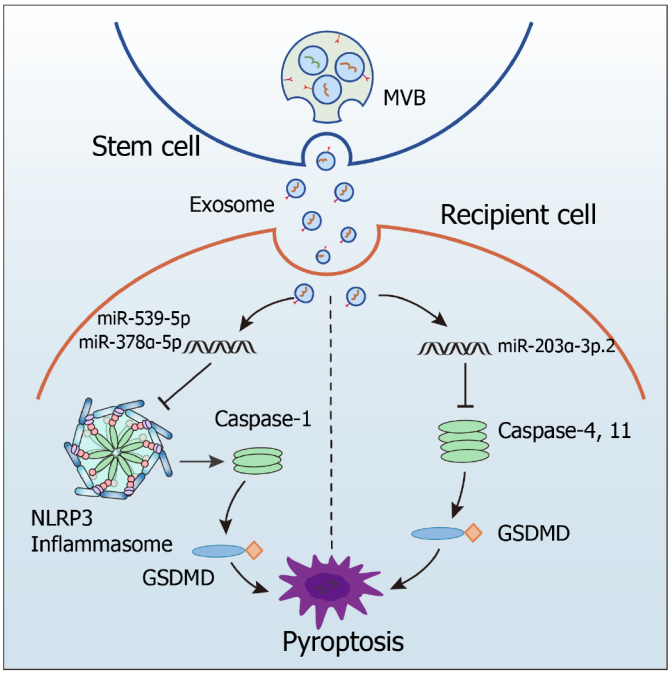

DOI: 10.3748/wjg.v30.i6.527

Figure 3 Inhibition of NOD-like receptor family pyrin domain containing 3 inflammasome activation by stem cell-derived exosomes in ulcerative colitis. NLRP3: NOD-like receptor family pyrin domain containing 3; MVB: Multivesicular bodies; GSDMD: Gasdermin D.

In conclusion, the therapeutic potential of exosomes has gained much attention since these vesicles transfer biologically active cargo between cells and could deliver drugs to treat diseases. However, because exosomes originating from different sources and exposed to specific intervention conditions have unique cargo composition and properties, selecting those most suitable for therapeutic use represents a challenge requiring substantial effort for clarification. Moreover, encapsulation and targeted delivery of drugs (*e.g.*, biologics and small molecule drugs) through exosomes is a novel approach that both reduce drugs toxicity and improve efficacy. Therefore, large-scale prospective clinical trials exploring therapeutic efficacy and adverse events of exosomes in UC will be the focus of upcoming studies on the basis of sufficient basic research evidence.

FOOTNOTES

Co-first authors: Xin Li and Li-Jiang Ji.

Author contributions: Li X and Ji LJ wrote the paper the paper, they are the co-first authors; Feng KD, Huang H, Liang MR, Cheng SJ performed the collected the data; Meng XD contributed to the review, and editing of the manuscript; all authors have read and approved the final manuscript.

Supported by Guizhou University of Traditional Chinese Medicine Doctoral Initiation Fund, No. 202306; and Changshu Municipal Science and Technology Bureau Supporting Project, No. CS202030.

Conflict-of-interest statement: Authors declare no conflict of interests for this article.

Country/Territory of origin: China

ORCID number: Li-Jiang Ji 0000-0003-2397-2181; Hua Huang 0000-0001-6111-8019; Xiu-Dong Meng 0000-0001-8353-7425.

S-Editor: Yan JP
L-Editor: Filipodia
P-Editor: Yuan YY

REFERENCES

1 **Feuerstein JD**, Moss AC, Farraye FA. Ulcerative Colitis. *Mayo Clin Proc* 2019; **94**: 1357-1373 [PMID: 31272578 DOI: 10.1016/j.mayocp.2019.01.018]

2 **Huang J**, Wang F, Tang X. Uncovering the shared molecule and mechanism between ulcerative colitis and atherosclerosis: an integrative genomic analysis. *Front Immunol* 2023; **14**: 1219457 [PMID: 37638002 DOI: 10.3389/fimmu.2023.1219457]

3 **Salim SY**, Söderholm JD. Importance of disrupted intestinal barrier in inflammatory bowel diseases. *Inflamm Bowel Dis* 2011; **17**: 362-381 [PMID: 20725949 DOI: 10.1002/ibd.21403]

4 **Zou J**, Liu C, Jiang S, Qian D, Duan J. Cross Talk between Gut Microbiota and Intestinal Mucosal Immunity in the Development of Ulcerative Colitis. *Infect Immun* 2021; **89**: e0001421 [PMID: 33526559 DOI: 10.1128/IAI.00014-21]

5 **Sun T**, Nguyen A, Gommerman JL. Dendritic Cell Subsets in Intestinal Immunity and Inflammation. *J Immunol* 2020; **204**: 1075-1083 [PMID: 32071090 DOI: 10.4049/jimmunol.1900710]

6 **Ji L**, Zhou Q, Huang J, Lu D. Macrophages in ulcerative colitis: A perspective from bibliometric and visual analysis. *Heliyon* 2023; **9**: e20195 [PMID: 37809606 DOI: 10.1016/j.heliyon.2023.e20195]

7 **Huang J**, Zhang J, Ma J, Liu J, Wang F, Tang X. Inhibiting Ferroptosis: A Novel Approach for Ulcerative Colitis Therapeutics. *Oxid Med Cell Longev* 2022; **2022**: 9678625 [PMID: 35378823 DOI: 10.1155/2022/9678625]

8 **Yan J**, Pandey SP, Barnes BJ, Turner JR, Abraham C. T Cell-Intrinsic IRF5 Regulates T Cell Signaling, Migration, and Differentiation and Promotes Intestinal Inflammation. *Cell Rep* 2020; **31**: 107820 [PMID: 32610123 DOI: 10.1016/j.celrep.2020.107820]

9 **Song Y**, Zhao Y, Ma Y, Wang Z, Rong L, Wang B, Zhang N. Biological functions of NLRP3 inflammasome: A therapeutic target in inflammatory bowel disease. *Cytokine Growth Factor Rev* 2021; **60**: 61-75 [PMID: 33773897 DOI: 10.1016/j.cytogfr.2021.03.003]

10 **Zhang Q**, Chen LH, Yang H, Fang YC, Wang SW, Wang M, Yuan QT, Wu W, Zhang YM, Liu ZJ, Nan FJ, Xie X. GPR84 signaling promotes intestinal mucosal inflammation *via* enhancing NLRP3 inflammasome activation in macrophages. *Acta Pharmacol Sin* 2022; **43**: 2042-2054 [PMID: 34912006 DOI: 10.1038/s41401-021-00825-y]

11 **Dubyak GR**. P2X7 receptor regulation of non-classical secretion from immune effector cells. *Cell Microbiol* 2012; **14**: 1697-1706 [PMID: 22882764 DOI: 10.1111/cmi.12001]

12 **Ansari MA**, Singh VV, Dutta S, Veettil MV, Dutta D, Chikoti L, Lu J, Everly D, Chandran B. Constitutive interferon-inducible protein 16-inflammasome activation during Epstein-Barr virus latency I, II, and III in B and epithelial cells. *J Virol* 2013; **87**: 8606-8623 [PMID: 23720728 DOI: 10.1128/JVI.00805-13]

13 **Kim J**, Gee HY, Lee MG. Unconventional protein secretion - new insights into the pathogenesis and therapeutic targets of human diseases. *J Cell Sci* 2018; **131** [PMID: 29941450 DOI: 10.1242/jcs.213686]

14 **Shi TT**, Zhao RX, Xin Z, Hou ZJ, Wang H, Xie RR, Li DM, Yang JK. Tear-derived exosomal biomarkers of Graves' ophthalmopathy. *Front Immunol* 2022; **13**: 1088606 [PMID: 36561758 DOI: 10.3389/fimmu.2022.1088606]

15 **Pegtel DM**, Gould SJ. Exosomes. *Annu Rev Biochem* 2019; **88**: 487-514 [PMID: 31220978 DOI: 10.1146/annurev-biochem-013118-111902]

16 **Kalluri R**, LeBleu VS. The biology, function, and biomedical applications of exosomes. *Science* 2020; **367** [PMID: 32029601 DOI: 10.1126/science.aau6977]

17 **Paktinat S**, Hashemi SM, Ghaffari Novin M, Mohammadi-Yeganeh S, Salehpour S, Karamian A, Nazarian H. Seminal exosomes induce interleukin-6 and interleukin-8 secretion by human endometrial stromal cells. *Eur J Obstet Gynecol Reprod Biol* 2019; **235**: 71-76 [PMID: 30807994 DOI: 10.1016/j.ejogrb.2019.02.010]

18 **Li Z**, Chen X, Tao J, Shi A, Zhang J, Yu P. Exosomes Regulate NLRP3 Inflammasome in Diseases. *Front Cell Dev Biol* 2021; **9**: 802509 [PMID: 35047512 DOI: 10.3389/fcell.2021.802509]

19 **Noonin C**, Thongboonkerd V. Exosome-inflammasome crosstalk and their roles in inflammatory responses. *Theranostics* 2021; **11**: 4436-4451 [PMID: 33754070 DOI: 10.7150/thno.54004]

20 **Xue Y**, Enosi Tuipulotu D, Tan WH, Kay C, Man SM. Emerging Activators and Regulators of Inflammasomes and Pyroptosis. *Trends Immunol* 2019; **40**: 1035-1052 [PMID: 31662274 DOI: 10.1016/j.it.2019.09.005]

21 **Agostini L**, Martinon F, Burns K, McDermott MF, Hawkins PN, Tschopp J. NALP3 forms an IL-1beta-processing inflammasome with increased activity in Muckle-Wells autoinflammatory disorder. *Immunity* 2004; **20**: 319-325 [PMID: 15030775 DOI: 10.1016/s1074-7613(04)00046-9]

22 **Seoane PI**, Lee B, Hoyle C, Yu S, Lopez-Castejon G, Lowe M, Brough D. The NLRP3-inflammasome as a sensor of organelle dysfunction. *J Cell Biol* 2020; **219** [PMID: 33044555 DOI: 10.1083/jcb.202006194]

23 **Malik A**, Kanneganti TD. Inflammasome activation and assembly at a glance. *J Cell Sci* 2017; **130**: 3955-3963 [PMID: 29196474 DOI: 10.1242/jcs.207365]

24 **Lu A**, Magupalli VG, Ruan J, Yin Q, Atianand MK, Vos MR, Schröder GF, Fitzgerald KA, Wu H, Egelman EH. Unified polymerization mechanism for the assembly of ASC-dependent inflammasomes. *Cell* 2014; **156**: 1193-1206 [PMID: 24630722 DOI: 10.1016/j.cell.2014.02.008]

25 **Liu L**, Wang D, Liu M, Yu H, Chen Q, Wu Y, Bao R, Zhang Y, Wang T. The development from hyperuricemia to gout: key mechanisms and natural products for treatment. *Acupunct Herbal Med* 2022; **2**: 25-32 [DOI: 10.1097/HM9.0000000000000016]

26 **Wang L**, Hauenstein AV. The NLRP3 inflammasome: Mechanism of action, role in disease and therapies. *Mol Aspects Med* 2020; **76**: 100889 [PMID: 32859386 DOI: 10.1016/j.mam.2020.100889]

27 **Bauernfeind FG**, Horvath G, Stutz A, Alnemri ES, MacDonald K, Speert D, Fernandes-Alnemri T, Wu J, Monks BG, Fitzgerald KA, Hornung V, Latz E. Cutting edge: NF-kappaB activating pattern recognition and cytokine receptors license NLRP3 inflammasome activation by regulating NLRP3 expression. *J Immunol* 2009; **183**: 787-791 [PMID: 19570822 DOI: 10.4049/jimmunol.0901363]

28 **Lin KM**, Hu W, Troutman TD, Jennings M, Brewer T, Li X, Nanda S, Cohen P, Thomas JA, Pasare C. IRAK-1 bypasses priming and directly links TLRs to rapid NLRP3 inflammasome activation. *Proc Natl Acad Sci U S A* 2014; **111**: 775-780 [PMID: 24379360 DOI: 10.1073/pnas.1320294111]

29 **Xing Y**, Yao X, Li H, Xue G, Guo Q, Yang G, An L, Zhang Y, Meng G. Cutting Edge: TRAF6 Mediates TLR/IL-1R Signaling-Induced Nontranscriptional Priming of the NLRP3 Inflammasome. *J Immunol* 2017; **199**: 1561-1566 [PMID: 28739881 DOI: 10.4049/jimmunol.1700175]

30 **Paik S**, Kim JK, Silwal P, Sasakawa C, Jo EK. An update on the regulatory mechanisms of NLRP3 inflammasome activation. *Cell Mol*

Immunol 2021; **18**: 1141-1160 [PMID: 33850310 DOI: 10.1038/s41423-021-00670-3]
31 **Miao EA**, Rajan JV, Aderem A. Caspase-1-induced pyroptotic cell death. *Immunol Rev* 2011; **243**: 206-214 [PMID: 21884178 DOI: 10.1111/j.1600-065X.2011.01044.x]
32 **Matikainen S**, Nyman TA, Cypryk W. Function and Regulation of Noncanonical Caspase-4/5/11 Inflammasome. *J Immunol* 2020; **204**: 3063-3069 [PMID: 32513874 DOI: 10.4049/jimmunol.2000373]
33 **Liu X**, Zhang Z, Ruan J, Pan Y, Magupalli VG, Wu H, Lieberman J. Inflammasome-activated gasdermin D causes pyroptosis by forming membrane pores. *Nature* 2016; **535**: 153-158 [PMID: 27383986 DOI: 10.1038/nature18629]
34 **Huang Y**, Xu W, Zhou R. NLRP3 inflammasome activation and cell death. *Cell Mol Immunol* 2021; **18**: 2114-2127 [PMID: 34321623 DOI: 10.1038/s41423-021-00740-6]
35 **Zanoni I**, Tan Y, Di Gioia M, Broggi A, Ruan J, Shi J, Donado CA, Shao F, Wu H, Springstead JR, Kagan JC. An endogenous caspase-11 ligand elicits interleukin-1 release from living dendritic cells. *Science* 2016; **352**: 1232-1236 [PMID: 27103670 DOI: 10.1126/science.aaf3036]
36 **Gaidt MM**, Ebert TS, Chauhan D, Schmidt T, Schmid-Burgk JL, Rapino F, Robertson AA, Cooper MA, Graf T, Hornung V. Human Monocytes Engage an Alternative Inflammasome Pathway. *Immunity* 2016; **44**: 833-846 [PMID: 27037191 DOI: 10.1016/j.immuni.2016.01.012]
37 **Hanaei S**, Sadr M, Rezaei A, Shahkarami S, Ebrahimi Daryani N, Bidoki AZ, Rezaei N. Association of NLRP3 single nucleotide polymorphisms with ulcerative colitis: A case-control study. *Clin Res Hepatol Gastroenterol* 2018; **42**: 269-275 [PMID: 29102545 DOI: 10.1016/j.clinre.2017.09.003]
38 **Zhang HX**, Wang ZT, Lu XX, Wang YG, Zhong J, Liu J. NLRP3 gene is associated with ulcerative colitis (UC), but not Crohn's disease (CD), in Chinese Han population. *Inflamm Res* 2014; **63**: 979-985 [PMID: 25297810 DOI: 10.1007/s00011-014-0774-9]
39 **Cao Y**, Oh J, Xue M, Huh WJ, Wang J, Gonzalez-Hernandez JA, Rice TA, Martin AL, Song D, Crawford JM, Herzon SB, Palm NW. Commensal microbiota from patients with inflammatory bowel disease produce genotoxic metabolites. *Science* 2022; **378**: eabm3233 [PMID: 36302024 DOI: 10.1126/science.abm3233]
40 **Ranson N**, Veldhuis M, Mitchell B, Fanning S, Cook AL, Kunde D, Eri R. NLRP3-Dependent and -Independent Processing of Interleukin (IL)-1β in Active Ulcerative Colitis. *Int J Mol Sci* 2018; **20** [PMID: 30583612 DOI: 10.3390/ijms20010057]
41 **Ma J**, Zhang J, Wang Y, Huang J, Yang X, Ma J, Liu Z, Wang F, Tang X. Modified Gegen Qinlian decoction ameliorates DSS-induced chronic colitis in mice by restoring the intestinal mucus barrier and inhibiting the activation of γδT17 cells. *Phytomedicine* 2023; **111**: 154660 [PMID: 36681051 DOI: 10.1016/j.phymed.2023.154660]
42 **Qu S**, Fan L, Qi Y, Xu C, Hu Y, Chen S, Liu W, Si J. Akkermansia muciniphila Alleviates Dextran Sulfate Sodium (DSS)-Induced Acute Colitis by NLRP3 Activation. *Microbiol Spectr* 2021; **9**: e0073021 [PMID: 34612661 DOI: 10.1128/Spectrum.00730-21]
43 **Zeng B**, Huang Y, Chen S, Xu R, Xu L, Qiu J, Shi F, Liu S, Zha Q, Ouyang D, He X. Dextran sodium sulfate potentiates NLRP3 inflammasome activation by modulating the KCa3.1 potassium channel in a mouse model of colitis. *Cell Mol Immunol* 2022; **19**: 925-943 [PMID: 35799057 DOI: 10.1038/s41423-022-00891-0]
44 **Bauer C**, Duewell P, Mayer C, Lehr HA, Fitzgerald KA, Dauer M, Tschopp J, Endres S, Latz E, Schnurr M. Colitis induced in mice with dextran sulfate sodium (DSS) is mediated by the NLRP3 inflammasome. *Gut* 2010; **59**: 1192-1199 [PMID: 20442201 DOI: 10.1136/gut.2009.197822]
45 **Bauer C**, Duewell P, Lehr HA, Endres S, Schnurr M. Protective and aggravating effects of Nlrp3 inflammasome activation in IBD models: influence of genetic and environmental factors. *Dig Dis* 2012; **30** Suppl 1: 82-90 [PMID: 23075874 DOI: 10.1159/000341681]
46 **Ning L**, Ye N, Ye B, Miao Z, Cao T, Lu W, Xu D, Tan C, Xu Y, Yan J. Qingre Xingyu recipe exerts inhibiting effects on ulcerative colitis development by inhibiting TNFα/NLRP3/Caspase-1/IL-1β pathway and macrophage M1 polarization. *Cell Death Discov* 2023; **9**: 84 [PMID: 36890151 DOI: 10.1038/s41420-023-01361-w]
47 **Perera AP**, Fernando R, Shinde T, Gundamaraju R, Southam B, Sohal SS, Robertson AAB, Schroder K, Kunde D, Eri R. MCC950, a specific small molecule inhibitor of NLRP3 inflammasome attenuates colonic inflammation in spontaneous colitis mice. *Sci Rep* 2018; **8**: 8618 [PMID: 29872077 DOI: 10.1038/s41598-018-26775-w]
48 **Du X**, Chen W, Wang Y, Chen C, Guo L, Ju R, Li J, Zhang D, Zhu L, Ye C. Therapeutic efficacy of carboxyamidotriazole on 2,4,6-trinitrobenzene sulfonic acid-induced colitis model is associated with the inhibition of NLRP3 inflammasome and NF-κB activation. *Int Immunopharmacol* 2017; **45**: 16-25 [PMID: 28152446 DOI: 10.1016/j.intimp.2017.01.015]
49 **Zhou W**, Liu X, Zhang X, Tang J, Li Z, Wang Q, Hu R. Oroxylin A inhibits colitis by inactivating NLRP3 inflammasome. *Oncotarget* 2017; **8**: 58903-58917 [PMID: 28938606 DOI: 10.18632/oncotarget.19440]
50 **Sun Y**, Zhao Y, Yao J, Zhao L, Wu Z, Wang Y, Pan D, Miao H, Guo Q, Lu N. Wogonoside protects against dextran sulfate sodium-induced experimental colitis in mice by inhibiting NF-κB and NLRP3 inflammasome activation. *Biochem Pharmacol* 2015; **94**: 142-154 [PMID: 25677765 DOI: 10.1016/j.bcp.2015.02.002]
51 **Huang J**, Zheng Y, Ma J, Lu M, Ma X, Wang F, Tang X. Exploration of the Potential Mechanisms of Wumei Pill for the Treatment of Ulcerative Colitis by Network Pharmacology. *Gastroenterol Res Pract* 2021; **2021**: 4227668 [PMID: 34970312 DOI: 10.1155/2021/4227668]
52 **Tucci M**, Mannavola F, Passarelli A, Stucci LS, Cives M, Silvestris F. Exosomes in melanoma: a role in tumor progression, metastasis and impaired immune system activity. *Oncotarget* 2018; **9**: 20826-20837 [PMID: 29755693 DOI: 10.18632/oncotarget.24846]
53 **Ventimiglia LN**, Fernández-Martín L, Martínez-Alonso E, Antón OM, Guerra M, Martínez-Menárguez JA, Andrés G, Alonso MA. Cutting Edge: Regulation of Exosome Secretion by the Integral MAL Protein in T Cells. *J Immunol* 2015; **195**: 810-814 [PMID: 26109641 DOI: 10.4049/jimmunol.1500891]
54 **Xu Z**, Zeng S, Gong Z, Yan Y. Exosome-based immunotherapy: a promising approach for cancer treatment. *Mol Cancer* 2020; **19**: 160 [PMID: 33183286 DOI: 10.1186/s12943-020-01278-3]
55 **Miao C**, Wang X, Zhou W, Huang J. The emerging roles of exosomes in autoimmune diseases, with special emphasis on microRNAs in exosomes. *Pharmacol Res* 2021; **169**: 105680 [PMID: 34010670 DOI: 10.1016/j.phrs.2021.105680]
56 **Barile L**, Moccetti T, Marbán E, Vassalli G. Roles of exosomes in cardioprotection. *Eur Heart J* 2017; **38**: 1372-1379 [PMID: 27443883 DOI: 10.1093/eurheartj/ehw304]
57 **Xu M**, Feng T, Liu B, Qiu F, Xu Y, Zhao Y, Zheng Y. Engineered exosomes: desirable target-tracking characteristics for cerebrovascular and neurodegenerative disease therapies. *Theranostics* 2021; **11**: 8926-8944 [PMID: 34522219 DOI: 10.7150/thno.62330]
58 **Lou G**, Chen Z, Zheng M, Liu Y. Mesenchymal stem cell-derived exosomes as a new therapeutic strategy for liver diseases. *Exp Mol Med* 2017; **49**: e346 [PMID: 28620221 DOI: 10.1038/emm.2017.63]
59 **Zhu L**, Li J, Gong Y, Wu Q, Tan S, Sun D, Xu X, Zuo Y, Zhao Y, Wei YQ, Wei XW, Peng Y. Exosomal tRNA-derived small RNA as a

promising biomarker for cancer diagnosis. *Mol Cancer* 2019; **18**: 74 [PMID: 30940133 DOI: 10.1186/s12943-019-1000-8]

60 **Soares Martins T**, Trindade D, Vaz M, Campelo I, Almeida M, Trigo G, da Cruz E Silva OAB, Henriques AG. Diagnostic and therapeutic potential of exosomes in Alzheimer's disease. *J Neurochem* 2021; **156**: 162-181 [PMID: 32618370 DOI: 10.1111/jnc.15112]

61 **Han Z**, Peng X, Yang Y, Yi J, Zhao D, Bao Q, Long S, Yu SX, Xu XX, Liu B, Liu YJ, Shen Y, Qiao L. Integrated microfluidic-SERS for exosome biomarker profiling and osteosarcoma diagnosis. *Biosens Bioelectron* 2022; **217**: 114709 [PMID: 36115123 DOI: 10.1016/j.bios.2022.114709]

62 **He C**, Zheng S, Luo Y, Wang B. Exosome Theranostics: Biology and Translational Medicine. *Theranostics* 2018; **8**: 237-255 [PMID: 29290805 DOI: 10.7150/thno.21945]

63 **Duya P**, Chen Y, Bai L, Li Z, Li J, Chai R, Bian Y, Zhao S. Nature products of traditional Chinese medicine provide new ideas in γδT cell for tumor immunotherapy. *Acupunct Herbal Med* 2022; **2**: 78-83 [DOI: 10.1097/HM9.0000000000000032]

64 **Li Q**, Wang H, Peng H, Huyan T, Cacalano NA. Exosomes: Versatile Nano Mediators of Immune Regulation. *Cancers (Basel)* 2019; **11** [PMID: 31615107 DOI: 10.3390/cancers11101557]

65 **Colletti M**, Galardi A, De Santis M, Guidelli GM, Di Giannatale A, Di Luigi L, Antinozzi C. Exosomes in Systemic Sclerosis: Messengers Between Immune, Vascular and Fibrotic Components? *Int J Mol Sci* 2019; **20** [PMID: 31487964 DOI: 10.3390/ijms20184337]

66 **Ocansey DKW**, Zhang L, Wang Y, Yan Y, Qian H, Zhang X, Xu W, Mao F. Exosome-mediated effects and applications in inflammatory bowel disease. *Biol Rev Camb Philos Soc* 2020; **95**: 1287-1307 [PMID: 32410383 DOI: 10.1111/brv.12608]

67 **Zhang H**, Wang L, Li C, Yu Y, Yi Y, Wang J, Chen D. Exosome-Induced Regulation in Inflammatory Bowel Disease. *Front Immunol* 2019; **10**: 1464 [PMID: 31316512 DOI: 10.3389/fimmu.2019.01464]

68 **Zheng X**, Chen F, Zhang Q, Liu Y, You P, Sun S, Lin J, Chen N. Salivary exosomal PSMA7: a promising biomarker of inflammatory bowel disease. *Protein Cell* 2017; **8**: 686-695 [PMID: 28523434 DOI: 10.1007/s13238-017-0413-7]

69 **Lian H**, Zhong XS, Xiao Y, Sun Z, Shen Y, Zhao K, Ma X, Li Y, Niu Q, Liu M, Powell DW, Liu C, Li Q. Exosomal miR-29b of Gut Origin in Patients With Ulcerative Colitis Suppresses Heart Brain-Derived Neurotrophic Factor. *Front Mol Biosci* 2022; **9**: 759689 [PMID: 35274002 DOI: 10.3389/fmolb.2022.759689]

70 **Xu AT**, Lu JT, Ran ZH, Zheng Q. Exosome in intestinal mucosal immunity. *J Gastroenterol Hepatol* 2016; **31**: 1694-1699 [PMID: 27061439 DOI: 10.1111/jgh.13413]

71 **Cai X**, Zhang ZY, Yuan JT, Ocansey DKW, Tu Q, Zhang X, Qian H, Xu WR, Qiu W, Mao F. hucMSC-derived exosomes attenuate colitis by regulating macrophage pyroptosis *via* the miR-378a-5p/NLRP3 axis. *Stem Cell Res Ther* 2021; **12**: 416 [PMID: 34294138 DOI: 10.1186/s13287-021-02492-6]

72 **Wang D**, Xue H, Tan J, Liu P, Qiao C, Pang C, Zhang L. Bone marrow mesenchymal stem cells-derived exosomes containing miR-539-5p inhibit pyroptosis through NLRP3/caspase-1 signalling to alleviate inflammatory bowel disease. *Inflamm Res* 2022; **71**: 833-846 [PMID: 35637388 DOI: 10.1007/s00011-022-01577-z]

73 **Chang Y**, Zhang Y, Jiang Y, Zhao L, Lv C, Huang Q, Guan J, Jin S. From Hair to Colon: Hair Follicle-Derived MSCs Alleviate Pyroptosis in DSS-Induced Ulcerative Colitis by Releasing Exosomes in a Paracrine Manner. *Oxid Med Cell Longev* 2022; **2022**: 9097530 [PMID: 36160717 DOI: 10.1155/2022/9097530]

74 **Xu Y**, Tang X, Fang A, Yan J, Kofi Wiredu Ocansey D, Zhang X, Mao F. HucMSC-Ex carrying miR-203a-3p.2 ameliorates colitis through the suppression of caspase11/4-induced macrophage pyroptosis. *Int Immunopharmacol* 2022; **110**: 108925 [PMID: 35724605 DOI: 10.1016/j.intimp.2022.108925]

75 **Heidari N**, Abbasi-Kenarsari H, Namaki S, Baghaei K, Zali MR, Ghaffari Khaligh S, Hashemi SM. Adipose-derived mesenchymal stem cell-secreted exosome alleviates dextran sulfate sodium-induced acute colitis by Treg cell induction and inflammatory cytokine reduction. *J Cell Physiol* 2021; **236**: 5906-5920 [PMID: 33728664 DOI: 10.1002/jcp.30275]

76 **Ocansey DKW**, Zhang Z, Xu X, Liu L, Amoah S, Chen X, Wang B, Zhang X, Mao F. Mesenchymal stem cell-derived exosome mitigates colitis *via* the modulation of the gut metagenomics-metabolomics-farnesoid X receptor axis. *Biomater Sci* 2022; **10**: 4822-4836 [PMID: 35858469 DOI: 10.1039/d2bm00559j]

77 **Liu H**, Liang Z, Wang F, Zhou C, Zheng X, Hu T, He X, Wu X, Lan P. Exosomes from mesenchymal stromal cells reduce murine colonic inflammation *via* a macrophage-dependent mechanism. *JCI Insight* 2019; **4** [PMID: 31689240 DOI: 10.1172/jci.insight.131273]

78 **Wang J**, Pei B, Yan J, Xu X, Fang AN, Ocansey DKW, Zhang X, Qian H, Xu W, Mao F. hucMSC-Derived Exosomes Alleviate the Deterioration of Colitis *via* the miR-146a/SUMO1 Axis. *Mol Pharm* 2022; **19**: 484-493 [PMID: 35084199 DOI: 10.1021/acs.molpharmaceut.1c00450]

79 **Qian W**, Huang L, Xu Y, Lu W, Wen W, Guo Z, Zhu W, Li Y. Hypoxic ASCs-derived Exosomes Attenuate Colitis by Regulating Macrophage Polarization *via* miR-216a-5p/HMGB1 Axis. *Inflamm Bowel Dis* 2023; **29**: 602-619 [PMID: 36287066 DOI: 10.1093/ibd/izac225]

80 **Heidari N**, Abbasi-Kenarsari H, Namaki S, Baghaei K, Zali MR, Mirsanei Z, Hashemi SM. Regulation of the Th17/Treg balance by human umbilical cord mesenchymal stem cell-derived exosomes protects against acute experimental colitis. *Exp Cell Res* 2022; **419**: 113296 [PMID: 35917844 DOI: 10.1016/j.yexcr.2022.113296]

81 **Yang S**, Liang X, Song J, Li C, Liu A, Luo Y, Ma H, Tan Y, Zhang X. A novel therapeutic approach for inflammatory bowel disease by exosomes derived from human umbilical cord mesenchymal stem cells to repair intestinal barrier *via* TSG-6. *Stem Cell Res Ther* 2021; **12**: 315 [PMID: 34051868 DOI: 10.1186/s13287-021-02404-8]

82 **Yang R**, Huang H, Cui S, Zhou Y, Zhang T. IFN-γ promoted exosomes from mesenchymal stem cells to attenuate colitis *via* miR-125a and miR-125b. *Cell Death Dis* 2020; **11**: 603 [PMID: 32733020 DOI: 10.1038/s41419-020-02788-0]

83 **Zhu F**, Wei C, Wu H, Shuai B, Yu T, Gao F, Yuan Y, Zuo D, Liu X, Zhang L, Fan H. Hypoxic mesenchymal stem cell-derived exosomes alleviate ulcerative colitis injury by limiting intestinal epithelial cells reactive oxygen species accumulation and DNA damage through HIF-1α. *Int Immunopharmacol* 2022; **113**: 109426 [PMID: 36461588 DOI: 10.1016/j.intimp.2022.109426]

84 **Gu L**, Ren F, Fang X, Yuan L, Liu G, Wang S. Exosomal MicroRNA-181a Derived From Mesenchymal Stem Cells Improves Gut Microbiota Composition, Barrier Function, and Inflammatory Status in an Experimental Colitis Model. *Front Med (Lausanne)* 2021; **8**: 660614 [PMID: 34249964 DOI: 10.3389/fmed.2021.660614]

85 **Ma ZJ**, Wang YH, Li ZG, Wang Y, Li BY, Kang HY, Wu XY. Immunosuppressive Effect of Exosomes from Mesenchymal Stromal Cells in Defined Medium on Experimental Colitis. *Int J Stem Cells* 2019; **12**: 440-448 [PMID: 31242720 DOI: 10.15283/ijsc18139]

86 **Tian J**, Zhu Q, Zhang Y, Bian Q, Hong Y, Shen Z, Xu H, Rui K, Yin K, Wang S. Olfactory Ecto-Mesenchymal Stem Cell-Derived Exosomes Ameliorate Experimental Colitis *via* Modulating Th1/Th17 and Treg Cell Responses. *Front Immunol* 2020; **11**: 598322 [PMID: 33362781

DOI: 10.3389/fimmu.2020.598322]

87 **Yang J**, Liu XX, Fan H, Tang Q, Shou ZX, Zuo DM, Zou Z, Xu M, Chen QY, Peng Y, Deng SJ, Liu YJ. Extracellular Vesicles Derived from Bone Marrow Mesenchymal Stem Cells Protect against Experimental Colitis *via* Attenuating Colon Inflammation, Oxidative Stress and Apoptosis. *PLoS One* 2015; **10**: e0140551 [PMID: 26469068 DOI: 10.1371/journal.pone.0140551]

88 **Barnhoorn MC**, Plug L, Jonge ESMM, Molenkamp D, Bos E, Schoonderwoerd MJA, Corver WE, van der Meulen-de Jong AE, Verspaget HW, Hawinkels LJAC. Mesenchymal Stromal Cell-Derived Exosomes Contribute to Epithelial Regeneration in Experimental Inflammatory Bowel Disease. *Cell Mol Gastroenterol Hepatol* 2020; **9**: 715-717.e8 [PMID: 31982571 DOI: 10.1016/j.jcmgh.2020.01.007]

89 **Mao F**, Wu Y, Tang X, Kang J, Zhang B, Yan Y, Qian H, Zhang X, Xu W. Exosomes Derived from Human Umbilical Cord Mesenchymal Stem Cells Relieve Inflammatory Bowel Disease in Mice. *Biomed Res Int* 2017; **2017**: 5356760 [PMID: 28589143 DOI: 10.1155/2017/5356760]

90 **Zhu Y**, Qin H, Sun C, Shao B, Li G, Qin Y, Kong D, Ren S, Wang H, Wang Z, Zhang J. Endometrial Regenerative Cell-Derived Exosomes Attenuate Experimental Colitis through Downregulation of Intestine Ferroptosis. *Stem Cells Int* 2022; **2022**: 3014123 [PMID: 36045952 DOI: 10.1155/2022/3014123]

91 **Chang CL**, Chen CH, Chiang JY, Sun CK, Chen YL, Chen KH, Sung PH, Huang TH, Li YC, Chen HH, Yip HK. Synergistic effect of combined melatonin and adipose-derived mesenchymal stem cell (ADMSC)-derived exosomes on amelioration of dextran sulfate sodium (DSS)-induced acute colitis. *Am J Transl Res* 2019; **11**: 2706-2724 [PMID: 31217848]

92 **Bauer KM**, Nelson MC, Tang WW, Chiaro TR, Brown DG, Ghazaryan A, Lee SH, Weis AM, Hill JH, Klag KA, Tran VB, Thompson JW, Ramstead AG, Monts JK, Marvin JE, Alexander M, Voth WP, Stephens WZ, Ward DM, Petrey AC, Round JL, O'Connell RM. CD11c+ myeloid cell exosomes reduce intestinal inflammation during colitis. *JCI Insight* 2022; **7** [PMID: 36214220 DOI: 10.1172/jci.insight.159469]

93 **Wang L**, Yu Z, Wan S, Wu F, Chen W, Zhang B, Lin D, Liu J, Xie H, Sun X, Wu Z. Exosomes Derived from Dendritic Cells Treated with Schistosoma japonicum Soluble Egg Antigen Attenuate DSS-Induced Colitis. *Front Pharmacol* 2017; **8**: 651 [PMID: 28959207 DOI: 10.3389/fphar.2017.00651]

94 **Yang X**, Meng S, Jiang H, Chen T, Wu W. Exosomes derived from interleukin-10-treated dendritic cells can inhibit trinitrobenzene sulfonic acid-induced rat colitis. *Scand J Gastroenterol* 2010; **45**: 1168-1177 [PMID: 20469967 DOI: 10.3109/00365521.2010.490596]

95 **Rao Q**, Ma G, Li M, Wu H, Zhang Y, Zhang C, Ma Z, Huang L. Targeted delivery of triptolide by dendritic cell-derived exosomes for colitis and rheumatoid arthritis therapy in murine models. *Br J Pharmacol* 2023; **180**: 330-346 [PMID: 36156794 DOI: 10.1111/bph.15958]

96 **Deng F**, Yan J, Lu J, Luo M, Xia P, Liu S, Wang X, Zhi F, Liu D. M2 Macrophage-Derived Exosomal miR-590-3p Attenuates DSS-Induced Mucosal Damage and Promotes Epithelial Repair *via* the LATS1/YAP/ β-Catenin Signalling Axis. *J Crohns Colitis* 2021; **15**: 665-677 [PMID: 33075119 DOI: 10.1093/ecco-jcc/jjaa214]

97 **Lu J**, Liu D, Tan Y, Deng F, Li R. M1 Macrophage exosomes MiR-21a-5p aggravates inflammatory bowel disease through decreasing E-cadherin and subsequent ILC2 activation. *J Cell Mol Med* 2021; **25**: 3041-3050 [PMID: 33569850 DOI: 10.1111/jcmm.16348]

98 **Yang C**, Zhang M, Sung J, Wang L, Jung Y, Merlin D. Autologous Exosome Transfer: A New Personalised Treatment Concept to Prevent Colitis in a Murine Model. *J Crohns Colitis* 2020; **14**: 841-855 [PMID: 31710674 DOI: 10.1093/ecco-jcc/jjz184]

99 **Wei M**, Gao X, Liu L, Li Z, Wan Z, Dong Y, Chen X, Niu Y, Zhang J, Yang G. Visceral Adipose Tissue Derived Exosomes Exacerbate Colitis Severity *via* Pro-inflammatory MiRNAs in High Fat Diet Fed Mice. *ACS Nano* 2020; **14**: 5099-5110 [PMID: 32275391 DOI: 10.1021/acsnano.0c01860]

100 **Chen Y**, Huang J, Li H, Li P, Xu C. Serum exosomes derived from Hp-positive gastritis patients inhibit MCP-1 and MIP-1α expression *via* NLRP12-Notch signaling pathway in intestinal epithelial cells and improve DSS-induced colitis in mice. *Int Immunopharmacol* 2020; **88**: 107012 [PMID: 33182033 DOI: 10.1016/j.intimp.2020.107012]

101 **Wong WY**, Lee MM, Chan BD, Kam RK, Zhang G, Lu AP, Tai WC. Proteomic profiling of dextran sulfate sodium induced acute ulcerative colitis mice serum exosomes and their immunomodulatory impact on macrophages. *Proteomics* 2016; **16**: 1131-1145 [PMID: 26806198 DOI: 10.1002/pmic.201500174]

102 **Guo Y**, Xu C, Gong R, Hu T, Zhang X, Xie X, Chi J, Li H, Xia X, Liu X. Exosomal CagA from Helicobacter pylori aggravates intestinal epithelium barrier dysfunction in chronic colitis by facilitating Claudin-2 expression. *Gut Pathog* 2022; **14**: 13 [PMID: 35331316 DOI: 10.1186/s13099-022-00486-0]

103 **Stremmel W**, Weiskirchen R, Melnik BC. Milk Exosomes Prevent Intestinal Inflammation in a Genetic Mouse Model of Ulcerative Colitis: A Pilot Experiment. *Inflamm Intest Dis* 2020; **5**: 117-123 [PMID: 32999884 DOI: 10.1159/000507626]

104 **Reif S**, Elbaum-Shiff Y, Koroukhov N, Shilo I, Musseri M, Golan-Gerstl R. Cow and Human Milk-Derived Exosomes Ameliorate Colitis in DSS Murine Model. *Nutrients* 2020; **12** [PMID: 32858892 DOI: 10.3390/nu12092589]

105 **Han G**, Cho H, Kim H, Jang Y, Jang H, Kim DE, Kim ES, Kim EH, Hwang KY, Kim K, Yang Y, Kim SH. Bovine colostrum derived-exosomes prevent dextran sulfate sodium-induced intestinal colitis *via* suppression of inflammation and oxidative stress. *Biomater Sci* 2022; **10**: 2076-2087 [PMID: 35315847 DOI: 10.1039/d1bm01797g]

106 **Liu Y**, Lou G, Li A, Zhang T, Qi J, Ye D, Zheng M, Chen Z. AMSC-derived exosomes alleviate lipopolysaccharide/d-galactosamine-induced acute liver failure by miR-17-mediated reduction of TXNIP/NLRP3 inflammasome activation in macrophages. *EBioMedicine* 2018; **36**: 140-150 [PMID: 30197023 DOI: 10.1016/j.ebiom.2018.08.054]

107 **Xia C**, Zeng Z, Fang B, Tao M, Gu C, Zheng L, Wang Y, Shi Y, Fang C, Mei S, Chen Q, Zhao J, Lin X, Fan S, Jin Y, Chen P. Mesenchymal stem cell-derived exosomes ameliorate intervertebral disc degeneration *via* anti-oxidant and anti-inflammatory effects. *Free Radic Biol Med* 2019; **143**: 1-15 [PMID: 31351174 DOI: 10.1016/j.freeradbiomed.2019.07.026]

108 **Tavakoli Dargani Z**, Singla DK. Embryonic stem cell-derived exosomes inhibit doxorubicin-induced TLR4-NLRP3-mediated cell death-pyroptosis. *Am J Physiol Heart Circ Physiol* 2019; **317**: H460-H471 [PMID: 31172809 DOI: 10.1152/ajpheart.00056.2019]

109 **Wang K**, Ru J, Zhang H, Chen J, Lin X, Lin Z, Wen M, Huang L, Ni H, Zhuge Q, Yang S. Melatonin Enhances the Therapeutic Effect of Plasma Exosomes Against Cerebral Ischemia-Induced Pyroptosis Through the TLR4/NF-κB Pathway. *Front Neurosci* 2020; **14**: 848 [PMID: 33013286 DOI: 10.3389/fnins.2020.00848]

110 **Zeng Q**, Zhou Y, Liang D, He H, Liu X, Zhu R, Zhang M, Luo X, Wang Y, Huang G. Exosomes Secreted From Bone Marrow Mesenchymal Stem Cells Attenuate Oxygen-Glucose Deprivation/Reoxygenation-Induced Pyroptosis in PC12 Cells by Promoting AMPK-Dependent Autophagic Flux. *Front Cell Neurosci* 2020; **14**: 182 [PMID: 32765221 DOI: 10.3389/fncel.2020.00182]

111 **Yan B**, Zhang Y, Liang C, Liu B, Ding F, Wang Y, Zhu B, Zhao R, Yu XY, Li Y. Stem cell-derived exosomes prevent pyroptosis and repair ischemic muscle injury through a novel exosome/circHIPK3/ FOXO3a pathway. *Theranostics* 2020; **10**: 6728-6742 [PMID: 32550900 DOI: 10.7150/thno.42259]

112 **Sun L**, Zhu M, Feng W, Lin Y, Yin J, Jin J, Wang Y. Exosomal miRNA Let-7 from Menstrual Blood-Derived Endometrial Stem Cells Alleviates Pulmonary Fibrosis through Regulating Mitochondrial DNA Damage. *Oxid Med Cell Longev* 2019; **2019**: 4506303 [PMID: 31949877 DOI: 10.1155/2019/4506303]

113 **Li Q**, Wang Z, Xing H, Wang Y, Guo Y. Exosomes derived from miR-188-3p-modified adipose-derived mesenchymal stem cells protect Parkinson's disease. *Mol Ther Nucleic Acids* 2021; **23**: 1334-1344 [PMID: 33717653 DOI: 10.1016/j.omtn.2021.01.022]

114 **Wang Y**, Xie W, Liu B, Huang H, Luo W, Zhang Y, Pan X, Yu XY, Shen Z, Li Y. Stem cell-derived exosomes repair ischemic muscle injury by inhibiting the tumor suppressor Rb1-mediated NLRP3 inflammasome pathway. *Signal Transduct Target Ther* 2021; **6**: 121 [PMID: 33727530 DOI: 10.1038/s41392-021-00520-8]

115 **Singla DK**, Johnson TA, Tavakoli Dargani Z. Exosome Treatment Enhances Anti-Inflammatory M2 Macrophages and Reduces Inflammation-Induced Pyroptosis in Doxorubicin-Induced Cardiomyopathy. *Cells* 2019; **8** [PMID: 31600901 DOI: 10.3390/cells8101224]

116 **Cheng HY**, Hsieh CH, Lin PH, Chen YT, Hsu DS, Tai SK, Chu PY, Yang MH. Snail-regulated exosomal microRNA-21 suppresses NLRP3 inflammasome activity to enhance cisplatin resistance. *J Immunother Cancer* 2022; **10** [PMID: 36002186 DOI: 10.1136/jitc-2022-004832]

117 **Zhao Y**, Chen Y, Wang Z, Xu C, Qiao S, Liu T, Qi K, Tong D, Li C. Bone Marrow Mesenchymal Stem Cell Exosome Attenuates Inflammasome-Related Pyroptosis *via* Delivering circ_003564 to Improve the Recovery of Spinal Cord Injury. *Mol Neurobiol* 2022; **59**: 6771-6789 [PMID: 36038697 DOI: 10.1007/s12035-022-03006-y]

118 **Liang C**, Liu Y, Xu H, Huang J, Shen Y, Chen F, Luo M. Exosomes of Human Umbilical Cord MSCs Protect Against Hypoxia/Reoxygenation-Induced Pyroptosis of Cardiomyocytes *via* the miRNA-100-5p/FOXO3/NLRP3 Pathway. *Front Bioeng Biotechnol* 2020; **8**: 615850 [PMID: 33520966 DOI: 10.3389/fbioe.2020.615850]

119 **Hu J**, Jiang Y, Wu X, Wu Z, Qin J, Zhao Z, Li B, Xu Z, Lu X, Wang X, Liu X. Exosomal miR-17-5p from adipose-derived mesenchymal stem cells inhibits abdominal aortic aneurysm by suppressing TXNIP-NLRP3 inflammasome. *Stem Cell Res Ther* 2022; **13**: 349 [PMID: 35883151 DOI: 10.1186/s13287-022-03037-1]

120 **Ye L**, Guo H, Wang Y, Peng Y, Zhang Y, Li S, Yang M, Wang L. Exosomal circEhmt1 Released from Hypoxia-Pretreated Pericytes Regulates High Glucose-Induced Microvascular Dysfunction *via* the NFIA/NLRP3 Pathway. *Oxid Med Cell Longev* 2021; **2021**: 8833098 [PMID: 33815662 DOI: 10.1155/2021/8833098]

121 **Haneklaus M**, Gerlic M, Kurowska-Stolarska M, Rainey AA, Pich D, McInnes IB, Hammerschmidt W, O'Neill LA, Masters SL. Cutting edge: miR-223 and EBV miR-BART15 regulate the NLRP3 inflammasome and IL-1β production. *J Immunol* 2012; **189**: 3795-3799 [PMID: 22984081 DOI: 10.4049/jimmunol.1200312]

122 **Zhang L**, Wang Q, Su H, Cheng J. Exosomes from adipose derived mesenchymal stem cells alleviate diabetic osteoporosis in rats through suppressing NLRP3 inflammasome activation in osteoclasts. *J Biosci Bioeng* 2021; **131**: 671-678 [PMID: 33849774 DOI: 10.1016/j.jbiosc.2021.02.007]

123 **Jiang L**, Zhang S, Hu H, Yang J, Wang X, Ma Y, Jiang J, Wang J, Zhong L, Chen M, Wang H, Hou Y, Zhu R, Zhang Q. Exosomes derived from human umbilical cord mesenchymal stem cells alleviate acute liver failure by reducing the activity of the NLRP3 inflammasome in macrophages. *Biochem Biophys Res Commun* 2019; **508**: 735-741 [PMID: 30528233 DOI: 10.1016/j.bbrc.2018.11.189]

124 **Kang X**, Jiang L, Chen X, Wang X, Gu S, Wang J, Zhu Y, Xie X, Xiao H, Zhang J. Exosomes derived from hypoxic bone marrow mesenchymal stem cells rescue OGD-induced injury in neural cells by suppressing NLRP3 inflammasome-mediated pyroptosis. *Exp Cell Res* 2021; **405**: 112635 [PMID: 34051241 DOI: 10.1016/j.yexcr.2021.112635]

125 **Hua T**, Yang M, Song H, Kong E, Deng M, Li Y, Li J, Liu Z, Fu H, Wang Y, Yuan H. Huc-MSCs-derived exosomes attenuate inflammatory pain by regulating microglia pyroptosis and autophagy *via* the miR-146a-5p/TRAF6 axis. *J Nanobiotechnology* 2022; **20**: 324 [PMID: 35836229 DOI: 10.1186/s12951-022-01522-6]

126 **Hu H**, Qi L, Ren C, Yan S. M2 Macrophage-Derived Exosomes Regulate Myocardial Ischemia-Reperfusion And Pyroptosis Via ROS/NLRP3 Pathway. *Heart Surg Forum* 2022; **25**: E698-E708 [PMID: 36317904 DOI: 10.1532/hsf.4919]

127 **Dessouki FBA**, Kukreja RC, Singla DK. Stem Cell-Derived Exosomes Ameliorate Doxorubicin-Induced Muscle Toxicity through Counteracting Pyroptosis. *Pharmaceuticals (Basel)* 2020; **13** [PMID: 33316945 DOI: 10.3390/ph13120450]

128 **Bottino LZMF**, Rodrigues-Junior DM, Farias IS, Branco LM, Iyer NG, de Albuquerque GE, Vettore AL, Bortoluci KR. Extracellular vesicles derived from head and neck squamous cells carcinoma inhibit NLRP3 inflammasomes. *Curr Res Immunol* 2021; **2**: 175-183 [PMID: 35492395 DOI: 10.1016/j.crimmu.2021.10.005]

129 **Hu LT**, Wang BY, Fan YH, He ZY, Zheng WX. Exosomal miR-23b from bone marrow mesenchymal stem cells alleviates oxidative stress and pyroptosis after intracerebral hemorrhage. *Neural Regen Res* 2023; **18**: 560-567 [PMID: 36018178 DOI: 10.4103/1673-5374.346551]

130 **Sun Z**, Gao Z, Wu J, Zheng X, Jing S, Wang W. MSC-Derived Extracellular Vesicles Activate Mitophagy to Alleviate Renal Ischemia/Reperfusion Injury *via* the miR-223-3p/NLRP3 Axis. *Stem Cells Int* 2022; **2022**: 6852661 [PMID: 35646124 DOI: 10.1155/2022/6852661]

131 **Yang T**, Li W, Peng A, Wang Q. Exosomes derived from heat shock preconditioned bone marrow mesenchymal stem cells alleviate cisplatin-induced ototoxicity in mice. *J Biol Eng* 2022; **16**: 24 [PMID: 36175910 DOI: 10.1186/s13036-022-00304-w]

132 **Zhang W**, Wang Y, Kong Y. Exosomes Derived From Mesenchymal Stem Cells Modulate miR-126 to Ameliorate Hyperglycemia-Induced Retinal Inflammation Via Targeting HMGB1. *Invest Ophthalmol Vis Sci* 2019; **60**: 294-303 [PMID: 30657854 DOI: 10.1167/iovs.18-25617]

133 **Qian J**, Wang X, Su G, Shu X, Huang Z, Jiang H, Zhu Q. Platelet-rich plasma-derived exosomes attenuate intervertebral disc degeneration by promoting NLRP3 autophagic degradation in macrophages. *Int Immunopharmacol* 2022; **110**: 108962 [PMID: 35753124 DOI: 10.1016/j.intimp.2022.108962]

134 **Huang Y**, Lu D, Ma W, Liu J, Ning Q, Tang F, Li L. miR-223 in exosomes from bone marrow mesenchymal stem cells ameliorates rheumatoid arthritis *via* downregulation of NLRP3 expression in macrophages. *Mol Immunol* 2022; **143**: 68-76 [PMID: 35042119 DOI: 10.1016/j.molimm.2022.01.002]

135 **Cui B**, Sun J, Li SP, Zhou GP, Chen XJ, Sun LY, Wei L, Zhu ZJ. CD80(+) dendritic cell derived exosomes inhibit CD8(+) T cells through down-regulating NLRP3 expression after liver transplantation. *Int Immunopharmacol* 2022; **109**: 108787 [PMID: 35490667 DOI: 10.1016/j.intimp.2022.108787]

136 **Dai Y**, Wang S, Chang S, Ren D, Shali S, Li C, Yang H, Huang Z, Ge J. M2 macrophage-derived exosomes carry microRNA-148a to alleviate myocardial ischemia/reperfusion injury *via* inhibiting TXNIP and the TLR4/NF-κB/NLRP3 inflammasome signaling pathway. *J Mol Cell Cardiol* 2020; **142**: 65-79 [PMID: 32087217 DOI: 10.1016/j.yjmcc.2020.02.007]

137 **Xia Y**, Zhou K, Sun M, Shu R, Qian J, Xie Y. The miR-223-3p Regulates Pyroptosis Through NLRP3-Caspase 1-GSDMD Signal Axis in Periodontitis. *Inflammation* 2021; **44**: 2531-2542 [PMID: 34637033 DOI: 10.1007/s10753-021-01522-y]

138 **Jiao Y**, Zhang T, Zhang C, Ji H, Tong X, Xia R, Wang W, Ma Z, Shi X. Exosomal miR-30d-5p of neutrophils induces M1 macrophage

polarization and primes macrophage pyroptosis in sepsis-related acute lung injury. *Crit Care* 2021; **25**: 356 [PMID: 34641966 DOI: 10.1186/s13054-021-03775-3]

139 **Liang M**, Chen X, Wang L, Qin L, Wang H, Sun Z, Zhao W, Geng B. Cancer-derived exosomal TRIM59 regulates macrophage NLRP3 inflammasome activation to promote lung cancer progression. *J Exp Clin Cancer Res* 2020; **39**: 176 [PMID: 32867817 DOI: 10.1186/s13046-020-01688-7]

140 **Zhang W**, Ma Y, Zhang Y, Yang J, He G, Chen S. Photo-Oxidative Blue-Light Stimulation in Retinal Pigment Epithelium Cells Promotes Exosome Secretion and Increases the Activity of the NLRP3 Inflammasome. *Curr Eye Res* 2019; **44**: 67-75 [PMID: 30198786 DOI: 10.1080/02713683.2018.1518458]

141 **Zhang L**, Liu H, Jia L, Lyu J, Sun Y, Yu H, Li H, Liu W, Weng Y, Yu W. Exosomes Mediate Hippocampal and Cortical Neuronal Injury Induced by Hepatic Ischemia-Reperfusion Injury through Activating Pyroptosis in Rats. *Oxid Med Cell Longev* 2019; **2019**: 3753485 [PMID: 31814872 DOI: 10.1155/2019/3753485]

142 **Wu XB**, Sun HY, Luo ZL, Cheng L, Duan XM, Ren JD. Plasma-derived exosomes contribute to pancreatitis-associated lung injury by triggering NLRP3-dependent pyroptosis in alveolar macrophages. *Biochim Biophys Acta Mol Basis Dis* 2020; **1866**: 165685 [PMID: 31953217 DOI: 10.1016/j.bbadis.2020.165685]

143 **Sur S**, Steele R, Isbell TS, Ray R, Ray RB. Circulatory Exosomes from COVID-19 Patients Trigger NLRP3 Inflammasome in Endothelial Cells. *mBio* 2022; **13**: e0095122 [PMID: 35587188 DOI: 10.1128/mbio.00951-22]

144 **Hou CC**, Ma HF, Ye JF, Luo D, Bao HF, Guan JL. Plasma exosomes derived from patients with intestinal Behçet's syndrome induce intestinal epithelial cell pyroptosis. *Clin Rheumatol* 2021; **40**: 4143-4155 [PMID: 33954847 DOI: 10.1007/s10067-021-05755-y]

145 **Li H**, Lu R, Pang Y, Li J, Cao Y, Fu H, Fang G, Chen Q, Liu B, Wu J, Zhou Y, Zhou J. Zhen-Wu-Tang Protects IgA Nephropathy in Rats by Regulating Exosomes to Inhibit NF-κB/NLRP3 Pathway. *Front Pharmacol* 2020; **11**: 1080 [PMID: 32765277 DOI: 10.3389/fphar.2020.01080]

146 **Shi X**, Xie X, Sun Y, He H, Huang H, Liu Y, Wu H, Dai M. Paeonol inhibits NLRP3 mediated inflammation in rat endothelial cells by elevating hyperlipidemic rats plasma exosomal miRNA-223. *Eur J Pharmacol* 2020; **885**: 173473 [PMID: 32800809 DOI: 10.1016/j.ejphar.2020.173473]

147 **Bai L**, Li J, Li H, Song J, Zhou Y, Lu R, Liu B, Pang Y, Zhang P, Chen J, Liu X, Wu J, Liang C, Zhou J. Renoprotective effects of artemisinin and hydroxychloroquine combination therapy on IgA nephropathy *via* suppressing NF-κB signaling and NLRP3 inflammasome activation by exosomes in rats. *Biochem Pharmacol* 2019; **169**: 113619 [PMID: 31465776 DOI: 10.1016/j.bcp.2019.08.021]

148 **Cypryk W**, Nyman TA, Matikainen S. From Inflammasome to Exosome-Does Extracellular Vesicle Secretion Constitute an Inflammasome-Dependent Immune Response? *Front Immunol* 2018; **9**: 2188 [PMID: 30319640 DOI: 10.3389/fimmu.2018.02188]

149 **Wozniak AL**, Adams A, King KE, Dunn W, Christenson LK, Hung WT, Weinman SA. The RNA binding protein FMR1 controls selective exosomal miRNA cargo loading during inflammation. *J Cell Biol* 2020; **219** [PMID: 32970791 DOI: 10.1083/jcb.201912074]

150 **Kato T**, Miyaki S, Ishitobi H, Nakamura Y, Nakasa T, Lotz MK, Ochi M. Exosomes from IL-1β stimulated synovial fibroblasts induce osteoarthritic changes in articular chondrocytes. *Arthritis Res Ther* 2014; **16**: R163 [PMID: 25092378 DOI: 10.1186/ar4679]

151 **Kang J**, Zhang L, Luo X, Ma X, Wang G, Yang Y, Yan Y, Qian H, Zhang X, Xu W, Mao F. Systematic Exposition of Mesenchymal Stem Cell for Inflammatory Bowel Disease and Its Associated Colorectal Cancer. *Biomed Res Int* 2018; **2018**: 9652817 [PMID: 30687760 DOI: 10.1155/2018/9652817]

152 **Asami T**, Ishii M, Fujii H, Namkoong H, Tasaka S, Matsushita K, Ishii K, Yagi K, Fujiwara H, Funatsu Y, Hasegawa N, Betsuyaku T. Modulation of murine macrophage TLR7/8-mediated cytokine expression by mesenchymal stem cell-conditioned medium. *Mediators Inflamm* 2013; **2013**: 264260 [PMID: 24191131 DOI: 10.1155/2013/264260]

World Journal of Gastroenterology

Submit a Manuscript: https://www.f6publishing.com

World J Gastroenterol 2024 February 14; 30(6): 542-555

DOI: 10.3748/wjg.v30.i6.542

ISSN 1007-9327 (print) ISSN 2219-2840 (online)

ORIGINAL ARTICLE

Retrospective Study

Preoperative prediction of lymphovascular and perineural invasion in gastric cancer using spectral computed tomography imaging and machine learning

Hui-Ting Ge, Jian-Wu Chen, Li-Li Wang, Tian-Xiu Zou, Bin Zheng, Yuan-Fen Liu, Yun-Jing Xue, Wei-Wen Lin

Specialty type: Gastroenterology and hepatology

Provenance and peer review: Invited article; Externally peer reviewed.

Peer-review model: Single blind

Peer-review report's scientific quality classification

Grade A (Excellent): 0
Grade B (Very good): B
Grade C (Good): 0
Grade D (Fair): 0
Grade E (Poor): 0

P-Reviewer: Osera S, Japan

Received: October 20, 2023
Peer-review started: October 20, 2023
First decision: December 5, 2023
Revised: December 18, 2023
Accepted: January 15, 2024
Article in press: January 15, 2024
Published online: February 14, 2024

Hui-Ting Ge, Tian-Xiu Zou, Yuan-Fen Liu, Yun-Jing Xue, Wei-Wen Lin, Department of Radiology, Fujian Medical University Union Hospital, Fuzhou 350001, Fujian Province, China

Hui-Ting Ge, Jian-Wu Chen, Li-Li Wang, Fujian Key Laboratory of Intelligent Imaging and Precision Radiotherapy for Tumors, Fujian Medical University, Fuzhou 350001, Fujian Province, China

Hui-Ting Ge, Jian-Wu Chen, Li-Li Wang, Digestive, Hematological and Breast Malignancies, Clinical Research Center for Radiology and Radiotherapy of Fujian Province, Fuzhou 350001, Fujian Province, China

Jian-Wu Chen, Department of Radiation Oncology, Fujian Medical University Union Hospital, Fuzhou 350001, Fujian Province, China

Li-Li Wang, Department of Diagnostic Radiology, Fujian Medical University Union Hospital, Fuzhou 350001, Fujian Province, China

Bin Zheng, School of Electrical and Computer Engineering, University of Oklahoma, Oklahoma, OK 73019, United States

Corresponding author: Wei-Wen Lin, PhD, Doctor, Professor, Researcher, Department of Radiology, Fujian Medical University Union Hospital, Xinquan Road, Gulou District, Fuzhou 350001, Fujian Province, China. wwl152559063@163.com

Abstract

BACKGROUND

Lymphovascular invasion (LVI) and perineural invasion (PNI) are important prognostic factors for gastric cancer (GC) that indicate an increased risk of metastasis and poor outcomes. Accurate preoperative prediction of LVI/PNI status could help clinicians identify high-risk patients and guide treatment decisions. However, prior models using conventional computed tomography (CT) images to predict LVI or PNI separately have had limited accuracy. Spectral CT provides quantitative enhancement parameters that may better capture tumor invasion. We hypothesized that a predictive model combining clinical and spectral CT parameters would accurately preoperatively predict LVI/PNI status in GC patients.

AIM
To develop and test a machine learning model that fuses spectral CT parameters and clinical indicators to predict LVI/PNI status accurately.

METHODS
This study used a retrospective dataset involving 257 GC patients (training cohort, n = 172; validation cohort, n = 85). First, several clinical indicators, including serum tumor markers, CT-TN stages and CT-detected extramural vein invasion (CT-EMVI), were extracted, as were quantitative spectral CT parameters from the delineated tumor regions. Next, a two-step feature selection approach using correlation-based methods and information gain ranking inside a 10-fold cross-validation loop was utilized to select informative clinical and spectral CT parameters. A logistic regression (LR)-based nomogram model was subsequently constructed to predict LVI/PNI status, and its performance was evaluated using the area under the receiver operating characteristic curve (AUC).

RESULTS
In both the training and validation cohorts, CT T3-4 stage, CT-N positive status, and CT-EMVI positive status are more prevalent in the LVI/PNI-positive group and these differences are statistically significant (P < 0.05). LR analysis of the training group showed preoperative CT-T stage, CT-EMVI, single-energy CT values of 70 keV of venous phase (VP-70 keV), and the ratio of standardized iodine concentration of equilibrium phase (EP-NIC) were independent influencing factors. The AUCs of VP-70 keV and EP-NIC were 0.888 and 0.824, respectively, which were slightly greater than those of CT-T and CT-EMVI (AUC = 0.793, 0.762). The nomogram combining CT-T stage, CT-EMVI, VP-70 keV and EP-NIC yielded AUCs of 0.918 (0.866-0.954) and 0.874 (0.784-0.936) in the training and validation cohorts, which are significantly higher than using each of single independent factors (P < 0.05).

CONCLUSION
The study found that using portal venous and EP spectral CT parameters allows effective preoperative detection of LVI/PNI in GC, with accuracy boosted by integrating clinical markers.

Key Words: Spectral computed tomography; Gastric cancer; Lymphovascular invasion; Perineural invasion

Core Tip: This study developed a machine learning model using clinical indicators and spectral computed tomography (CT) imaging parameters to preoperatively predict lymphovascular and perineural invasive risk in gastric cancer patients. The model combining CT staging, extramural vein invasive based on CT, and quantitative spectral CT measures had high accuracy for noninvasive prediction of these important histological features.

Citation: Ge HT, Chen JW, Wang LL, Zou TX, Zheng B, Liu YF, Xue YJ, Lin WW. Preoperative prediction of lymphovascular and perineural invasion in gastric cancer using spectral computed tomography imaging and machine learning. *World J Gastroenterol* 2024; 30(6): 542-555
URL: https://www.wjgnet.com/1007-9327/full/v30/i6/542.htm
DOI: https://dx.doi.org/10.3748/wjg.v30.i6.542

INTRODUCTION

Currently, gastric cancer (GC) ranks fifth in global cancer incidence and fourth in mortality[1]. Accurate preoperative evaluation of GC stage and tumor invasiveness is important for developing personalized treatment. In GC development, nerves, blood vessels, and lymphatic connections constitute the tumor microenvironment, and cancer cells can spread throughout the body by invading lymphatic blood vessels, and nerve fiber sheaths. Therefore, lymphovascular invasion (LVI) and perineural invasion (PNI) are closely related to tumor stage, depth of invasion, lymphatic metastasis, and distant metastasis in GC patients. As a result, the LVI and PNI can be used to predict tumor invasion and patient prognosis (or patient response to treatment)[2-4]. Previous studies have shown that a positive LVI/PNI can be used as an indicator of the efficacy of neoadjuvant and adjuvant therapies in GC patients[5,6]. At present, LVI/PNI can be diagnosed or determined only by postoperative pathology. Therefore, preoperative assessment of LVI and the PNI may assist oncologists in preoperatively identifying high-risk categories and predicting outcomes in GC patients.

In addition to postoperative pathology methods, other diagnostic methods have been identified. For example, one previous study showed a correlation among gastric wall invasion, lymph node metastasis, and the PNI[7]. Chen *et al*[8] reported that clinical T staging, N staging, American Joint Committee on Cancer (AJCC) staging, and enhanced computed tomography (CT) radiomics could be used to predict LVI. Yardımcı *et al*[9] confirmed that machine learning-based CT texture analysis was more successful at predicting LVI than was the PNI. However, these studies were usually based on conventional CT images used to construct models to predict LVI status or PNI status separately.

As a new scanning mode, spectral CT imaging has a variety of quantitative parameters, which enables CT imaging to enter the field of microscopic quantitative research from macroscopic morphology[10]. Previous studies have proven that the quantitative assessment of spectral CT image parameters could be used to evaluate the histological classification, staging, lymph node metastasis, and prognosis of GC patients[11-13]. Ren *et al* showed that cancer antigen 125 (CA125) levels, histological grade, Borrmann grade and energy-based spectrum CT parameters could be used to evaluate LVI and the PNI[14]. However, these studies need further validation. To our knowledge, few studies have focused on assessing the value of using spectral CT imaging and machine learning algorithms to predict LVI and PNI in GC patients preoperatively.

To better address this clinical issue, we hypothesized that optimal fusion of spectral CT parameters and clinical markers using a machine learning method could more accurately predict LVI or PNI status in GC patients preoperatively. Thus, the objective of this study is to test our hypothesis. Specifically, we first used a logistic regression (LR) method to analyze a number of important clinical indicators, including preoperative CT evaluation of gastric wall invasion depth (CT-T stage), lymph node metastasis (CT-N stage), CT-detected extramural vein invasion (CT-EMVI), and serum tumor markers, as well as quantitative spectral CT parameters, and then build a LR-based nomogram model that optimally fuses quantitative spectral CT parameters and clinical indicators (or markers), to predict histological LVI and PNI statuses in GC.

MATERIALS AND METHODS

Patients

This was a retrospective study in which we selected data from patients with gastric adenocarcinoma who underwent surgical resection and were pathologically diagnosed from December 2017 to June 2023 in our hospital. The inclusion criteria are as follows: (1) Diagnosis of gastric adenocarcinoma with clear LVI and PNI information; (2) Abdominal three-phase enhanced spectral CT scan performed within 2 wk before surgery; and (3) No local or systemic treatment performed before CT examination or surgery. The exclusion criteria were as follows: (1) Unclear lesion on CT image; (2) Poor gastric filling, (3) Poor image quality; and (4) Incomplete clinical information. Using the above criteria, the clinical information and preoperative spectral CT images of 257 patients were obtained in this study. According to the postoperative pathological results, patients with LVI and/or PNI were classified as the positive group (LVI/PNI positive, n = 162), and patients without LVI and PNI were classified as the negative group (LVI/PNI negative, n = 95), as shown in Figure 1.

Clinical information

Clinical data, including sex, age, serum tumor marker levels, and pathological information, were collected by a senior attending physician. The serum tumor markers included CA72-4, alfa fetoprotein (AFP), carcinoembryonic antigen (CEA), CA19-9 and CA125. The pathological information included histological type and complete LVI and PNI data.

CT examination

All preoperative CT images were acquired using a GE Healthcare Revolution CT ascending spectral scanner. Before examination, all patients were asked to fast for 8 h and drink 800-1000 mL of water. The acquisition parameters were as follows: (1) Scanning range; (2) Mid-upper abdomen; (3) Tube voltage, 80 kVp to 140 kVp instantaneous switch; (4) Tube current, 200 mAs; (5) Width of detector, 80 mm; (6) Pitch, 0.992:1; (7) Speed, 0.6-0.8 s/revolution; and (8) Image matrix, 512 × 512. A single-energy image at 70 keV was reconstructed with an image slice thickness of 1.25 mm. Before CT examination, a nonionic water-soluble contrast agent (Dimyron 400 mg/mL, Shanghai Bracco Sine Pharmaceutical Corp. Ltd.) used was injected through the cubital vein of the patient with a high-pressure syringe. The dose was 1.5 mL/kg, and the injection rate was 2.5-3 mL/s. Images in the arterial phase (AP), portal venous phase (VP) and equilibrium phase (EP) were scanned at 20-25 s, 60 s, and 3 min after the start of contrast medium injection.

Imaging analysis

First, two senior attending radiologists (with 7 and 13 years of experience in abdominal radiology, respectively) were blinded to the clinical information and independently and retrospectively reviewed the CT images. All TN stages and EMVIs were evaluated on multiplanar reconstruction images constructed using an AW4.6 workstation. The TN staging and EMVI scores were assigned based on the consensus between the two radiologists. Any discrepancies were resolved by a third senior radiologist (with 32 years of experience in abdominal radiology).

TN staging was performed on the CT images according to the 7th edition of AJCC guidelines and the study by Kim *et al* [15]. CT-EMVI was defined and scored based on the criteria outlined by Yang *et al*[16]. A positive CT-EMVI was defined as a GC lesion directly invading the extramural vascular lumen, resulting in vascular dilation or filling defects, and connecting with the primary tumor mass. EMVI scores of 0-2 and 3-4 are considered negative, and positive CT-EMVI, respectively. The CT-EMVI scoring criteria are described below Figure 2.

Quantitative image analysis was performed on a GE AW4.6 workstation using GSI Viewer software, as depicted in Figure 3. An experienced abdominal radiologist (7 years) who was blinded to the clinical data delineated circular or elliptical regions of interests (ROIs) on the largest cross-sectional area of each tumor, encompassing approximately two-thirds of the lesion volume while avoiding necrotic regions. Each lesion ROI was measured three times, and the average values were calculated. The following spectral CT parameters across three contrast phases were obtained including: (1) Single-energy CT values of 40 keV, 70 keV, 120 keV and 140 keV; (2) Iodine concentration (IC); and (3) Effective atomic

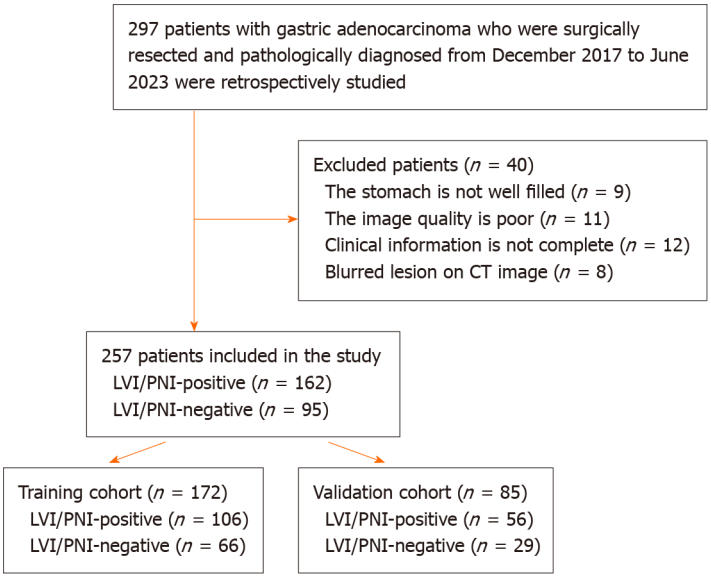

DOI: 10.3748/wjg.v30.i6.542

Figure 1 Flowchart of the inclusion and exclusion criteria. LVI: Lymphovascular invasion; PNI: Perineural invasion; CT: Computed tomography.

number (Zeff). Two additional metrics were also derived, namely: (1) The spectral curve slope, calculated as K40-70 = (CT40 keV-CT70 keV)/30; and (2) The normalized IC ratio (NIC), defined as the lesion IC divided by the thoracic aortic IC at the same level. Thus, a total of 24 parameters were extracted and computed from the spectral CT images.

In this study, the inter- and intraclass correlation coefficients (ICCs) were also calculated to assess the reproducibility of the spectral CT parameters extracted from the ROIs delineated by two radiologists. Radiologist A, who has 7 years of experience, first completed the ROI outlines for all the patients. Radiologist B, who has 13 years of experience, independently outlined the ROIs for a randomly selected subset of 50 patients to evaluate interobserver agreement. Radiologist A also repeated the ROI outlines for the same 50 patients after one month to allow assessment of intraobserver agreement. Spectral CT parameters with ICC values ≥ 0.75 were considered adequately reproducible and were retained for further analysis.

Feature engineering

Figure 4 outlines the steps of computing, selecting features, building a machine learning model and evaluating model performance. First, a total of 257 patients diagnosed with GC were divided into the original in the training cohort (n = 172) and validation cohort (n = 85) in chronological order at a ratio of 2:1. Since 34 features (including 24 spectral CT parameters and 10 clinical indicators) were extracted and computed, some of the features may be redundant. To increase the robustness of the multifeature fusion-based machine learning model, a feature dimensionality reduction step was conducted to select optimal parameters and remove redundant parameters from the whole training cohort *via* the following steps: (1) Univariate analysis was applied to calculate the associations between clinical characteristics and the status of LVI/PNI. Clinical features that showed statistically significant associations were retained for further analysis; and (2) A correlation-based feature selection subset evaluator was used in conjunction with a best-first heuristic feature search and selection method for feature selection. The InfoGainAttributeEval tool was then utilized to evaluate the worth of attributes by measuring their information gain relative to the class. This was paired with a Ranker tool employing a 0.2 average merit threshold for further selection of informative spectral CT parameters. Step 2 was embedded inside a tenfold cross-validation-based iteration cycle to minimize case partition bias, and variance.

A machine learning-based individualized prediction model

Using the selected clinical characteristics and spectral CT parameters, the machine learning algorithm LR was developed using the Akaike information criterion as the stopping criterion. Model performance was evaluated by the area under the receiver operating characteristic curve (AUC) in the training and independent testing cohorts. The Hosmer-Lemeshow test, calibration curves, and bootstrapping (500 resamples) were used to assess model calibration. The AUCs were compared between cohorts *via* DeLong testing. DCA was used to quantify the potential net benefit of the nomogram.

Statistical methods

SPSS 26.0 statistical software was used, and single-factor statistical tests, including the χ^2 test, Fisher's exact test, the Mann-Whitney U test and independent sample t tests were used. Weka software (version 3.8.6) was used for feature selection, and R software (version 3.4.3) was used for prediction model construction and plotting. $P < 0.05$ was considered to indicate statistical significance.

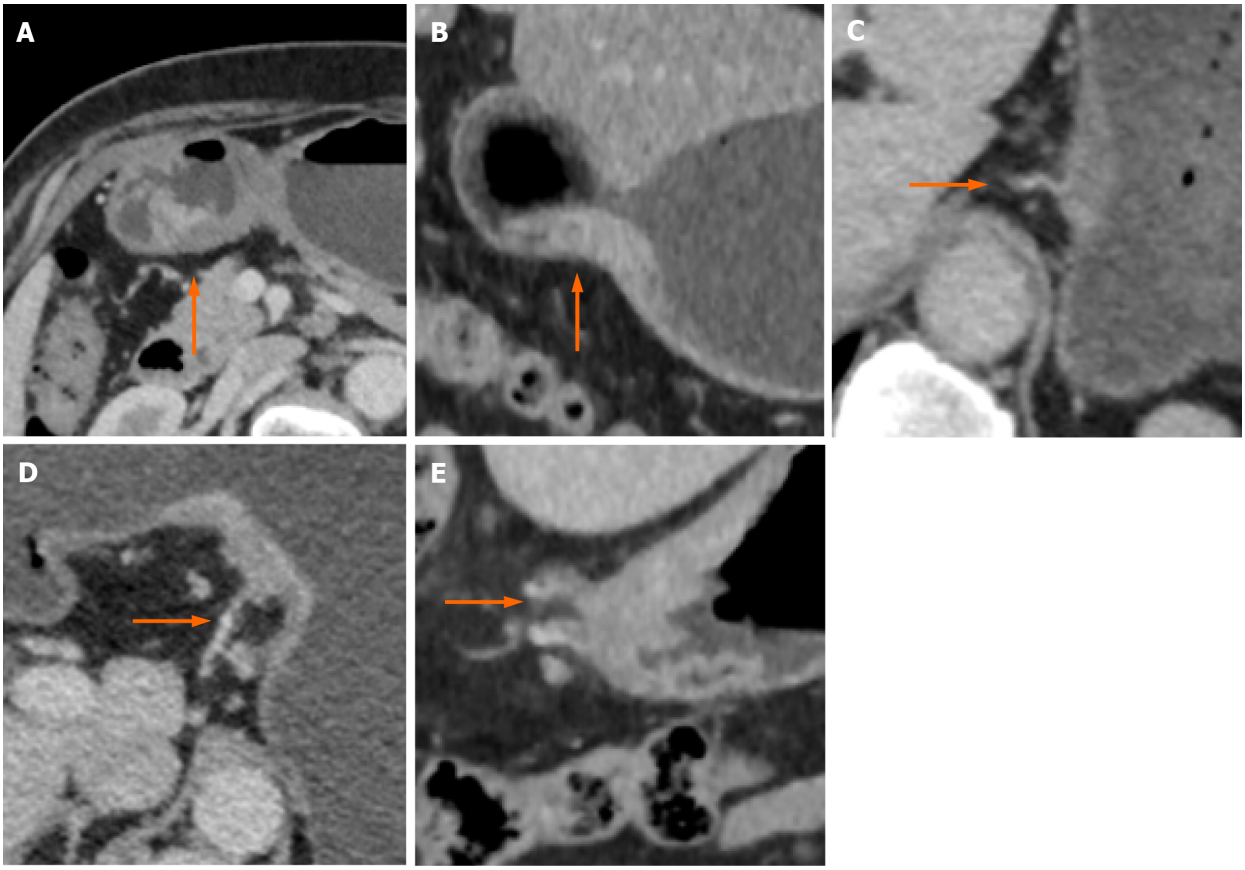

DOI: 10.3748/wjg.v30.i6.542

Figure 2 Example of a computed tomography-detected extramural vein invasion score on computed tomography images of gastric cancer patients. A: Score 0: The tumor has not penetrated the gastric wall, and there are no extramural vessels beside the lesion (arrow) in the transverse position of the venous phase (VP); B: Score 1: The transverse view of the VP shows that the tumor has permeated the gastric wall, and there are no extramural vessels beside the lesion (arrow); C: Score 2: In the VP, the coronal lesion has penetrated the gastric wall, and there are tortuous blood vessels connected with the lesion (arrow), but no tumor density shadow is observed in the vascular lumen; D: Score 3: The transverse view of the VP shows that the mass has penetrated through the gastric wall, the involved blood vessels appear slightly tortuous and dilated, and the tumor density shadow is visible (arrow); E: Score 4: In the coronary view of the VP, the tumor permeated the gastric wall, the extramural vascular lumen was significantly dilated, and a slight low-density filling defect was visible inside (arrow).

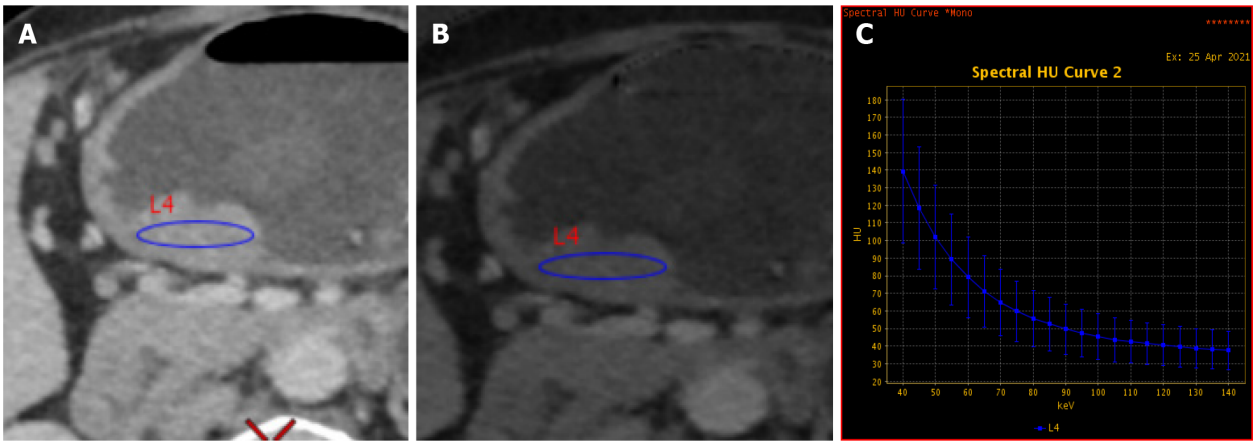

DOI: 10.3748/wjg.v30.i6.542

Figure 3 Example of the energy spectrum data measurement. A: 70 keV single-energy image; B: The iodine base image; C: The energy spectrum curve. Elliptical regions of interests were drawn at the largest level of the lesion in the lesser curvature of the gastric horn, as shown in A and B.

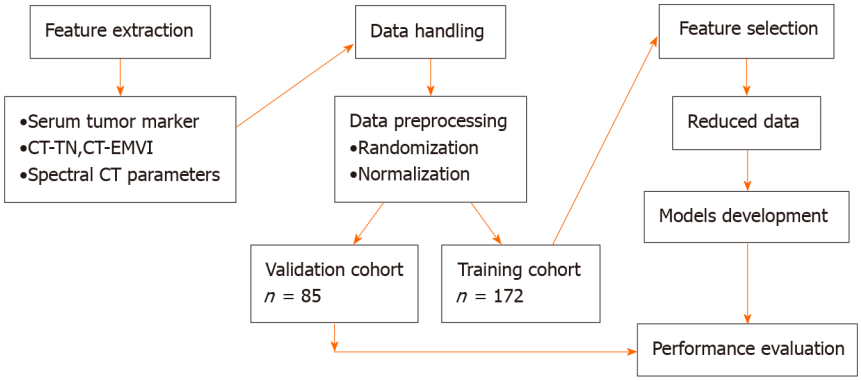

DOI: 10.3748/wjg.v30.i6.542

Figure 4 Technical study pipeline. CT-EMVI: Computed tomography-detected extramural vein invasion; CT: Computed tomography.

Comparison of clinical characteristics and quantitative three-phase spectral CT parameters between groups

Figure 5 shows examples of CT and histopathology images of two patients, as well as the energy spectral curves. As shown in Table 1, there were no significant differences between the positive and negative groups in either the training or validation cohorts in terms of sex or age distribution ($P > 0.05$). The data in Table 1 also show the following statistics data analysis results: (1) In both the training and validation cohorts, CT T3-4 stage, CT-N positive status, and CT-EMVI positive status are more prevalent in the LVI/PNI-positive group and these differences are statistically significant ($P < 0.05$); (2) In the training cohort, serum CA72-4 and CA19-9 levels are significantly higher in the LVI/PNI-positive group compared to the LVI/PNI-negative group ($P < 0.05$), however this is not observed in the validation cohort ($P > 0.05$); and (3) There were no significant differences in AFP, CEA, or CA125 levels between the two groups ($P > 0.05$).

The CT values of 40 keV, 70 keV, 120 keV, and 140 keV, K40-70, Zeff, IC, and NIC are higher in the LVI/PNI-positive group compared to the LVI/PNI-negative group at the AP, VP, and EP ($P < 0.05$). The interobserver ICCs for these spectral CT parameters ranged from 0.766 to 0.955, while the intraobserver ICCs ranged from 0.759 to 0.945, indicating good inter- and intraobserver agreement, as all the ICCs exceeded 0.75. These reproducible spectral CT parameters were retained for subsequent feature selection.

Feature selection

After removing 29 redundant features, five features-CT-T stage, CT-N stage, CT-EMVI, single-energy CT values of 70 keV of VP-70 keV, and the ratio of standardized IC of EP (EP-NIC)-were frequently selected by the BestFirst method with ≥ 90% probability. The CT-N stage was then removed after applying InfoGainAttributeEval with a 0.2 average merit threshold. The remaining four features (CT-T stage, CT-EMVI, VP-70 keV CT value, and EP-NIC) were selected and incorporated into LR models. The confusion matrices of clinical and spectral CT features and details of the feature selection process are presented in Tables 1 and 2.

Model performance evaluation

Using training cohort, LR demonstrated that CT-T stage [odds ratio (OR) = 2.683, 95% confidence interval (CI): 1.103-6.523], CT-EMVI (OR = 3.396, 95%CI: 1.277-9.027), VP-70 keV CT value (OR = 1.047, 95%CI: 1.021-1.074), and EP-NIC (OR = 117.723, 95%CI: 4.867-2847.564) were independent influencing factors for predicting LVI/PNI status.

According to the ROC analysis (Table 3 and Figure 6), the AUC of the established LR model was 0.918 (95%CI: 0.866-0.954) in the training cohort, which was greater than that of the single independent factors (0.762-0.888). According to the DeLong tests, the differences between the AUC generated by the LR model and each of the 4 parameters (CT-T, CT-EMVI, VP-70 keV, and EP-NIC) were significant (P values ranging from 0.0428 to 0.0001). A nomogram was constructed for clinical use (Figure 6).

The AUC of the LR model in the validation cohort was 0.874 (95%CI: 0.784-0.936); when each of the 4 parameters was used individually, the AUC ranged from 0.735 to 0.824. There are no significant differences between the paired ROC curves using the same features or LR model applying to the training and validation cohorts with P value > 0.05, such as $P = 0.3564$ using LR model.

Additionally, the calibration curve and Hosmer-Lemeshow test showed good fit of the nomogram (Figure 6), with no significant differences ($P = 0.6051$). The decision curve analysis confirmed that, compared to the treat-none and treat-all strategies, using the nomogram can help stratify patients based on their predicted risk of LVI/PNI positivity for threshold probabilities between 0.10 and 0.95.

DISCUSSION

This study analyzed quantitative spectral CT parameters, CT-determined TN stage, CT-detected EMVI, and serum tumor markers using a machine learning algorithm. Feature reduction and subsequent LR analysis demonstrated that CT-T stage, CT-EMVI, the VP-70 keV CT value, and the EP-NIC were independent predictors of histological LVI/PNI status.

Table 1 Comparative analysis of clinical indicators and spectral computed tomography parameters between groups

Variables	Training cohort (*n* = 172)			Validation cohort (*n* = 85)		
	LVI/PNI (+)	LVI/PNI (-)	*P* value	LVI/PNI (+)	LVI/PNI (-)	*P* value
Gender, *n* (%)						
Male	77 (61.1)	49 (38.9)	0.818	47 (70.2)	20 (29.8)	0.109
Female	29 (63.0)	17 (37.0)		9 (50.0)	9 (50.0)	
Age, yr, *n* (%)						
< 60	33 (66.0)	17 (34.0)	0.450	19 (67.9)	9 (32.1)	0.788
≥ 60	73 (59.8)	49 (40.2)		37 (64.9)	20 (35.1)	
CT-T						
T1/2	23 (30.3)	53 (69.7)	< 0.001[a]	9 (28.1)	23 (71.9)	< 0.001[a]
T3/4	83 (86.5)	13 (13.5)		47 (88.7)	6 (11.3)	
CT-N						
N0	29 (34.9)	54 (65.1)	< 0.001[a]	19 (55.8)	24 (44.2)	< 0.001[a]
N1/2/3	77 (86.5)	12 (13.5)		36 (12.2)	5 (87.8)	
CT-EMVI						
Negative	44 (41.5)	62 (58.5)	< 0.001[a]	20 (45.5)	24 (54.5)	< 0.001[a]
Positive	62 (6.1)	4 (93.9)		36 (87.8)	5 (12.2)	
CA72-4, *n* (%)						
Negative	86 (57.3)	64 (42.7)	0.002[a]	46 (63.9)	26 (36.1)	0.528
Positive	20 (90.9)	2 (9.1)		10 (76.9)	3 (23.1)	
AFP, *n* (%)						
Negative	104 (61.5)	65 (38.5)	1.000	54 (65.9)	28 (34.1)	1.000
Positive	2 (66.7)	1 (33.3)		2 (66.7)	1 (33.3)	
CEA, *n* (%)						
Negative	91 (61.1)	58 (38.9)	0.704	42 (61.8)	26 (38.2)	0.109
Positive	15 (65.2)	8 (34.8)		14 (82.4)	3 (17.6)	
CA199, *n* (%)						
Negative	89 (58.6)	63 (41.4)	0.022[a]	48 (64.0)	27 (36.0)	0.483
Positive	17 (85.0)	3 (15.0)		8 (80.0)	2 (20.0)	
CA125, *n* (%)						
Negative	101 (60.5)	66 (39.5)	0.158	54 (65.9)	28 (34.1)	1.000
Positive	5 (100.0)	0 (0.0)		2 (66.7)	1 (33.3)	
VP-70 kev, mean ± SD	92.46 ± 18.29	64.54 ± 15.90	< 0.001[a]	89.87 ± 20.34	66.30 ± 18.65	< 0.001[a]
EP-NIC, mean ± SD	0.68 ± 0.16	0.49 ± 0.13	< 0.001[a]	0.69 ± 0.15	0.51 ± 0.12	< 0.001[a]

[a]*P* value < 0.05.

P was calculated from univariate association of characteristics with lymphovascular invasion/perineural invasion status in gastric cancer cohorts. LVI: Lymphovascular invasion; PNI: Perineural invasion; (+): Positive; (-): Negative; CT-EMVI: Computed tomography-detected extramural vein invasion; VP-70 keV: Single-energy computed tomography value of 70 keV in the venous phase; EP-NIC: Ratio of the standardized iodine concentration in the equilibrium phase; CA: Cancer antigen; CEA: Carcinoembryonic antigen; AFP: Alfa fetoprotein.

The LR model demonstrated promising results, with comparable accuracy in predicting LVI/PNI across independent training and testing cohorts.

The present study suggested a greater possibility of vascular nerve invasion in the T3-4 stage, which aligns with the findings of previous studies[9] that identified clinical T stage as a predictive factor for LVI. Although CT-determined N status differed significantly according to the χ^2 test, it was removed by the InfoGainAttributeEval tool, which evaluates

Table 2 Risk factors of lymphovascular invasion and perineural invasion in gastric cancer

Variables	Feature selection		Individual nomogram		
	BestFirst with probability (%)	InfoGainAttributeEval with average merit	*Z* value	OR (95%CI)	*P* value
CT-EMVI	100	0.203 ± 0.016	2.451	3.396 (1.277-9.027)	0.014
CT-T	100	0.263 ± 0.018	2.177	2.683 (1.103-6.523)	0.029
VP-70kev	90	0.356 ± 0.016	3.565	1.047 (1.021-1.074)	< 0.001
EP-NIC	90	0.239 ± 0.016	2.934	117.723 (4.867-2847.564)	0.003
CT-N	100	0.197 ± 0.014			

CT-EMVI: Computed tomography-detected extramural vein invasion; VP-70 keV: Single-energy computed tomography value of 70 keV in the venous phase; EP-NIC: Ratio of the standardized iodine concentration in the equilibrium phase; OR: Odds ratio; CI: Confidence interval.

Table 3 Performance of the individual nomogram and single independent factors

	AUC (95%CI)	Sensitivity	Specificity	PPV	NPV	Accuracy
Nomogram						
Training cohort	0.918 (0.866-0.954)	85.9	83.3	89.2	78.6	84.9
Validation cohort	0.874 (0.784-0.936)	87.5	75.9	87.5	75.9	83.5
CT-EMVI						
Training cohort	0.762 (0.691-0.824)	58.5	93.9	93.9	58.5	72.1
Validation cohort	0.735 (0.628-0.825)	64.3	82.8	87.8	54.5	70.6
CT-T						
Training cohort	0.793 (0.725-0.851)	78.3	80.3	86.5	69.7	79.1
Validation cohort	0.816 (0.717-0.892)	83.9	79.3	88.7	71.9	82.4
VP-70kev						
Training cohort	0.888 (0.831-0.931)	84.9	71.2	82.6	74.6	79.7
Validation cohort	0.804 (0.703-0.882)	92.9	55.2	80.0	80.0	80.0
EP-NIC						
Training cohort	0.824 (0.758-0.877)	82.1	62.1	77.7	68.3	74.4
Validation cohort	0.824 (0.726-0.898)	85.7	58.6	80.0	68.0	76.5

CT-EMVI: Computed tomography-detected extramural vein invasion; VP-70 keV: Single-energy computed tomography value of 70 keV in the venous phase; EP-NIC: Ratio of the standardized iodine concentration in the equilibrium phase; AUC: Area under the receiver operating characteristic curve; CI: Confidence interval; PPV: Positive predictive value; NPV: Negative predictive value.

attribute worth by measuring information gain relative to the class. This may be because preoperative CT has lower accuracy for N staging than for T staging, as reported previously[17,18].

The presence of an EMVI in CT images is another independent risk factor for LVI/PNI. Previous studies have shown that EMVI usually coexists with invasion of the perigastric nerves, blood vessels, and lymphatic vessels and is considered a route for tumor spread through neurovascular bundles[19]. Our study also confirmed that CT-EMVI is closely related to LVI/PNI status. Patients with positive CT-EMVI findings had a greater probability of having positive LVI/PNI (OR = 3.396, 95%CI: 1.277-9.027).

Serum tumor markers are produced by tumor cells or the body's autoimmune response during tumor growth. CA72-4, AFP, CEA, CA19-9, CA125, and other markers are widely used to diagnose and evaluate the prognosis and treatment efficacy in GC patients[20-22]. Significant differences were found for CA72-4 and CA19-9 in the training cohort ($P < 0.05$) but not in the verification cohort ($P > 0.05$), indicating population-level differences. In contrast, AFP, CEA, and CA125 did not significantly differ ($P > 0.05$). In contrast to our results, Ren *et al*[14] reported higher CA125 levels in LVI/PNI-positive patients. Other studies have shown that GC patients with nerve, vascular, or serosal infiltration and lymph node metastasis have a greater probability of having increased CA72-4[20]. These findings further indicate that serum tumor

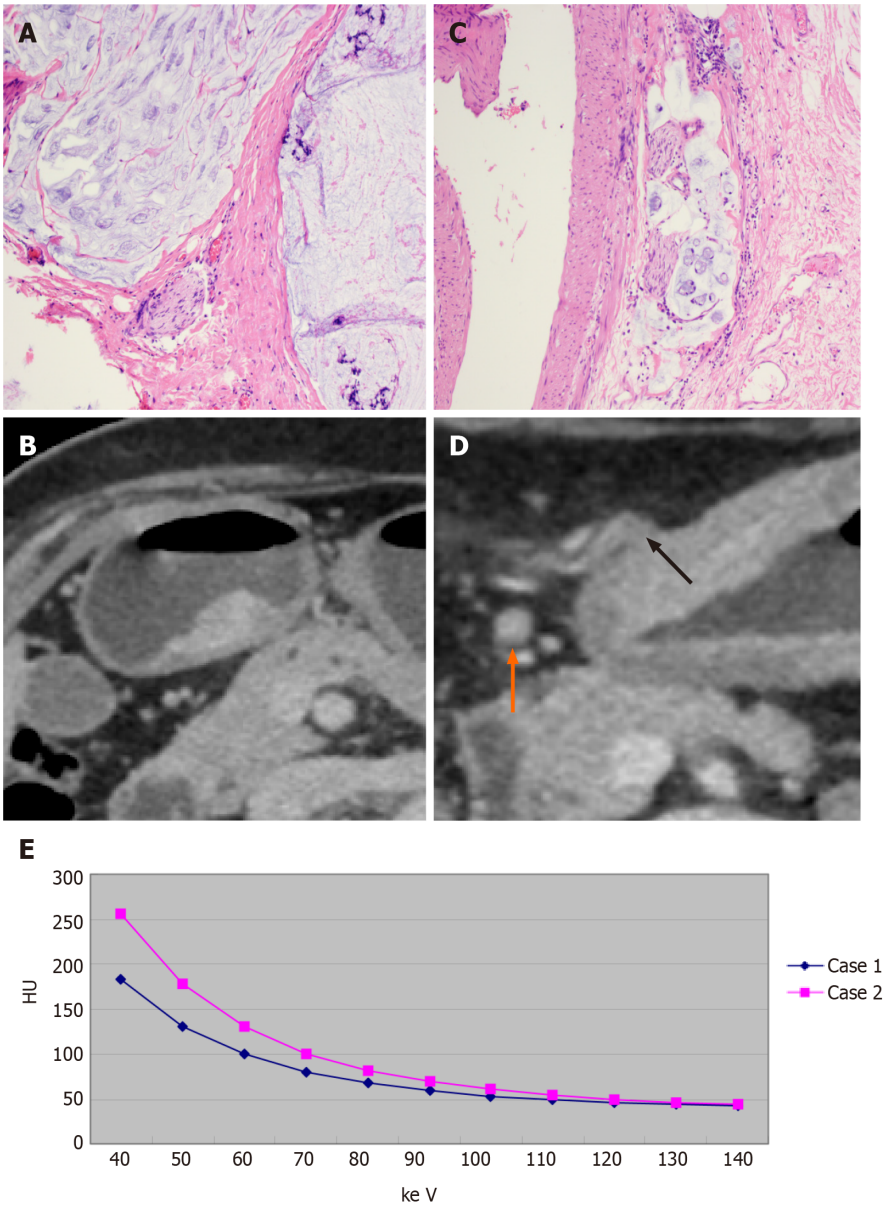

DOI: 10.3748/wjg.v30.i6.542

Figure 5 Comparative imaging and spectral analysis of pathological gastric adenocarcinoma in two patients with different lymphovascular and perineural invasion status. A and B: Patient 1: The patient was a 75-year-old female with pathological gastric adenocarcinoma, and both lymphovascular invasion (LVI) and perineural invasion (PNI) were negative (HE, × 200); the equilibrium phase (EP) transverse view shows that the gastric cancer (GC) lesion was immersed in the submucosal low-density layer, and the infiltration depth was more than 50% of the lesion; however, the low-density zone was still visible with an intact outer membrane. No suspicious metastatic lymph nodes were found on the computed tomography (CT) image, and no extramural blood vessels were found around the lesion. The CT stage was CT-T2N0, and CT-detected extramural vein invasion (CT-EMVI) was 0 and negative. The slopes of the energy spectrum curves in the EP were K40-70 = 3.43, IC = 18.46 (100 μg/cm^3), normalized iodine concentration (NIC) = 0.40, and effective atomic number (Zeff) = 8.68; C and D: Patient 2: The patient was a 77-year-old male with pathological gastric adenocarcinoma, and both LVI and PNI were positive (HE, × 200). The GC lesion in the transverse position in the equilibrium stage permeated the gastric wall, and a cord-like thickened vascular shadow was observed in the fat space around the lesion. An endovascular low-density filling defect (black arrow) was observed. Enlarged lymph nodes were observed around the lesion, the short diameter was 7 mm (orange arrow), the CT stage was CT-T4aN1, and the CT-EMVI score was 4, indicating positivity. The slopes of the energy spectrum curves in the EP are K40-70 = 5.18, IC = 27.41 (100 μg/cm^3), NIC = 0.59, and Zeff = 9.14; E: The energy spectrum curve shows that the CT value at 40-140 keV in patient 2 is greater than that in patient 1, and the value of the slope is greater. The spectral parameters of patient 2 are greater than those of patient 1.

marker levels differ across populations.

The single-energy CT value, IC, and NIC in energy spectrum CT can reflect the degree of blood supply to lesions[23]. Previous studies have indicated that LVI/PNI-positive patients exhibit greater angiogenesis activity and greater microvascular density, resulting in greater lesion enhancement[24]. Therefore, iodine uptake rates (IC and NIC) and single-energy CT values were greater in the positive group than in the negative group. The energy spectrum curve slope and Zeff were also greater in the LVI/PNI-positive group ($P > 0.05$), indicating differences in attenuation characteristics between the groups. An increased lesion mass from the vasculature and endoneurial tumor embolus formation leads to increased Zeff[14].

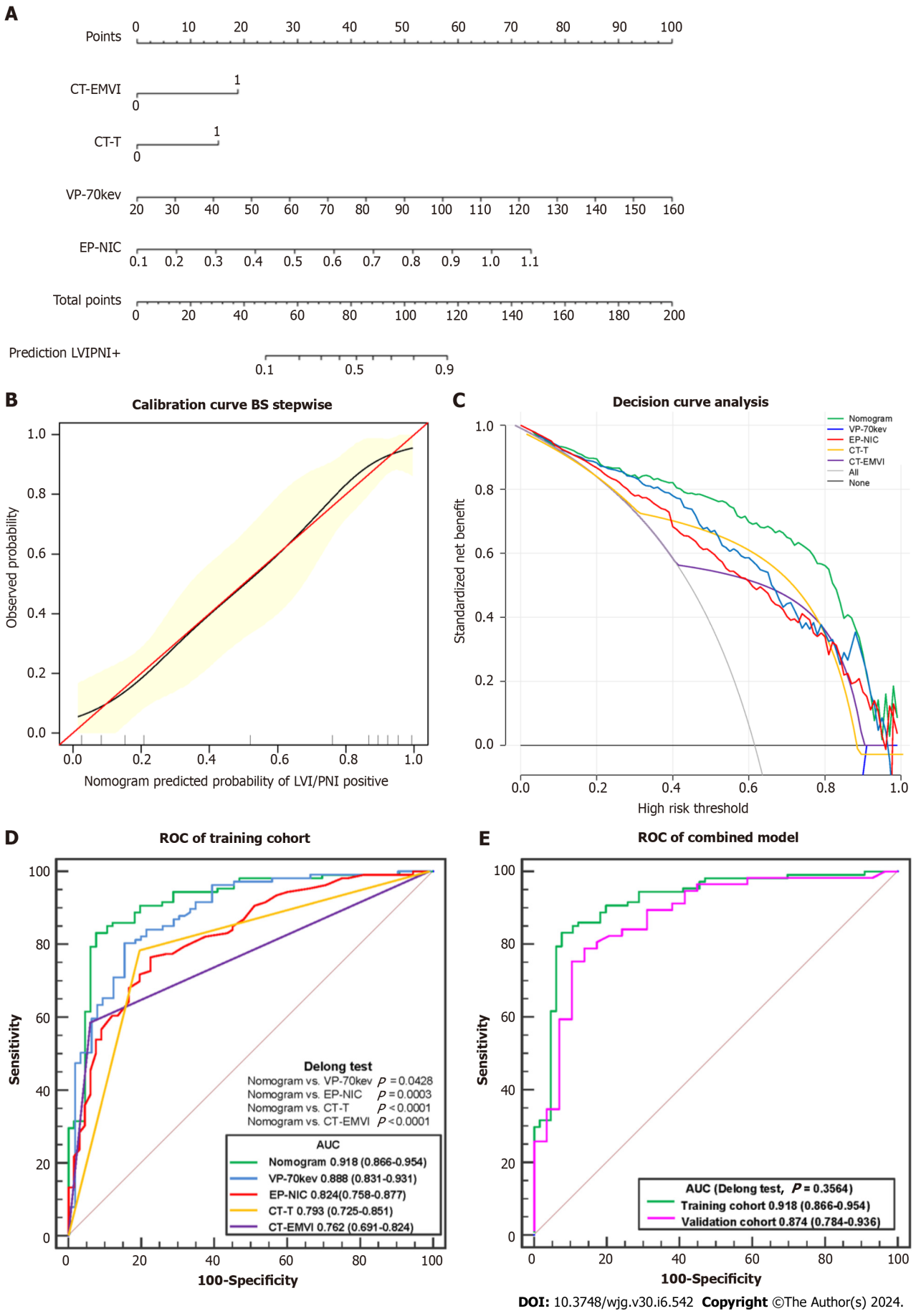

DOI: 10.3748/wjg.v30.i6.542

Figure 6 Comprehensive analysis of predictive models. A: Individual nomogram; B: Calibration curve; C: Decision curve analysis of the training cohort; D:

Receiver operating characteristic (ROC) curves of the application of the nomogram, VP-70 keV, EP-NIC, CT-T and CT-EMVI to the training cohort. The DeLong test showed that the differences were significant between the nomogram and each single independent factor; E: ROC curve of the application of the nomogram to the training cohort and the validation cohort. CT-EMVI: Computed tomography-detected extramural vein invasion; VP-70 keV: Single-energy computed tomography value of 70 keV in the venous phase; EP-NIC: Ratio of the standardized iodine concentration in the equilibrium phase; ROC: Receiver operating characteristic; AUC: Area under the receiver operating characteristic curve.

Among the spectral CT quantitative parameters, VP-CT70 keV and EP-NIC were identified as independent predictors of LVI/PNI status by multivariate LR, while arterial-phase parameters were excluded. This may be because the AP mainly reflects intravascular blood supply, whereas the venous and EPs can more effectively reflect blood supply distribution, especially the extracellular lesion space. Thus, venous and EP parameters had better predictive performance than AP parameters. Ren *et al*[14] and Li *et al*[25] also reported superior diagnostic performance for LVI/PNI status using venous-phase spectral parameters. In our study, 70 keV single-energy CT values in the VP were selected as an independent risk factor. This is likely because 70 keV images have the lowest noise, even below that of conventional mixed-energy images, providing the best signal-to-noise ratio[24,26].

Multivariate LR was used to construct predictive models for LVI/PNI status. The AUC of spectral CT quantitative parameters in the venous and EPs for predicting LVI/PNI status was 0.888 and 0.824, respectively, slightly higher than CT-T and CT-EMVI (AUC = 0.793, 0.762). This finding suggested that venous and EP spectral CT alone enables effective assessment. However, the nomogram constructed using combined parameters provides even greater sensitivity and positive predictive value. This allows preoperative identification of high-risk LVI/PNI patients, allowing oncologists to stratify patients into risk categories and adopt more aggressive treatment if warranted. In summary, our study demonstrated the utility of a multiparametric approach using spectral CT for preoperatively identifying high-risk categories and predicting outcomes in GC patients.

This study has several limitations. First, the sample size was relatively small, and there were unequal numbers of patients in the positive and negative LVI/PNI groups. Second, this study focused solely on gastric adenocarcinoma and did not evaluate other histological tumor types. Third, traditional clinicopathological factors were not incorporated into our prediction models. Fourth, as a single-center study, our results may have limited generalizability. Further multicenter studies are warranted to verify the clinical feasibility of implementing these predictive models more broadly.

CONCLUSION

In conclusion, despite these limitations, this study demonstrated the feasibility of using multiphasic spectral CT parameters to preoperatively predict lymphovascular and PNI risk in gastric adenocarcinoma patients. Further validation of this noninvasive approach may enable individualized risk stratification and outcome prediction to optimize treatment.

ARTICLE HIGHLIGHTS

Research background

The research background involves the critical role of lymphovascular invasion (LVI) and perineural invasion (PNI) as prognostic factors in gastric cancer (GC), indicating an increased risk of metastasis and poor patient outcomes. The ability to accurately predict LVI/PNI status preoperatively is significant for identifying high-risk patients and guiding treatment decisions. Conventional models using standard computed tomography (CT) images to predict these invasions have had limited success; thus, this study proposes a new approach using spectral CT imaging and machine learning to improve prediction accuracy.

Research motivation

The research is motivated by the necessity to improve preoperative predictions of LVI and PNI in GC patients, addressing the limitations of conventional CT imaging techniques. The primary objective is to develop a more precise predictive model by integrating spectral CT imaging parameters with clinical markers through machine learning algorithms. Successfully achieving this could refine preoperative assessments, aid in risk stratification, inform treatment planning, and potentially elevate future diagnostic strategies in the field of GC.

Research objectives

The primary objective of the research is to test the hypothesis that an optimal fusion of spectral CT parameters with clinical markers using a machine learning method can more accurately predict LVI or PNI status in GC patients before surgery. Specifically, the study analyzed a set of clinical indicators, such as preoperative CT evaluation of gastric wall invasion depth, lymph node metastasis, extramural vein invasion, and serum tumor markers, along with quantitative spectral CT parameters. The research aimed to develop a logistic regression (LR)-based nomogram model that integrates these clinical indicators with spectral CT parameters to predict histological LVI and PNI statuses in GC. Realizing these objectives has significant implications for improving preoperative staging and tailoring appropriate treatment plans for GC patients, thus advancing future research and diagnostic strategies in this field.

Research methods

The research adopted a retrospective dataset and a LR-based nomogram model that incorporated clinical indicators with quantitative spectral CT parameters for the preoperative prediction of lymphovascular and PNI in GC patients. Methods included using statistical software for univariate analysis and correlation-based feature selection, along with 10-fold cross-validation and information gain ranking within a training-validation cohort framework to select significant features. The model's performance was evaluated through receiver operating characteristic (ROC) analysis, calibration using the Hosmer-Lemeshow test and bootstrapping, and decision curve analysis to quantify potential net benefits. These methods highlighted novel approaches in integrating machine learning with available clinical and imaging data to potentially improve preoperative assessment and treatment planning.

Research results

The research results demonstrated that CT values and parameters such as iodine concentration and normalized iodine concentration were significantly higher in the LVI/PNI-positive group across all phases (arterial, venous, and equilibrium) when compared to the LVI/PNI-negative group, with statistical significance ($P < 0.05$). Good inter- and intra-observer agreement was observed for these spectral CT parameters, as indicated by the inter-observer intraclass correlation coefficients (ICC) values ranging from 0.766 to 0.955 and intra-observer ICC values from 0.759 to 0.945. This reproducibility led to their retention for feature selection in developing the predictive model. These findings contribute to the overall research in the field by introducing reproducible and quantifiable spectral CT parameters as reliable predictors for LVI/PNI status in GC patients. The study opens avenues for further investigation into refining and validating these spectral CT-based assessment methods, possibly addressing existing challenges in preoperative staging and treatment planning.

Research conclusions

The study proposes a novel application of spectral CT imaging integrated with machine learning to preoperatively predict lymphovascular and PNI in patients with GC. Through the use of a logistic regression-based nomogram model, the research introduces a new method for combining clinical indicators with quantitative imaging parameters to improve the accuracy of preoperative assessments. This contributes to the field by proposing an alternative to the current postoperative pathology methods and could improve treatment planning by enabling non-invasive, individualized risk stratification prior to surgery.

Research perspectives

The direction of future research following this study is anticipated to focus on validating the noninvasive spectral CT-based machine learning model in prospective multicenter studies to confirm its clinical utility in preoperative risk stratification. Additionally, further research may explore the integration of this model in routine clinical practice to assess its impact on patient management, particularly in the identification of those who may benefit from more aggressive treatment strategies preoperatively. By refining and expanding the predictive capabilities of spectral CT imaging, future research could pave the way for improved individualized treatment planning and outcomes in GC care.

ACKNOWLEDGEMENTS

We thank all the authors for their contributions to the manuscript and for their recognition of the data and conclusions.

FOOTNOTES

Co-first authors: Hui-Ting Ge and Jian-Wu Chen.

Co-corresponding authors: Yun-Jing Xue and Wei-Wen Lin.

Author contributions: Ge HT, Chen JW, and Wang LL contributed equally to this work; Ge HT, Chen JW, and Wang LL designed the research study and performed the research; Ge HT wrote the manuscript and collected data; Zou TX contributed new software and analytic tools; Wang LL and Zheng B analyzed the data; Liu YF provided methods; Xue YJ and Lin WW searched literature and managed the project; Xue YJ and Lin WW contributed equally to this work; and all authors have read and approve the final manuscript.

Supported by Science and Technology Project of Fujian Province, No. 2022Y0025.

Institutional review board statement: The study was reviewed and approved by the Ethical Review Board of Fujian Medical University Union Hospital (Fuzhou, China), approval No. 2022KJT016.

Informed consent statement: The requirement for informed consent was waived.

Conflict-of-interest statement: All the authors report no relevant conflicts of interest for this article.

Data sharing statement: Technical appendix, statistical code, and dataset available from the corresponding author at wwl152559063@163.com. Participants gave informed consent for data sharing but the presented data are anonymized and risk of identification is low.

Country/Territory of origin: China

ORCID number: Yun-Jing Xue 0000-0003-4563-4763; Wei-Wen Lin 0009-0005-2317-3996.

S-Editor: Wang JJ
L-Editor: A
P-Editor: Zhao YQ

REFERENCES

1 **Sung H**, Ferlay J, Siegel RL, Laversanne M, Soerjomataram I, Jemal A, Bray F. Global Cancer Statistics 2020: GLOBOCAN Estimates of Incidence and Mortality Worldwide for 36 Cancers in 185 Countries. *CA Cancer J Clin* 2021; **71**: 209-249 [PMID: 33538338 DOI: 10.3322/caac.21660]

2 **Tan X**, Yang X, Hu S, Chen X, Sun Z. A nomogram for predicting postoperative complications based on tumor spectral CT parameters and visceral fat area in gastric cancer patients. *Eur J Radiol* 2023; **167**: 111072 [PMID: 37666073 DOI: 10.1016/j.ejrad.2023.111072]

3 **Hsu CP**, Chuang CY, Hsu PK, Chien LI, Lin CH, Yeh YC, Hsu HS, Wu YC. Lymphovascular Invasion as the Major Prognostic Factor in Node-Negative Esophageal Cancer After Primary Esophagectomy. *J Gastrointest Surg* 2020; **24**: 1459-1468 [PMID: 31273552 DOI: 10.1007/s11605-019-04310-0]

4 **Dobrițoiu M**, Stepan AE, Vere CC, Simionescu CE. Evaluation of Gastric Carcinomas Histological Patterns in Relation to Tumors Aggressiveness Parameters. *Curr Health Sci J* 2018; **44**: 342-346 [PMID: 31123609 DOI: 10.12865/CHSJ.44.04.03]

5 **Ajani JA**, D'Amico TA, Almhanna K, Bentrem DJ, Chao J, Das P, Denlinger CS, Fanta P, Farjah F, Fuchs CS, Gerdes H, Gibson M, Glasgow RE, Hayman JA, Hochwald S, Hofstetter WL, Ilson DH, Jaroszewski D, Johung KL, Keswani RN, Kleinberg LR, Korn WM, Leong S, Linn C, Lockhart AC, Ly QP, Mulcahy MF, Orringer MB, Perry KA, Poultsides GA, Scott WJ, Strong VE, Washington MK, Weksler B, Willett CG, Wright CD, Zelman D, McMillian N, Sundar H. Gastric Cancer, Version 3.2016, NCCN Clinical Practice Guidelines in Oncology. *J Natl Compr Canc Netw* 2016; **14**: 1286-1312 [PMID: 27697982 DOI: 10.6004/jnccn.2016.0137]

6 **Huang ZN**, Chen QY, Zheng CH, Li P, Xie JW, Wang JB, Lin JX, Lu J, Cao LL, Lin M, Tu RH, Lin JL, Zheng HL, Huang CM. Are the indications for postoperative radiotherapy in the NCCN guidelines for patients with gastric adenocarcinoma too broad? A study based on the SEER database. *BMC Cancer* 2018; **18**: 1064 [PMID: 30390644 DOI: 10.1186/s12885-018-4957-6]

7 **Selçukbiricik F**, Tural D, Büyükünal E, Serdengeçti S. Perineural invasion independent prognostic factors in patients with gastric cancer undergoing curative resection. *Asian Pac J Cancer Prev* 2012; **13**: 3149-3152 [PMID: 22994725]

8 **Chen X**, Yang Z, Yang J, Liao Y, Pang P, Fan W, Chen X. Radiomics analysis of contrast-enhanced CT predicts lymphovascular invasion and disease outcome in gastric cancer: a preliminary study. *Cancer Imaging* 2020; **20**: 24 [PMID: 32248822 DOI: 10.1186/s40644-020-00302-5]

9 **Yardımcı AH**, Koçak B, Turan Bektaş C, Sel İ, Yarıkkaya E, Dursun N, Bektaş H, Usul Afşar Ç, Gürsu RU, Kılıçkesmez Ö. Tubular gastric adenocarcinoma: machine learning-based CT texture analysis for predicting lymphovascular and perineural invasion. *Diagn Interv Radiol* 2020; **26**: 515-522 [PMID: 32990246 DOI: 10.5152/dir.2020.19507]

10 **Goo HW**, Goo JM. Dual-Energy CT: New Horizon in Medical Imaging. *Korean J Radiol* 2017; **18**: 555-569 [PMID: 28670151 DOI: 10.3348/kjr.2017.18.4.555]

11 **Li R**, Li J, Wang X, Liang P, Gao J. Detection of gastric cancer and its histological type based on iodine concentration in spectral CT. *Cancer Imaging* 2018; **18**: 42 [PMID: 30413174 DOI: 10.1186/s40644-018-0176-2]

12 **Hong YL**, Zhang YS, Ye F, Liu ZJ, Kang JH, Wang JA, Zeng Q. [Value of dual-layer spectral detector CT in preoperative prediction of lymph node metastasis of gastric cancer]. *Zhonghua Yi Xue Za Zhi* 2022; **102**: 1747-1752 [PMID: 35705478 DOI: 10.3760/cma.j.cn112137-20220207-00245]

13 **Wang R**, Li J, Fang MJ, Dong D, Liang P, Gao JB. [The value of spectral CT-based radiomics in preoperative prediction of lymph node metastasis of advanced gastric cancer]. *Zhonghua Yi Xue Za Zhi* 2020; **100**: 1617-1622 [PMID: 32486595 DOI: 10.3760/cma.j.cn112137-20191113-02468]

14 **Ren T**, Zhang W, Li S, Deng L, Xue C, Li Z, Liu S, Sun J, Zhou J. Combination of clinical and spectral-CT parameters for predicting lymphovascular and perineural invasion in gastric cancer. *Diagn Interv Imaging* 2022; **103**: 584-593 [PMID: 35934616 DOI: 10.1016/j.diii.2022.07.004]

15 **Kim JW**, Shin SS, Heo SH, Choi YD, Lim HS, Park YK, Park CH, Jeong YY, Kang HK. Diagnostic performance of 64-section CT using CT gastrography in preoperative T staging of gastric cancer according to 7th edition of AJCC cancer staging manual. *Eur Radiol* 2012; **22**: 654-662 [PMID: 21965037 DOI: 10.1007/s00330-011-2283-3]

16 **Yang YT**, Dong SY, Zhao J, Wang WT, Zeng MS, Rao SX. CT-detected extramural venous invasion is corelated with presence of lymph node metastasis and progression-free survival in gastric cancer. *Br J Radiol* 2020; **93**: 20200673 [PMID: 33002375 DOI: 10.1259/bjr.20200673]

17 **Wang Y**, Liu W, Yu Y, Liu JJ, Xue HD, Qi YF, Lei J, Yu JC, Jin ZY. CT radiomics nomogram for the preoperative prediction of lymph node metastasis in gastric cancer. *Eur Radiol* 2020; **30**: 976-986 [PMID: 31468157 DOI: 10.1007/s00330-019-06398-z]

18 **Borggreve AS**, Goense L, Brenkman HJF, Mook S, Meijer GJ, Wessels FJ, Verheij M, Jansen EPM, van Hillegersberg R, van Rossum PSN, Ruurda JP. Imaging strategies in the management of gastric cancer: current role and future potential of MRI. *Br J Radiol* 2019; **92**: 20181044 [PMID: 30789792 DOI: 10.1259/bjr.20181044]

19 **Tan CH**, Vikram R, Boonsirikamchai P, Bhosale P, Marcal L, Faria S, Charnsangavej C. Extramural venous invasion by gastrointestinal malignancies: CT appearances. *Abdom Imaging* 2011; **36**: 491-502 [PMID: 21184063 DOI: 10.1007/s00261-010-9667-8]

20 **Xu Y**, Zhang P, Zhang K, Huang C. The application of CA72-4 in the diagnosis, prognosis, and treatment of gastric cancer. *Biochim Biophys*

Acta Rev Cancer 2021; **1876**: 188634 [PMID: 34656687 DOI: 10.1016/j.bbcan.2021.188634]

21 **Feng F**, Tian Y, Xu G, Liu Z, Liu S, Zheng G, Guo M, Lian X, Fan D, Zhang H. Diagnostic and prognostic value of CEA, CA19-9, AFP and CA125 for early gastric cancer. *BMC Cancer* 2017; **17**: 737 [PMID: 29121872 DOI: 10.1186/s12885-017-3738-y]

22 **He B**, Zhang HQ, Xiong SP, Lu S, Wan YY, Song RF. Changing patterns of Serum CEA and CA199 for Evaluating the Response to First-line Chemotherapy in Patients with Advanced Gastric Adenocarcinoma. *Asian Pac J Cancer Prev* 2015; **16**: 3111-3116 [PMID: 25921105 DOI: 10.7314/apjcp.2015.16.8.3111]

23 **Wan Y**, Li Z, Ji N, Gao J. Comparison of gastric vascular anatomy by monochromatic and polychromatic dual-energy spectral computed tomography imaging. *J Int Med Res* 2014; **42**: 26-34 [PMID: 24435514 DOI: 10.1177/0300060513504703]

24 **Lv P**, Lin XZ, Chen K, Gao J. Spectral CT in patients with small HCC: investigation of image quality and diagnostic accuracy. *Eur Radiol* 2012; **22**: 2117-2124 [PMID: 22618521 DOI: 10.1007/s00330-012-2485-3]

25 **Li J**, Wang Y, Wang R, Gao JB, Qu JR. Spectral CT for preoperative prediction of lymphovascular invasion in resectable gastric cancer: With external prospective validation. *Front Oncol* 2022; **12**: 942425 [PMID: 36267965 DOI: 10.3389/fonc.2022.942425]

26 **Matsumoto K**, Jinzaki M, Tanami Y, Ueno A, Yamada M, Kuribayashi S. Virtual monochromatic spectral imaging with fast kilovoltage switching: improved image quality as compared with that obtained with conventional 120-kVp CT. *Radiology* 2011; **259**: 257-262 [PMID: 21330561 DOI: 10.1148/radiol.11100978]

World Journal of Gastroenterology

Submit a Manuscript: https://www.f6publishing.com

World J Gastroenterol 2024 February 14; 30(6): 556-564

DOI: 10.3748/wjg.v30.i6.556

ISSN 1007-9327 (print) ISSN 2219-2840 (online)

ORIGINAL ARTICLE

Clinical Trials Study

Optimized sequential therapy *vs* 10- and 14-d concomitant therapy for eradicating *Helicobacter pylori*: A randomized clinical trial

Hassan Seddik, Jihane Benass, Sanaa Berrag, Asmae Sair, Reda Berraida, Hanae Boutallaka

Specialty type: Gastroenterology and hepatology

Provenance and peer review: Unsolicited article; Externally peer reviewed.

Peer-review model: Single blind

Peer-review report's scientific quality classification

Grade A (Excellent): 0
Grade B (Very good): 0
Grade C (Good): C, C
Grade D (Fair): 0
Grade E (Poor): 0

P-Reviewer: Bordin DS, Russia; Cheng H, China

Received: October 6, 2023
Peer-review started: October 6, 2023
First decision: November 12, 2023
Revised: November 26, 2023
Accepted: December 29, 2023
Article in press: December 29, 2023
Published online: February 14, 2024

Hassan Seddik, Jihane Benass, Asmae Sair, Reda Berraida, Hanae Boutallaka, Department of Gastroenterology II, Mohammed V Military Teaching Hospital of Rabat, Rabat 10100, Morocco

Hassan Seddik, Jihane Benass, Sanaa Berrag, Asmae Sair, Reda Berraida, Hanae Boutallaka, Department of Gastroenterology, Mohammed V University in Rabat, Rabat 10100, Morocco

Sanaa Berrag, Department of Gastroenterology I, Mohammed V Military Teaching Hospital of Rabat, Rabat 10100, Morocco

Corresponding author: Jihane Benass, MD, Senior Resident, Department of Gastroenterology II, Mohammed V Military Teaching Hospital of Rabat, Avenue des Forces Armées Royales, Rabat 10100, Morocco. jihane.benass@gmail.com

Abstract

BACKGROUND

A cure for *Helicobacter pylori* (*H. pylori*) remains a problem of global concern. The prevalence of antimicrobial resistance is widely rising and becoming a challenging issue worldwide. Optimizing sequential therapy seems to be one of the most attractive strategies in terms of efficacy, tolerability and cost. The most common sequential therapy consists of a dual therapy [proton-pump inhibitors (PPIs) and amoxicillin] for the first period (5 to 7 d), followed by a triple therapy for the second period (PPI, clarithromycin and metronidazole). PPIs play a key role in maintaining a gastric pH at a level that allows an optimal efficacy of antibiotics, hence the idea of using new generation molecules.

AIM

To compare an optimized sequential therapy with the standard non-bismuth quadruple therapies of 10 and 14 d, in terms of efficacy, incidence of adverse effects (AEs) and cost.

METHODS

This open-label prospective study randomized 328 patients with confirmed *H. pylori* infection into three groups (1:1:1): The first group received quadruple therapy consisting of twice-daily (bid) omeprazole 20 mg, amoxicillin 1 g, clarithromycin 500 mg and metronidazole 500 mg for 10 d (QT-10), the second group received a 14 d quadruple therapy following the same regimen (QT-14), and the third group received an optimized sequential therapy consisting of bid rabe-

prazole 20 mg plus amoxicillin 1 g for 7 d, followed by bid rabeprazole 20 mg, clarithromycin 500 mg and metronidazole 500 mg for the next 7 d (OST-14). AEs were recorded throughout the study, and the *H. pylori* eradication rate was determined 4 to 6 wk after the end of treatment, using the 13C urea breath test.

RESULTS

In the intention-to-treat and per-protocol analysis, the eradication rate was higher in the OST-14 group compared to the QT-10 group: (93.5%, 85.5% $P = 0.04$) and (96.2%, 89.5% $P = 0.03$) respectively. However, there was no statistically significant difference in eradication rates between the OST-14 and QT-14 groups: (93.5%, 91.8% $P = 0.34$) and (96.2%, 94.4% $P = 0.35$), respectively. The overall incidence of AEs was significantly lower in the OST-14 group ($P = 0.01$). Furthermore, OST-14 was the most cost-effective among the three groups.

CONCLUSION

The optimized 14-d sequential therapy is a safe and effective alternative. Its eradication rate is comparable to that of the 14-d concomitant therapy while causing fewer AEs and allowing a gain in terms of cost.

Key Words: *Helicobacter pylori*; Quadruple therapy; Sequential; Proton-pump inhibitor; Optimization

Core Tip: *Helicobacter pylori* infection remains a common infection worldwide. The decline in the efficacy of traditional triple therapies since 2010 has required new combinations of antibiotics. The last guidelines of Maastricht VI recommend bismuth quadruple therapies or concomitant quadruple therapies to reach an eradication rate of at least 90%. These values remain higher than those obtained with standard sequential therapy but are associated with a higher cost and more adverse effects (AEs). The results of the present study demonstrate that optimizing sequential therapy by using second-generation proton-pump inhibitors improved eradication rates and reduced AE incidence. This combination can thus be suggested for use in clinical practice.

Citation: Seddik H, Benass J, Berrag S, Sair A, Berraida R, Boutallaka H. Optimized sequential therapy *vs* 10- and 14-d concomitant therapy for eradicating *Helicobacter pylori*: A randomized clinical trial. *World J Gastroenterol* 2024; 30(6): 556-564
URL: https://www.wjgnet.com/1007-9327/full/v30/i6/556.htm
DOI: https://dx.doi.org/10.3748/wjg.v30.i6.556

INTRODUCTION

A cure for *Helicobacter pylori* (*H. pylori*) remains a problem of global concern[1]. This bacterium is a well-known cause of peptic ulcer, gastritis, gastric mucosa-associated lymphoid tissue lymphoma and gastric malignancies[2-4]. *H. pylori* eradication is thus an effective strategy in preventing gastric malignancies[5,6].

Even though *H. pylori* infection management is evolving, no regimen can currently achieve a cure rate of 100%. The most recent Maastricht VI consensus recommends (in the absence of antibiotic susceptibility testing) quadruple Bismuth therapy or non-Bismuth quadruple concomitant therapy to achieve a cure rate of at least 90% despite the association of both regimens with a significant rate of adverse effects (AEs)[7]. Furthermore, the prevalence of antimicrobial resistance is widely rising and becoming a problem of great interest worldwide[8]; in Morocco, a previous study showed clarithromycin resistance of more than 15%[9]. Therefore, the best strategy to increase *H. pylori* eradication rate would be a personalized treatment based on antibiotic susceptibility[10].

However, this strategy is not possible in many developing countries, which is why many studies have instead focused on optimizing the recommended regimens[11]. It can either be an optimization by extending the length of the protocol [12], using a higher dose and/or second-generation proton-pump inhibitors (PPIs) or switching to vonoprazan[13,14], changing the antibiotics used and their posology, or associating other molecules to the eradication protocol, such as probiotics[15].

Optimizing the sequential therapy seems to be one of the most attractive strategies in terms of efficacy, tolerability and cost. The most common sequential therapy consists of a dual therapy (PPI and amoxicillin) for the first period (5 to 7 d), followed by a triple therapy for the second period (PPI, clarithromycin and metronidazole). PPIs play a key role in maintaining a gastric pH at a level that allows optimal antibiotic efficacy[16], hence the idea of using new generation molecules.

The primary aim of this study was to compare the efficacy of the 14-d sequential therapy (optimized by using a second-generation PPI) and standard non-bismuth quadruple therapies of 10 and 14 d. The secondary aims were to compare the tolerability and AEs among the groups, as well as their cost-effectiveness.

MATERIALS AND METHODS

Study design and patient selection

This was a single center, prospective, open-label, randomized study, conducted between January 2018 and March 2020, at the Mohammed V Military Teaching Hospital of Rabat. We included adult patients with *H. pylori* infection confirmed by histological analysis of gastric biopsies performed during upper endoscopy. Five gastric biopsy samples were taken systematically according to the recommended Sydney system (antrum, incisura, greater and lesser curvature)[17], and then studied for the presence of *H. pylori* using Hematoxylin and eosin staining at the pathology laboratory of our hospital. Patients who previously received an eradication therapy, PPI, H_2-blockers, non-steroidal anti-inflammatory drugs or Bismuth containing compounds 4 wk prior to the study, and/or patients who were allergic to the prescribed antibiotics were excluded from the study. Pregnant and breastfeeding females, patients with history of gastric surgery, kidney or liver failure, or severe psychiatric conditions were also excluded. All patients provided written informed consent to be included in the study. The protocol followed Helsinki Declaration guidelines and was approved by our local scientific committee at Mohammed V Military Teaching Hospital of Rabat. Our clinical trial was registered in the Pan African Clinical Trial Registry (www.pactr.org) on December 7, 2021, registration number: PACTR202112632957229.

Randomization and treatment

Patients were randomly assigned into three groups in a 1:1:1 ratio, using a computer-generated table: QT-14, QT-10 and OST-14. Allocations were concealed in a sealed opaque envelope which was to be opened during the consultation day. The QT-14 and QT-10 groups received omeprazole 20 mg, amoxicillin 1 g, clarithromycin 500 mg and metronidazole 500 mg, all twice daily for 14 and 10 d, respectively. The OST-14 group received an optimized sequential therapy consisting of twice daily rabeprazole 20 mg and amoxicillin 1 g during 7 d, followed by rabeprazole 20 mg, clarithromycin 500 mg and metronidazole 500 mg, all twice daily for the remaining 7 d. PPI was administered 30 min before breakfast and supper, whereas antibiotics were administered every 12 h after meals.

Follow-up and outcomes

The *H. pylori* eradication was assessed at least 4 wk after the last day of the treatment using the 13C-urea breath test (UBT), which was performed blindly at the same laboratory for all patients. The cut-off value for the UBT was 2.5 per thousand. The patients did not undergo additional therapy with PPI after completion of eradication therapy.

All patients were evaluated 2 wk after the start of the treatment and at its end to assess AEs and compliance. Drug compliance was defined by taking at least 90% of the prescribed protocol drugs and was assessed at the end of the protocol. AEs were assessed using a pre-established structured questionnaire consisting of dichotomous questions about the occurrence and intensity of AEs including diarrhea, nausea and/or vomiting, gastralgia, metallic taste, dysgeusia, symptoms related to an allergic reaction, headache, dizziness, asthenia, or any other AE.

Cost-effectiveness analysis was assessed by comparing the overall cost of each protocol. The cost of every drug was calculated using a national website: www.medicament.ma. The cost-effectiveness ratio for each regimen was calculated by dividing the total cost for 100 patients treated by the percent of patients treated.

Statistical analysis

This study sample size was determined as follows. We presumed the eradication rate of OST-14 to be 95% and the eradication rate of QT-10 to be 83% (lowest eradication rate of the three treatment regimens). By setting the bilateral significance level to 0.05, the power to 80% and the drop-out rate to 5%, at least 104 patients were required in each group. Our hypothesis on the QT-10 eradication rate was based on a previous meta-analysis[18].

The primary endpoint of the study was the eradication rate of *H. pylori*, which was assessed by intention to treat (ITT) and per-protocol (PP) analyses. The safety population included all randomized patients who received at least one treatment dose during the study, ITT population included all patients who received at least one treatment dose during the study and who were examined during the first visit, while the PP population included only patients who completed the study. Therapeutic failure was recorded as outcome for patients with missing data due to incomplete treatment. The secondary outcomes were the incidence of AEs, the therapeutic compliance and the cost-effectiveness of the protocols.

Descriptive and inferential statistical analyses were performed using Software Package Social Science SPSS® for mac OS version 22.0 (IBM Corp, Armonk, NY, United States). For all statistical analyses, P value less than 0.05 was considered statistically significant. Qualitative variables (eradication rates of the three groups) were compared using χ^2 test and Fisher's exact test. Continuous variables were compared between the three groups using a one-way ANOVA test.

RESULTS

Population characteristics

A total of 328 patients were enrolled in the study. They were included in the ITT analysis and randomized into the three groups. After eliminating the dropped-out patients from the study, the PP analysis included 317 patients. The study flow chart is shown in Figure 1. Demographic and clinical characteristics of the three groups are shown in Table 1 and were not significantly different between the groups.

Table 1 Basic overall population and group characteristics

Characteristic	Overall, *n* = 317	QT-14, *n* = 107	QT-10, *n* = 105	OST-14, *n* = 105	*P* value
Age in yr, mean ± SD	44.13 ± 15.30	43.37 ± 14.40	43.36 ± 15.9	45.67 ± 15.53	0.46
Sex ratio as male/female	0.98	1.03	1	0.92	0.91
Smoking habit	49 (14.9)	18 (16.4)	14 (12.7)	17 (15.7)	0.62
Gastroduodenal ulcer	47 (14.3)	22 (20)	13 (11.8)	12 (11.1)	0.16
Gastric atrophy	51 (15.5)	14 (12.7)	18 (16.4)	19 (17.6)	0.58
Gastric metaplasia	18 (5.5)	7 (6.4)	8 (7.3)	3 (2.8)	0.26
HP antral density					0.30
+	114 (34.9)	37 (33.9)	37 (33.6)	40 (37)	
++	170 (52)	58 (53.2)	56 (50.9)	56 (51.9)	
+++	35 (10.7)	11 (10.1)	12 (10.9)	12 (11.1)	
HP fundic density					0.74
+	147 (44.8)	54 (49.1)	46 (41.8)	47 (43.5)	
++	62 (18.9)	20 (18.2)	22 (20)	20 (18.5)	
+++	7 (2.1)	1 (0.9)	2 (1.8)	4 (3.7)	

All values are expressed as *n* (%) unless otherwise stated. +: Sparse; ++: Moderate; +++: Marked. HP: *Helicobacter pylori*; SD: Standard deviation.

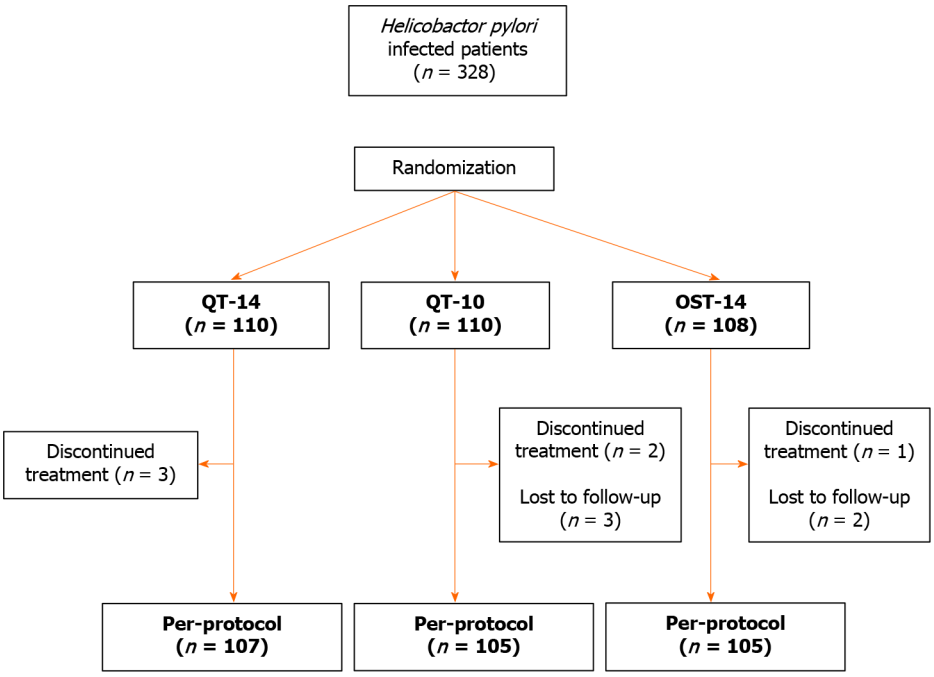

DOI: 10.3748/wjg.v30.i6.556

Figure 1 Flow-chart of study patients.

Eradication rates

In the ITT analysis, *H. pylori* eradication was achieved in 85.5% of patients in the QT-10 group, 91.8% of patients in the QT-14 group, and 93.5% of patients in the OST-14 group. In the PP analysis, the results were as follows: 89.5%, 94.4%, and 96.2% in the QT-10, QT-14, and OST-14 groups, respectively.

Comparison of eradication rates

The eradication rate in the OST-14 group was higher compared to the QT-10 group in the ITT analysis (P = 0.04) and in the PP analysis (0.03). However, there was no statistically significant difference between the eradication rate of OST-14 and QT-14 groups (in ITT analysis: P = 0.34, in PP analysis P = 0.35).

Safety

The treatment tolerance was better in the OST-14 group, with an incidence of AEs of 24.7% compared to 42.7% and 39% in the QT-14 and QT-10, respectively (P = 0.03) (Table 2). However, the treatment was globally well tolerated among the three groups, and AEs were mild to moderate in all patients. The drug compliance was excellent among the three groups: 97%, 95% and 98.9% in the QT-10, QT-14 and OST-14, respectively (P = 0.48).

Cost-effectiveness

The overall cost was lower in the OST-14 group [427.10 Moroccan dirhams (MAD)], compared to QT-14 and QT-10 groups (691.90 MAD and 587.10 MAD, respectively). The cost-effectiveness ratio was lower in the OST-14 group, as shown in Table 3.

DISCUSSION

According to the Maastricht VI consensus, the most recommended empirical regimens for *H. pylori* infection are Bismuth quadruple therapy and non-Bismuth quadruple concomitant therapy[7]. However, eradication rates widely vary geographically due to varying antimicrobial resistance, especially to clarithromycin and metronidazole[19].

It is important to note that the *H. pylori* eradication rate is significantly influenced by antibiotic resistance. Furthermore, the bismuth agent is not available in all areas. Therefore, in areas where *H. pylori* is highly resistant to clarithromycin, non-bismuth quadruple therapies are still recommended when the bismuth agent is not available.

Several non-bismuth regimens have been tested to improve the management of *H. pylori* infection[20,21]. One of them is modified sequential therapy[12,22]. In the present study, we aimed to compare the results of the standard 10- and 14-d non-bismuth quadruple therapies to an optimized sequential therapy by using a second-generation PPI.

Overall, we found that the optimized 14-d sequential regimen using rabeprazole (OST-14) achieves a higher cure rate than the standard quadruple therapy without bismuth for 10 d (85.5% and 93.5%, respectively, P = 0.04), while there was no statistically significant difference between OST-14 and the 14-d quadruple therapy (93.2% and 91.8%, respectively, P = 0.34). OST-14 allowed a greater tolerance with fewer AEs compared to quadruple therapies (P = 0.01), and there was no difference in term of drugs compliance between the three groups. Furthermore, the cost-effectiveness ratio was lower in the OST-14 group.

The sequential therapy was introduced for the first time in 2000 in Italy by Zullo *et al*[23]. We personally demonstrated its superiority compared to the standard triple therapy in a previous study[24]. A recent metanalysis by Wang *et al*[18] showed that there is no difference in terms of eradication rate between a 14-d sequential and a 14-d concomitant therapy. Another study showed that a 14-d sequential therapy is equivalent to 10 d bismuth quadruple therapy in terms of eradication rate (91.3% and 91.6%, respectively), but bismuth therapy led to more AEs[25]. In a metanalysis, the same team demonstrated that a 14-d sequential therapy is more effective than a 14-d triple therapy[26].

In the present study, the gain in terms of eradication rate can be explained by the use of a second generation PPI (rabeprazole 20 mg bid) in the OST-14 group. In fact, the last Maastricht consensus states that switching omeprazole 20 mg twice daily to rabeprazole 20 mg bid or esomeprazole 40 mg bid may increase eradication rate by 8%-12%[7]. The advantage of PPIs lies in the fact that the majority of proposed regimens are pH-dependent and become less effective when the intragastric pH is low[27], hence the use of higher dose PPIs and second-generation substances. A possible explanation for the superiority of second-generation PPIs (rabeprazole and esomeprazole) may be their metabolism, which is less dependent on CYP2C19 genetic variables and their higher acid inhibition power[28]. A further metanalysis by McNichol *et al*[29] confirmed that both esomeprazole and rabeprazole led to higher eradication rates compared to first generation PPIs (omeprazole, lansoprazole and pantoprazole). High doses of PPIs also improved the efficacy of eradication therapy. In strains resistant to clarithromycin, the eradication rate can be increased using PPI-amoxicillin dual therapy[30].

All therapeutic regimens currently recommended are associated with gastrointestinal AEs[31]. Herein, OST-14 allowed a gain in terms of AE incidence compared to quadruple concomitant therapies. These findings confirm those of previous studies[32-34]. The 14-d sequential therapy consists of the same antibiotics as the 14-d concomitant regimen but for a shorter duration. It should therefore lead to fewer AEs. This was the case in our study with a benefit of 18% in terms of AE occurrence (31.3% *vs* 49.5%; P = 0.03). Because treatment cost is a determining factor, especially in developing countries, we carried-out cost- effectiveness analysis and showed that OST-14 is the most cost-effective among our study's groups. The same result was previously reported by Farhoud *et al*[33], who found that 14-d sequential therapy is cheaper than 14-d triple therapy. Further, Kate *et al*[35] confirmed in a metanalysis that sequential therapies are cheaper than standard therapies. Other cost-analysis studies have shown the same results and found that sequential therapy is the most economically attractive option[36,37]. This benefit can be explained by the fact that clarithromycin is the most expensive drug used in different protocols, and it is used for a shorter duration in sequential therapy.

One of the limitations of this study is that we did not perform *H. pylori* cultures and did not have any data about antibiotic susceptibility. However, a recent study showed that in Morocco, the local primary resistance to clarithromycin was 29%, 40% to metronidazole and 0% to amoxicillin[9]. Another potential limitation is that second line treatments were not included, which makes it difficult to interpret the cost effectiveness analysis. Additionally, it is difficult to generalize our results to other areas, as the study was conducted in a single center. Nonetheless, the sample size was reasonable to allow for correct statistical analysis. However, our results should be validated by further studies in different geographic areas. Other studies could further compare these eradication regimens to others containing vonoprazan. For the moment, this molecule is still not available in Morocco.

Table 2 Incidence of adverse effects among the study groups

Analysis	QT-10	QT-14	OST-14	*P* value[1]
ITT	39%	42.7%	24.7%	0.03
PP	45.1%	49.5%	31.3%	0.01

[1]*P* value of χ^2 test.
ITT: Intention to treat; PP: Per-protocol.

Table 3 Cost-effectiveness ratio in the three protocols costs, expressed in Moroccan dirhams

Therapeutic protocol	Overall cost of 100 patients	Effectiveness	Cost-effectiveness ratio
QT-10	58710	89.5%	655
QT-14	69190	94.4%	732
OST-14	42710	98.1%	435

CONCLUSION

In conclusion, the results of the present study showed that the 14-d sequential therapy using rabeprazole appears to be an optimal therapy that is comparable to 14-d concomitant therapy while causing fewer AEs and allowing a gain in terms of cost.

ARTICLE HIGHLIGHTS

Research background

A cure for *Helicobacter pylori* (*H. pylori*) remains a problem of global concern and none of the currently available treatments can achieve a cure rate of 100%. With the global rising issue of antibiotic resistance and the difficulty to establish personalized treatments according to antibiotic susceptibility in developing countries, optimizing sequential therapy seems to be one of the most attractive strategies in terms of efficacy, tolerability and cost.

Research motivation

H. pylori eradication rate is significantly influenced by antibiotic resistance. According to the Maastricht VI consensus, the most recommended empirical regimens for *H. pylori* infection are Bismuth quadruple therapy and non-Bismuth quadruple concomitant therapy when the Bismuth agent is not available. Many studies showed that switching to high doses of second-generation proton-pump inhibitors (PPIs) and using a PPI-amoxicillin dual therapy can improve the eradication rate and could lead to fewer adverse effects (AEs). The cost of treatment is also a determining factor, especially in developing countries.

Research objectives

In the present study, we aimed to compare the results of the standard 10- and 14-d non-bismuth quadruple therapies to an optimized sequential therapy by using a second-generation PPI, in terms of efficacy, tolerability and cost-effectiveness. The 14-d sequential therapy using rabeprazole appears to be an optimal therapy that is comparable to 14-d concomitant therapy while causing fewer AEs and allowing a gain in terms of cost. Other studies could further validate the standard eradication regimens *vs* the 14-d sequential therapy using rabeprazole *vs* other regimens containing vonoprazan. For the moment, this molecule is still not available in Morocco.

Research methods

We conducted a single center, prospective, open-label, randomized study with patients randomly assigned into three groups in a 1:1:1 ratio using a computer-generated table: QT-14, QT-10 and OST-14. Allocations were concealed in a sealed opaque envelope to be opened during the consultation day.

Research results

This study showed that the 14-d sequential therapy using rabeprazole appears to be an optimal therapy that is comparable to 14-d concomitant therapy while causing fewer AEs and allowing a gain in terms of cost.

Research conclusions

According to the Maastricht VI consensus, the most recommended empirical regimens for *H. pylori* infection are Bismuth

quadruple therapy and non-Bismuth quadruple concomitant therapy. This study suggests the use of an optimized 14-d sequential regimen using rabeprazole to achieve the same eradication rate as the non-bismuth quadruple concomitant therapy while leading to fewer AEs and being more economically attractive.

Research perspectives

Given our study's limitations, these are several future research perspectives: (1) Conduct a multicenter trial (in different geographical areas) to validate our results; (2) Compare the sequential therapy to other therapies containing vonoprazan; and (3) Compare the use of esomeprazole and rabeprazole in a sequential therapy in terms of efficacy, tolerability and cost-effectiveness.

FOOTNOTES

Author contributions: Seddik H was responsible for study concept and planning and supervised the statistical analysis and manuscript revision; Benass J and Boutallaka H were involved in performing the statistical analysis and writing the manuscript, with input from all authors; Berrag S, Sair A, and Berraida R were involved in patient enrollment and data collection and were involved in manuscript preparation; All authors reviewed the manuscript.

Institutional review board statement: An Institutional Review Board (Scientific committee at Mohammed V Military Teaching Hospital of Rabat) reviewed and approved the trial protocol. Our study was performed in accordance with the ethical standards as laid down in the 1964 Declaration of Helsinki and its later amendments.

Clinical trial registration statement: Our clinical trial has been retrospectively registered in the Pan African Clinical Trial Registry (www.pactr.org) on December 7, 2021, Registration No.: PACTR202112632957229.

Informed consent statement: All patients included in the study provided written informed consent before being enrolled in the trial.

Conflict-of-interest statement: The authors report having no relevant conflicts of interest for this article.

Data sharing statement: The datasets generated and/or analyzed during the study are available from the corresponding author on reasonable request.

CONSORT 2010 statement: The authors have read the CONSORT 2010 Statement, and the manuscript was prepared and revised according to the CONSORT 2010 Statement.

Country/Territory of origin: Morocco

ORCID number: Hassan Seddik 0000-0002-6801-210X; Jihane Benass 0000-0002-8525-1516; Sanaa Berrag 0000-0001-5993-4068; Reda Berraida 0000-0002-8138-0785; Hanae Boutallaka 0000-0002-8496-694X.

S-Editor: Wang JJ
L-Editor: Filipodia
P-Editor: Yuan YY

REFERENCES

1 **Gatta L**, Vakil N, Vaira D, Scarpignato C. Global eradication rates for Helicobacter pylori infection: systematic review and meta-analysis of sequential therapy. *BMJ* 2013; **347**: f4587 [PMID: 23926315 DOI: 10.1136/bmj.f4587]
2 **Malfertheiner P**, Megraud F, O'Morain CA, Atherton J, Axon AT, Bazzoli F, Gensini GF, Gisbert JP, Graham DY, Rokkas T, El-Omar EM, Kuipers EJ; European Helicobacter Study Group. Management of Helicobacter pylori infection--the Maastricht IV/ Florence Consensus Report. *Gut* 2012; **61**: 646-664 [PMID: 22491499 DOI: 10.1136/gutjnl-2012-302084]
3 **Uemura N**, Okamoto S, Yamamoto S, Matsumura N, Yamaguchi S, Yamakido M, Taniyama K, Sasaki N, Schlemper RJ. Helicobacter pylori infection and the development of gastric cancer. *N Engl J Med* 2001; **345**: 784-789 [PMID: 11556297 DOI: 10.1056/NEJMoa001999]
4 **Alakkari A**, Zullo A, O'Connor HJ. Helicobacter pylori and nonmalignant diseases. *Helicobacter* 2011; **16** Suppl 1: 33-37 [PMID: 21896083 DOI: 10.1111/j.1523-5378.2011.00878.x]
5 **Herrero R**, Park JY, Forman D. The fight against gastric cancer - the IARC Working Group report. *Best Pract Res Clin Gastroenterol* 2014; **28**: 1107-1114 [PMID: 25439075 DOI: 10.1016/j.bpg.2014.10.003]
6 **Tsukamoto T**, Nakagawa M, Kiriyama Y, Toyoda T, Cao X. Prevention of Gastric Cancer: Eradication of Helicobacter Pylori and Beyond. *Int J Mol Sci* 2017; **18** [PMID: 28771198 DOI: 10.3390/ijms18081699]
7 **Malfertheiner P**, Megraud F, Rokkas T, Gisbert JP, Liou JM, Schulz C, Gasbarrini A, Hunt RH, Leja M, O'Morain C, Rugge M, Suerbaum S,

Tilg H, Sugano K, El-Omar EM; European Helicobacter and Microbiota Study group. Management of Helicobacter pylori infection: the Maastricht VI/Florence consensus report. *Gut* 2022 [PMID: 35944925 DOI: 10.1136/gutjnl-2022-327745]

8 **Meyer JM**, Silliman NP, Wang W, Siepman NY, Sugg JE, Morris D, Zhang J, Bhattacharyya H, King EC, Hopkins RJ. Risk factors for Helicobacter pylori resistance in the United States: the surveillance of H. pylori antimicrobial resistance partnership (SHARP) study, 1993-1999. *Ann Intern Med* 2002; **136**: 13-24 [PMID: 11777360 DOI: 10.7326/0003-4819-136-1-200201010-00008]

9 **Bouihat N**, Burucoa C, Benkirane A, Seddik H, Sentissi S, Al Bouzidi A, Elouennas M, Benouda A. Helicobacter pylori Primary Antibiotic Resistance in 2015 in Morocco: A Phenotypic and Genotypic Prospective and Multicenter Study. *Microb Drug Resist* 2017; **23**: 727-732 [PMID: 27996373 DOI: 10.1089/mdr.2016.0264]

10 **Liou JM**, Chen PY, Kuo YT, Wu MS; Taiwan Gastrointestinal Disease and Helicobacter Consortium. Toward population specific and personalized treatment of Helicobacter pylori infection. *J Biomed Sci* 2018; **25**: 70 [PMID: 30285834 DOI: 10.1186/s12929-018-0471-z]

11 **Gisbert JP**, McNicholl AG. Optimization strategies aimed to increase the efficacy of H. pylori eradication therapies. *Helicobacter* 2017; **22** [PMID: 28464347 DOI: 10.1111/hel.12392]

12 **Zullo A**, De Francesco V, Hassan C, Ridola L, Repici A, Bruzzese V, Vaira D. Modified sequential therapy regimens for Helicobacter pylori eradication: a systematic review. *Dig Liver Dis* 2013; **45**: 18-22 [PMID: 23022424 DOI: 10.1016/j.dld.2012.08.025]

13 **Sachs G**, Shin JM, Munson K, Vagin O, Lambrecht N, Scott DR, Weeks DL, Melchers K. Review article: the control of gastric acid and Helicobacter pylori eradication. *Aliment Pharmacol Ther* 2000; **14**: 1383-1401 [PMID: 11069309 DOI: 10.1046/j.1365-2036.2000.00837.x]

14 **Li M**, Oshima T, Horikawa T, Tozawa K, Tomita T, Fukui H, Watari J, Miwa H. Systematic review with meta-analysis: Vonoprazan, a potent acid blocker, is superior to proton-pump inhibitors for eradication of clarithromycin-resistant strains of Helicobacter pylori. *Helicobacter* 2018; **23**: e12495 [PMID: 29873436 DOI: 10.1111/hel.12495]

15 **Seddik H**, Boutallaka H, Elkoti I, Nejjari F, Berraida R, Berrag S, Loubaris K, Sentissi S, Benkirane A. Saccharomyces boulardii CNCM I-745 plus sequential therapy for Helicobacter pylori infections: a randomized, open-label trial. *Eur J Clin Pharmacol* 2019; **75**: 639-645 [PMID: 30694338 DOI: 10.1007/s00228-019-02625-0]

16 **Miner P Jr**, Katz PO, Chen Y, Sostek M. Gastric acid control with esomeprazole, lansoprazole, omeprazole, pantoprazole, and rabeprazole: a five-way crossover study. *Am J Gastroenterol* 2003; **98**: 2616-2620 [PMID: 14687806 DOI: 10.1111/j.1572-0241.2003.08783.x]

17 **Misiewicz JJ**. The Sydney System: a new classification of gastritis. Introduction. *J Gastroenterol Hepatol* 1991; **6**: 207-208 [PMID: 1912430 DOI: 10.1111/j.1440-1746.1991.tb01467.x]

18 **Wang Y**, Zhao R, Wang B, Zhao Q, Li Z, Zhu-Ge L, Yin W, Xie Y. Sequential versus concomitant therapy for treatment of Helicobacter pylori infection: an updated systematic review and meta-analysis. *Eur J Clin Pharmacol* 2018; **74**: 1-13 [PMID: 28990120 DOI: 10.1007/s00228-017-2347-7]

19 **Flores-Treviño S**, Mendoza-Olazarán S, Bocanegra-Ibarias P, Maldonado-Garza HJ, Garza-González E. Helicobacter pylori drug resistance: therapy changes and challenges. *Expert Rev Gastroenterol Hepatol* 2018; **12**: 819-827 [PMID: 29976092 DOI: 10.1080/17474124.2018.1496017]

20 **Yang JC**, Lu CW, Lin CJ. Treatment of Helicobacter pylori infection: current status and future concepts. *World J Gastroenterol* 2014; **20**: 5283-5293 [PMID: 24833858 DOI: 10.3748/wjg.v20.i18.5283]

21 **Georgopoulos SD**, Papastergiou V, Karatapanis S. Treatment of Helicobacter Pylori infection: optimization strategies in a high resistance era. *Expert Opin Pharmacother* 2015; **16**: 2307-2317 [PMID: 26330278 DOI: 10.1517/14656566.2015.1084503]

22 **Liao XM**, Nong GH, Chen MZ, Huang XP, Cong YY, Huang YY, Wu BH, Wei JQ. Modified sequential therapy vs quadruple therapy as initial therapy in patients with Helicobacter infection. *World J Gastroenterol* 2015; **21**: 6310-6316 [PMID: 26034367 DOI: 10.3748/wjg.v21.i20.6310]

23 **Zullo A**, Rinaldi V, Winn S, Meddi P, Lionetti R, Hassan C, Ripani C, Tomaselli G, Attili AF. A new highly effective short-term therapy schedule for Helicobacter pylori eradication. *Aliment Pharmacol Ther* 2000; **14**: 715-718 [PMID: 10848654 DOI: 10.1046/j.1365-2036.2000.00766.x]

24 **Seddik H**, Ahid S, El Adioui T, El Hamdi FZ, Hassar M, Abouqal R, Cherrah Y, Benkirane A. Sequential therapy versus standard triple-drug therapy for Helicobacter pylori eradication: a prospective randomized study. *Eur J Clin Pharmacol* 2013; **69**: 1709-1715 [PMID: 23695545 DOI: 10.1007/s00228-013-1524-6]

25 **Liou JM**, Chen CC, Fang YJ, Chen PY, Chang CY, Chou CK, Chen MJ, Tseng CH, Lee JY, Yang TH, Chiu MC, Yu JJ, Kuo CC, Luo JC, Hsu WF, Hu WH, Tsai MH, Lin JT, Shun CT, Twu G, Lee YC, Bair MJ, Wu MS; Members of the Taiwan Gastrointestinal Disease and Helicobacter Consortium. 14 day sequential therapy versus 10 day bismuth quadruple therapy containing high-dose esomeprazole in the first-line and second-line treatment of Helicobacter pylori: a multicentre, non-inferiority, randomized trial. *J Antimicrob Chemother* 2018; **73**: 2510-2518 [PMID: 29846605 DOI: 10.1093/jac/dky183]

26 **Liou JM**, Chen CC, Lee YC, Chang CY, Wu JY, Bair MJ, Lin JT, Chen MJ, Wu MS; Taiwan Gastrointestinal Disease and Helicobacter Consortium. Systematic review with meta-analysis: 10- or 14-day sequential therapy vs. 14-day triple therapy in the first line treatment of Helicobacter pylori infection. *Aliment Pharmacol Ther* 2016; **43**: 470-481 [PMID: 26669729 DOI: 10.1111/apt.13495]

27 **Graham DY**, Lu H, Dore MP. Relative potency of proton-pump inhibitors, Helicobacter pylori therapy cure rates, and meaning of double-dose PPI. *Helicobacter* 2019; **24**: e12554 [PMID: 30440097 DOI: 10.1111/hel.12554]

28 **Ierardi E**, Losurdo G, Fortezza RF, Principi M, Barone M, Leo AD. Optimizing proton pump inhibitors in Helicobacter pylori treatment: Old and new tricks to improve effectiveness. *World J Gastroenterol* 2019; **25**: 5097-5104 [PMID: 31558859 DOI: 10.3748/wjg.v25.i34.5097]

29 **McNicholl AG**, Linares PM, Nyssen OP, Calvet X, Gisbert JP. Meta-analysis: esomeprazole or rabeprazole vs. first-generation pump inhibitors in the treatment of Helicobacter pylori infection. *Aliment Pharmacol Ther* 2012; **36**: 414-425 [PMID: 22803691 DOI: 10.1111/j.1365-2036.2012.05211.x]

30 **Xu X**, He C, Zhu Y. Treatment of refractory Helicobacter pylori infection: A new challenge for clinicians. *Front Microbiol* 2022; **13**: 998240 [PMID: 36329840 DOI: 10.3389/fmicb.2022.998240]

31 **Kwon SB**, Lee KL, Kim JS, Lee JK, Kim W, Jung YJ, Jeong JB, Kim JW, Kim BG. Antibiotics-associated diarrhea and other gastrointestinal abnormal responses regarding Helicobacter pylori eradication. *Korean J Gastroenterol* 2010; **56**: 229-235 [PMID: 20962558 DOI: 10.4166/kjg.2010.56.4.229]

32 **Eisig JN**, Navarro-Rodriguez T, Teixeira AC, Silva FM, Mattar R, Chinzon D, Haro C, Diniz MA, Moraes-Filho JP, Fass R, Barbuti RC. Standard Triple Therapy versus Sequential Therapy in Helicobacter pylori Eradication: A Double-Blind, Randomized, and Controlled Trial. *Gastroenterol Res Pract* 2015; **2015**: 818043 [PMID: 26064098 DOI: 10.1155/2015/818043]

33 **Farhoud NS**, Ibrahim OM, Ezzat SE. Efficacy and Cost-effectiveness Comparison of 10-Day, 14-Day Sequential Versus 14-Day Triple

Therapies for Treating Helicobacter pylori Infection in Egyptian Patients. *J Clin Gastroenterol* 2020; **54**: 806-812 [PMID: 31904681 DOI: 10.1097/MCG.0000000000001278]

34 **Kim JS**, Park SM, Kim BW. Sequential or concomitant therapy for eradication of Helicobacter pylori infection: A systematic review and meta-analysis. *J Gastroenterol Hepatol* 2015; **30**: 1338-1345 [PMID: 25867718 DOI: 10.1111/jgh.12984]

35 **Kate V**, Kalayarasan R, Ananthakrishnan N. Sequential therapy versus standard triple-drug therapy for Helicobacter pylori eradication: a systematic review of recent evidence. *Drugs* 2013; **73**: 815-824 [PMID: 23625272 DOI: 10.1007/s40265-013-0053-z]

36 **Valooran GJ**, Kate V, Jagdish S, Basu D. Sequential therapy versus standard triple drug therapy for eradication of Helicobacter pylori in patients with perforated duodenal ulcer following simple closure. *Scand J Gastroenterol* 2011; **46**: 1045-1050 [PMID: 21627398 DOI: 10.3109/00365521.2011.584894]

37 **Zhou YQ**, Xu L, Wang BF, Fan XM, Wu JY, Wang CY, Guo CY, Xu XF. Modified Sequential Therapy Regimen versus Conventional Triple Therapy for Helicobacter Pylori Eradication in Duodenal Ulcer Patients in China: A Multicenter Clinical Comparative Study. *Gastroenterol Res Pract* 2012; **2012**: 405425 [PMID: 22550478 DOI: 10.1155/2012/405425]

World Journal of Gastroenterology

Submit a Manuscript: https://www.f6publishing.com

World J Gastroenterol 2024 February 14; 30(6): 565-578

DOI: 10.3748/wjg.v30.i6.565

ISSN 1007-9327 (print) ISSN 2219-2840 (online)

ORIGINAL ARTICLE

Basic Study

Role of deubiquitinase JOSD2 in the pathogenesis of esophageal squamous cell carcinoma

Wen-Peng Wang, Dan Shi, Duo Yun, Jun Hu, Jie-Fu Wang, Jia Liu, Yan-Peng Yang, Ming-Rui Li, Jun-Feng Wang, Da-Lu Kong

Specialty type: Gastroenterology and hepatology

Provenance and peer review: Unsolicited article; Externally peer reviewed.

Peer-review model: Single blind

Peer-review report's scientific quality classification
Grade A (Excellent): A
Grade B (Very good): 0
Grade C (Good): 0
Grade D (Fair): 0
Grade E (Poor): 0

P-Reviewer: Alcántara-Hernández R, Mexico

Received: December 4, 2023
Peer-review started: December 4, 2023
First decision: December 8, 2023
Revised: December 20, 2023
Accepted: January 16, 2024
Article in press: January 16, 2024
Published online: February 14, 2024

Wen-Peng Wang, Jun Hu, Jie-Fu Wang, Jia Liu, Yan-Peng Yang, Jun-Feng Wang, Da-Lu Kong, Department of Colorectal Oncology, Tianjin Medical University Cancer Institute and Hospital, National Clinical Research Center for Cancer, Tianjin's Clinical Research Center for Cancer, Key Laboratory of Cancer Prevention and Therapy, Tianjin 300060, China

Dan Shi, Department of Gastrointestinal Surgery, Tianjin Nan Kai Hospital, Tianjin Medical University, Tianjin Key Laboratory of Acute Abdomen Disease Associated Organ Injury and ITCWM Repair, Institute of Integrative Medicine for Acute Abdominal Diseases, Tianjin 300100, China

Duo Yun, Department of Oncology, The First Hospital of Hohhot, Hohhot 010000, Inner Mongolia Autonomous Region, China

Ming-Rui Li, Department of Endocrinology, Dazhou Central Hospital, Dazhou 635000, Sichuan Province, China

Corresponding author: Da-Lu Kong, BMed, Chief Physician, Director, Doctor, Department of Colorectal Oncology, Tianjin Medical University Cancer Institute and Hospital, National Clinical Research Center for Cancer, Tianjin's Clinical Research Center for Cancer, Key Laboratory of Cancer Prevention and Therapy, Huanhuxi Road, Hexi District, Tianjin 300060, China. kongdalu2021@126.com

Abstract

BACKGROUND

Esophageal squamous cell carcinoma (ESCC) is a deadly malignancy with limited treatment options. Deubiquitinases (DUBs) have been confirmed to play a crucial role in the development of malignant tumors. JOSD2 is a DUB involved in controlling protein deubiquitination and influencing critical cellular processes in cancer.

AIM

To investigate the impact of JOSD2 on the progression of ESCC.

METHODS

Bioinformatic analyses were employed to explore the expression, prognosis, and enriched pathways associated with JOSD2 in ESCC. Lentiviral transduction was utilized to manipulate JOSD2 expression in ESCC cell lines (KYSE30 and

KYSE150). Functional assays, including cell proliferation, colony formation, drug sensitivity, migration, and invasion, were performed, revealing the impact of JOSD2 on ESCC cell lines. JOSD2's role in xenograft tumor growth and drug sensitivity *in vivo* was also assessed. The proteins that interacted with JOSD2 were identified using mass spectrometry.

RESULTS

Preliminary research indicated that JOSD2 was highly expressed in ESCC tissues, which was associated with poor prognosis. Further analysis demonstrated that JOSD2 was upregulated in ESCC cell lines compared to normal esophageal cells. JOSD2 knockdown inhibited ESCC cell activity, including proliferation and colony-forming ability. Moreover, JOSD2 knockdown decreased the drug resistance and migration of ESCC cells, while JOSD2 overexpression enhanced these phenotypes. *In vivo* xenograft assays further confirmed that JOSD2 promoted tumor proliferation and drug resistance in ESCC. Mechanistically, JOSD2 appears to activate the MAPK/ERK and PI3K/AKT signaling pathways. Mass spectrometry was used to identify crucial substrate proteins that interact with JOSD2, which identified the four primary proteins that bind to JOSD2, namely USP47, IGKV2D-29, HSP90AB1, and PRMT5.

CONCLUSION

JOSD2 plays a crucial role in enhancing the proliferation, migration, and drug resistance of ESCC, suggesting that JOSD2 is a potential therapeutic target in ESCC.

Key Words: Esophageal squamous cell carcinoma; JOSD2; Ubiquitination; Biomarker; Targeted therapy; Drug resistance

Core Tip: JOSD2, a deubiquitinating enzyme, is a key player in the aggressive pathogenesis of esophageal squamous cell carcinoma (ESCC). Elevated JOSD2 expression in ESCC tissues is associated with poor prognosis. Functional analyses, including *in vivo* xenograft assays, highlight JOSD2's role in promoting tumor proliferation and drug resistance. Mechanistically, JOSD2 activates the MAPK/ERK and PI3K/AKT signaling pathways. Mass spectrometry identified key interacting proteins, including USP47, IGKV2D-29, HSP90AB1, and PRMT5. This study underscores the potential role of JOSD2 as a therapeutic target in ESCC.

Citation: Wang WP, Shi D, Yun D, Hu J, Wang JF, Liu J, Yang YP, Li MR, Wang JF, Kong DL. Role of deubiquitinase JOSD2 in the pathogenesis of esophageal squamous cell carcinoma. *World J Gastroenterol* 2024; 30(6): 565-578
URL: https://www.wjgnet.com/1007-9327/full/v30/i6/565.htm
DOI: https://dx.doi.org/10.3748/wjg.v30.i6.565

INTRODUCTION

Esophageal squamous cell carcinoma (ESCC) ranks among the deadliest malignancies worldwide, posing a significant public health concern[1]. Despite advances in early detection and therapeutic interventions, ESCC remains a formidable challenge due to its mostly late-stage diagnosis and limited treatment options. To explore the potential therapeutic targets of ESCC, there has been an increasing focus on the genetic underpinnings of this aggressive cancer. Deubiquitinases (DUBs), responsible for cleaving ubiquitin chains from their protein targets, are crucial for controlling protein ubiquitination and preserving protein homeostasis. DUBs influence important cellular processes such as tumor cell proliferation, drug resistance, distant metastasis, and immune evasion by stabilizing the expression of key cancer proteins[2-6]. The research on DUBs provides new avenues for developing treatment options for cancers lacking effective therapeutic strategies. However, the role of DUBs in malignant tumors is far from fully elucidated. Currently, an increasing number of small molecule inhibitors targeting DUBs are being developed and reported, with preclinical and clinical trials underway, demonstrating significant potential in this research field[7].

JOSD2, also known as Josephin domain-containing 2, is a member of the Machado-Joseph disease protein family. It consists of 188 amino acids and contains only one highly conserved catalytic Josephin domain, possessing enzymatic activity. Several recent studies have shed light on the involvement of JOSD2 in some malignant tumors[8-12]. JOSD2 has been found to interact with key signaling pathways, such as the Hippo pathway, Wnt/β-catenin pathway, and DNA repair mechanisms[8,9,11]. Dysregulation of JOSD2 expression has been implicated in cancer initiation, tumor growth, and resistance to chemotherapy[8,11]. There is a lack of relevant research on the association between JOSD2 and ESCC. The elucidation of the function of JOSD2 in ESCC will be helpful to identify individuals at higher risk and devise personalized treatment strategies. Therefore, we aimed to explore the function of JOSD2 in ESCC, shedding light on its potential as a promising avenue for further investigation and clinical applications.

MATERIALS AND METHODS

Analyses of JOSD2 expression, prognosis and enriched pathways in ESCC tissue

The University of Alabama at Birmingham CANcer database (https://ualcan.path.uab.edu/) was used to analyze the differential expression of JOSD2 mRNA between ESCC and normal esophageal tissues[13,14]. The online survival database Kaplan–Meier Plotter (https://kmplot.com/analysis/) was used to assess the impact of high *vs* low JOSD2 mRNA expression on the survival prognosis of patients with ESCC[15]. Clinical and RNA-seq data from ESCC patients were downloaded from The Cancer Genome Atlas (TCGA) database (https://portal.gdc.cancer.gov/), and a nomogram predicting the 1-, 3- and 5-year survival probability of ESCC patients was constructed and visualized using the "survival" and "rms" packages in R (4.2.1).

The top 500 genes that have a similar expression pattern to JOSD2 in ESCC were downloaded from the Gene Expression Profiling Interactive Analysis 2 database (http://gepia2.cancer-pku.cn/#index) and listed in Supplementary Table 1. The Search Tool for the Retrieval of Interacting Genes/Proteins database (https://string-db.org/) was used to plot a protein-protein interaction (PPI) network of the top 100 genes associated with JOSD2.

Gene Ontology (GO) (Supplementary Table 2) and Kyoto Encyclopedia of Genes and Genomes (KEGG) (Supplementary Table 3) enrichment analyses of the top 500 genes that have a similar expression pattern to JOSD2 were conducted using the R packages "clusterProfiler", "enrichplot", and "ggplot2". The differentially expressed genes between the high and low JOSD2 expression groups based on TCGA database were determined using the R package "DESeq2" and listed in Supplementary Table 4. A Gene Set Enrichment Analysis (GSEA) was then conducted using the R packages "clusterProfiler" and "ggplot2" (Supplementary Table 5), based on the C2. CP. KEGG.v7.2 gene sets from the Molecular Signatures Database (MSigDB). Single-cell sequencing data from GSE160269 dataset was also analyzed to determine JOSD2 expression of different cell types (including B cell, CD4 T cell, CD8 T cell, DC, endothelial cell, fibroblasts, malignant cell, mast cell, mono/macro cell, pericytes, plasma cell, T proliferation cell, and Treg cell) using the Tumor Immune Single-Cell Hub 2 online tool (http://tisch.comp-genomics.org/home/).

Cell culture

A normal esophageal epithelial cell line, Het-1A, was obtained from the American Type Culture Collection and cultured in Dulbecco's modified Eagle's medium (Thermo Fisher Scientific, United States) supplemented with 10% fetal bovine serum (FBS) (Sigma, United States), penicillin (100 U/mL) and streptomycin (0.1 mg/mL) (Sigma, United States). Four ESCC cell lines (KYSE30, KYSE140, KYSE150, and KYSE410) were obtained from the Chinese Academy of Sciences Cell Bank and cultured in Roswell Park Memorial Institute (RPMI)-1640 medium (Thermo Fisher Scientific, United States) supplemented with 10% FBS (Sigma, United States), penicillin (100 U/mL), and streptomycin (0.1 mg/mL) (Sigma, United States). These cells were cultured at 37°C in a 5% CO_2 incubator.

Lentiviral packaging and transduction

Two independent small hairpin RNA (shRNA) sequences targeting JOSD2 (sh1: CGATGAGATCTG-CAAGAGGTT; sh2: GTGTCTACTACAACCTGGACT) were designed, cloned into a PSIH1 vector (GenePharma, China), and used for lentivirus packaging in 293T cells. The lentiviral supernatant was collected. KYSE150 cells (which had the highest JOSD2 expression among the ESCC cell lines) were transduced with the lentivirus and selected with puromycin 72 h later.

The JOSD2 gene was cloned into the lentiviral expression vector pLVX-IRES-Neo to create the overexpression plasmid pLVX-G418 JOSD2-Flag (GenePharma, China). The lentivirus was packaged and used to infect KYSE30 cells (which had the lowest JOSD2 expression among the ESCC cell lines), which were then selected with G418 72 h later.

RNA extraction and real-time fluorescent quantitative polymerase chain reaction

The total RNA was extracted using an RNApure Tissue/Cell Kit (Cwbiotech, China). The isolated RNA was used as a template for reverse transcription reaction using a HiFiScript cDNA Synthesis Kit (Cwbiotech, China). Real-time fluorescent quantitative polymerase chain reaction (RT-qPCR) was performed using SYBR Fast qPCR Mix (TaKaRa, Japan) and a CFX96 Real-Time System (Bio-Rad, United States). The primer sequences for JOSD2 were as follows: Forward: 5′-CCCACCGTGTACCACGAAC-3′; reverse: 5′-CTCCTGGCTAAAGAGCTGCTG-3′. The primer sequences for GAPDH were as follows: Forward: 5′-GATTCCACCCATGGCAAATTC-3′; reverse: 5′-CTGGAAGATGGTGATGGGATT-3′.

Cell protein extraction and western blotting

Approximately 1×10^6 cells were placed in each well of a 6-well culture plate. The cells were lysed by adding radioimmunoprecipitation assay buffer (10 μL) and a phosphatase inhibitor (1 μL) for every 100000 cells. The protein lysate was centrifuged at 17000g for 30 min to obtain the supernatant. The protein concentration was measured using a bicinchoninic acid assay. A mixture containing 10 μg of protein was then boiled at 95 °C for 10 min to denature the proteins.

Gel electrophoresis and transfer were carried out using a Mini Gel Tank chamber system (Thermo Fisher Scientific, United States) following the detailed procedures and reagents provided in the manufacturer's instructions. Gel electrophoresis was performed with constant voltage, starting at 70 V for 20 min, followed by an adjustment to 100 V for 50 min. The proteins were then transferred to a polyvinylidene fluoride membrane using a constant voltage of 10 V for 50 min.

The membrane was blocked with 5% skim milk for 1 h. The membrane was then incubated with one of the following primary antibodies overnight at 4 °C: JOSD2 antibody (sab2103354, 1:500, Sigma-Aldrich, United States), phosphorylated p44/42 MAPK (Erk1/2) (Thr202/Tyr204) antibody (9101, 1:1000, Cell Signaling Technology, United States), p44/42 MAPK (Erk1/2) (L34F12) antibody (4696, 1:1000, Cell Signaling Technology, United States), phosphorylated Akt (Ser473)

(D9E) antibody (4060, 1:2000, Cell Signaling Technology, United States), phosphorylated Akt (Thr308) antibody (13038, 1:1000, Cell Signaling Technology, United States), or Akt (pan) (40D4) antibody (2920, 1:2000, Cell Signaling Technology, United States). The membrane was then incubated with one of the following secondary antibodies at room temperature for 1 h: Anti-rabbit (7074, 1:1000, Cell Signaling Technology, United States) or anti-mouse (7076, 1:1000, Cell Signaling Technology, United States) horseradish peroxidase-linked antibody. The membrane was subjected to enhanced chemiluminescence (ECL) detection using SignalFire ECL reagent (Cell Signaling Technology, United States), and images were captured and saved using an automated imaging system. Anti-β-actin antibody (4967, 1:1000, Cell Signaling Technology, United States) was then added and incubated at room temperature for 1 h, followed by detection and image capture.

Cell proliferation assays

The Cell Counting Kit-8 (CCK-8) assay (Solarbio, China) was performed according to the manufacturer's instructions. Cells were seeded in a 96-well culture plate with approximately 1000 cells per well, and incubated at 37 °C in a 5% CO_2 incubator for 24, 48, 72, or 96 h. Subsequently, 10 μL of CCK-8 reagent was added to the cells, and the absorbance at 450 nm was measured using a microplate reader.

Colony formation assay

After exposure to shRNA1, shRNA2, or negative control, 1000 cells in the logarithmic growth phase were suspended in RPMI-1640 medium with 10% FBS and seeded in each well of 6-well plates. Following a 12-d incubation, the cells were fixed with methanol for 15 min and then stained with 0.5% crystal violet for 3 min at room temperature. After three washes with distilled water, the plates were air-dried and the cell colonies were manually counted. A positive colony was defined as a cluster containing at least 50 cells.

Drug sensitivity assay

Cells in the logarithmic growth phase, with knocked-down or overexpressed JOSD2, and their respective control cells, were divided into different groups and seeded into 96-well plates with each well containing 1×10^4 cells. After cell adhesion, cisplatin (Med-ChemExpress, United States) was added to each well at concentration gradients of 0, 10, 20, 40, 60, and 80 μg/mL in JOSD2 knock-down cell group. For the JOSD2 overexpression cell group, cisplatin was added at concentration gradients of 0, 20, 40, 60, 80, and 100 μg/mL. After 48 h, the sensitivity of the tumor cells to cisplatin was assessed using a 3-(4,5-dimethylthiazol-2-yl)-2,5-diphenyltetrazolium bromide assay kit (Sangon Biotech, China).

Migration assay

Transwell chambers (Corning, United States) were preloaded with 5×10^4 cells suspended in 100 μL of RPMI-1640 medium without FBS. The chambers were then placed in a 24-well plate, with each well containing 500 μL of RPMI-1640 medium supplemented with 10% FBS, and incubated in a 37 °C, 5% CO_2 incubator. After 24 h, the medium in the chambers was removed, and the cells in the chambers were gently wiped away with a cotton swab. The cells on the chambers were fixed on a new 24-well plate with 4% paraformaldehyde for 20 min. Next, the chambers were removed, followed by crystal violet staining for 20 min. Excess crystal violet solution was washed off with phosphate-buffered saline (PBS), and cell images were captured using a microscope.

Invasion assay

Approximately 60 μL of diluted Matrigel (1:8, Becton, Dickinson and Company, United States) was added to Transwell chambers. The chambers were incubated in a 37 °C, 5% CO_2 incubator for 3 h, excess liquid was removed from the chambers, and 100 μL of RPMI-1640 medium without FBS was added. The chambers were then placed in the 37 °C, 5% CO_2 incubator for 30 min to hydrate the basement membrane. Subsequently, 100 μL of cell suspension comprising 5×10^4 cells in FBS-free RPMI-1640 medium was added to the chambers. The chambers were then placed in a 24-well plate, with each well containing 500 μL of RPMI-1640 medium with 10% FBS, and incubated in the 37 °C, 5% CO_2 incubator. After 24 h, the medium in the chambers was removed, and the Matrigel and the cells in the chambers were gently wiped away with a cotton swab. As in the Transwell migration assays, a new 24-well plate with 4% paraformaldehyde was used to fix the cells on the chambers for 20 min, the chambers were removed, crystal violet staining was performed for 20 min, excess crystal violet solution was rinsed off with PBS, and cell images were captured using a microscope.

Xenograft and drug sensitivity assays

Xenograft assays were conducted by subcutaneously injecting JOSD2-knockdown KYSE150 cells and JOSD2-overexpressing KYSE30 cells under the armpits of BALB/c nude mice. Tumor dimensions, including length and width, were assessed using a vernier caliper every 3 d. Tumor volume was determined as $0.52 \times \text{length} \times \text{width}^2$, and growth curves were plotted. From subcutaneous injection until tumor growth on the 19th day, the tumor tissues were harvested and their weights were recorded.

Additionally, the role of JOSD2 in cisplatin sensitivity *in vivo* was studied using xenograft and drug sensitivity assays. JOSD2-knockdown KYSE150 cells or JOSD2-overexpressing KYSE30 cells were injected under the armpits of BALB/c nude mice. When the tumor volume reached 10 mm^3, cisplatin was intraperitoneally injected (6 mg/kg, every 3 d for 15 d) and the tumor volume was measured at the same time. At approximately 2 wk after the first administration of cisplatin, the tumor tissues were excised and weighed.

Mass spectrometry

To explore the proteins that interact with JOSD2, KYSE30 cells with Flag-tagged JOSD2 (Flag-JOSD2 sequence: GATTACAAGGATGACGACGATAAG) were lysed with protein lysis buffer to obtain the total proteins. Flag-JOSD2 was then enriched by immunoprecipitation. After obtaining the protein precipitate interacting with Flag-JOSD2, the protein complex was subjected to SDS-PAGE, followed by silver staining for band visualization. Specific bands were then subjected to mass spectrometry analysis (Beijing Protein Innovation Co., Ltd., China).

Statistical methods

ImageJ software was used to quantify the protein expression levels in Western blot analysis. Graphs were constructed and statistical analyses were performed using GraphPad Prism 10 software (GraphPad Software, Inc., United States). A P value less than 0.05 was considered statistically significant. Student's t-test was used to determine the significance of differences between two groups, while analysis of variance was employed to compare differences among more than two groups.

RESULTS

JOSD2 is highly expressed in ESCC tissues, which is associated with poor prognosis

JOSD2 expression was significantly higher in ESCC tissues than normal esophageal tissues (P < 0.0001) (Figure 1A). Additionally, ESCC patients with high JOSD2 expression had a worse prognosis than those with low expression (P = 0.025), providing a basis for predicting the prognosis of ESCC (Figure 1B and C).

To determine the biological functions of JOSD2, GO and KEGG enrichment analyses were performed. The top five most enriched biological process, cellular component, and molecular function (MF) terms are shown in Figure 1D (only one MF term was enriched), and the top five most enriched KEGG pathways are shown in Figure 1E. The top five gene sets in the GSEA, comprising CROMER Tumorigenesis Up, UROSEVIC Response to Imiquimod, MOSERLE IFNA Response, GNATENKO Platelet Signature, and RADAEVA Response to IFNA1 Up, are shown in Figure 1F. A PPI diagram based on the top 100 genes associated with JOSD2 is depicted in Supplementary Figure 1.

JOSD2 expression in ESCC cells

To determine whether JOSD2 is expressed in ESCC cells, single-cell sequencing data in GSE160269 was utilized and JOSD2 was highly expressed in ESCC cells (Figure 2). Additionally, JOSD2 mRNA and protein expression in a normal esophageal epithelial cell line (Het-1A) and ESCC cell lines (KYSE30, KYSE140, KYSE150, and KYSE410) was assessed using RT-qPCR and western blotting, respectively. The results showed that both JOSD2 mRNA (Figure 3A) and protein (Figure 3B) expression were consistently upregulated in ESCC cell lines compared to the normal esophageal cell line.

JOSD2 knockdown inhibits activity of ESCC cells

To confirm the function of JOSD2 in ESCC cells, two shRNAs targeting JOSD2 were designed and knockdown assays in the KYSE150 cell line (which had the highest JOSD2 expression among the ESCC cell lines) were conducted. RT-qPCR results showed that both shRNAs achieved effective knockdown (Figure 4A).

Subsequently, CCK-8 cell viability assays were performed to study the influence of JOSD2 knockdown on cell proliferation. The results indicated that both shRNAs significantly inhibited the proliferation of KYSE150 cells (P < 0.0001 for both) (Figure 4B). Colony formation assays were conducted to investigate the effect of JOSD2 knockdown on tumor-forming ability. JOSD2 knockdown significantly suppressed the colony-forming ability of KYSE150 cells (Figure 4C).

JOSD2 enhances ESCC cell proliferation, drug resistance, and migration in vitro

Chemoresistance and distant metastasis are major contributors to the poor prognosis of ESCC patients. Therefore, the next step was to investigate whether JOSD2 also affects the drug resistance and migratory ability of ESCC cells. JOSD2 knockdown increased the sensitivity of KYSE150 cells to 48-h treatment with various concentrations of cisplatin (P < 0.0001 for both) (Figure 5A). Transwell migration and invasion assays also demonstrated that JOSD2 knockdown significantly inhibited the migratory (P < 0.01) and invasion (P < 0.0001) ability of KYSE150 cells (Figure 5B). To validate the promoting role of JOSD2 in the development of ESCC cells, exogenous JOSD2 was overexpressed in KYSE30 cells (which had the lowest JOSD2 expression among the ESCC cell lines). The results showed that JOSD2 overexpression significantly promoted the proliferation (P < 0.0001), drug resistance (P < 0.0001), migration (P < 0.01), and invasion (P < 0.001) capability of KYSE30 cells (Figure 5C-E).

JOSD2 promotes ESCC cell proliferation and drug resistance in vivo

Xenograft assays were conducted in nude mice using JOSD2-knockdown KYSE150 cells, JOSD2-overexpressing KYSE30 cells, and their respective control cells. The mice in each group were divided into subgroups with and without cisplatin treatment to study the effects of JOSD2 on ESCC cell proliferation and drug sensitivity *in vivo*. JOSD2-knockdown KYSE150 cells exhibited significantly slower tumor growth and a more pronounced reduction in tumor volume under cisplatin treatment compared to control cells (P < 0.001 for tumor volume, P < 0.0001 for tumor weight) (Figure 6A and B). On the other hand, JOSD2-overexpressing KYSE30 cells not only had faster tumor growth but also exhibited significantly increased resistance to cisplatin (P < 0.0001 for tumor volume, P < 0.0001 for tumor weight) (Figure 6C and D). These findings suggested that JOSD2 has a vital role in promoting the development of ESCC.

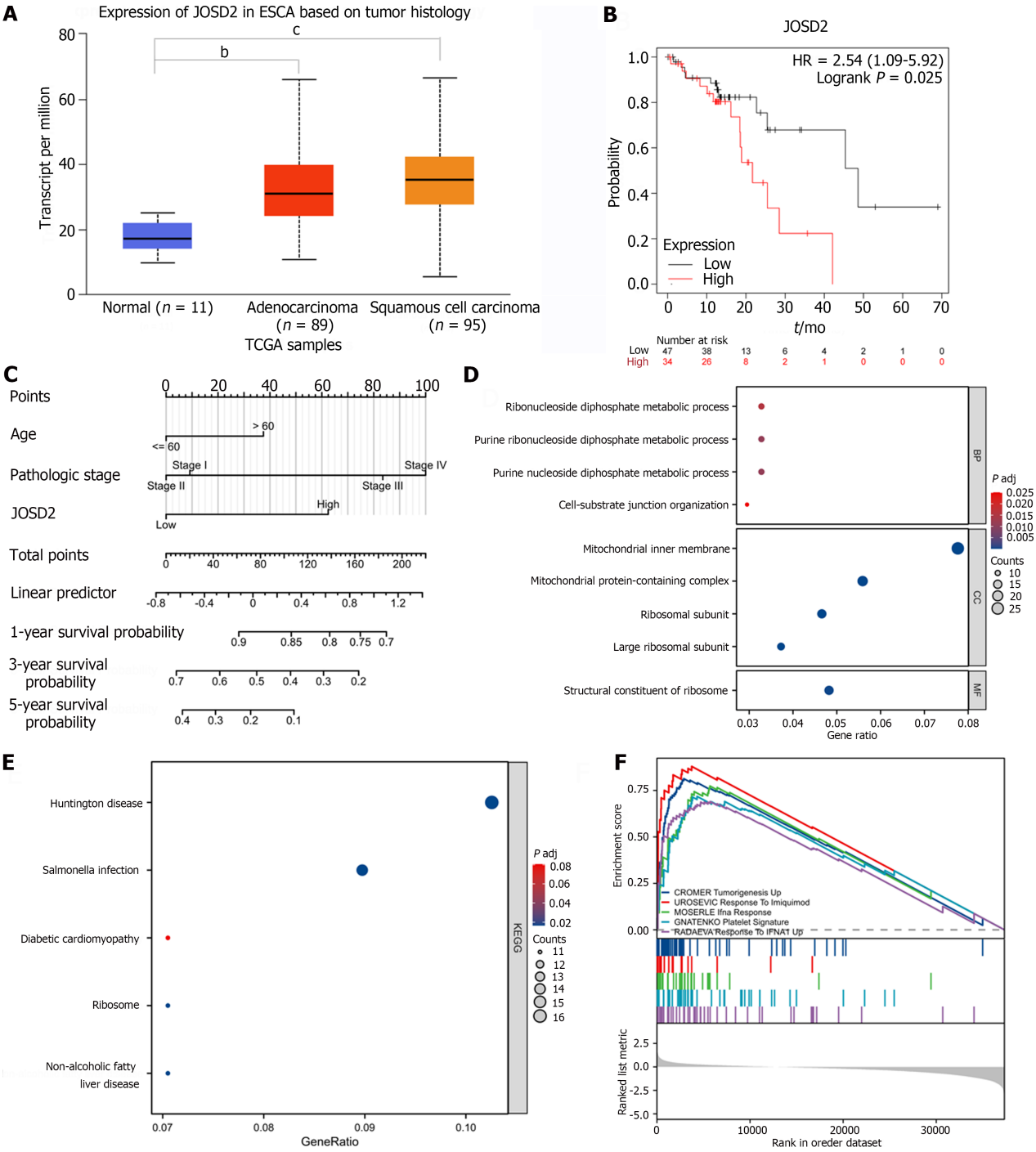

DOI: 10.3748/wjg.v30.i6.565

Figure 1 Expression level, survival analysis, and enrichment analyses of JOSD2 in esophageal squamous cell carcinoma tissues. A: Boxplots of JOSD2 expression in esophageal squamous cell carcinoma (ESCC) tissues and normal esophageal tissues based on University of Alabama at Birmingham CANcer database; B: Kaplan-Meier plot showing the survival difference between ESCC patients with high *vs* low JOSD2 expression based on the Kaplan-Meier Plotter database; C: Nomogram of JOSD2 expression predicting 1-, 3- and 5-year survival probability of ESCC patients; D-F: Gene Ontology (D), Kyoto Encyclopedia of Genes and Genomes (E) and Gene Set Enrichment Analysis (F) enrichment analyses of JOSD2. $^{b}P < 0.001$; $^{c}P < 0.0001$.

JOSD2 facilitates activation of cancer-related pathways in ESCC cells

To explore the molecular mechanisms by which JOSD2 promotes ESCC, the effects of JOSD2 on the phosphorylation pathways MAPK/ERK and PI3K/AKT, which play important roles in carcinogenesis, were assessed. Western blotting results showed that JOSD2 knockdown in ESCC cells inhibited the phosphorylation levels of ERK1/2 and AKT (Figure 7A), while JOSD2 overexpression in ESCC cells led to the activation of MAPK/ERK and PI3K/AKT signaling pathways (Figure 7B). These results indicated that the activation of the MAPK/ERK and PI3K/AKT signaling pathways serves as a pivotal downstream mechanism in facilitating the oncogenic function of JOSD2.

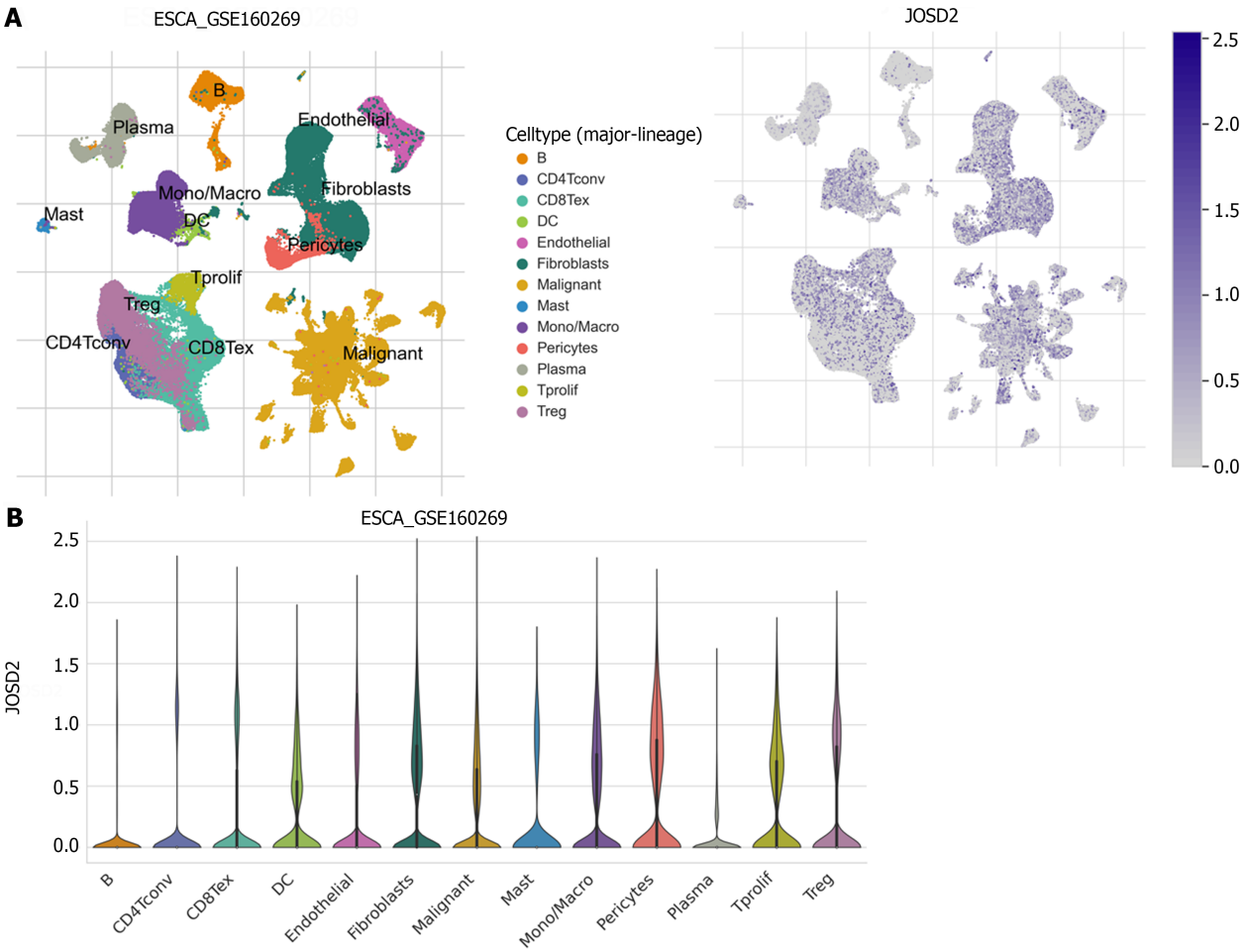

DOI: 10.3748/wjg.v30.i6.565

Figure 2 Single-cell sequencing data of esophageal squamous cell carcinoma in GSE160269. A: Uniform manifold approximation and projection plots showing the grouping of different cell types (left) and the expression profile of JOSD2 (right) in different cell types; B: Violin plots showing JOSD2 expression in different cell types.

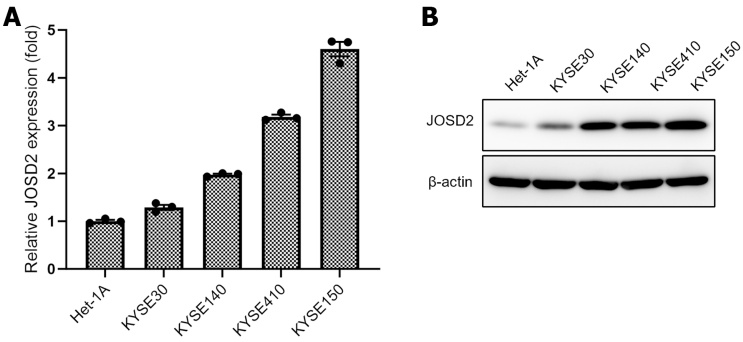

DOI: 10.3748/wjg.v30.i6.565

Figure 3 JOSD2 expression in esophageal squamous cell carcinoma cell lines. Real-time fluorescence quantitative polymerase chain reaction and western blotting results showing JOSD2 mRNA (A) and protein (B) expression in esophageal squamous cell carcinoma cell lines and a normal esophageal epithelial cell line. A: JOSD2 mRNA; B: Protein.

Proteins potentially binding to JOSD2 were identified by mass spectrometry

To identify key substrate proteins interacting with JOSD2, anti-Flag magnetic beads were used to enrich Flag-JOSD2 protein and its interacting proteins in KYSE30 cells with exogenous Flag-JOSD2 overexpression. As indicated by the blue arrows in Figure 8A, silver staining of the SDS-PAGE gel revealed numerous protein bands in the overexpression group but not in the control group, indicating that these proteins were specifically immunoprecipitated along with Flag-JOSD2. Mass spectrometry showed that JOSD2 had the highest score (validating the reliability of its enrichment) and the other top-ranked proteins were USP47, IGKV2D-29, HSP90AB1, and PRMT5 (Figure 8B), which indicated that these proteins

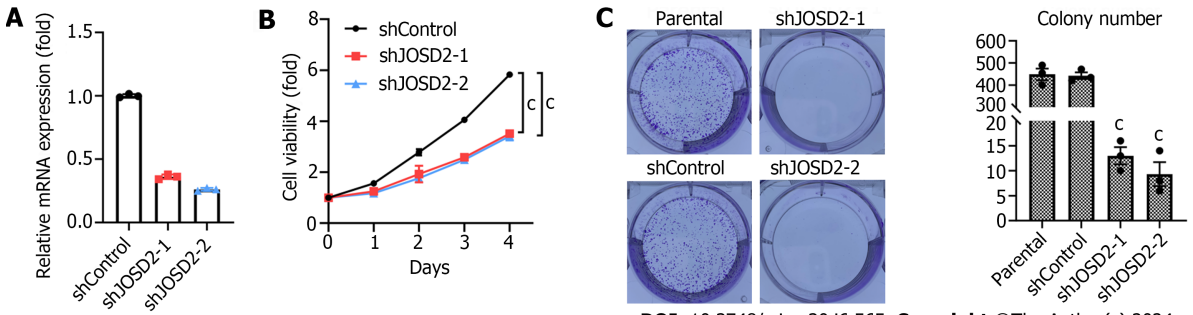

DOI: 10.3748/wjg.v30.i6.565

Figure 4 JOSD2 knockdown significantly suppresses the activity of esophageal squamous cell carcinoma cells. A: JOSD2 was successfully knocked down using shRNA1/2 directed against JOSD2 in KYSE150 cells; B: JOSD2 knockdown significantly inhibited cell proliferation; C: JOSD2 knockdown significantly inhibited the ability of the cells to form colonies. $^{c}P < 0.0001$.

may be the significant substrates that bind to JOSD2.

DISCUSSION

In recent years, an increasing number of studies have shown that DUBs play a crucial role in the development of malignant tumors[11,16]. There has been a substantial amount of research on DUBs in five common malignant tumors, namely non-small cell lung cancer, hepatocellular cancer, gastric cancer, colorectal cancer, and breast cancer[8,17-20]. For instance, USP9X, DUB3, and USP7 have been identified in these malignant tumors[21-23]. There has been less research on DUBs in ESCC, and this research has mostly focused on the impact of the known DUBs on the metastatic process of ESCC [24-27]. PSMD14, OTUB1, USP26, and EIF3H, by stabilizing Snail, promote the occurrence of metastasis[24-27]. This redundancy in the regulatory mechanism makes using individual DUBs as effective therapeutic targets challenging.

This study is the first to report on the role of JOSD2 in ESCC. The preliminary findings indicated that JOSD2 is not only highly expressed in ESCC tissues, but its high expression is significantly associated with a poor prognosis. Subsequent analyses revealed that JOSD2 significantly enhanced the proliferation, migration, and drug resistance of ESCC cells. The *in vivo* results confirmed that altering JOSD2 expression, either by overexpression or knockdown, modulates the resistance of ESCC to the chemotherapy drug cisplatin (one of the primary chemotherapy drugs used to treat ESCC). This highlights the potential significance of using JOSD2 as a therapeutic target in order to overcome cisplatin resistance in ESCC.

Norberg *et al*[28] reported the role of JOSD2 in lung adenocarcinoma. They analyzed the metabolic profile of lung adenocarcinoma and found that PHGDH, a critical rate-limiting enzyme in serine synthesis, was highly expressed in a subgroup with poor prognosis[28]. Tumors with high PHGDH expression exhibited rapid proliferation and migration. Subsequently, the authors discovered that the protein expression of PHGDH is regulated by the ubiquitin proteasome system pathway. The authors screened for DUBs that stabilize PHGDH by using a siRNA library targeting 99 DUBs for transient knockdown. Targeting the DUB JOSD2, among these 99 DUBs, led to the largest significant reduction (> 80%) in PHGDH protein expression. Thus, JOSD2 affected the metabolism of lung adenocarcinoma by stabilizing PHGDH and promoting tumor growth. The same research team further explored and revealed the relationship between JOSD2 and metabolism[29]. They found that both *in vitro* and *in vivo*, JOSD2 directly regulated the metabolic enzyme complex comprising aldolase A, phosphofructokinase 1, and PHGDH. Wild-type JOSD2, but not its enzymatic mutant, stabilized this complex *via* deubiquitination, enhancing its activity, and thereby increasing the glycolytic rate of cancer cells. The absence of JOSD2 inhibited various cancer cells (including non-small cell lung cancer, breast cancer, and ovarian cancer cells) and reduced glycolysis. In summary, JOSD2 effectively integrated glycometabolism and serine metabolism by stabilizing the metabolic enzyme complex. For cancer types that are highly reliant on glycolysis for their energy supply, increased JOSD2 expression significantly promoted cell proliferation and growth. This finding suggests that JOSD2 is a potential therapeutic target in cancer cells that are dependent on glycolytic metabolism.

Qian *et al*[11] reported the role of JOSD2 in the progression of cholangiocarcinoma (CCA)[11]. They identified JOSD2 as a crucial regulator that stabilizes Yes-associated protein/Transcriptional co-activator with PDZ-binding motif (YAP/TAZ), which are involved in the malignant progression of CCA. Depleting JOSD2 led to the degradation of YAP/TAZ and thereby significantly inhibited CCA proliferation both *in vitro* and *in vivo*. Additionally, there was a positive association between JOSD2 and YAP abundance in CCA patient samples, suggesting that JOSD2 is a potential target for treatment in patients with YAP/TAZ-related CCA. Moreover, Huang *et al*[9] identified JOSD2 as a novel prognostic indicator for individuals with hepatocellular cancer and identified CTNNB1 as a significant collaborator and downstream protein targeted by JOSD2[9]. However, Lei *et al*[10] reported that, in acute myeloid leukemia, JOSD2 is a tumor suppressor and PKM2 is a newfound JOSD2-interacting partner, which suggests that JOSD2 has different functions and mechanisms in different malignant tumors[10].

The MAPK/ERK and PI3K/AKT signaling pathways are crucial for key cancer characteristics, including cell proliferation, differentiation, migration, and genomic stability[30,31]. Therefore, we assessed the effects of JOSD2 on these pathways. The results revealed that the phosphorylation activation of MAPK/ERK and PI3K/AKT was a critical

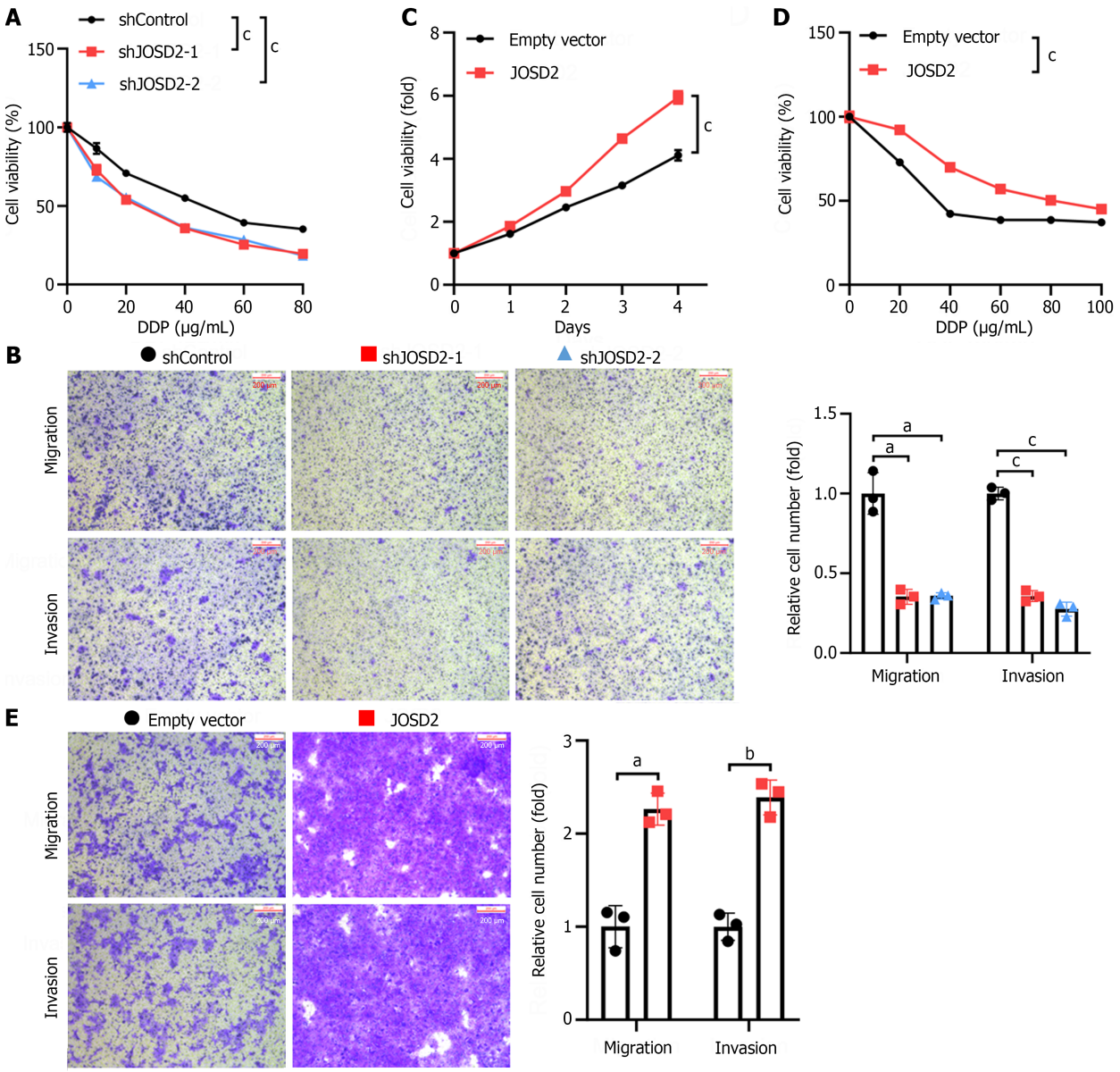

DOI: 10.3748/wjg.v30.i6.565

Figure 5 JOSD2 contributes to the proliferation, drug resistance, and metastatic capability of esophageal squamous cell carcinoma cells. A: JOSD2-knockdown KYSE150 cells exhibited increased sensitivity to 48-h treatment with various concentrations of cisplatin; B: JOSD2-knockdown KYSE150 cells exhibited significantly decreased migration and invasion in Transwell migration and invasion assays; C: JOSD2-overexpressing KYSE30 cells exhibited significantly increased cell growth in cell proliferation assays; D: JOSD2-overexpressing KYSE30 cells exhibited increased resistance to 48-h treatment with various concentrations of cisplatin; E: JOSD2-overexpressing KYSE30 cells exhibited significantly increased migration and invasion in Transwell migration and invasion assays. $^{a}P < 0.01$; $^{b}P < 0.001$; $^{c}P < 0.0001$.

downstream event mediating the oncogenic function of JOSD2.

Regarding the key substrate proteins interacting with JOSD2, we found that USP47, IGKV2D-29, HSP90AB1, and PRMT5 were the top four binding proteins of JOSD2 and may also be substrates for JOSD2's activity. USP47, a DUB, can counteract the functions of E3 ubiquitin ligases, playing a role in cell growth and survival processes[32]. Several studies have provided evidence that USP47 is involved in the advancement of diverse cancer types[33-35]. There is limited research on the IGKV2D-29 gene, but polymorphism in this gene was shown to lower the recombination frequency in B cells and to be especially important for immune responses to *Haemophilus influenzae* type b polysaccharide[36]. HSP90AB1 is a crucial participant in oncogene activity and the preservation of cancer cell viability[37]. This is due to its chaperone mechanism in cancer cells, safeguarding significant amounts of mutated and excessively expressed oncogenic proteins from undergoing misfolding and degradation[37]. Lastly, PRMT5 plays a crucial oncogenic role in various malignancies and has been a key target in recent cancer therapies[38,39]. However, there have been no studies reporting its deubiquitination modification. PRMT5's role in various malignancies implies that it is likely a key substrate protein for JOSD2's oncogenic function, and JOSD2's deubiquitination of PRMT5 may have significant implications for the treatment of ESCC.

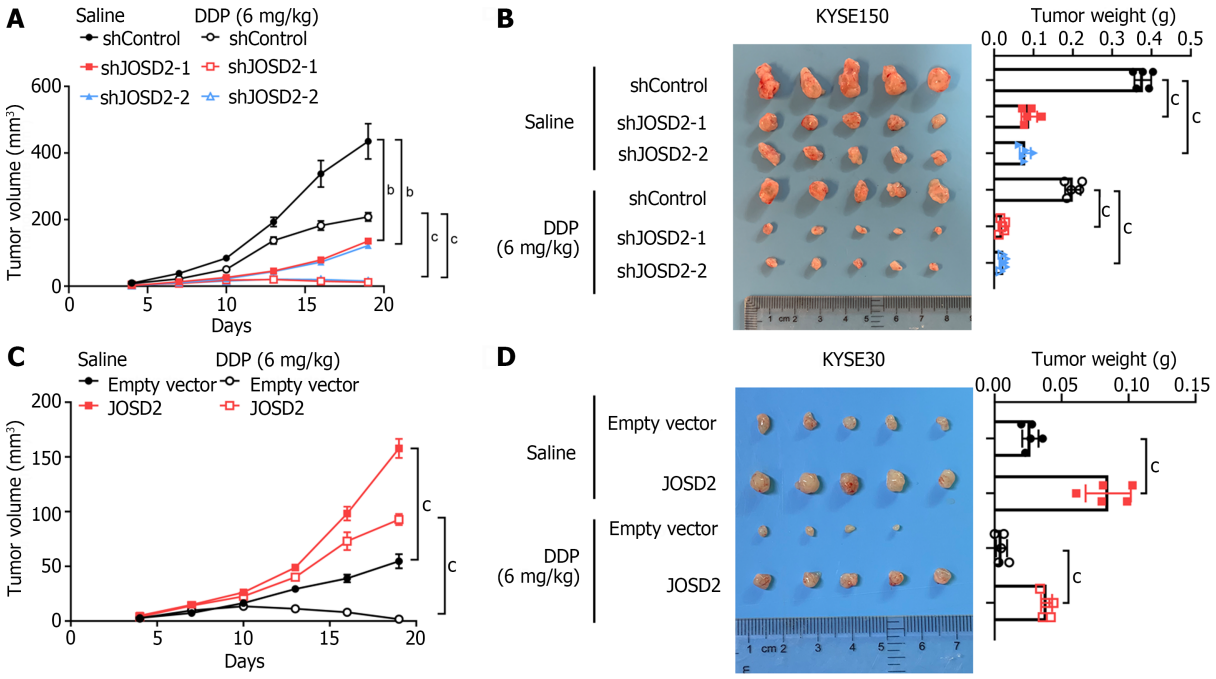

DOI: 10.3748/wjg.v30.i6.565

Figure 6 JOSD2 promotes *in vivo* esophageal squamous cell carcinoma cell proliferation and cisplatin resistance. A and B: JOSD2-knockdown cisplatin-treated KYSE150 cells exhibited significantly decreased tumor growth in both volume (A) and weight (B) compared to cisplatin-treated control cells; C and D: JOSD2-overexpressing cisplatin-treated KYSE30 cells exhibited significantly increased tumor growth in both volume (C) and weight (D) compared to cisplatin-treated control cells. $^{b}P < 0.001$; $^{c}P < 0.0001$.

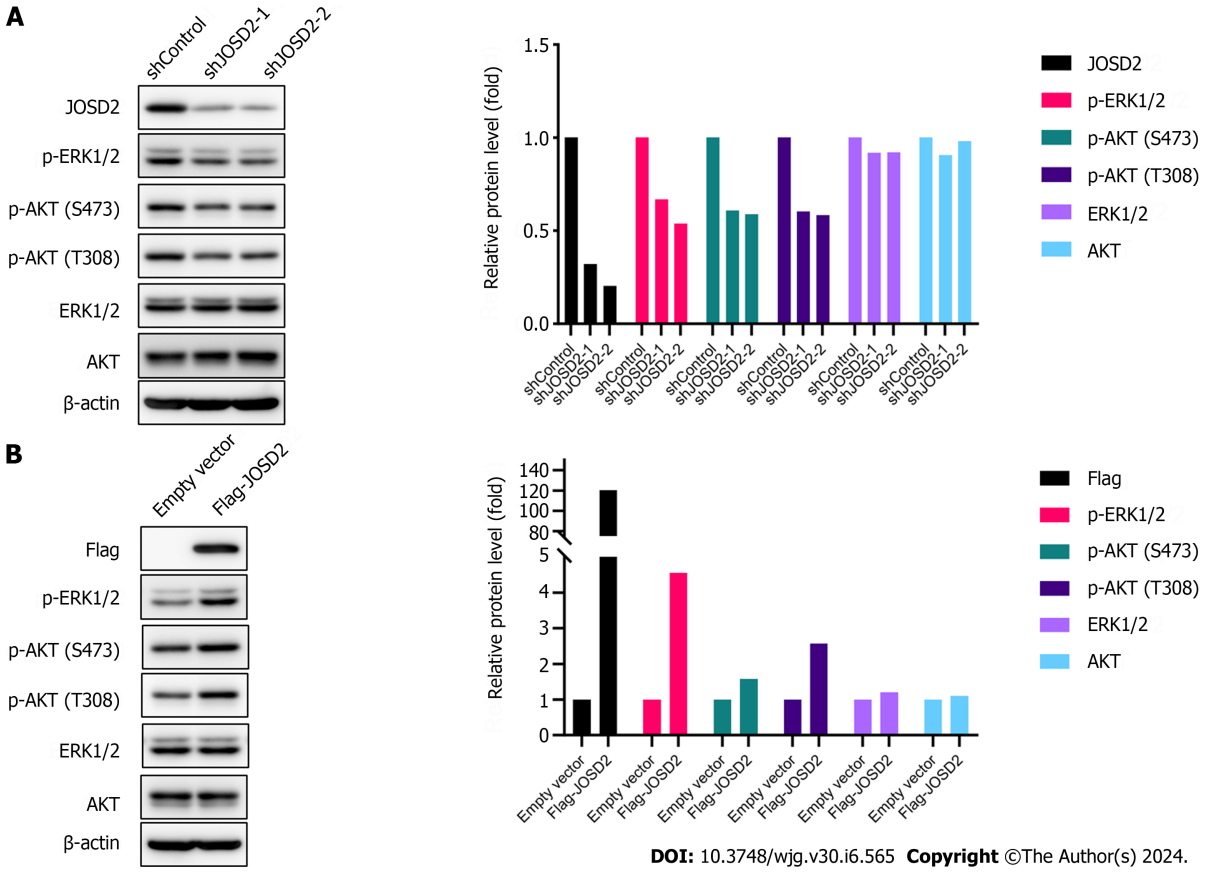

DOI: 10.3748/wjg.v30.i6.565

Figure 7 JOSD2 enhances the activation of phosphorylation pathways in esophageal squamous cell carcinoma. A: Western blotting showing that JOSD2 knockdown in esophageal squamous cell carcinoma (ESCC) cells decreased the phosphorylation of ERK1/2 and AKT; B: Western blotting showing that JOSD2 overexpression in ESCC cells activated the MAPK/ERK and PI3K/AKT signaling pathways.

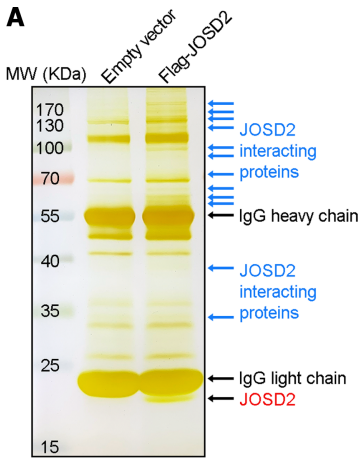

B

Top 5 proteins identified by MS

Proteins	Unique peptide numbers	MS score
JOSD2	25	3476
USP47	57	1450
IGKV2D-29	4	1371
HSP90AB1	20	897
PRMT5	40	857

DOI: 10.3748/wjg.v30.i6.565

Figure 8 Mass spectrometry analysis of proteins that bind to JOSD2 protein. A: Protein bands after SDS-PAGE gel silver staining; B: Proteins that potentially interact with JOSD2.

CONCLUSION

In conclusion, this study reveals the tumorigenic role of JOSD2 in the advancement of ESCC. In terms of the mechanism, JOSD2 influences the phosphorylation activation of MAPK/ERK and PI3K/AKT. USP47, IGKV2D-29, HSP90AB1, and PRMT5 are the four primary proteins that interact with JOSD2 and may serve as substrates for JOSD2's functional activity, especially PRMT5. In 2019, Grasty *et al*[40] elucidated the molecular structure of the JOSD2 protein, which will facilitate the development of molecular targeted inhibitors of JOSD2. However, there are currently no report on JOSD2 inhibitors. Consequently, there is a need for further exploration of the effects of specific and potent JOSD2 inhibitors on the clinical outlook for ESCC patients.

ARTICLE HIGHLIGHTS

Research background

Esophageal squamous cell carcinoma (ESCC) is a highly lethal malignancy with limited treatment options. Deubiquitinases (DUBs), crucial for maintaining protein homeostasis, are emerging as key players influencing vital cellular processes in ESCC, offering new treatment avenues. In addition, the ongoing development of small molecule inhibitors targeting DUBs shows significant promise, with several preclinical and clinical trials underway.

Research motivation

Recognizing the crucial involvement of DUBs in malignant tumor development, JOSD2, a specific DUB, has been identified as playing a pivotal role in controlling protein deubiquitination and impacting essential cellular processes in cancer. Nevertheless, the function of JOSD2 in ESCC remains uncertain.

Research objectives

The objective of this study was to explore the impact of JOSD2 on the progression of ESCC.

Research methods

Bioinformatics analyses were used to investigate the expression patterns, prognosis, and enriched pathways of JOSD2 in ESCC tissues. Manipulation of JOSD2 expression in ESCC cell lines (KYSE30 and KYSE150) was achieved through lentiviral transduction. Comprehensive functional assays, encompassing cell proliferation, colony formation, drug sensitivity, migration, and invasion assays, were conducted to unveil the influence of JOSD2 on ESCC cell lines. Additionally, the effects of JOSD2 on xenograft tumor growth and drug sensitivity *in vivo* were assessed. Proteins interacting with JOSD2 were determined by mass spectrometry.

Research results

The initial results suggested that JOSD2 was highly expressed in ESCC tissues and was associated with a poor prognosis. Subsequent investigations revealed upregulation of JOSD2 in ESCC cell lines compared to normal esophageal cells. JOSD2 knockdown inhibited various ESCC cell activities, including proliferation, colony formation, and migration, as well as reducing drug resistance. Conversely, JOSD2 overexpression enhanced these phenotypes. *In vivo* xenograft assays confirmed that JOSD2 promoted tumor proliferation and drug resistance in ESCC. Mechanistically, JOSD2 appears to activate the MAPK/ERK and PI3K/AKT signaling pathways. Mass spectrometry identified four primary proteins

interacting with JOSD2: USP47, IGKV2D-29, HSP90AB1, and PRMT5.

Research conclusions

JOSD2 promotes cell proliferation, migration, and drug resistance in ESCC.

Research perspectives

JOSD2 is a promising therapeutic target for the treatment of ESCC.

FOOTNOTES

Co-first authors: Wen-Peng Wang and Dan Shi.

Co-corresponding authors: Jun-Feng Wang and Da-Lu Kong.

Author contributions: Wang WP and Shi D contributed equally to this work; Kong DL and Wang JF were co-corresponding authors; The study was conceptualized and designed by Kong DL, Wang JF, and Wang WP; Shi D and Yun D were in charge of acquiring public data; Bioinformatic and statistical analyses were conducted by Wang WP, Shi D, Yun D, Hu J, Wang JF, and Liu J; Wang WP, Shi D, Yun D, Yang YP, and Li MR carried out both *in vitro* and *in vivo* experiments; Figures and tables were prepared, and the initial draft of the manuscript was written by Wang WP, Shi D, Wang JF and Yun D; Manuscript revisions were performed by Kong DL, Wang JF, and Wang WP; All authors have reviewed and approved the final version of the manuscript for publication.

Supported by Tianjin Key Medical Discipline (Specialty) Construction Project, No. TJYXZDXK-009A; Tianjin Medical University Cancer Hospital National Natural Science Foundation Cultivation Program, No. 220108; National Natural Science Foundation of China, No. 82373134; Science and Technology Development Fund of Tianjin Education Commission for Higher Education, No. 2022KJ228; Chinese Anti-Cancer Association-Heng Rui Anti-angiogenesis Targeted Tumor Research Fund, No. 2021001045; and Scientific Research Translational Foundation of Wenzhou Safety (Emergency) Institute of Tianjin University, No. TJUWYY2022025.

Institutional review board statement: The study was reviewed and approved by the Institutional Review Board of Tianjin Medical University Cancer Institute and Hospital, No. Ek2023018.

Institutional animal care and use committee statement: All procedures involving animals were reviewed and approved by the Tianjin Cancer Institute Animal Ethics Committee, No. NSFC-AE-2023n2.

Informed consent statement: All study participants or their legal guardian provided informed written consent about personal and medical data collection prior to study enrolment.

Conflict-of-interest statement: The authors declare no conflict of interest.

Data sharing statement: The data used and/or analyzed during the current study are available from the corresponding author on reasonable request.

ARRIVE guidelines statement: The authors have read the ARRIVE guidelines, and the manuscript was prepared and revised according to the ARRIVE guidelines.

Country/Territory of origin: China

ORCID number: Duo Yun 0000-0001-7999-5626; Yan-Peng Yang 0000-0002-0075-7420; Da-Lu Kong 0000-0002-5666-8777.

S-Editor: Fan JR
L-Editor: A
P-Editor: Cai YX

REFERENCES

1 **Zheng R**, Zhang S, Zeng H, Wang S, Sun K, Chen R, Li L, Wei W, He J. Cancer incidence and mortality in China, 2016. *J Nati Cancer Cent* 2022; **2**: 1-9 [DOI: 10.1016/j.jncc.2022.02.002]

2 **Ge Z**, Leighton JS, Wang Y, Peng X, Chen Z, Chen H, Sun Y, Yao F, Li J, Zhang H, Liu J, Shriver CD, Hu H; Cancer Genome Atlas Research Network, Piwnica-Worms H, Ma L, Liang H. Integrated Genomic Analysis of the Ubiquitin Pathway across Cancer Types. *Cell Rep* 2018; **23**: 213-226.e3 [PMID: 29617661 DOI: 10.1016/j.celrep.2018.03.047]

3 **Leznicki P**, Kulathu Y. Mechanisms of regulation and diversification of deubiquitylating enzyme function. *J Cell Sci* 2017; **130**: 1997-2006 [PMID: 28476940 DOI: 10.1242/jcs.201855]

4 **Zhang X**, Smits AH, van Tilburg GB, Jansen PW, Makowski MM, Ovaa H, Vermeulen M. An Interaction Landscape of Ubiquitin Signaling. *Mol Cell* 2017; **65**: 941-955.e8 [PMID: 28190767 DOI: 10.1016/j.molcel.2017.01.004]

5 **Zhang S**, Zhang M, Jing Y, Yin X, Ma P, Zhang Z, Wang X, Di W, Zhuang G. Deubiquitinase USP13 dictates MCL1 stability and sensitivity to BH3 mimetic inhibitors. *Nat Commun* 2018; **9**: 215 [PMID: 29335437 DOI: 10.1038/s41467-017-02693-9]

6 **Lim SO**, Li CW, Xia W, Cha JH, Chan LC, Wu Y, Chang SS, Lin WC, Hsu JM, Hsu YH, Kim T, Chang WC, Hsu JL, Yamaguchi H, Ding Q, Wang Y, Yang Y, Chen CH, Sahin AA, Yu D, Hortobagyi GN, Hung MC. Deubiquitination and Stabilization of PD-L1 by CSN5. *Cancer Cell* 2016; **30**: 925-939 [PMID: 27866850 DOI: 10.1016/j.ccell.2016.10.010]

7 **Harrigan JA**, Jacq X, Martin NM, Jackson SP. Deubiquitylating enzymes and drug discovery: emerging opportunities. *Nat Rev Drug Discov* 2018; **17**: 57-78 [PMID: 28959952 DOI: 10.1038/nrd.2017.152]

8 **Ge F**, Liu X, Zhang H, Yuan T, Zhu H, Yang B, He Q. Deubiquitinating enzyme JOSD2 affects susceptibility of non-small cell lung carcinoma cells to anti-cancer drugs through DNA damage repair. *Zhejiang Da Xue Xue Bao Yi Xue Ban* 2023; **52**: 533-543 [PMID: 37899394 DOI: 10.3724/zdxbyxb-2023-0256]

9 **Huang Y**, Zeng J, Liu T, Xu Q, Song X. Deubiquitinating enzyme JOSD2 promotes hepatocellular carcinoma progression through interacting with and inhibiting CTNNB1 degradation. *Cell Biol Int* 2022; **46**: 1089-1097 [PMID: 35568970 DOI: 10.1002/cbin.11812]

10 **Lei H**, Yang L, Wang Y, Zou Z, Liu M, Xu H, Wu Y. JOSD2 regulates PKM2 nuclear translocation and reduces acute myeloid leukemia progression. *Exp Hematol Oncol* 2022; **11**: 42 [PMID: 35836282 DOI: 10.1186/s40164-022-00295-w]

11 **Qian M**, Yan F, Wang W, Du J, Yuan T, Wu R, Zhao C, Wang J, Lu J, Zhang B, Lin N, Dong X, Dai X, Yang B, Zhu H, He Q. Deubiquitinase JOSD2 stabilizes YAP/TAZ to promote cholangiocarcinoma progression. *Acta Pharm Sin B* 2021; **11**: 4008-4019 [PMID: 35024322 DOI: 10.1016/j.apsb.2021.04.003]

12 **Wang Y**, Li ZX, Wang JG, Li LH, Shen WL, Dang XW. Deubiquitinating enzyme Josephin-2 stabilizes PHGDH to promote a cancer stem cell phenotype in hepatocellular carcinoma. *Genes Genomics* 2023; **45**: 215-224 [PMID: 36583817 DOI: 10.1007/s13258-022-01356-4]

13 **Chandrashekar DS**, Bashel B, Balasubramanya SAH, Creighton CJ, Ponce-Rodriguez I, Chakravarthi BVSK, Varambally S. UALCAN: A Portal for Facilitating Tumor Subgroup Gene Expression and Survival Analyses. *Neoplasia* 2017; **19**: 649-658 [PMID: 28732212 DOI: 10.1016/j.neo.2017.05.002]

14 **Chandrashekar DS**, Karthikeyan SK, Korla PK, Patel H, Shovon AR, Athar M, Netto GJ, Qin ZS, Kumar S, Manne U, Creighton CJ, Varambally S. UALCAN: An update to the integrated cancer data analysis platform. *Neoplasia* 2022; **25**: 18-27 [PMID: 35078134 DOI: 10.1016/j.neo.2022.01.001]

15 **Győrffy B**. Discovery and ranking of the most robust prognostic biomarkers in serous ovarian cancer. *Geroscience* 2023; **45**: 1889-1898 [PMID: 36856946 DOI: 10.1007/s11357-023-00742-4]

16 **Jin X**, Yan Y, Wang D, Ding D, Ma T, Ye Z, Jimenez R, Wang L, Wu H, Huang H. DUB3 Promotes BET Inhibitor Resistance and Cancer Progression by Deubiquitinating BRD4. *Mol Cell* 2018; **71**: 592-605.e4 [PMID: 30057199 DOI: 10.1016/j.molcel.2018.06.036]

17 **Li L**, Liu T, Li Y, Wu C, Luo K, Yin Y, Chen Y, Nowsheen S, Wu J, Lou Z, Yuan J. The deubiquitinase USP9X promotes tumor cell survival and confers chemoresistance through YAP1 stabilization. *Oncogene* 2018; **37**: 2422-2431 [PMID: 29449692 DOI: 10.1038/s41388-018-0134-2]

18 **Wang J**, Liu R, Mo H, Xiao X, Xu Q, Zhao W. Deubiquitinase PSMD7 promotes the proliferation, invasion, and cisplatin resistance of gastric cancer cells by stabilizing RAD23B. *Int J Biol Sci* 2021; **17**: 3331-3342 [PMID: 34512150 DOI: 10.7150/ijbs.61128]

19 **Wu J**, Liu C, Wang T, Liu H, Wei B. Deubiquitinase inhibitor PR-619 potentiates colon cancer immunotherapy by inducing ferroptosis. *Immunology* 2023; **170**: 439-451 [PMID: 37526037 DOI: 10.1111/imm.13683]

20 **Ning Z**, Guo X, Liu X, Lu C, Wang A, Wang X, Wang W, Chen H, Qin W, Zhou L, Ma C, Du J, Lin Z, Luo H, Otkur W, Qi H, Chen D, Xia T, Liu J, Tan G, Xu G, Piao HL. USP22 regulates lipidome accumulation by stabilizing PPARγ in hepatocellular carcinoma. *Nat Commun* 2022; **13**: 2187 [PMID: 35449157 DOI: 10.1038/s41467-022-29846-9]

21 **Zhang Q**, Zhang ZY, Du H, Li SZ, Tu R, Jia YF, Zheng Z, Song XM, Du RL, Zhang XD. DUB3 deubiquitinates and stabilizes NRF2 in chemotherapy resistance of colorectal cancer. *Cell Death Differ* 2019; **26**: 2300-2313 [PMID: 30778200 DOI: 10.1038/s41418-019-0303-z]

22 **Zhang FK**, Ni QZ, Wang K, Cao HJ, Guan DX, Zhang EB, Ma N, Wang YK, Zheng QW, Xu S, Zhu B, Chen TW, Xia J, Qiu XS, Ding XF, Jiang H, Qiu L, Wang X, Chen W, Cheng SQ, Xie D, Li JJ. Targeting USP9X-AMPK Axis in ARID1A-Deficient Hepatocellular Carcinoma. *Cell Mol Gastroenterol Hepatol* 2022; **14**: 101-127 [PMID: 35390516 DOI: 10.1016/j.jcmgh.2022.03.009]

23 **Dai X**, Lu L, Deng S, Meng J, Wan C, Huang J, Sun Y, Hu Y, Wu B, Wu G, Lovell JF, Jin H, Yang K. USP7 targeting modulates anti-tumor immune response by reprogramming Tumor-associated Macrophages in Lung Cancer. *Theranostics* 2020; **10**: 9332-9347 [PMID: 32802195 DOI: 10.7150/thno.47137]

24 **Zhu R**, Liu Y, Zhou H, Li L, Li Y, Ding F, Cao X, Liu Z. Deubiquitinating enzyme PSMD14 promotes tumor metastasis through stabilizing SNAIL in human esophageal squamous cell carcinoma. *Cancer Lett* 2018; **418**: 125-134 [PMID: 29331416 DOI: 10.1016/j.canlet.2018.01.025]

25 **Zhou H**, Liu Y, Zhu R, Ding F, Cao X, Lin D, Liu Z. OTUB1 promotes esophageal squamous cell carcinoma metastasis through modulating Snail stability. *Oncogene* 2018; **37**: 3356-3368 [PMID: 29559747 DOI: 10.1038/s41388-018-0224-1]

26 **Li L**, Zhou H, Zhu R, Liu Z. USP26 promotes esophageal squamous cell carcinoma metastasis through stabilizing Snail. *Cancer Lett* 2019; **448**: 52-60 [PMID: 30763716 DOI: 10.1016/j.canlet.2019.02.007]

27 **Guo X**, Zhu R, Luo A, Zhou H, Ding F, Yang H, Liu Z. EIF3H promotes aggressiveness of esophageal squamous cell carcinoma by modulating Snail stability. *J Exp Clin Cancer Res* 2020; **39**: 175 [PMID: 32867821 DOI: 10.1186/s13046-020-01678-9]

28 **Zhang B**, Zheng A, Hydbring P, Ambroise G, Ouchida AT, Goiny M, Vakifahmetoglu-Norberg H, Norberg E. PHGDH Defines a Metabolic Subtype in Lung Adenocarcinomas with Poor Prognosis. *Cell Rep* 2017; **19**: 2289-2303 [PMID: 28614715 DOI: 10.1016/j.celrep.2017.05.067]

29 **Krassikova L**, Zhang B, Nagarajan D, Queiroz AL, Kacal M, Samakidis E, Vakifahmetoglu-Norberg H, Norberg E. The deubiquitinase JOSD2 is a positive regulator of glucose metabolism. *Cell Death Differ* 2021; **28**: 1091-1109 [PMID: 33082514 DOI: 10.1038/s41418-020-00639-1]

30 **Sun Y**, Liu WZ, Liu T, Feng X, Yang N, Zhou HF. Signaling pathway of MAPK/ERK in cell proliferation, differentiation, migration, senescence and apoptosis. *J Recept Signal Transduct Res* 2015; **35**: 600-604 [PMID: 26096166 DOI: 10.3109/10799893.2015.1030412]

31 **Akbarzadeh M**, Mihanfar A, Akbarzadeh S, Yousefi B, Majidinia M. Crosstalk between miRNA and PI3K/AKT/mTOR signaling pathway in cancer. *Life Sci* 2021; **285**: 119984 [PMID: 34592229 DOI: 10.1016/j.lfs.2021.119984]

32 **Shi J**, Liu Y, Xu X, Zhang W, Yu T, Jia J, Liu C. Deubiquitinase USP47/UBP64E Regulates β-Catenin Ubiquitination and Degradation and Plays a Positive Role in Wnt Signaling. *Mol Cell Biol* 2015; **35**: 3301-3311 [PMID: 26169834 DOI: 10.1128/MCB.00373-15]

33 **Peng J**, Li W, Tan N, Lai X, Jiang W, Chen G. USP47 stabilizes BACH1 to promote the Warburg effect and non-small cell lung cancer development *via* stimulating Hk2 and Gapdh transcription. *Am J Cancer Res* 2022; **12**: 91-107 [PMID: 35141006]

34 **Zhang S**, Ju X, Yang Q, Zhu Y, Fan D, Su G, Kong L, Li Y. USP47 maintains the stemness of colorectal cancer cells and is inhibited by parthenolide. *Biochem Biophys Res Commun* 2021; **562**: 21-28 [PMID: 34030041 DOI: 10.1016/j.bbrc.2021.05.017]

35 **Lei H**, Xu HZ, Shan HZ, Liu M, Lu Y, Fang ZX, Jin J, Jing B, Xiao XH, Gao SM, Gao FH, Xia L, Yang L, Liu LG, Wang WW, Liu CX, Tong Y, Wu YZ, Zheng JK, Chen GQ, Zhou L, Wu YL. Targeting USP47 overcomes tyrosine kinase inhibitor resistance and eradicates leukemia stem/progenitor cells in chronic myelogenous leukemia. *Nat Commun* 2021; **12**: 51 [PMID: 33397955 DOI: 10.1038/s41467-020-20259-0]

36 **Padyukov L**, Hahn-Zoric M, Blomqvist SR, Ulanova M, Welch SG, Feeney AJ, Lau YL, Hanson LA. Distribution of human kappa locus IGKV2-29 and IGKV2D-29 alleles in Swedish Caucasians and Hong Kong Chinese. *Immunogenetics* 2001; **53**: 22-30 [PMID: 11261927 DOI: 10.1007/s002510000291]

37 **Haase M**, Fitze G. HSP90AB1: Helping the good and the bad. *Gene* 2016; **575**: 171-186 [PMID: 26358502 DOI: 10.1016/j.gene.2015.08.063]

38 **Jarrold J**, Davies CC. PRMTs and Arginine Methylation: Cancer's Best-Kept Secret? *Trends Mol Med* 2019; **25**: 993-1009 [PMID: 31230909 DOI: 10.1016/j.molmed.2019.05.007]

39 **Yang Y**, Bedford MT. Protein arginine methyltransferases and cancer. *Nat Rev Cancer* 2013; **13**: 37-50 [PMID: 23235912 DOI: 10.1038/nrc3409]

40 **Grasty KC**, Weeks SD, Loll PJ. Structural insights into the activity and regulation of human Josephin-2. *J Struct Biol X* 2019; **3**: 100011 [PMID: 32647816 DOI: 10.1016/j.yjsbx.2019.100011]

World Journal of Gastroenterology

Submit a Manuscript: https://www.f6publishing.com

World J Gastroenterol 2024 February 14; 30(6): 579-598

DOI: 10.3748/wjg.v30.i6.579

ISSN 1007-9327 (print) ISSN 2219-2840 (online)

META-ANALYSIS

Urea breath test for *Helicobacter pylori* infection in adult dyspeptic patients: A meta-analysis of diagnostic test accuracy

Fabian Fellipe Bueno Lemos, Caroline Tianeze de Castro, Marcel Silva Luz, Gabriel Reis Rocha, Gabriel Lima Correa Santos, Luís Guilherme de Oliveira Silva, Mariana Santos Calmon, Cláudio Lima Souza, Ana Carla Zarpelon-Schutz, Kádima Nayara Teixeira, Dulciene Maria de Magalhães Queiroz, Fabrício Freire de Melo

Specialty type: Gastroenterology and hepatology

Provenance and peer review: Invited article; Externally peer reviewed.

Peer-review model: Single blind

Peer-review report's scientific quality classification

Grade A (Excellent): 0
Grade B (Very good): B
Grade C (Good): 0
Grade D (Fair): 0
Grade E (Poor): 0

P-Reviewer: Huang YQ, China

Received: November 14, 2023
Peer-review started: November 14, 2023
First decision: December 5, 2023
Revised: December 16, 2023
Accepted: January 16, 2024
Article in press: January 16, 2024
Published online: February 14, 2024

Fabian Fellipe Bueno Lemos, Marcel Silva Luz, Gabriel Reis Rocha, Gabriel Lima Correa Santos, Luís Guilherme de Oliveira Silva, Mariana Santos Calmon, Cláudio Lima Souza, Fabrício Freire de Melo, Instituto Multidisciplinar em Saúde, Universidade Federal da Bahia, Vitória da Conquista 45029-094, Bahia, Brazil

Caroline Tianeze de Castro, Instituto de Saúde Coletiva, Universidade Federal da Bahia, Salvador 40110040, Bahia, Brazil

Ana Carla Zarpelon-Schutz, Kádima Nayara Teixeira, Campus Toledo, Universidade Federal do Paraná, Toledo 85919-899, Paraná, Brazil

Dulciene Maria de Magalhães Queiroz, Laboratory of Research in Bacteriology, UFMG, Belo Horizonte 30130-100, Minas Gerais, Brazil

Corresponding author: Fabrício Freire de Melo, PhD, Professor, Instituto Multidisciplinar em Saúde, Universidade Federal da Bahia, Estrada do Bem Querer, No. 3293-3391- Candeias, Vitória da Conquista 45029-094, Bahia, Brazil. freiremeloufba@gmail.com

Abstract

BACKGROUND

Helicobacter pylori (*H. pylori*) infection has been well-established as a significant risk factor for several gastrointestinal disorders. The urea breath test (UBT) has emerged as a leading non-invasive method for detecting *H. pylori*. Despite numerous studies confirming its substantial accuracy, the reliability of UBT results is often compromised by inherent limitations. These findings underscore the need for a rigorous statistical synthesis to clarify and reconcile the diagnostic accuracy of the UBT for the diagnosis of *H. pylori* infection.

AIM

To determine and compare the diagnostic accuracy of ^{13}C-UBT and ^{14}C-UBT for *H. pylori* infection in adult patients with dyspepsia.

METHODS

We conducted an independent search of the PubMed/MEDLINE, EMBASE, and Cochrane Central databases until April 2022. Our search included diagnostic accuracy studies that evaluated at least one of the index tests (^{13}C-UBT or ^{14}C-UBT) against a reference standard. We used the QUADAS-2 tool to assess the methodo-

logical quality of the studies. We utilized the bivariate random-effects model to calculate sensitivity, specificity, positive and negative test likelihood ratios (LR+ and LR-), as well as the diagnostic odds ratio (DOR), and their 95% confidence intervals. We conducted subgroup analyses based on urea dosing, time after urea administration, and assessment technique. To investigate a possible threshold effect, we conducted Spearman correlation analysis, and we generated summary receiver operating characteristic (SROC) curves to assess heterogeneity. Finally, we visually inspected a funnel plot and used Egger's test to evaluate publication bias.

RESULTS

The titles and abstracts of 4621 studies were screened; 79 articles were retrieved and selected for full-text reading. Finally, 60 studies were included in the diagnostic test accuracy meta-analysis. Our analysis demonstrates superior diagnostic accuracy of ^{13}C-UBT over ^{14}C-UBT, indicated by higher sensitivity (96.60% *vs* 96.15%), specificity (96.93% *vs* 89.84%), likelihood ratios (LR+ 22.00 *vs* 10.10; LR- 0.05 *vs* 0.06), and area under the curve (AUC; 0.979 *vs* 0.968). Notably, ^{13}C-UBT's DOR (586.47) significantly outperforms ^{14}C-UBT (DOR 226.50), making it the preferred diagnostic tool for dyspeptic individuals with *H. pylori* infection. Correlation analysis revealed no threshold effect (^{13}C-UBT: r = 0.48; ^{14}C-UBT: r = -0.01), and SROC curves showed consistent accuracy. Both ^{13}C-UBT and ^{14}C-UBT showed high AUC values (^{13}C-UBT 0.979; ^{14}C-UBT 0.968) near 1.00, reinforcing their excellent accuracy and endorsing both as reliable diagnostic tools in clinical practice.

CONCLUSION

In summary, our study has demonstrated that ^{13}C-UBT has been found to outperform the ^{14}C-UBT, making it the preferred diagnostic approach. Additionally, our results emphasize the significance of carefully considering urea dosage, assessment timing, and measurement techniques for both tests to enhance diagnostic precision. Nevertheless, it is crucial for researchers and clinicians to evaluate the strengths and limitations of our findings before implementing them in practice.

Key Words: *Helicobacter pylori*; Urea breath test; Diagnosis; Diagnostic test accuracy; Meta-analysis

Core Tip: The urea breath test (UBT) is a pivotal noninvasive method for detecting *Helicobacter pylori* (*H. pylori*); however, its reliability is challenging. This meta-analysis aimed to compare the precision of the ^{13}C-UBT and ^{14}C-UBT in diagnosing *H. pylori* among adults with dyspepsia, providing insights to enhance clinical strategies.

Citation: Lemos FFB, Castro CT, Silva Luz M, Rocha GR, Correa Santos GL, de Oliveira Silva LG, Calmon MS, Souza CL, Zarpelon-Schutz AC, Teixeira KN, Queiroz DMM, Freire de Melo F. Urea breath test for *Helicobacter pylori* infection in adult dyspeptic patients: A meta-analysis of diagnostic test accuracy. *World J Gastroenterol* 2024; 30(6): 579-598
URL: https://www.wjgnet.com/1007-9327/full/v30/i6/579.htm
DOI: https://dx.doi.org/10.3748/wjg.v30.i6.579

INTRODUCTION

Helicobacter pylori (*H. pylori*) is a spiral-shaped, gram-negative microaerophilic bacterium that infects approximately 43% of the global population[1]. While the majority of infected individuals remain asymptomatic, chronic gastritis inevitably ensues, leading to a significant burden of morbidity and mortality[2,3]. Adults who are infected with *H. pylori* are at increased risk of developing peptic ulcer disease, gastric cancer, and mucosa-associated lymphoid tissue lymphoma[4-6]. To address this, current guidelines advocate for either a test-and-treat or a scope-and-treat approach in managing uninvestigated dyspepsia, underscoring the importance of timely diagnosis and intervention[7,8].

Diagnostic testing for *H. pylori* infection typically involves two primary categories: Invasive (endoscopic) and non-invasive testing, depending on the application of upper endoscopy[9]. For individuals aged 50 years or older or those with alarm features, the recommended standard diagnostic approach involves upper endoscopy, followed by histopathological examination (HE) or rapid urease test (RUT), and occasionally, culture[8]. In contrast, in dyspeptic patients under 50 years without specific risk factors or alarm symptoms, non-invasive methods such as urea breath testing (UBT), stool antigen testing, and serology are preferred[8,10].

Among non-invasive diagnostic techniques, the UBT has emerged as a prominent method. This approach capitalizes on the urease activity of *H. pylori*, initiating the hydrolysis of ingested urea and consequent release of labeled carbon dioxide[11]. Two commonly utilized isotopic variants, ^{13}C-UBT and ^{14}C-UBT, offer distinctive features. In ^{13}C-UBT, a stable isotope (carbon-13) is employed, and breath samples are collected and analyzed for labeled carbon dioxide using various methods such as mass spectrometry and infrared spectrometry[12]. This method presents important advantages, notably the absence of ionizing radiation, rendering it suitable for repeated application and applicable in vulnerable populations,

including pregnant women and children[11,13]. In contrast, ^{14}C-UBT utilizes a radioactive isotope (carbon-14) and primarily relies on scintillation counting for detection[14,15]. Despite its historical use, concerns regarding radiation exposure have diminished its preference in contemporary clinical practice.

In a prior meta-analysis, Ferwana *et al*[16] assessed the diagnostic accuracy of the UBT, encompassing both ^{13}C-UBT and ^{14}C-UBT, for detecting *H. pylori* infection in adult dyspeptic patients. Despite its high accuracy, the reliability of UBT results was constrained by significant unexplained heterogeneity, persisting even after subgroup analysis[16]. This pattern persisted in subsequent studies, with Zhou *et al*[17] finding analogous challenges in calculating pooled estimates of diagnostic accuracy for ^{14}C-UBT. Moreover, a subsequent systematic review emphasized that the variability in thresholds and reference standards across studies limited the data available for pooling accuracy measures at specific UBT thresholds[18].

These findings underscore the need for a rigorous statistical synthesis to clarify and reconcile the diagnostic accuracy of the UBT for the diagnosis of *H. pylori* infection, addressing challenges identified in prior research. To address this gap in the evidence, we conducted a systematic review and meta-analysis to determine the diagnostic accuracy of the UBT for *H. pylori* infection in adult patients with dyspepsia.

MATERIALS AND METHODS

This study adhered to the guidelines outlined in the PRISMA-DTA[19]. These guidelines encompass a 27-item checklist and a 3-phase flowchart, both designed to enhance the transparency of systematic review reporting. Accordingly, our study protocol has been officially registered in the PROSPERO database under the registration number CRD42023449854.

Literature search

This search strategy was designed following the Cochrane Handbook for Systematic Reviews of Diagnostic Test Accuracy (Version 2.0, 2022)[20]. We performed independent, computer-assisted searches of the: (1) PubMed/MEDLINE; (2) EMBASE; and (3) Cochrane Library databases. MeSH (Medical Subject Headings) and Emtree (EMBASE Subject Headings) index terms and free-text words were combined. Search terms included "urea breath test," "breath test," "13C-urea breath test," "14C-urea breath test," "13C-UBT," "14C-UBT," "*Helicobacter pylori*," "*H. pylori*," and "dyspepsia." Boolean operators (AND, OR) were also used to narrow or broaden the search as required. No language restriction was applied. To identify additional studies, reference lists were also scanned. Finally, we conducted a "citing reference" search (by searching articles which cited the included studies) in PubMed/MEDLINE and EMBASE. Following the search, all identified citations were collated and uploaded into the Rayyan (https://www.rayyan.ai/) tool, and all duplicates were removed.

Selection of studies

Two independent reviewers, Lemos FFB and Calmon MS, screened the references against predefined eligibility criteria. In the case of disagreement, a 3rd researcher, Silva Luz M, was consulted. Full-text papers were obtained for references considered relevant. If any study was not retrieved, the authors were contacted. Two authors, Lemos FFB and Correa Santos GL, independently screened the full-text papers against the eligibility criteria. In the case of disagreement, consensus was reached.

We included diagnostic accuracy studies that evaluated at least one of the index tests (^{13}C- or ^{14}C-UBTs) against a reference standard (biopsy fragments followed by culture or HE or RUT and/or not serology/stool antigen-based tests in adult dyspeptic patients. Exclusion criteria were as follows: (1) Studies that enrolled children or adolescents under 18 years of age; (2) studies that included only patients with acute upper gastrointestinal bleeding; (3) studies that enrolled subjects who presented for reasons other than dyspeptic symptoms, complicated dyspeptic cases that need surgery, those who received previous therapy for *H. pylori* within the last 3 months, or long-term use of corticosteroids and immunosuppressant drugs; (4) screening studies; (5) studies that did not report true positive, false positive, false negative, and true negative data and the threshold used for the index tests; (6) case-control studies because these are prone to bias[21]; and (7) full-text articles not available or articles not available in English, Spanish, or Portuguese.

Data extraction and management

Two review authors, Rocha GR and Correa Santos GL, independently extracted data from each included study using a pre-piloted data extraction form. In case of discrepancies, a 3rd researcher, Lemos FFB, was consulted. The extracted data included: (1) Information about the studies, such as the first author, publication year, and country; (2) details about the study design, including the type of study (prospective and retrospective cohort studies, cross-sectional studies, or randomized clinical trials), the reference standards used, blinding of the index test and reference standard, and the flow and timing (retrospective/prospective); (3) participant information, *i.e.*, the total number of participants and population characteristics (age, mean ± SD, sex, and disease prevalence); (4) reference standard details, including the time interval between the index test and the reference standard; index test information, including the model (^{13}C- or ^{14}C-UBT), cut-off values, urea dosing, time for measurement after urea administration (min), and measurement technique; and (5) diagnostic accuracy data, including the number of true positives, false positives, false negatives, and true negatives.

Assessment of methodological quality

Two independent reviewers, Silva Luz M and de Oliveira Silva LG, conducted critical appraisal using the QUADAS-2 tool. In cases of disagreement, they consulted a 3rd researcher, Lemos FFB. The QUADAS-2 tool is applied in four phases

[21]: Summarizing the review question, tailoring the tool and producing review-specific guidance, constructing a flow diagram for the primary study, and evaluating bias and applicability. This tool comprises four domains: patient selection, index test, reference standard, and flow and timing. Each domain is assessed for the risk of bias, and the first three domains are also evaluated for concerns regarding applicability. It's important to note that "risk of bias" refers to internal validity, *i.e.*, whether there are systematic errors in conducting the study with respect to the specific domain, while "applicability concern" pertains to external validity, *i.e.*, whether there are concerns that the population, index test, or reference standard used in the studies align with the review question. Signaling questions were also included to assist in assessing the risk of bias.

Statistical analysis and data synthesis

Eligible studies were subjected to data extraction, and we organized the data into 2 × 2 tables. In our analysis, we selected only the optimal threshold values for *H. pylori* positivity in cases where multiple thresholds were presented. We added 0.5 to values equal to zero to ensure computational stability and prevent potential issues[22].

To address the anticipated diversity in meta-analyses of diagnostic accuracy studies, we utilized the random-effects model to calculate sensitivity, specificity, positive and negative test likelihood ratios (LR+ and LR-), as well as the diagnostic odds ratio (DOR)[23]. We also determined the corresponding 95% confidence intervals (95%CIs). The results of the ^{13}C- and ^{14}C-UBT are presented separately. Subgroup analyses were conducted with a focus on urea dosing, time for measurement after urea administration (in minutes), and the assessment technique employed. To investigate the possibility of a threshold effect in the analysis, we conducted Spearman correlation analysis. A substantial threshold effect was recognized when the correlation coefficient reached or exceeded 0.6[24].

We performed a bivariate random-effects meta-analysis and generated summary receiver operating characteristic (SROC) curves to visually assess heterogeneity. Furthermore, these curves allowed us to predict accuracy by summarizing diagnostic performance as the area under the curve (AUC)[25]. We categorized accuracy levels as follows: fail (0.50-0.60), poor (0.61-0.70), fair (0.71-0.80), good (0.81-0.90), and excellent (0.91-1.00)[22].

To evaluate publication bias, we conducted a visual inspection of a funnel plot and employed Egger's tests for statistical assessment. The creation of this plot and the assessment of the risk of data due to missing data required a minimum of ten studies.

All analyses were performed using R version 4.2.1, an environment for statistical computing in Vienna, Austria, utilizing the "meta" package (version 6.5-0), "dmetar" package (version 0.1.0), and the "mada" package (version 0.5.11).

RESULTS

Study selection

Database searches initially yielded 10902 reports, from which duplicates were removed. No additional references were discovered through alternative search methods. Subsequently, the titles and abstracts of 4621 studies underwent screening, resulting in the retrieval and selection of 79 articles for full-text examination. Ultimately, 60 studies fulfilled the inclusion criteria. The reasons for exclusion were as follows: Incorrect population (n = 8), unsuitable reference standard (n = 4), insufficient accuracy measures (n = 2), missing threshold information (n = 2), failure to compare against the reference standard (n = 1), writing in a foreign language (n = 1), and involvement of the same sample (n = 1). Figure 1 illustrates the flow of information through various phases of the systematic review.

General characteristics of included studies

Among all the studies, 39 (comprising 65%) employed the ^{13}C-UBT as their primary diagnostic test, featuring a median population size of 200 individuals (lower to upper quartile: 84.5-254). Cross-sectional study design was predominant, making up 97.5% of the total, while only one study (2.5%) adopted a randomized controlled trial approach. For the ^{13}C-UBT, the median pre-test probability was 51.2% (lower to upper quartile: 47.8-67.6). Various reference standards were used, with the most common being "*H. pylori* culture (*Hp*C) or (HE and RUT)," accounting for 22.5% of cases. Other reference standards included "HE and RUT" (17.5%), "HE" (12.5%), "HE or *Hp*C" (12.5%), "HE or (RUT and serology)" (5%), "RUT" (5%), "HE, *Hp*C, and RUT" (5%), and "*Hp*C" (2.5%). Some studies also combined reference standards, such as "RUT or HE" and "(HE, *Hp*C, RUT) at least two positives," each constituting 2.5% of the sample, as shown in Table 1.

On the other hand, the ^{14}C-UBT accounted for 35% of the total (21 studies) with a median population size of 108.5 (lower to upper quartile: 63.5-125.5). For the ^{14}C-UBT, the median pre-test probability was 64.9% (lower to upper quartile: 43.6-73.1). Various reference standards were employed in these studies, with "HE" being the most prevalent, accounting for 38.1% of cases. Other reference standards included "HE and RUT" (14.3%) and "HpC or HE" (9.5%). Some studies also used combinations of reference standards, such as "HE, RUT, Serology (at least two positive)" and "HpC or [HE and (RUT or Gram staining)]," each comprising 4.8% of the sample, as detailed in Table 2.

Methodological quality assessment

Supplementary Figure 1 and Figure 2 provide a visual representation of the comprehensive methodological quality assessment of the included studies. In the patient selection domain, 22 studies (35.5%) were categorized as having a low risk of bias, 36 studies (58.1%) were associated with a high risk of bias, and 2 studies (3.2%) were considered to have an unclear risk of bias. In terms of patient selection applicability, 40 studies (64.5%) exhibited low concern, 17 studies (27.4%) showed high concern, and 3 studies (4.8%) had unclear concern.

Table 1 Characteristics of the included studies that assessed the diagnostic test accuracy of the ^{13}C-urea breath test

Ref.	Country	Design	Population, *n*	Prevalence (%)	Reference standard	Index test (model)	Optimal cut-off	Urea dosing (mg)	Time after administration (min)	Measurement tecnique	TP	FP	TN	FN
Wang *et al*[29], 2021	China	Cross-sectional	217	65.9	HE	^{13}C-UBT	10.4‰ DOB	50	30	IS	120	14	60	23
Alzoubi *et al* [33], 2020	Jordan	Cross-sectional	30	56.7	RUT or HE	^{13}C-UBT	4‰ DOB	75	30	IS	16	3	10	1
Nawacki *et al* [34], 2018	Poland	Cross-sectional	50	36.0	RUT	^{13}C-UBT	9.5‰ DOB	NR	30	IS	16	0	32	2
Som *et al*[27], 2014	India	Cross-sectional	83	59.0	RUT	^{13}C-UBT	1.47‰	75	Multiple times	ICOS	49	0	34	0
Bruden *et al* [35], 2011	United States	Cross-sectional	280	53.2	HE or (HpC and RUT)	^{13}C-UBT	7 DOB	NR	NR	NR	139	16	115	10
Peng *et al* [36], 2009	Taiwan	Cross-sectional	100	53.0	HpC or (HE and RUT)	^{13}C-UBT	4.8‰ DOB	100	15	IS	53	7	40	0
Jordaan *et al* [37], 2008	South Africa	Cross-sectional	103	58.3	HE	^{13}C-UBT	4.5‰ DOB	75	NR	GCMS	55	3	40	5
Gatta *et al*[26], 2006	Italy	RCT	100	43.0	HE and RUT	^{13}C-UBT	4.40‰-6.26‰ DOB	25	30	IRMS	43	0	57	0
Peng *et al*[38], 2005	Taiwan	Cross-sectional	50	36.0	HpC or (HE and RUT)	^{13}C-UBT	5‰ DOB	100	15	IRMS	18	0	32	0
Kato *et al*[39], 2004	Japan	Cross-sectional	254	51.1	HpC or (HE and RUT)	^{13}C-UBT	2.5‰ DOB	100	20	IRMS	252	5	242	6
Ohara *et al*[40], 2004	Japan	Cross-sectional	254	51.2	HpC or (HE and RUT)	^{13}C-UBT	2.5‰ DOB	100	Multiple times	IRMS	127	2	122	3
Chen *et al*[41], 2003	Taiwan	Cross-sectional	554	66.6	HpC or (HE and RUT)	^{13}C-UBT	3.5‰ DOB	100	20	IS	361	6	179	8
Valdepérez *et al*[42], 2003	Spain	Cross-sectional	85	76.8	HE and RUT	^{13}C-UBT	NR	100	30	NR	61	0	19	2
Gatta *et al*[43], 2003	Italy	Cross-sectional	200	56.5	HpC or (HE and RUT)	^{13}C-UBT	3.11‰-6.84‰ DOB	75	30	IRMS	113	0	87	0
Wong *et al*[44], 2003	China	Cross-sectional	200	49.5	HE and RUT	^{13}C-UBT	2.1‰ DOB	50	20	IRMS	99	0	101	0
Ng *et al*[45], 2002	China	Cross-sectional	213	54.9	HE and RUT	^{13}C-UBT	4.0‰-6.5‰ DOB	75	30	IRMS	112	2	94	5

Wong *et al*[46], 2001	China	Cross-sectional	101	48.1	HE and RUT	^{13}C-UBT	7.0-8.0‰ DOB	50	20	IRMS	99	4	103	0
Wong *et al*[47], 2001	China	Cross-sectional	294	55.4	HE, HpC, CLO (RUT), in-house RUT, PCR, UBT (at least four positive)	^{13}C-UBT	5‰ DOB	75	30	IRMS	151	4	127	12
Shirin *et al*[48], 2001	United States	Cross-sectional	97	47.4	HE and RUT	^{13}C-UBT	Positive: > 6‰ DOB (> 2 points)/negative: < 3‰ DOB (> 2 points)	75	5	MCS	45	2	49	1
Pilotto *et al* [49], 2000	Italy	Cross-sectional	96	51.0	HE, HpC, and RUT	^{13}C-UBT	5‰ DOB	100	30	IRMS	49	2	45	0
Sheu *et al*[50], 2000	Taiwan	Cross-sectional	177	47.5	HE or HpC	^{13}C-UBT	3.5 DOB	50	15	IS	81	1	92	3
Wong *et al*[51], 2000	China	Cross-sectional	202	56.4	HE and RUT	^{13}C-UBT	4.5‰ DOB	75	30	IRMS	108	2	86	6
Hahn *et al*[52], 2000	United States	Cross-sectional	67	6.0	HE and at least two positives of (definitive presence of *H. pylori* organisms in HE, UBT, Serology)	^{13}C-UBT	2.4‰ DOB	125	30	IRMS	4	9	54	0
Chen *et al*[53], 2000	Japan	Cross-sectional	162	83.3	HE and Serology	^{13}C-UBT	2.5‰ DOB	100	20	IRMS	135	1	26	0
Peng *et al*[54], 2000	Taiwan	Cross-sectional	136	59.6	HpC or (HE and RUT)	^{13}C-UBT	4.8‰ DOB	100	15	IRMS	76	6	49	5
Riepl *et al*[55], 2000	Germany	Cross-sectional	84	35.7	HE, HpC, and RUT	^{13}C-UBT	6.5‰ DOB	75	15	IS	30	0	54	0
D'Elios *et al* [56], 2000	Italy	Cross-sectional	256	45.3	HE	^{13}C-UBT	4‰ DOB	75	30	IRMS	113	2	138	3
van der Hulst *et al*[57], 1999	Italy	Cross-sectional	544	52.2	HE or HpC	^{13}C-UBT	7.5‰ DOB ± 0.8	100	30	LOGES	260	21	239	24
Leodolter *et al* [58], 1999	Germany	Cross-sectional	320	48.1	HpC or (HE and RUT)	^{13}C-UBT	4‰ DOB	75	30	IRMS	142	2	164	12
Mock *et al*[59], 1999	Canada	Cross-sectional	98	19.8	HE or (RUT and Serology)	^{13}C-UBT	3‰ DOB	75	30	IRMS	17	2	75	2
Mock *et al*[59], 1999	Korea	Cross-sectional	107	68.2	HE or (RUT and Serology)	^{13}C-UBT	3‰ DOB	75	30	IRMS	69	1	33	4
Perri *et al*[60], 1998	Belgium	Cross-sectional	172	73.3	HE or HpC	^{13}C-UBT	1.15‰ DOB	75	60	IRMS	121	1	45	5
Ohara *et al*[61], 1998	Japan	Cross-sectional	213	77.5	HpC or at least two positives of (HE, RUT, Serology)	^{13}C-UBT	2.5‰ DOB	100	20	IRMS	162	1	47	3

Leodolter *et al* [62], 1998	Germany	Cross-sectional	40	50.0	HpC or (HE and RUT)	^{13}C-UBT	4‰ DOB	75	10	IRMS	20	0	20	0
Andersen *et al* [63], 1998	Denmark	Cross-sectional	97	54.6	HE or HpC	^{13}C-UBT	5‰ DOB	100	Multiple times	IRMS	46	4	40	7
Ellenrieder *et al* [64], 1997	Germany	Cross-sectional	132	43.2	(HE, HpC, RUT) at least two positives	^{13}C-UBT	3.5‰ DOB	NR	30	IS	52	8	67	5
Epple *et al*[65], 1997	Germany	Cross-sectional	126	61.1	HE	^{13}C-UBT	1.3‰ DOB	75	30	IRMS	74	7	42	3
Labenz *et al* [66], 1996	Germany	Cross-sectional	70	67.1	HE or HpC	^{13}C-UBT	4‰ DOB	75	30	IRMS	46	0	23	1
Logan *et al*[67], 1991	England	Cross-sectional	56	68.0	HE	^{13}C-UBT	4.5‰ DOB	125	Multiple times	IRMS	32	1	15	2
Dill *et al*[68], 1990	Scotland	Cross-sectional	69	49.3	HpC	^{13}C-UBT	3‰ c-PDR	250	20	IRMS	33	0	35	1

CLO: Campylobacter-like organism; GCMS: Gas chromatography-mass spectrometry; HE: Histopathological examination; HpC: *Helicobacter pylori* culture; ICOS: Integrated Cavity Output Spectrometry; IRMS: Isotope ratio mass spectrometry; IS: Infrared spectrometry; LOGES: Laser opto-galvanic Effect Spectroscopy; MCS: Molecular correlation spectrometry; NR: Not reported; RUT: Rapid urease test; UBT: Urea breath test; DOB: Delta over baseline; RCT: Randomized clinical trial.

Within the index test selection domain, 33 studies (53.2%) were rated as having a low risk of bias, 26 studies (41.9%) were identified with a high risk, and 1 study (1.6%) had an unclear risk of bias. Concerning index test applicability, 57 studies (91.9%) displayed low concern, while 3 studies (4.8%) raised high concern.

In the reference standard domain, 47 studies (75.8%) demonstrated a low risk of bias, 12 studies (19.4%) showed a high risk of bias, and 1 study (1.6%) had an unclear risk of bias. Notably, none of the studies raised concerns about the applicability of the reference standard.

Lastly, in the flow and timing domain, 23 studies (37.1%) were associated with a low risk of bias, 23 studies (37.1%) exhibited a high risk of bias, and 7 studies (11.3%) had an unclear risk of bias.

Overall accuracy of the ^{13}C-UBT

The ^{13}C-UBT test was evaluated for its diagnostic accuracy in 39 studies *via* a comprehensive meta-analysis The results demonstrated a high sensitivity of 96.60% (95%CI: 95.64-97.56; P value < 0.01; I^2 = 65.0%) and an equally impressive specificity of 96.93% (95%CI: 96.04-97.82; P value < 0.01; I^2 = 58.0%) for this test (Figure 3). Additionally, the DOR was calculated at 586.47 (95%CI: 340.03-1011.51), with a positive likelihood ratio (LR+) of 22.00 (95%CI: 15.60-30.10) and a negative likelihood ratio (LR-) of 0.05 (95%CI: 0.04-0.06) as presented in Supplementary Table 1.

Subgroup analysis of the ^{13}C-UBT - Urea dosing

Among the thirty-six studies that documented the urea dosage, a 25 mg urea dose demonstrated notably high sensitivity (98.85%; 95%CI: 95.68-100.00) and specificity (99.13%; 95%CI: 96.73-100.00), as illustrated in Supplementary Figure 2. Increasing the urea dose to 50 mg across four studies resulted in a sensitivity of 95.28% (95%CI: 88.51-100.00) and a specificity of 94.91% (95%CI: 87.67-100.00). Seventeen studies explored the use of 75 mg of urea in the ^{13}C-UBT, revealing

Table 2 Characteristics of the included studies that assessed the diagnostic test accuracy of the ^{14}C-urea breath test

Ref.	Country	Design	Population, n	Prevalence (%)	Reference standard	Index test (model)	Optimal cut-off	Urea dosing (μCi)	Time after administration (min)	Measurement tecnique	TP	TN	FP	FN
Han *et al*[30], 2023	China	Cross-sectional	205	42.4	HE and RUT	^{14}C-UBT	100 dpm	0.75	20	SC	83	3	115	4
Wang *et al*[29], 2021	China	Cross-sectional	267	71.9	HE	^{14}C-UBT	238 dpm	0.75	25	NR	158	12	63	34
Miftahussurur [69], 2021	Indonesia	Cross-sectional	55	23.6	HE	^{14}C-UBT	57 cpm	1	10	HA	12	1	41	1
Cosgun *et al*[70], 2016	Turkey	Cross-sectional	126	92.1	HpC or HE	^{14}C-UBT	NR	1	10	HA	112	7	3	4
Atli *et al*[71], 2012	Turkey	Cross-sectional	100	35.0	HE	^{14}C-UBT	Positive: > 50 cpm/suspicious: 25-50 cpm /negative: < 25 dpm	1	10	HA	32	4	61	3
Alarcón-Rivera *et al*[72], 2011	Mexico	Cross-sectional	84	70.2	HE	^{14}C-UBT	Positive: > 50 ppm/indeterminate: 25-50 ppm/negative: < 25 ppm	1	10-15	HA	56	1	24	3
Mansour-Ghanaei *et al*[73], 2011	Iran	Cross-sectional	125	56.8	HE, RUT, Serology (at least two positive)	^{14}C-UBT	50 cpm	1	15	HA	67	0	54	4
Ozdemir *et al*[74], 2008	Turkey	Cross-sectional	89	66.3	HE, RUT, PCR (at least two positive)	^{14}C-UBT	Positive: > 50 cpm/equivocal: 25-50 cpm; negative: < 25 dpm	1	10	HA	57	0	30	2
Rasool *et al*[75], 2007	Pakistan	Cross-sectional	94	64.9	RUT	^{14}C-UBT	50 cpm	1	10	β-SC	60	3	30	1
Gurbuz *et al*[76], 2005	Turkey	Cross-sectional	65	44.6	HE	^{14}C-UBT	Positive: > 50 cpm/suspicious: 25-50 cpm /negative: < 25 dpm	1	10	HA	26	8	28	3
Gatta *et al*[31], 2003	Italy	Cross-sectional	117	65.0	HpC or (HE and RUT)	^{14}C-UBT	130-136 dpm (dpm at sample-dpm at T0)	1	12.5	LSC	73	2	39	3
González *et al*[77], 2003	Chile	Cross-sectional	NR	71.9	Two or more positives	^{14}C-UBT	200 dpm	1	10	LSC	61	14	11	3
Oztürk *et al*[78], 2009	Turkey	Cross-sectional	75	65.8	HE	^{14}C-UBT	100 dpm	1	10	LSC	48	5	20	0
Gomes *et al*[79], 2002	Brazil	Cross-sectional	137	83.9	HE and RUT	^{14}C-UBT	1000 cpm	5	15	LSC	114	1	21	1
Desroches *et al* [80], 1997	Canada	Cross-sectional	56	80.4	HE or HpC	^{14}C-UBT	0.33‰ AS ($^{14}CO_2$ specific activity)	5	20	LSC	44	0	11	1
Allardyce *et al*	New	Cross-	63	34.9	HE and RUT	^{14}C-UBT	49 dpm	1	30	β-SC	22	2	39	0

[81], 1997	Zealand	sectional												
Faigel *et al*[82], 1996	United States	Cross-sectional	50	42.6	HE or RUT	^{14}C-UBT	Positive: > 200 dpm in any sample/borderline: 100-200 dpm (as the peak count)/negative: < 100 dpm (in all samples)	1	Multiple times	LSC	18	1	26	2
Goh *et al*[83], 1995	Malaysia	Cross-sectional	63	50.8	HpC or [HE and (RUT or Gram staining)]	^{14}C-UBT	1275 dpm	5	15	LSC	32	0	31	0
Kao *et al*[84], 1993	China	Cross-sectional	184	53.8	HpC or RUT	^{14}C-UBT	150‰	5	10	LSC	99	14	71	0
Vivas *et al*[85], 1993	Venezuela	Cross-sectional	15	53.3	HE	^{14}C-UBT	100 dpm	1	20	β-SC	8	1	6	0
Novis *et al*[28], 1991	Israel	Cross-sectional	64	80.3	HE	^{14}C-UBT	4,7‰	10	Multiple times	LSC	59	3	12	2

CLO: Campylobacter-like organism; HA: Heliprobe Analyser; HE: histopathological examination; HpC: *Helicobacter pylori* culture; LSC: Liquid scintillation counting; NR: Not reported; RUT: Rapid urease test; SC: Solid scintillation counting; UBT: Urea breath test; β-SC: Beta-scintillation counting.

a sensitivity of 96.47% (95%CI: 95.14-97.79) and a specificity of 98.33% (95%CI: 97.59-99.07). In cases where 100 mg of urea was used (in 12 studies), the ^{13}C-UBT demonstrated a sensitivity of 97.31% (95%CI: 95.92-98.70) and a specificity of 96.08% (95%CI: 94.34-97.82). Two studies employing 125 mg of urea showed a sensitivity of 93.76% (95%CI: 86.13-100.00) and a specificity of 88.66% (95%CI: 81.07-96.25). Lastly, in a single study using 250 mg of urea, the ^{13}C-UBT exhibited a sensitivity of 97.06% (95%CI: 91.38-100.00) and a specificity of 98.59% (95%CI: 94.72-100.00).

Subgroup analysis of the ^{13}C-UBT - Time for assessment after urea administration

Among the 36 studies that provided information on the time after urea administration, optimal sensitivity (98.87%; 95%CI: 98.14-99.60) and specificity (98.14%; 95%CI: 96.98-99.30) were achieved when the assessment was conducted 20 min after urea administration [in 7 studies (Supplementary Figure 3)]. Notably, there were variations in sensitivity and specificity for different time intervals following urea administration.

For tests conducted 5 min post-urea administration (in one study), sensitivity was 97.83% (95%CI: 93.61-100.0), and specificity was 96.08% (95%CI: 90.75-100.00). Tests performed 10 min after urea administration (based on one study) yielded a sensitivity of 97.56% (95%CI: 90.88-100.0) and a specificity of 97.56% (95%CI: 90.88-100.00).

Similarly, in the case of tests carried out at 15 min post-urea administration (as reported in five studies), sensitivity averaged at 97.61% (95%CI: 95.68-99.55), with specificity at 95.85% (95%CI: 91.33-100.00). Longer intervals, such as 30 min and 60 min, as well as tests conducted at multiple time points after urea administration, displayed some variability. For instance, tests performed 30 min after urea administration (in 19 studies) had a sensitivity of 95.15% (95%CI: 93.30-96.92) and a specificity of 96.18% (95%CI: 94.48-97.87). A single study conducting tests 60 min post-urea administration reported a sensitivity of 96.03% (95%CI: 92.62-99.44) and a specificity of 97.83% (95%CI: 93.61-100.00). In the case of four studies investigating multiple time points after urea administration, the sensitivity was 96.13% (95%CI: 92.13-100.0), and the specificity was 97.95% (95%CI: 96.08-99.81).

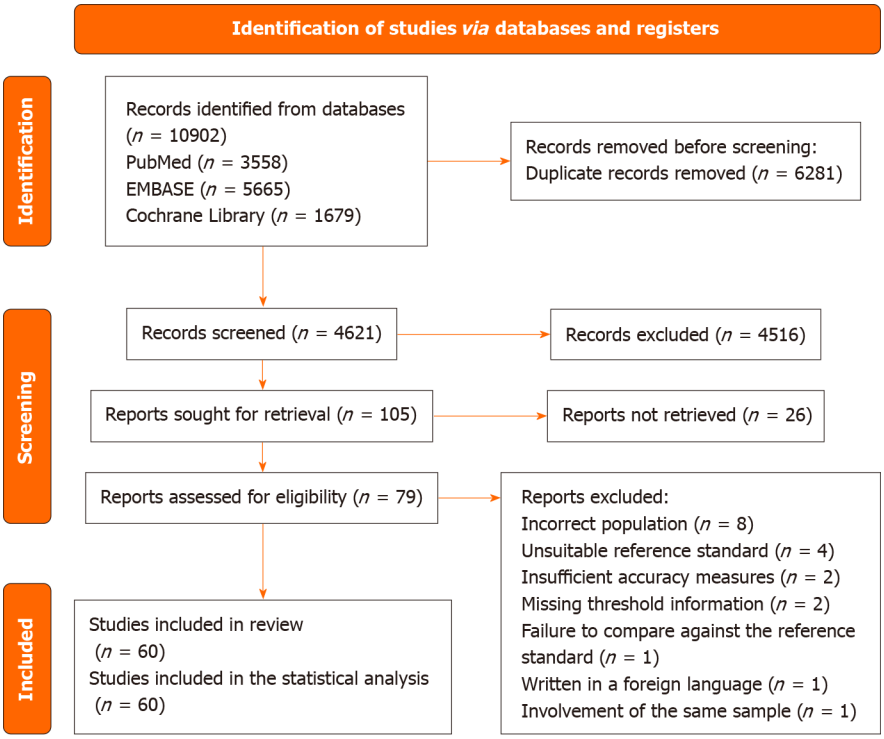

DOI: 10.3748/wjg.v30.i6.579

Figure 1 PRISMA 2020 flow diagram. This flowchart delineates the progression of information throughout various phases of the systematic review, illustrating the quantities of records identified, included, and excluded, along with the rationales for study exclusion.

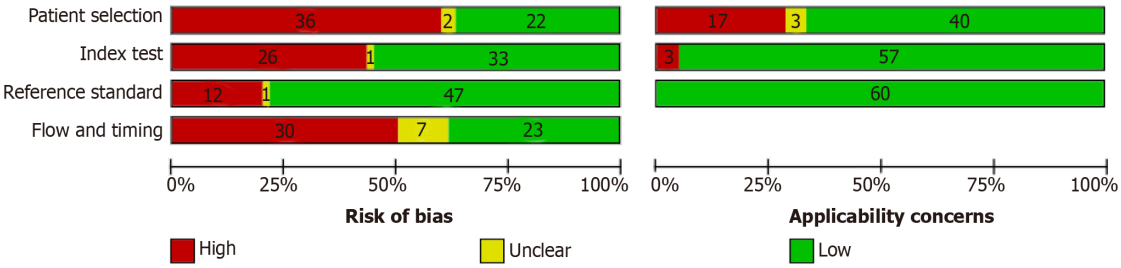

DOI: 10.3748/wjg.v30.i6.579

Figure 2 QUADAS-2 methodological quality graph. The QUADAS-2 methodological quality graph consists of four sections, each representing one of the key domains assessed.

Subgroup analysis of the ^{13}C-UBT - Assessment technique

In our analysis of 38 studies that included data on the ^{13}C-UBT assessment technique, Integrated Cavity Output Spectrometry (ICOS) for measuring CO_2 Isotope Ratios exhibited exceptional performance. ICOS demonstrated a sensitivity of 98.99% (95%CI: 96.20-100.00) and a specificity of 98.55% (95%CI: 94.56-100.00), as visualized in Supplementary Figure 4. In contrast, Infrared spectrometry, assessed in 8 studies, displayed a sensitivity of 94.72% (95%CI: 90.91-98.54) and a specificity of 98.55% (95%CI: 88.17-98.22).

Gas chromatography-mass spectrometry, investigated in a single study, yielded a sensitivity of 91.67% (95%CI: 84.67-98.66) and a specificity of 93.02% (95%CI: 85.41-100.00). Isotope-ratio mass spectrometry, scrutinized in 17 studies, demonstrated a sensitivity of 97.37% (95%CI: 96.45-98.28) and a specificity of 98.38% (95%CI: 84.67-98.66). Molecular correlation spectrometry, examined in a solitary study, exhibited a sensitivity of 97.83% (95%CI: 93.61-100.00) and a specificity of 96.08% (95%CI: 90.75-100.00). Similarly, Laser opto-galvanic effect spectroscopy, reported in one study, recorded a sensitivity of 91.65% (95%CI: 88.31-94.78) and a specificity of 91.92% (95%CI: 88.61-98.21).

Overall accuracy of the ^{14}C-UBT

A total of 21 studies investigated the diagnostic accuracy of the ^{14}C-UBT, revealing a combined sensitivity of 96.15% (95%CI: 94.47-97.82; *P* value < 0.01; I^2 = 62.0%) and specificity of 89.84% (95%CI: 84.90-94.77; *P* value < 0.01; I^2 = 78.0%), as depicted in Figure 4. Within this dataset, a DOR of 226.50 (95%CI: 102.57-500.15), a positive likelihood ratio (LR+) of 10.10 (95%CI: 5.74-16.90), and a negative likelihood ratio (LR-) of 0.06 (95%CI: 0.04-0.08) were observed, as summarized in Supplementary Table 1.

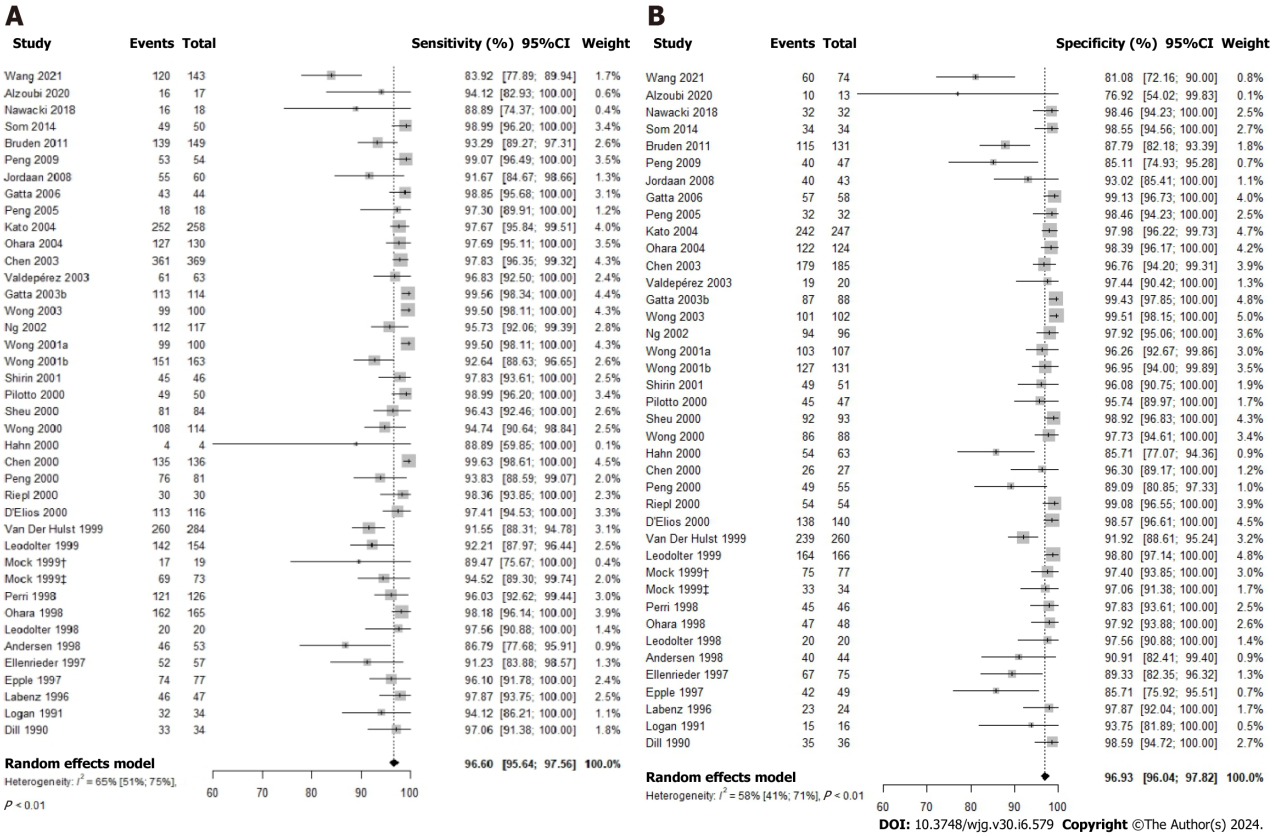

Figure 3 Forest plot for studies based on the ^{13}C-urea breath test for *Helicobacter pylori* infection in dyspeptic patients. A: Forest plot for overall sensitivity; B: Forest plot for overall specificity. 95%CI: 95% confidence interval.

Subgroup analysis of the ^{14}C-UBT - Urea dosing

Twenty-one studies investigated varying urea dosages in the context of the ^{14}C-UBT. Among these, the use of a 5 μCi marked urea dose, as examined in four studies, demonstrated exceptional sensitivity (99.21%; 95%CI: 98.20-100.00) and specificity (93.43%; 95%CI 86.45-100.00), as depicted in Supplementary Figure 5. Elevating the urea dose to 10 μCi, as explored in a single study, resulted in a sensitivity of 96.72% (95%CI: 92.15-100.00) and a specificity of 80.00% (95%CI: 56.76-100.00). Conversely, when employing 1 μCi of marked urea (in 14 studies), the ^{14}C-UBT exhibited a sensitivity of 96.78% (95%CI: 95.46-98.09) and a specificity of 87.19% (95%CI: 59.76-95.81). Lastly, two studies using 0.75 μCi of urea reported a sensitivity of 88.94% (95%CI: 76.10-100.00) and a specificity of 91.32% (95%CI: 78.18-100.00).

Subgroup analysis of the ^{14}C-UBT - Time for measurement after marked urea administration

When considering the time for measurement after urea administration, an analysis of all included studies consistently revealed the highest sensitivity (98.39%; 95%CI: 96.36-100.00) and specificity (98.71%; 95%CI: 96.58-100.00) when the tests were conducted 15 minutes after urea administration, as illustrated in Supplementary Figure 6.

In studies conducted shortly after urea administration (within 10 minutes, n = 9), the sensitivity was consistently high at 97.83% (95%CI: 96.34-99.33), while specificity was somewhat lower at 79.90% (95%CI: 66.15-93.65). A single study, conducted at 12.5 minutes post-administration, reported a sensitivity of 96.05% (95%CI: 91.67-100.00) and a specificity of 95.12% (95%CI: 88.53-100.00). Studies conducted between 10- and 15-minutes post-urea administration (n = 3) showed a sensitivity of 94.92% (95%CI: 89.31-100.00) and a specificity of 96.00% (95%CI: 88.32-100.00).

However, longer intervals (20, 25, and 30 min), as well as tests conducted at various time points after urea administration, exhibited more variability. For instance, studies conducted at 20 min post-administration (n = 3) showed a sensitivity of 96.52% (95%CI: 93.50-97.55) and a specificity of 97.23% (95%CI: 94.48-99.97). A single study conducted at 25 min post-urea administration reported a sensitivity of 82.29% (95%CI: 76.89-87.69) and a specificity of 84.00% (95%CI: 75.70-92.30). A study conducted at 30 minutes post-administration yielded a sensitivity of 97.78% (95%CI: 91.69-100.00) and a specificity of 95.12% (95%CI: 88.53-100.00). In the case of two studies that investigated multiple time points after urea administration, the sensitivity was 96.03% (95%CI: 91.79-100.00), and the specificity was 91.02% (95%CI: 76.07-100.00).

Subgroup analysis of the ^{14}C-UBT - Assessment technique

In the assessment of 20 studies with available data on the assessment technique, it was observed that liquid scintillation counting yielded a higher sensitivity of 98.79% (95%CI: 97.90-99.69) while maintaining a specificity of 87.24% (95%CI: 77.69-96.79). Conversely, Solid Scintillation UBT (scintillation counting) demonstrated higher specificity, reaching 97.46% (95%CI: 94.62-100.00), with a sensitivity of 95.40% (95%CI: 91.00-99.80), as illustrated in Supplementary Figure 7.

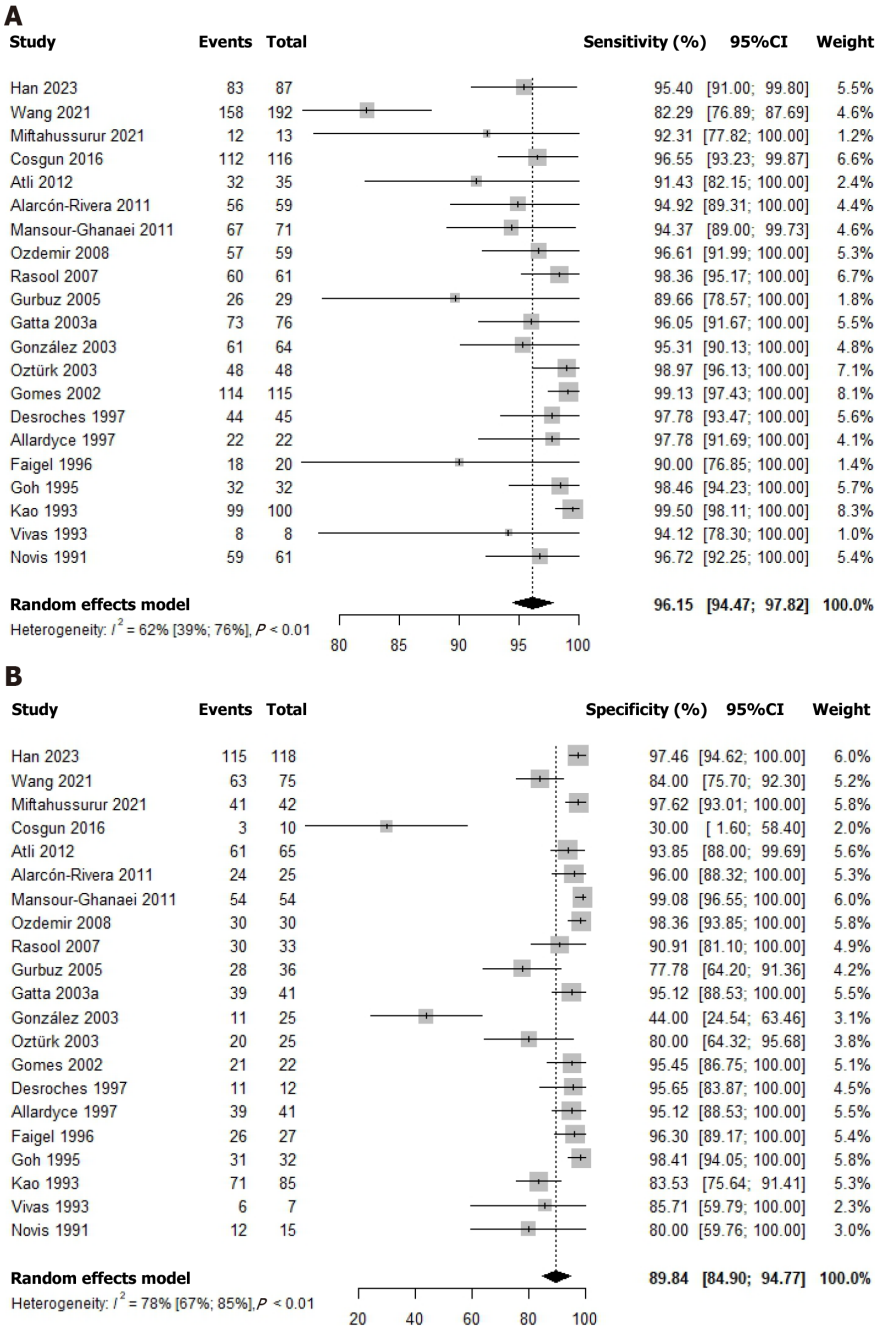

DOI: 10.3748/wjg.v30.i6.579

Figure 4 Forest plot for studies based on the ^{14}C-urea breath test for *Helicobacter pylori* infection in dyspeptic patients by time after urea administration. A: Forest plot for overall sensitivity; B: Forest plot for overall specificity. 95%CI: 95% confidence interval.

In contrast, the Heliprobe Analyser, assessed in 7 studies, displayed a sensitivity of 95.41% (95%CI: 93.32-97.50) and a specificity of 88.10% (95%CI: 74.43-100.00). Ultimately, the use of Beta-scintillation counter for the assessment of ^{14}C-UBT resulted in a sensitivity of 98.11% (95%CI: 95.33-100.00) and a specificity of 93.47% (95%CI: 88.11-98.82).

Threshold effect and SROC curve

Spearman's correlation analysis for studies evaluating ^{13}C-UBT revealed a correlation coefficient (r) of 0.48, indicating the absence of a threshold effect. Similarly, ^{14}C-UBT studies exhibited a negligible correlation (r = -0.01), also suggesting the absence of a threshold effect. Visual inspection of the SROC curves did not reveal any significant heterogeneity. Both the ^{13}C-UBT (AUC = 0.979; Figure 5A) and the ^{14}C-UBT (AUC = 0.968; Figure 5B) displayed excellent diagnostic accuracy.

Publication bias

The funnel plot visualization exposed asymmetry in both the ^{13}C-UBT (Figure 6A) and ^{14}C-UBT (Figure 6B) models. Additionally, Egger's test confirmed the presence of publication bias in both tests. The intercept was 2.54 with a P value < 0.001 for ^{13}C-UBT and 3.04 with a P value < 0.001 for ^{14}C-UBT.

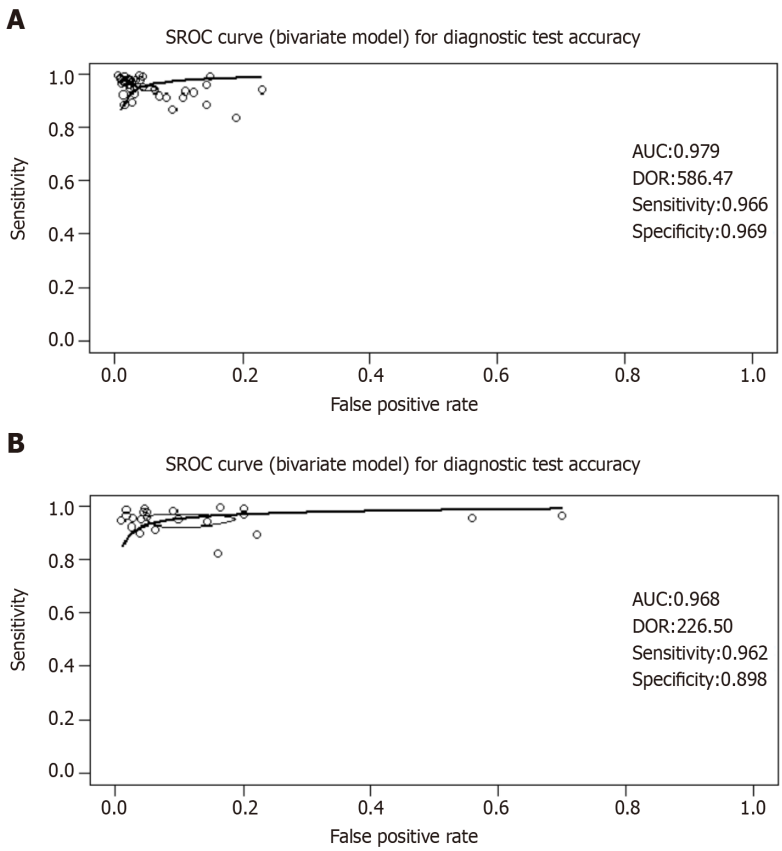

DOI: 10.3748/wjg.v30.i6.579

Figure 5 Summary operating characteristics curve curves for studies based on the ^{13}C-urea breath test and the ^{14}C-urea breath test for *Helicobacter pylori* infection in dyspeptic patients. The summary operating characteristics curve (SROC) curve is a graphical representation that combines sensitivity and specificity data from multiple studies or diagnostic tests. It illustrates how these measures change with different threshold settings or study parameters. The curve is accompanied by the area under the curve (AUC), which provides a quantitative assessment of the test's overall performance. A higher AUC value indicates better discriminatory ability across tested thresholds. Furthermore, the diagnostic odds ratio (DOR) is derived from the ROC curve and offers an evaluation of the test's diagnostic precision. A higher DOR signifies stronger discriminatory power, reflecting the odds of a positive test result in individuals with the condition compared to those without it. A: SROC curve for studies based on the ^{13}C-urea breath test (UBT) for *Helicobacter pylori* (*H. pylori*) infection in dyspeptic patients; B: SROC curve for studies based on the ^{14}C-UBT for *H. pylori* infection in dyspeptic patients. SROC: Summary operating characteristics curve; AUC: Area under the curve; DOR: Diagnostic odds ratio.

DISCUSSION

Insights from ^{13}C- and ^{14}C-UBT performance analysis

Our analysis has revealed that the ^{13}C-UBT outperforms the ^{14}C-UBT in terms of diagnostic accuracy, as evidenced by the following values: DOR, Likelihood Ratios (LR+ and LR-), and AUC values. Specifically, the ^{13}C-UBT has sensitivity and specificity values of 96.60% (95%CI: 95.64-97.56; P value < 0.01; I^2 = 65.0%) and 96.93% (95%CI: 96.04-97.82; P value < 0.01; I^2 = 58.0%), respectively. In contrast, the ^{14}C-UBT has sensitivity and specificity values of 96.15% (95%CI: 94.47-97.82; P value < 0.01; I^2 = 62.0%) and 89.84% (95%CI: 84.90-94.77; P value < 0.01; I^2 = 78.0%). The LR+ values for the ^{13}C-UBT and ^{14}C-UBT are 22.00 and 10.10, respectively, indicating the likelihood of positive results in individuals with *H. pylori* infection. Conversely, the LR- values, suggesting a reduced likelihood of negative test results for individuals with the infection, are 0.05 for the ^{13}C-UBT and 0.06 for the ^{14}C-UBT.

Furthermore, the DOR values show a substantial difference between the two tests. The ^{13}C-UBT yields a significantly higher DOR of 586.47 compared to the ^{14}C-UBT's DOR of 226.50. These results indicate that the ^{13}C-UBT is statistically superior at distinguishing dyspeptic individuals with and without *H. pylori* infection, making it the preferred diagnostic tool in this clinical context.

Finally, it is essential to emphasize that our correlation analysis, utilizing both the ^{13}C-UBT (r = 0.48) and the ^{14}C-UBT (r = -0.01), yielded no evidence of a threshold effect. Visual examination of the SROC curves revealed no heterogeneity, indicating consistent accuracy assessments across the studies. Additionally, both the ^{13}C-UBT and the ^{14}C-UBT displayed remarkably high AUC values: 0.979 for the ^{13}C-UBT and 0.968 for the ^{14}C-UBT, which approaching 1.00 reinforces the excellent accuracy of these tests in detecting *H. pylori* infection in individuals with dyspepsia. These findings strongly support the reliability of the ^{13}C-UBT and the ^{14}C-UBT as valuable diagnostic tools in clinical practice.

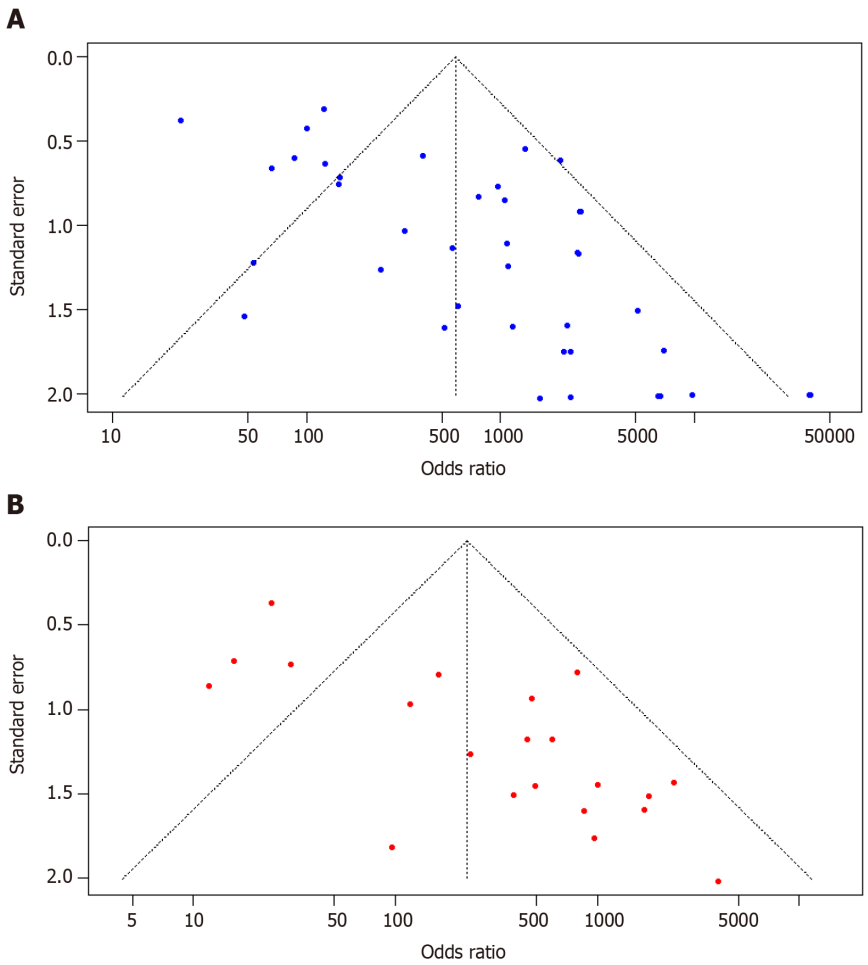

DOI: 10.3748/wjg.v30.i6.579

Figure 6 Funnel plots for studies based on ^{13}C-urea breath test and ^{14}C-urea breath test for *Helicobacter pylori* infection in dyspeptic patients. A: Funnel plot for studies based on ^{13}C-urea breath test (UBT); B: Funnel plot for studies based on ^{14}C-UBT.

^{13}C-UBT performance: Urea dose, assessment timing, and measurement technique selection

Our analysis highlights the critical importance of selecting the appropriate urea dose when conducting the ^{13}C-UBT for diagnosing *H. pylori* infection. While the 25 mg urea dose displays the highest sensitivity (98.85%) and specificity (99.13%), concerns regarding the generalizability of these results arise due to the fact that these findings are primarily based on a single study[26]. In contrast, the use of 75 mg and 100 mg doses is supported by a larger body of evidence, maintaining excellent diagnostic accuracy with sensitivity and specificity exceeding 96%. Conversely, higher doses, such as 125 mg or 250 mg, exhibit a modest reduction in accuracy, particularly in terms of specificity. These findings strongly advocate for the consideration of 75 mg and 100 mg doses when aiming to optimize both sensitivity and specificity.

A crucial factor affecting the performance of the ^{13}C-UBT is the timing of the assessment following urea administration. Our observations reveal that the optimal sensitivity and specificity, both exceeding 98%, are achieved at the 20-minute mark post-urea administration. Tests conducted at shorter intervals, such as 5 min and 10 min, also demonstrate high sensitivity and specificity, albeit slightly lower than the 20-min assessment. Conversely, assessments at 15 min maintain excellent accuracy, with sensitivity close to 98% and specificity around 95%. However, assessments at longer intervals, such as 30 min, 60 min, and multiple time points, exhibit some variability, with sensitivity and specificity values slightly lower than the 20-min assessment. These results highlight the 20-min assessment as the most reliable time point, offering a balance between high sensitivity and specificity. Nevertheless, the test remains accurate when conducted at shorter intervals.

The choice of assessment technique is also crucial for test accuracy. ICOS is the most accurate technique, with a sensitivity of 98.99% and a specificity of 98.55%. However, it is important to note that ICOS was evaluated in a single study[27], potentially limiting the generalizability of these results. To address this limitation, Isotope-ratio mass spectrometry is a more advisable option. In contrast, Infrared spectrometry, gas chromatography-mass spectrometry, isotope-ratio mass spectrometry, molecular correlation spectrometry, and Laser opto-galvanic effect spectroscopy yield varying levels of sensitivity and specificity. These findings underscore the significance of selecting the right assessment technique. While ICOS may be preferred when available due to its exceptional accuracy, other factors such as cost, availability, and local expertise should also be considered when making this choice.

^{14}C-UBT performance: Urea dose, assessment timing, and measurement technique selection

Our research indicates that the urea dosage utilized in the ^{14}C-UBT can also impact test accuracy. Specifically, a urea dose of 5 μCi was examined in four studies and was found to possess exceptional sensitivity (99.21%) and specificity (93.43%). These findings underscore the potential benefits of employing a 5 μCi dose for the ^{14}C-UBT, as it offers a high level of accuracy in detecting *H. pylori* infection. However, increasing the urea dose to 10 μCi, as investigated in a single study [28], resulted in a slightly lower sensitivity (96.72%) and a specificity of 80.00%. This suggests that while higher urea dosages may still provide reliable results, they may be associated with a decrease in specificity, which could lead to more false-positive results.

On the other hand, the use of 1 μCi of marked urea, which was the most commonly used dosage in 14 studies, resulted in a sensitivity of 96.78% and a specificity of 87.19%. This indicates that a 1 μCi dose remains a viable option for the ^{14}C-UBT, offering a good balance between sensitivity and specificity. Two recent studies using 0.75 μCi of urea reported a sensitivity of 88.94% and a specificity of 91.32%, suggesting that even lower urea doses can provide reasonable diagnostic accuracy[29,30].

Regarding the time for measurement, tests conducted 15 min after urea administration consistently exhibited the highest sensitivity (98.39%) and specificity (98.71%). This indicates that the 15-min time point is optimal for maximizing test accuracy. Tests conducted within 10 min post-administration maintained high sensitivity (97.83%) but had a somewhat lower specificity (79.90%). A single study conducted at 12.5 min post-administration reported favorable sensitivity (96.05%) and specificity (95.12%)[31]. In contrast, longer intervals (20, 25, and 30 min) showed more variability, with varying levels of sensitivity and specificity. This suggests that measurements taken beyond 15 min may not be as reliable for *H. pylori* detection. Clinicians should carefully consider the timing of the ^{14}C-UBT to ensure accurate results, with a preference for the 15-min mark when feasible.

Lastly, our analysis of assessment techniques uncovered differences in sensitivity and specificity. Liquid scintillation counting demonstrated the highest sensitivity (98.79%) but had a specificity of 87.24%. In contrast, Solid Scintillation UBT (scintillation counting) showed higher specificity (97.46%) at the expense of sensitivity (95.40%). The Heliprobe Analyser and Beta-scintillation counter also demonstrated moderate sensitivity and specificity. When choosing the assessment technique, the trade-off between sensitivity and specificity should be considered in relation to the clinical context. For instance, if high sensitivity is paramount to avoid missing positive cases, liquid scintillation counting may be the preferred method. Conversely, if high specificity is crucial to minimize false positives, solid scintillation counting could be a better choice.

Strengths and limitations

This meta-analysis adhered to established guidelines and rigorous methodological principles, enhancing the validity and reliability of our findings. We used a bivariate random-effects model to calculate sensitivity, specificity, likelihood ratios, and the DOR, alongside generating SROC curves for a comprehensive statistical analysis of the included studies. Subgroup analyses based on urea dosing, measurement timing, and assessment technique were conducted to explore potential sources of variation, while Spearman correlation analysis was used to assess the threshold effect's impact on diagnostic accuracy. Additionally, we assessed publication bias through visual inspections of funnel plots and Egger's tests.

However, it's important to acknowledge inherent limitations in our analysis. These include potential language bias, reliance on available data, and challenges associated with the inherent heterogeneity in diagnostic accuracy studies. Although we did not impose language restrictions in our search, the inclusion of studies conducted in English, Spanish, or Portuguese may introduce language bias[32]. The exclusion of studies due to unavailability of full-text articles or articles not in these specified languages could potentially lead to the omission of essential data.

Furthermore, the quality of our meta-analysis is closely tied to the quality of the primary studies we included. Biases within these primary studies can affect our analysis outcomes. In particular, we have concerns regarding the inclusion of patients, as there was no reported consecutive patient inclusion in some studies, and the index test was not always performed using a pre-specified threshold. Moreover, the diversity in diagnostic accuracy studies can present challenges when consolidating results, and despite subgroup analyses, residual heterogeneity may impact the broad applicability of our findings. Encouragingly, the visual examination of the SROC curves indicates consistent accuracy assessments across the included studies. Nevertheless, it is imperative to underscore that the reliability of our meta-analysis hinges on the data provided in these included studies. The absence or inconsistency of critical data points can significantly affect the precision of our analysis. Researchers and clinicians should consider these strengths and limitations when applying our findings in their practice.

CONCLUSION

In summary, our study offers crucial insights for selecting optimal diagnostic methods to detect *H. pylori* infection in clinical settings. We found that the ^{13}C-UBT outperforms the ^{14}C-UBT in terms of diagnostic accuracy, making it the preferred diagnostic approach. Furthermore, our findings highlight the significance of precise considerations when choosing urea dosage, assessment timing, and measurement techniques for both the ^{13}C-UBT and ^{14}C-UBT, thus enhancing diagnostic precision. These insights provide practical guidance to healthcare practitioners when choosing the most suitable diagnostic method for *H. pylori* infection, tailored to their specific clinical context. Factors like diagnostic accuracy, cost, and availability should be carefully weighed in this decision-making process. Our findings also have the potential to contribute significantly to the standardization of testing procedures, ensuring consistent and reliable results,

especially for patients with dyspepsia or suspected *H. pylori* infection. Nevertheless, it's essential for researchers and clinicians to consider the strengths and limitations when applying our findings in their practice.

ARTICLE HIGHLIGHTS

Research background

The urea breath test (UBT) has become a widely accepted non-invasive method for detecting *Helicobacter pylori* (*H. pylori*). While numerous studies have confirmed its high accuracy, its reliability is often hindered by inherent limitations.

Research motivation

In a previous investigation, the diagnostic accuracy of the UBT, which encompasses both ^{13}C-UBT and ^{14}C-UBT, was evaluated in adult patients with dyspepsia to determine the presence of *H. pylori* infection. Although the test demonstrated a high degree of precision, its reliability was compromised by significant and unexplained heterogeneity, which persisted even after conducting subgroup analyses. This trend continued in subsequent studies, with similar challenges encountered in determining pooled estimates of diagnostic accuracy for ^{14}C-UBT. Furthermore, a subsequent systematic review revealed that the variability in thresholds and reference standards across studies limited the available data for pooling accuracy measures at specific UBT thresholds. These findings underscore the need for a rigorous statistical synthesis to clarify and reconcile the diagnostic accuracy of the UBT for the diagnosis of *H. pylori* infection, addressing challenges identified in prior research.

Research objectives

To evaluate and contrast the diagnostic accuracy of ^{13}C-UBT and ^{14}C-UBT for *H. pylori* infection in adult patients with dyspepsia.

Research methods

We conducted independent searches of PubMed/MEDLINE, EMBASE, and Cochrane Central databases until April 2022, focusing on diagnostic accuracy studies that evaluated at least one of the index tests (^{13}C-UBT or ^{14}C-UBT) against a reference standard. We utilized the QUADAS-2 tool to assess the methodological quality of the studies, and we calculated sensitivity, specificity, positive and negative test likelihood ratios (LR+ and LR-), as well as the diagnostic odds ratio (DOR) and their 95% confidence intervals using the bivariate random-effects model. We conducted subgroup analyses based on urea dosing, time after urea administration, and assessment technique. To investigate a possible threshold effect, we conducted Spearman correlation analysis, and we generated summary receiver operating characteristic (SROC) curves to assess heterogeneity. Lastly, we visually inspected a funnel plot and used Egger's test to evaluate publication bias.

Research results

A screening of 4621 studies led to the selection of 60 articles for inclusion in a diagnostic test accuracy meta-analysis after full-text reading. Our analysis highlights the superior diagnostic accuracy of ^{13}C-UBT compared to ^{14}C-UBT, as evidenced by higher sensitivity (96.60% *vs* 96.15%), specificity (96.93% *vs* 89.84%), likelihood ratios (LR+ 22.00 *vs* 10.10; LR- 0.05 *vs* 0.06), and AUC values (0.979 *vs* 0.968). Particularly noteworthy is the significantly higher DOR of ^{13}C-UBT (586.47) compared to ^{14}C-UBT (DOR 226.50), establishing ^{13}C-UBT as the preferred diagnostic tool for individuals with dyspepsia and *H. pylori* infection. Correlation analysis indicated no threshold effect for both ^{13}C-UBT (r = 0.48) and ^{14}C-UBT (r = -0.01), and the SROC curves consistently demonstrated accurate performance for both tests. The high AUC values (^{13}C-UBT: 0.979; ^{14}C-UBT: 0.968), nearing 1.00, further affirm the excellent accuracy of both UBT variants, solidifying their reliability as diagnostic tools in clinical practice.

Research conclusions

Our study establishes ^{13}C-UBT as the superior diagnostic approach over ^{14}C-UBT. Furthermore, our findings underscore the critical importance of meticulously considering factors such as urea dosage, assessment timing, and measurement techniques for both tests to optimize diagnostic accuracy. However, it is paramount for researchers and clinicians to thoroughly evaluate the strengths and limitations of our conclusions before integrating them into clinical practice.

Research perspectives

Future research should focus on improving the comprehension, practicality, and dependability of UBTs for *H. pylori* infection. This endeavor involves refining techniques, examining sources of variability, exploring threshold effects, conducting longitudinal and comparative investigations, addressing biases, and assessing cost-effectiveness.

FOOTNOTES

Author contributions: Lemos FFB, Castro CT, Silva Luz M, Queiroz DMM, and Freire de Melo F contributed to the conceptualization of the manuscript; Lemos FFB, Castro CT, Queiroz DMM and Freire de Melo F designed the study methodology; Lemos FFB, Castro CT,

Calmon MS, Silva Luz M, Rocha GR, Correa Santos GL, de Oliveira Silva LG, Calmon MS were responsible for manuscript visualization; Lemos FFB, Castro CT, Calmon MS, Silva Luz M, Rocha GR, Correa Santos GL, de Oliveira Silva LG, Calmon MS contributed to the investigation; Lemos FFB, Castro CT, Calmon MS, Silva Luz M, Rocha GR, Correa Santos GL, de Oliveira Silva LG, Calmon MS performed formal analysis; Lemos FFB and Castro CT wrote the original draft; Castro CT and Queiroz DMM were responsible for manuscript editing; Castro CT, Teixeira KN, Souza CL, and Queiroz DMM were responsible for manuscript writing and review; Freire de Melo F supervised the writing of the original draft.

Supported by Scientific Initiation Scholarship Programme (PIBIC) of the Bahia State Research Support Foundation; the Doctorate Scholarship Program of the Coordination of Improvement of Higher Education Personnel; the Scientific Initiation Scholarship Programme (PIBIC) of the National Council for Scientific and Technological Development; and the CNPq Research Productivity Fellowship.

Conflict-of-interest statement: The authors declare no conflict of interest.

PRISMA 2009 Checklist statement: The authors have read the PRISMA 2009 Checklist, and the manuscript was prepared and revised according to the PRISMA 2009 Checklist.

Country/Territory of origin: Brazil

ORCID number: Fabian Fellipe Bueno Lemos 0000-0002-4686-7086; Caroline Tianeze de Castro 0000-0002-9445-8842; Marcel Silva Luz 0000-0003-1650-5807; Gabriel Reis Rocha 0000-0002-3090-0726; Gabriel Lima Correa Santos 0000-0003-3673-9889; Luís Guilherme de Oliveira Silva 0000-0001-7275-7182; Mariana Santos Calmon 0000-0002-3871-7408; Cláudio Lima Souza 0000-0002-8094-8357; Ana Carla Zarpelon-Schutz 0000-0002-8320-3633; Kádima Nayara Teixeira 0000-0002-2928-9181; Dulciene Maria de Magalhães Queiroz 0000-0003-1334-9423; Fabrício Freire de Melo 0000-0002-5680-2753.

S-Editor: Lin C
L-Editor: A
P-Editor: Zhao YQ

REFERENCES

1 **Li Y**, Choi H, Leung K, Jiang F, Graham DY, Leung WK. Global prevalence of Helicobacter pylori infection between 1980 and 2022: a systematic review and meta-analysis. *Lancet Gastroenterol Hepatol* 2023; **8**: 553-564 [PMID: 37086739 DOI: 10.1016/S2468-1253(23)00070-5]

2 **Sugano K**, Tack J, Kuipers EJ, Graham DY, El-Omar EM, Miura S, Haruma K, Asaka M, Uemura N, Malfertheiner P; faculty members of Kyoto Global Consensus Conference. Kyoto global consensus report on Helicobacter pylori gastritis. *Gut* 2015; **64**: 1353-1367 [PMID: 26187502 DOI: 10.1136/gutjnl-2015-309252]

3 **Malfertheiner P**, Camargo MC, El-Omar E, Liou JM, Peek R, Schulz C, Smith SI, Suerbaum S. Helicobacter pylori infection. *Nat Rev Dis Primers* 2023; **9**: 19 [PMID: 37081005 DOI: 10.1038/s41572-023-00431-8]

4 **Narayanan M**, Reddy KM, Marsicano E. Peptic Ulcer Disease and Helicobacter pylori infection. *Mo Med* 2018; **115**: 219-224 [PMID: 30228726]

5 **Usui Y**, Taniyama Y, Endo M, Koyanagi YN, Kasugai Y, Oze I, Ito H, Imoto I, Tanaka T, Tajika M, Niwa Y, Iwasaki Y, Aoi T, Hakozaki N, Takata S, Suzuki K, Terao C, Hatakeyama M, Hirata M, Sugano K, Yoshida T, Kamatani Y, Nakagawa H, Matsuda K, Murakami Y, Spurdle AB, Matsuo K, Momozawa Y. Helicobacter pylori, Homologous-Recombination Genes, and Gastric Cancer. *N Engl J Med* 2023; **388**: 1181-1190 [PMID: 36988593 DOI: 10.1056/NEJMoa2211807]

6 **Lemos FFB**, de Castro CT, Calmon MS, Silva Luz M, Pinheiro SLR, Faria Souza Mendes Dos Santos C, Correa Santos GL, Marques HS, Delgado HA, Teixeira KN, Souza CL, Oliveira MV, Freire de Melo F. Effectiveness of Helicobacter pylori eradication in the treatment of early-stage gastric mucosa-associated lymphoid tissue lymphoma: An up-to-date meta-analysis. *World J Gastroenterol* 2023; **29**: 2202-2221 [PMID: 37122607 DOI: 10.3748/wjg.v29.i14.2202]

7 **Liou JM**, Malfertheiner P, Lee YC, Sheu BS, Sugano K, Cheng HC, Yeoh KG, Hsu PI, Goh KL, Mahachai V, Gotoda T, Chang WL, Chen MJ, Chiang TH, Chen CC, Wu CY, Leow AH, Wu JY, Wu DC, Hong TC, Lu H, Yamaoka Y, Megraud F, Chan FKL, Sung JJ, Lin JT, Graham DY, Wu MS, El-Omar EM; Asian Pacific Alliance on Helicobacter and Microbiota (APAHAM). Screening and eradication of Helicobacter pylori for gastric cancer prevention: the Taipei global consensus. *Gut* 2020; **69**: 2093-2112 [PMID: 33004546 DOI: 10.1136/gutjnl-2020-322368]

8 **Malfertheiner P**, Megraud F, Rokkas T, Gisbert JP, Liou JM, Schulz C, Gasbarrini A, Hunt RH, Leja M, O'Morain C, Rugge M, Suerbaum S, Tilg H, Sugano K, El-Omar EM; European Helicobacter and Microbiota Study group. Management of Helicobacter pylori infection: the Maastricht VI/Florence consensus report. *Gut* 2022 [PMID: 35944925 DOI: 10.1136/gutjnl-2022-327745]

9 **Talebi Bezmin Abadi A**. Diagnosis of Helicobacter pylori Using Invasive and Noninvasive Approaches. *J Pathog* 2018; **2018**: 9064952 [PMID: 29951318 DOI: 10.1155/2018/9064952]

10 **Kayali S**, Aloe R, Bonaguri C, Gaiani F, Manfredi M, Leandro G, Fornaroli F, Di Mario F, De' Angelis GL. Non-invasive tests for the diagnosis of helicobacter pylori: state of the art. *Acta Biomed* 2018; **89**: 58-64 [PMID: 30561419 DOI: 10.23750/abm.v89i8-S.7910]

11 **Sankararaman S**, Moosavi L. Urea Breath Test. In: StatPearls [Internet]. Treasure Island (FL): StatPearls Publishing; 2023 [PMID:

31194426]
12 **Savarino V**, Vigneri S, Celle G. The 13C urea breath test in the diagnosis of Helicobacter pylori infection. *Gut* 1999; **45** Suppl 1: I18-I22 [PMID: 10457031 DOI: 10.1136/gut.45.2008.i18]
13 **Leal YA**, Flores LL, Fuentes-Pananá EM, Cedillo-Rivera R, Torres J. 13C-urea breath test for the diagnosis of Helicobacter pylori infection in children: a systematic review and meta-analysis. *Helicobacter* 2011; **16**: 327-337 [PMID: 21762274 DOI: 10.1111/j.1523-5378.2011.00863.x]
14 **Balon H**, Gold CA, Dworkin HJ, McCormick VA, Freitas JE. Procedure guideline for carbon-14-urea breath test. Society of Nuclear Medicine. *J Nucl Med* 1998; **39**: 2012-2014 [PMID: 9829599]
15 **Balon HR**, Roff E. C-14-urea breath test: a new product and a word of caution. *J Nucl Med* 1998; **39**: 1306 [PMID: 9669416]
16 **Ferwana M**, Abdulmajeed I, Alhajiahmed A, Madani W, Firwana B, Hasan R, Altayar O, Limburg PJ, Murad MH, Knawy B. Accuracy of urea breath test in Helicobacter pylori infection: meta-analysis. *World J Gastroenterol* 2015; **21**: 1305-1314 [PMID: 25632206 DOI: 10.3748/wjg.v21.i4.1305]
17 **Zhou Q**, Li L, Ai Y, Pan Z, Guo M, Han J. Diagnostic accuracy of the (14)C-urea breath test in Helicobacter pylori infections: a meta-analysis. *Wien Klin Wochenschr* 2017; **129**: 38-45 [PMID: 27848071 DOI: 10.1007/s00508-016-1117-3]
18 **Best LM**, Takwoingi Y, Siddique S, Selladurai A, Gandhi A, Low B, Yaghoobi M, Gurusamy KS. Non-invasive diagnostic tests for Helicobacter pylori infection. *Cochrane Database Syst Rev* 2018; **3**: CD012080 [PMID: 29543326 DOI: 10.1002/14651858.CD012080.pub2]
19 **McInnes MDF**, Moher D, Thombs BD, McGrath TA, Bossuyt PM; and the PRISMA-DTA Group, Clifford T, Cohen JF, Deeks JJ, Gatsonis C, Hooft L, Hunt HA, Hyde CJ, Korevaar DA, Leeflang MMG, Macaskill P, Reitsma JB, Rodin R, Rutjes AWS, Salameh JP, Stevens A, Takwoingi Y, Tonelli M, Weeks L, Whiting P, Willis BH. Preferred Reporting Items for a Systematic Review and Meta-analysis of Diagnostic Test Accuracy Studies: The PRISMA-DTA Statement. *JAMA* 2018; **319**: 388-396 [PMID: 29362800 DOI: 10.1001/jama.2017.19163]
20 **Deeks JJ**, Bossuyt PM, Leeflang MM, Takwoingi Y. Cochrane Handbook for Systematic Reviews of Diagnostic Test Accuracy. 1st ed. New Jersey: John Wiley, 2023 [DOI: 10.1002/9781119756194]
21 **Whiting PF**, Rutjes AW, Westwood ME, Mallett S, Deeks JJ, Reitsma JB, Leeflang MM, Sterne JA, Bossuyt PM; QUADAS-2 Group. QUADAS-2: a revised tool for the quality assessment of diagnostic accuracy studies. *Ann Intern Med* 2011; **155**: 529-536 [PMID: 22007046 DOI: 10.7326/0003-4819-155-8-201110180-00009]
22 **Reiman MP**, Thorborg K, Goode AP, Cook CE, Weir A, Hölmich P. Diagnostic Accuracy of Imaging Modalities and Injection Techniques for the Diagnosis of Femoroacetabular Impingement/Labral Tear: A Systematic Review With Meta-analysis. *Am J Sports Med* 2017; **45**: 2665-2677 [PMID: 28129509 DOI: 10.1177/0363546516686960]
23 **Macaskill P**, Takwoingi Y, Deeks JJ, Gatsonis C. Understanding meta-analysis. In: Cochrane Handbook for Systematic Reviews of Diagnostic Test Accuracy. 1st ed. Deeks JJ, Bossuyt PM, Leeflang MM, Takwoingi Y, editors. New Jersey: John Wiley, 2023: 203-247 [DOI: 10.1002/9781119756194.ch9]
24 **Kim KW**, Lee J, Choi SH, Huh J, Park SH. Systematic Review and Meta-Analysis of Studies Evaluating Diagnostic Test Accuracy: A Practical Review for Clinical Researchers-Part I. General Guidance and Tips. *Korean J Radiol* 2015; **16**: 1175-1187 [PMID: 26576106 DOI: 10.3348/kjr.2015.16.6.1175]
25 **Lee J**, Kim KW, Choi SH, Huh J, Park SH. Systematic Review and Meta-Analysis of Studies Evaluating Diagnostic Test Accuracy: A Practical Review for Clinical Researchers-Part II. Statistical Methods of Meta-Analysis. *Korean J Radiol* 2015; **16**: 1188-1196 [PMID: 26576107 DOI: 10.3348/kjr.2015.16.6.1188]
26 **Gatta L**, Ricci C, Tampieri A, Osborn J, Perna F, Bernabucci V, Vaira D. Accuracy of breath tests using low doses of 13C-urea to diagnose Helicobacter pylori infection: a randomised controlled trial. *Gut* 2006; **55**: 457-462 [PMID: 16162678 DOI: 10.1136/gut.2005.078626]
27 **Som S**, Maity A, Banik GD, Ghosh C, Chaudhuri S, Daschakraborty SB, Ghosh S, Pradhan M. Excretion kinetics of 13C-urea breath test: influences of endogenous CO2 production and dose recovery on the diagnostic accuracy of Helicobacter pylori infection. *Anal Bioanal Chem* 2014; **406**: 5405-5412 [PMID: 24939135 DOI: 10.1007/s00216-014-7951-0]
28 **Novis BH**, Gabay G, Leichtmann G, Peri M, Bernheim J, Pomeranz IS. Two point analysis 15-minute 14C-urea breath test for diagnosing Helicobacter pylori infection. *Digestion* 1991; **50**: 16-21 [PMID: 1804728 DOI: 10.1159/000200735]
29 **Wang X**, Zhang S, Chua EG, He Y, Li X, Liu A, Chen H, Wise MJ, Marshall BJ, Sun D, Tay CY. A re-testing range is recommended for (13)C- and (14)C-urea breath tests for Helicobacter pylori infection in China. *Gut Pathog* 2021; **13**: 38 [PMID: 34118962 DOI: 10.1186/s13099-021-00435-3]
30 **Han YH**, Zhang W, Wang YT, Xiong ZJ, Du Q, Xie Y, Lu H. Performance evaluation of a novel 14C-urea breath test (solid scintillation) for the diagnosis of helicobacter pylori infection. *Medicine (Baltimore)* 2023; **102**: e33107 [PMID: 36862867 DOI: 10.1097/MD.0000000000033107]
31 **Gatta L**, Ricci C, Stanghellini V, Alì A, Menegatti M, Morselli Labate AM, Corinaldesi R, Miglioli M, Vaira D. Best cut-off values for [14C]-urea breath tests for Helicobacter pylori detection. *Scand J Gastroenterol* 2003; **38**: 1144-1148 [PMID: 14686717 DOI: 10.1080/00365520310006261]
32 **Stern C**, Kleijnen J. Language bias in systematic reviews: you only get out what you put in. *JBI Evid Synth* 2020; **18**: 1818-1819 [PMID: 32925418 DOI: 10.11124/JBIES-20-00361]
33 **Alzoubi H**, Al-Mnayyis A, Al Rfoa I, Aqel A, Abu-Lubad M, Hamdan O, Jaber K. The Use of (13)C-Urea Breath Test for Non-Invasive Diagnosis of Helicobacter pylori Infection in Comparison to Endoscopy and Stool Antigen Test. *Diagnostics (Basel)* 2020; **10** [PMID: 32635179 DOI: 10.3390/diagnostics10070448]
34 **Nawacki Ł**, Czyż A, Bryk P, Kozieł D, Stępień R, Głuszek S. Can urea breath test (UBT) replace rapid urea test (RUT)? *Pol Przegl Chir* 2018; **90**: 44-48 [PMID: 30426947 DOI: 10.5604/01.3001.0012.0669]
35 **Bruden DL**, Bruce MG, Miernyk KM, Morris J, Hurlburt D, Hennessy TW, Peters H, Sacco F, Parkinson AJ, McMahon BJ. Diagnostic accuracy of tests for Helicobacter pylori in an Alaska Native population. *World J Gastroenterol* 2011; **17**: 4682-4688 [PMID: 22180710 DOI: 10.3748/wjg.v17.i42.4682]
36 **Peng NJ**, Lai KH, Lo GH, Hsu PI. Comparison of noninvasive diagnostic tests for Helicobacter pylori infection. *Med Princ Pract* 2009; **18**: 57-61 [PMID: 19060493 DOI: 10.1159/000163048]
37 **Jordaan M**, Laurens JB. Diagnosis of Helicobacter pylori infection with the (13)C-urea breath test by means of GC-MS analysis. *J Sep Sci* 2008; **31**: 329-335 [PMID: 18196527 DOI: 10.1002/jssc.200700385]
38 **Peng NJ**, Lai KH, Liu RS, Lee SC, Tsay DG, Lo CC, Tseng HH, Huang WK, Lo GH, Hsu PI. Capsule 13C-urea breath test for the diagnosis of Helicobacter pylori infection. *World J Gastroenterol* 2005; **11**: 1361-1364 [PMID: 15761976 DOI: 10.3748/wjg.v11.i9.1361]
39 **Kato S**, Nakayama K, Minoura T, Konno M, Tajiri H, Matsuhisa T, Iinuma K; Japanese pediatric Helicobacter study group. Comparison

between the 13C-urea breath test and stool antigen test for the diagnosis of childhood Helicobacter pylori infection. *J Gastroenterol* 2004; **39**: 1045-1050 [PMID: 15580396 DOI: 10.1007/s00535-004-1442-6]

40 **Ohara S**, Kato M, Saito M, Fukuda S, Kato C, Hamada S, Nagashima R, Obara K, Suzuki M, Honda H, Asaka M, Toyota T. Comparison between a new 13C-urea breath test, using a film-coated tablet, and the conventional 13C-urea breath test for the detection of Helicobacter pylori infection. *J Gastroenterol* 2004; **39**: 621-628 [PMID: 15293131 DOI: 10.1007/s00535-004-1356-3]

41 **Chen TS**, Chang FY, Chen PC, Huang TW, Ou JT, Tsai MH, Wu MS, Lin JT. Simplified 13C-urea breath test with a new infrared spectrometer for diagnosis of Helicobacter pylori infection. *J Gastroenterol Hepatol* 2003; **18**: 1237-1243 [PMID: 14535979 DOI: 10.1046/j.1440-1746.2003.03139.x]

42 **Valdepérez J**, Vicente R, Novella MP, Valle L, Sicilia B, Yus C, Gomollón F. [Is the breath test reliable in primary care diagnosis of Helicobacter pylori infection?]. *Aten Primaria* 2003; **31**: 93-97 [PMID: 12609106 DOI: 10.1016/s0212-6567(03)79144-6]

43 **Gatta L**, Vakil N, Ricci C, Osborn JF, Tampieri A, Perna F, Miglioli M, Vaira D. A rapid, low-dose, 13C-urea tablet for the detection of Helicobacter pylori infection before and after treatment. *Aliment Pharmacol Ther* 2003; **17**: 793-798 [PMID: 12641501 DOI: 10.1046/j.1365-2036.2003.01490.x]

44 **Wong WM**, Lam SK, Lai KC, Chu KM, Xia HH, Wong KW, Cheung KL, Lin SK, Wong BC. A rapid-release 50-mg tablet-based 13C-urea breath test for the diagnosis of Helicobacter pylori infection. *Aliment Pharmacol Ther* 2003; **17**: 253-257 [PMID: 12534410 DOI: 10.1046/j.1365-2036.2003.01417.x]

45 **Ng FH**, Lai KC, Wong BC, Wong WM, Wong SY, Chow KC, Yuen ST, Leung SY, Lam SK. [13C]-urea breath test without prior fasting and without test meal is accurate for the detection of Helicobacter pylori infection in Chinese. *J Gastroenterol Hepatol* 2002; **17**: 834-838 [PMID: 12164957 DOI: 10.1046/j.1440-1746.2002.02833.x]

46 **Wong WM**, Wong BC, Li TM, Wong KW, Cheung KL, Fung FM, Xia HH, Lam SK. Twenty-minute 50 mg 13C-urea breath test without test meal for the diagnosis of Helicobacter pylori infection in Chinese. *Aliment Pharmacol Ther* 2001; **15**: 1499-1504 [PMID: 11552925 DOI: 10.1046/j.1365-2036.2001.01078.x]

47 **Wong BC**, Wong WM, Wang WH, Tang VS, Young J, Lai KC, Yuen ST, Leung SY, Hu WH, Chan CK, Hui WM, Lam SK. An evaluation of invasive and non-invasive tests for the diagnosis of Helicobacter pylori infection in Chinese. *Aliment Pharmacol Ther* 2001; **15**: 505-511 [PMID: 11284779 DOI: 10.1046/j.1365-2036.2001.00947.x]

48 **Shirin H**, Kenet G, Shevah O, Wardi J, Birkenfeld S, Shahmurov M, Bruck R, Niv Y, Moss SF, Avni Y. Evaluation of a novel continuous real time (13)C urea breath analyser for Helicobacter pylori. *Aliment Pharmacol Ther* 2001; **15**: 389-394 [PMID: 11207514 DOI: 10.1046/j.1365-2036.2001.00926.x]

49 **Pilotto A**, Franceschi M, Leandro G, Rassu M, Zagari RM, Bozzola L, Furlan F, Bazzoli F, Di Mario F, Valerio G. Noninvasive diagnosis of Helicobacter pylori infection in older subjects: comparison of the 13C-urea breath test with serology. *J Gerontol A Biol Sci Med Sci* 2000; **55**: M163-M167 [PMID: 10795730 DOI: 10.1093/gerona/55.3.m163]

50 **Sheu BS**, Lee SC, Lin PW, Wang ST, Chang YC, Yang HB, Chuang CH, Lin XZ. Carbon urea breath test is not as accurate as endoscopy to detect Helicobacter pylori after gastrectomy. *Gastrointest Endosc* 2000; **51**: 670-675 [PMID: 10840298 DOI: 10.1067/mge.2000.105719]

51 **Wong WM**, Wong BC, Wong KW, Fung FM, Lai KC, Hu WH, Yuen ST, Leung SY, Lau GK, Lai CL, Chan CK, Go R, Lam SK. (13)C-urea breath test without a test meal is highly accurate for the detection of Helicobacter pylori infection in Chinese. *Aliment Pharmacol Ther* 2000; **14**: 1353-1358 [PMID: 11012482 DOI: 10.1046/j.1365-2036.2000.00843.x]

52 **Hahn M**, Fennerty MB, Corless CL, Magaret N, Lieberman DA, Faigel DO. Noninvasive tests as a substitute for histology in the diagnosis of Helicobacter pylori infection. *Gastrointest Endosc* 2000; **52**: 20-26 [PMID: 10882957 DOI: 10.1067/mge.2000.106686]

53 **Chen X**, Haruma K, Kamada T, Mihara M, Komoto K, Yoshihara M, Sumii K, Kajiyama G. Factors that affect results of the 13C urea breath test in Japanese patients. *Helicobacter* 2000; **5**: 98-103 [PMID: 10849059 DOI: 10.1046/j.1523-5378.2000.00015.x]

54 **Peng NJ**, Hsu PI, Lee SC, Tseng HH, Huang WK, Tsay DG, Ger LP, Lo GH, Lin CK, Tsai CC, Lai KH. A 15-minute [13C]-urea breath test for the diagnosis of Helicobacter pylori infection in patients with non-ulcer dyspepsia. *J Gastroenterol Hepatol* 2000; **15**: 284-289 [PMID: 10764029 DOI: 10.1046/j.1440-1746.2000.02159.x]

55 **Riepl RL**, Folwaczny C, Otto B, Klauser A, Blendinger C, Wiebecke B, König A, Lehnert P, Heldwein W. Accuracy of 13C-urea breath test in clinical use for diagnosis of Helicobacter pylori infection. *Z Gastroenterol* 2000; **38**: 13-19 [PMID: 10689743 DOI: 10.1055/s-2000-15278]

56 **D'Elios MM**, Amedei A, Benagiano M, Azzurri A, Del Prete G. Usefulness of (13)C-urea breath test in the diagnosis of gastric helicobacter pylori infection. *Int J Immunopathol Pharmacol* 2000; **13**: 27-30 [PMID: 12749775 DOI: 10.1177/039463200001300104]

57 **van der Hulst RW**, Hensen EF, van der Ende A, Kruizinga SP, Homan A, Tytgat GN. [Laser-assisted 13C-urea breath test; a new noninvasive detection method for Helicobacter pylori infection]. *Ned Tijdschr Geneeskd* 1999; **143**: 400-404 [PMID: 10221110]

58 **Leodolter A**, Domínguez-Muñoz JE, Von Arnim U, Malfertheiner P. Citric acid or orange juice for the 13C-urea breath test: the impact of pH and gastric emptying. *Aliment Pharmacol Ther* 1999; **13**: 1057-1062 [PMID: 10468681 DOI: 10.1046/j.1365-2036.1999.00557.x]

59 **Mock T**, Yatscoff R, Foster R, Hyun JH, Chung IS, Shim CS, Yacyshyn B. Clinical validation of the Helikit: a 13C urea breath test used for the diagnosis of Helicobacter pylori infection. *Clin Biochem* 1999; **32**: 59-63 [PMID: 10074893 DOI: 10.1016/s0009-9120(98)00082-4]

60 **Perri F**, Clemente R, Festa V, Quitadamo M, Conoscitore P, Niro G, Ghoos Y, Rutgeerts P, Andriulli A. Relationship between the results of pre-treatment urea breath test and efficacy of eradication of Helicobacter pylori infection. *Ital J Gastroenterol Hepatol* 1998; **30**: 146-150 [PMID: 9675647]

61 **Ohara S**, Kato M, Asaka M, Toyota T. The UBiT-100 13CO2 infrared analyzer: comparison between infrared spectrometric analysis and mass spectrometric analysis. *Helicobacter* 1998; **3**: 49-53 [PMID: 9546118 DOI: 10.1046/j.1523-5378.1998.08046.x]

62 **Leodolter A**, Domínguez-Muñoz JE, von Arnim U, Manes G, Malfertheiner P. 13C-urea breath test for the diagnosis of Helicobacter pylori infection. A further simplification for clinical practice. *Scand J Gastroenterol* 1998; **33**: 267-270 [PMID: 9580391 DOI: 10.1080/00365529850170847]

63 **Andersen LP**, Kiilerick S, Pedersen G, Thoreson AC, Jørgensen F, Rath J, Larsen NE, Børup O, Krogfelt K, Scheibel J, Rune S. An analysis of seven different methods to diagnose Helicobacter pylori infections. *Scand J Gastroenterol* 1998; **33**: 24-30 [PMID: 9489904 DOI: 10.1080/00365529850166167]

64 **Ellenrieder V**, Glasbrenner B, Stoffels C, Weiler S, Bode G, Möller P, Adler G. Qualitative and semi-quantitative value of a modified 13C-urea breath test for identification of Helicobacter pylori infection. *Eur J Gastroenterol Hepatol* 1997; **9**: 1085-1089 [PMID: 9431899 DOI: 10.1097/00042737-199711000-00011]

65 **Epple HJ**, Kirstein FW, Bojarski C, Frege J, Fromm M, Riecken EO, Schulzke JD. 13C-urea breath test in Helicobacter pylori diagnosis and eradication. Correlation to histology, origin of 'false' results, and influence of food intake. *Scand J Gastroenterol* 1997; **32**: 308-314 [PMID:

9140151 DOI: 10.3109/00365529709007677]

66 **Labenz J**, Bärsch G, Peitz U, Aygen S, Hennemann O, Tillenburg B, Becker T, Stolte M. Validity of a novel biopsy urease test (HUT) and a simplified 13C-urea breath test for diagnosis of Helicobacter pylori infection and estimation of the severity of gastritis. *Digestion* 1996; **57**: 391-397 [PMID: 8913700 DOI: 10.1159/000201366]

67 **Logan RP**, Polson RJ, Misiewicz JJ, Rao G, Karim NQ, Newell D, Johnson P, Wadsworth J, Walker MM, Baron JH. Simplified single sample 13Carbon urea breath test for Helicobacter pylori: comparison with histology, culture, and ELISA serology. *Gut* 1991; **32**: 1461-1464 [PMID: 1773948 DOI: 10.1136/gut.32.12.1461]

68 **Dill S**, Payne-James JJ, Misiewicz JJ, Grimble GK, McSwiggan D, Pathak K, Wood AJ, Scrimgeour CM, Rennie MJ. Evaluation of 13C-urea breath test in the detection of Helicobacter pylori and in monitoring the effect of tripotassium dicitratobismuthate in non-ulcer dyspepsia. *Gut* 1990; **31**: 1237-1241 [PMID: 2253905 DOI: 10.1136/gut.31.11.1237]

69 **Miftahussurur M**. Noninvasive Helicobacter pylori Diagnostic Methods in Indonesia. *Gut Liver* 2020; **14**: 553-559 [PMID: 31693853 DOI: 10.5009/gnl19264]

70 **Cosgun Y**, Yildirim A, Yucel M, Karakoc AE, Koca G, Gonultas A, Gursoy G, Ustun H, Korkmaz M. Evaluation of Invasive and Noninvasive Methods for the Diagnosis of Helicobacter Pylori Infection. *Asian Pac J Cancer Prev* 2016; **17**: 5265-5272 [PMID: 28125872 DOI: 10.22034/APJCP.2016.17.12.5265]

71 **Atli T**, Sahin S, Arslan BU, Varli M, Yalcin AE, Aras S. Comparison of the C14 urea breath test and histopathology in the diagnosis of Helicobacter pylori in the elderly. *J Pak Med Assoc* 2012; **62**: 1061-1065 [PMID: 23866448]

72 **Alarcón-Rivera G**, Vázquez-Jiménez G, de la Cruz-Patiño E, Abarca M, Leyva E, Delgado F, Ruíz-Juárez I, Grube-Pagola P, Roesch-Dietlen F, Remes-Troche JM. [Comparative analysis between breath test, serological immunoassay and rapid-urease test for detection of Helicobacter pylori infection in Mexican patients with non-investigated dyspepsia]. *Rev Gastroenterol Mex* 2011; **76**: 322-329 [PMID: 22188957]

73 **Mansour-Ghanaei F**, Sanaei O, Joukar F. Clinical Validation of an Office-Based C-UBT (Heliprobe) for H. pylori Diagnosis in Iranian Dyspeptic Patients. *Gastroenterol Res Pract* 2011; **2011**: 930941 [PMID: 21760778 DOI: 10.1155/2011/930941]

74 **Ozdemir E**, Karabacak NI, Degertekin B, Cirak M, Dursun A, Engin D, Unal S, Unlü M. Could the simplified (14)C urea breath test be a new standard in noninvasive diagnosis of Helicobacter pylori infection? *Ann Nucl Med* 2008; **22**: 611-616 [PMID: 18756364 DOI: 10.1007/s12149-008-0168-6]

75 **Rasool S**, Abid S, Jafri W. Validity and cost comparison of 14carbon urea breath test for diagnosis of H Pylori in dyspeptic patients. *World J Gastroenterol* 2007; **13**: 925-929 [PMID: 17352025 DOI: 10.3748/wjg.v13.i6.925]

76 **Gurbuz AK**, Ozel AM, Narin Y, Yazgan Y, Baloglu H, Demirturk L. Is the remarkable contradiction between histology and 14C urea breath test in the detection of Helicobacter pylori due to false-negative histology or false-positive 14C urea breath test? *J Int Med Res* 2005; **33**: 632-640 [PMID: 16372580 DOI: 10.1177/147323000503300604]

77 **González P**, Galleguillos C, Massardo T, Rivera M, Morales A, Smok G, Moyano L, Pimentel C, Alay R, Otárola S. Could the [14C]urea breath test be proposed as a 'gold standard' for detection of Helicobacter pylori infection ? *Med Sci Monit* 2003; **9**: CR363-CR368 [PMID: 12942033]

78 **Oztürk E**, Yeşilova Z, Ilgan S, Ozgüven M, Dağalp K. Performance of acidified 14C-urea capsule breath test during pantoprazole and ranitidine treatment. *J Gastroenterol Hepatol* 2009; **24**: 1248-1251 [PMID: 19486449 DOI: 10.1111/j.1440-1746.2009.05845.x]

79 **Gomes AT**, Coelho LK, Secaf M, Módena JL, Troncon LE, Oliveira RB. Accuracy of the 14C-urea breath test for the diagnosis of Helicobacter pylori. *Sao Paulo Med J* 2002; **120**: 68-71 [PMID: 12163895 DOI: 10.1590/s1516-31802002000300002]

80 **Desroches JJ**, Lahaie RG, Picard M, Morais J, Dumont A, Gaudreau C, Picard D, Chartrand R. Methodological validation and clinical usefulness of carbon-14-urea breath test for documentation of presence and eradication of Helicobacter pylori infection. *J Nucl Med* 1997; **38**: 1141-1145 [PMID: 9225808]

81 **Allardyce RA**, Chapman BA, Tie AB, Burt MJ, Yeo KJ, Keenan JI, Bagshaw PF. 37 kBq 14C-urea breath test and gastric biopsy analyses of H. pylori infection. *Aust N Z J Surg* 1997; **67**: 31-34 [PMID: 9033373 DOI: 10.1111/j.1445-2197.1997.tb01890.x]

82 **Faigel DO**, Childs M, Furth EE, Alavi A, Metz DC. New noninvasive tests for Helicobacter pylori gastritis. Comparison with tissue-based gold standard. *Dig Dis Sci* 1996; **41**: 740-748 [PMID: 8674395 DOI: 10.1007/BF02213130]

83 **Goh KL**, Parasakthi N, Peh SC, Ong KK. 14C-urea breath test: a useful non-invasive test in the diagnosis of Helicobacter pylori infection. *Med J Malaysia* 1995; **50**: 208-211 [PMID: 8926896]

84 **Kao CH**, Huang CK, Wang SJ, Hsu CY, Lin WY, Chen GH. Accuracy of a rapid 10-minute carbon-14 urea breath test for the diagnosis of Helicobacter pylori-associated peptic ulcer disease. *Eur J Nucl Med* 1993; **20**: 708-711 [PMID: 8404959 DOI: 10.1007/BF00181763]

85 **Vivas J**, Contreras M, Mathew C, Peraza S, Maury de Tami I, Oliver W, Cano E, Castro D, Andrade O, Sanchez V. [The use of urea carbon 14 in breath tests as diagnostic method for Helicobacter pylori infections]. *G E N* 1993; **47**: 150-156 [PMID: 8112551]

World Journal of Gastroenterology

Submit a Manuscript: https://www.f6publishing.com

World J Gastroenterol 2024 February 14; 30(6): 599-606

DOI: 10.3748/wjg.v30.i6.599

ISSN 1007-9327 (print) ISSN 2219-2840 (online)

CASE REPORT

Y–Z deformable magnetic ring for the treatment of rectal stricture: A case report and review of literature

Miao-Miao Zhang, Huan-Chen Sha, Yuan-Fa Qin, Yi Lyu, Xiao-Peng Yan

Specialty type: Gastroenterology and hepatology

Provenance and peer review: Unsolicited article; Externally peer reviewed.

Peer-review model: Single blind

Peer-review report's scientific quality classification

Grade A (Excellent): 0
Grade B (Very good): B
Grade C (Good): 0
Grade D (Fair): 0
Grade E (Poor): 0

P-Reviewer: Nakaji K, Japan

Received: December 11, 2023
Peer-review started: December 11, 2023
First decision: December 15, 2023
Revised: December 18, 2023
Accepted: January 16, 2024
Article in press: January 16, 2024
Published online: February 14, 2024

Miao-Miao Zhang, Huan-Chen Sha, Yuan-Fa Qin, Yi Lyu, Xiao-Peng Yan, Department of Hepatobiliary Surgery, The First Affiliated Hospital of Xi'an Jiaotong University, Xi'an 710061, Shaanxi Province, China

Miao-Miao Zhang, Yi Lyu, Xiao-Peng Yan, National Local Joint Engineering Research Center for Precision Surgery & Regenerative Medicine, The First Affiliated Hospital of Xi'an Jiaotong University, Xi'an 710061, Shaanxi Province, China

Corresponding author: Xiao-Peng Yan, MD, PhD, Associate Research Scientist, Department of Hepatobiliary Surgery, The First Affiliated Hospital of Xi'an Jiaotong University, No. 277 West Yanta Road, Xi'an 710061, Shaanxi Province, China. yanxiaopeng9966@163.com

Abstract

BACKGROUND

Treatment of postoperative anastomotic stenosis for colorectal cancer is often challenging, especially for patients who do not respond well to endoscopy. In cases where patients have undergone an enterostomy, the stenosis can be easily resolved through magnetic compression. However, common magnetic compression techniques cannot be performed on those without enterostomy. We designed a novel Y–Z deformable magnetic ring (Y–Z DMR) and successfully applied it to a patient with a stenosis rectal anastomosis and without enterostomy after rectal cancer surgery.

CASE SUMMARY

We here report the case of a 57-year-old woman who had undergone a laparoscopic radical rectum resection (Dixon) for rectal cancer. However, she started facing difficulty in defecation 6 months after surgery. Her colonoscopy indicated stenosis of the rectal anastomosis. Endoscopic balloon dilation was performed six times on her. However, the stenosis still showed a trend of gradual aggravation. Because the patient did not undergo an enterostomy, the conventional endoscopic magnetic compression technique could not be performed. Hence, we implemented a Y–Z DMR implemented through the anus under single channel. The magnetic ring fell off nine days after the operation and the rectal stenosis was relieved. The patient was followed up for six months and reported good defecation.

CONCLUSION

The Y–Z DMR deformable magnetic ring is an excellent treatment strategy for patients with rectal stenosis and without enterostomy.

Key Words: Anastomotic stenosis; Colorectal cancer; Magnetosurgery; Magnetic compression technique; Magnetic surgery clinic; Case report

Core Tip: The magnetic compression technique can be used to treat patients with rectal stenosis that have also undergone an enterostomy. However, the existing magnetic ring cannot be used in patients without enterostomy. We designed a Y–Z deformable magnetic ring (Y–Z DMR), which can realize the single channel of the magnet placed through the anus. This paper reports the first successful clinical case of using the Y–Z DMR for the treatment of rectal stenosis.

Citation: Zhang MM, Sha HC, Qin YF, Lyu Y, Yan XP. Y–Z deformable magnetic ring for the treatment of rectal stricture: A case report and review of literature. *World J Gastroenterol* 2024; 30(6): 599-606
URL: https://www.wjgnet.com/1007-9327/full/v30/i6/599.htm
DOI: https://dx.doi.org/10.3748/wjg.v30.i6.599

INTRODUCTION

Rectal stenosis is a common postoperative complication of rectal cancer. Endoscopic treatment is generally preferred for such conditions. Balloon dilation[1,2], stent placement[3,4], and endoscopic radial incision[5] are some of the commonly used procedures that provide satisfactory treatment results in most patients. However, these procedures still lead to poor results in some patients, resulting in the need for surgical resection of anastomotic stenosis[6] or even permanent enterostomy. In addition, patients who have not undergone a prophylactic ileostomy or in whom stenosis occurs after ostomy reduction need urgent treatment.

Magnetic compression anastomosis (MCA) is a novel technique for the anastomosis of cavity organs through "non-contact" magnetic force. The current basic and clinical studies on MCA cover esophageal anastomosis[7-9], gastrointestinal anastomosis[10,11], and colorectal anastomosis[12,13] of the digestive system. MCA can be used for vascular anastomosis[14-16] and therapeutic ostomy[17-19] for non-gastrointestinal conditions. Magnetic compression technique can be used for stricture diseases such as the biliary stricture after liver transplantation[20-22], ureteric occlusion[23], esophageal stricture[24-26], colorectal stricture[27], and hypopharynx stenosis[28]. As for the basic research on MCA, some scholars have extensively discussed the characteristics of tissue healing in different periods and established the stage of digestion for magnetic anastomosis (Yan–Zhang's stage)[29].

Herein, we present a patient with the stenosis of rectal anastomosis and no enterostomy. For this case, we specially designed a Y–Z deformable magnetic ring (Y–Z DMR) and successfully achieved narrow recanalization in a single passage through the anus. The defecation status remained good even after 6 months of follow-up. This is the first study to report the clinical application of Y–Z DMR, which is of great clinical significance.

CASE PRESENTATION

Chief complaints

A 57-year-old woman presented to us in May 2023 for having difficulty in passing stools. She had undergone laparoscopic rectal cancer surgery 16 months ago (January 2022) and had started facing difficulty defecating 4 months after the surgery.

History of present illness

The patient had undergone laparoscopic radical rectum resection (Dixon) for rectal cancer at a local hospital 16 months ago and had recovered well after surgery. This patient did not undergo chemo-radio therapy before or after surgery. However, she started facing difficulties in defecation 1 year ago (May 2022). As a result, a colonoscopy was performed on her at a local hospital, which indicated stenosis of the rectal anastomosis. She underwent endoscopic balloon dilation treatment six times for the condition. However, the results were not satisfactory. For further treatment, the patient was admitted to the Magnetic Surgery Clinic of the First Affiliated Hospital of Xi'an Jiaotong University.

History of past illness

The patient had no history of acute or chronic infectious diseases, heart disease, hypertension or diabetes, or surgery other than laparoscopic radical rectum resection.

Personal and family history

The patient did not have any relevant family medical history.

Physical examination

The patient's vital signs were stable, with no obvious abnormalities in the physical examination of both her lungs and heart. Her abdomen was flat and soft, with no abdominal tenderness. Shifting dullness in the abdomen was negative, and bowel sounds were also normal.

Laboratory examinations

The patient's hematology results were normal.

Imaging examinations

After admission to our hospital, the patient underwent further colonoscopy. The result indicated that the rectal anastomosis was severely narrowed (5 cm) from the anus. In addition, no obvious lumen was observed. Hence, an attempt was made to insert a 14 Fr nasogastric tube through the anus to pass through the stenosis. Colography was performed by injecting approximately 100 mL of iohexol through the nasogastric tube. The results showed that the stenosis of the rectum was 0.4 mm in diameter and 1 cm in length (Figure 1).

FINAL DIAGNOSIS

The patient was diagnosed with rectum stenosis based on her medical history and the imaging examination and colonoscopy results.

TREATMENT

The patient refused further endoscopic treatment and surgery. Instead, she opted for minimally invasive magnetic surgery technique. The surgical plan was decided after a discussion with the Magnetic Surgery Multi-Disciplinary Treatment of the First Affiliated Hospital of Xi'an Jiaotong University (Figure 2). The patient agreed to the surgical protocol and signed the informed consent. The surgical plan was also approved by the Medical Department of the First Affiliated Hospital of Xi'an Jiaotong University. The S–O-shaped magnetic anastomosing ring designed by the author was used in the surgical plan. As the magnetic ring was designed, we named it the Y–Z DMR, also referred to as the Y–Z DMR. The Y–Z DMR was composed of two semicircular magnetic rings. The daughter magnetic ring was "S" shaped during the implantation process. It passed through the narrow section of the rectum in a serpentine motion. The daughter magnetic rings were manipulated by a control line to transform it from the "S" to the "O" shape. After adjusting the daughter magnetic ring to a suitable position, the two O-shaped parent magnetic rings were inserted through the anus. The daughter magnetic ring and the parent magnetic ring attracted each other and compressed the narrow section of the rectum. After a certain period, the scar of the narrow section and the magnetic rings fell off and were discharged through the anus.

The patient was administered intravenous anesthesia and the lithotomy position was adopted. A disposable anoscope was inserted through the anus. Rectal stenosis could be seen directly with the naked eye. An S-shaped magnetic ring was inserted through the anus, which was passed through the narrow part of the rectum under X-ray surveillance (Figure 3A). After the control line was pulled, the magnetic ring changed its S shape to O shape (Figure 3B). The catheter was inserted through the anus so that the balloon passed through the narrow part of the rectum and the center of the O-ring. The catheter balloon was dilated by injecting 10 mL of diluted iohexol solution. The catheter was vertically pulled so that the O-shaped magnetic ring became perpendicular to the longitudinal axis of the rectum and close to the rectal stenosis (Figure 3C). Two O-shaped parent magnetic rings were inserted through the end of the catheter and pushed along the catheter to the narrow anal side of the rectum. The daughter and parent magnetic rings were attracted toward each other, compressing the narrow section of the rectum (Figure 3D). The catheter was placed in the rectum and the procedure was completed. On the 9th day after surgery, the magnet rings and catheter were pulled out through the anus (Figure 4A), establishing the MCA. Colonoscopy showed no bleeding, mucosal edema, or erosion at the anastomotic orifice (Figure 4B). The colonoscope successfully passed through the anastomotic orifice (Figure 4C). Further colonography showed that the stenosis of the rectum widened significantly (Figure 4D and E). The patient was discharged 10 d after surgery. The patient was strongly advised to use a 20-mm-diameter anal reaming stick 3 times a day for 5 min each time for 3 months after discharge to prevent restenosis.

OUTCOME AND FOLLOW-UP

The 6-month follow-up of the patient showed a generally good condition with normal bowel movements.

DISCUSSION

Before admission to our hospital, the patient had undergone balloon dilations six times. However, the stenosis kept

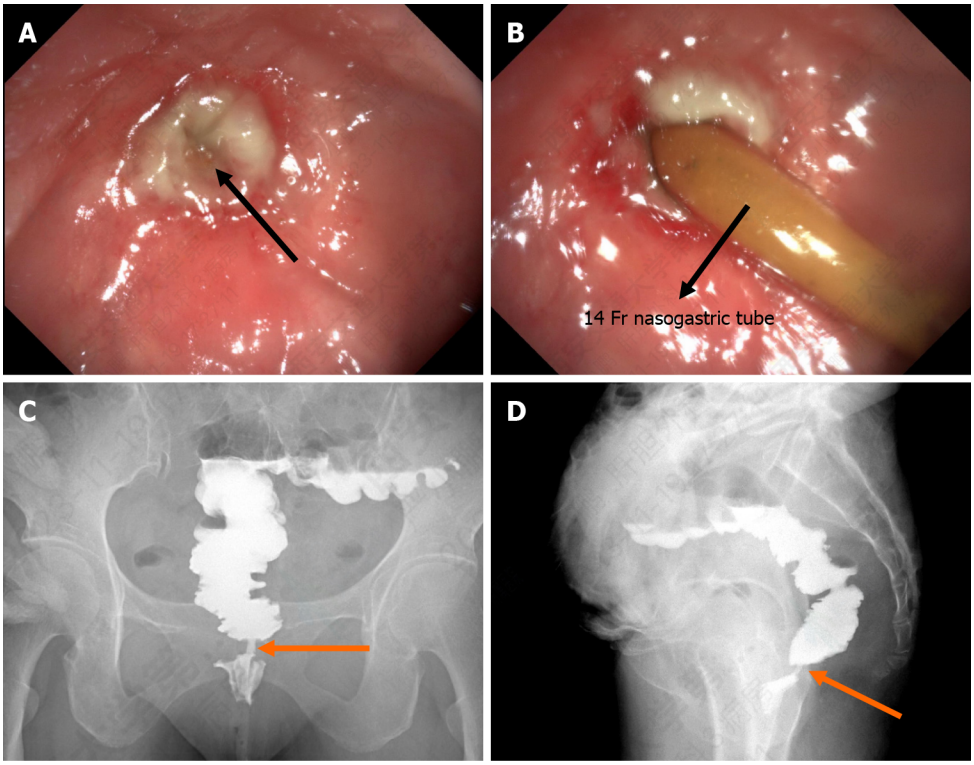

DOI: 10.3748/wjg.v30.i6.599

Figure 1 Colonoscopy and colography. A: Rectal anastomosis stoma; B: Rectal stenosis can only be achieved through a 14 Fr nasogastric tube; C: Anteroposterior colography; D: Lateral colography.

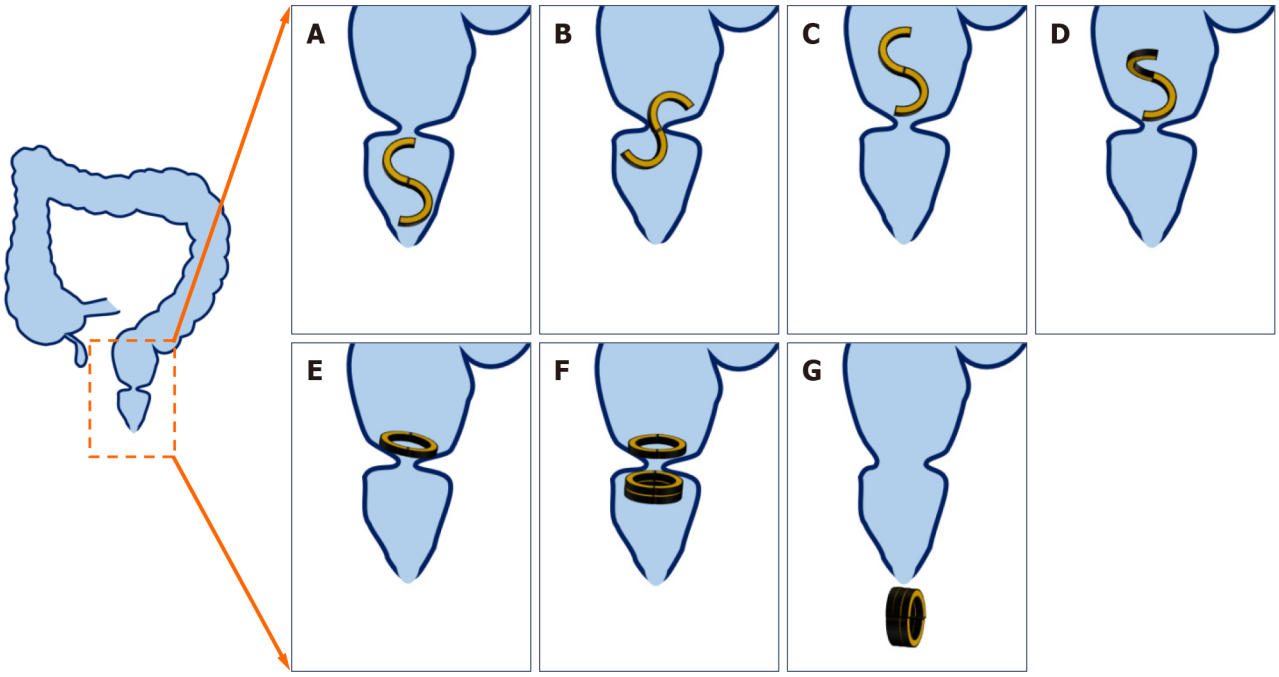

DOI: 10.3748/wjg.v30.i6.599

Figure 2 Operation plan. A: An S-shaped magnetic ring is inserted through the anus; B: The S-shaped magnetic ring passes through the rectal stenosis; C: The S-shaped magnetic ring successfully passed the narrow rectum; D: Deformation of the S-shaped magnetic ring; E: The S-shaped magnetic ring deforms to an O-shape; F: The daughter ring and the parent ring attract each other and compress the narrow section of the rectum; G: Rectum stenosis recanalizes and the magnetic ring is discharged through the anus.

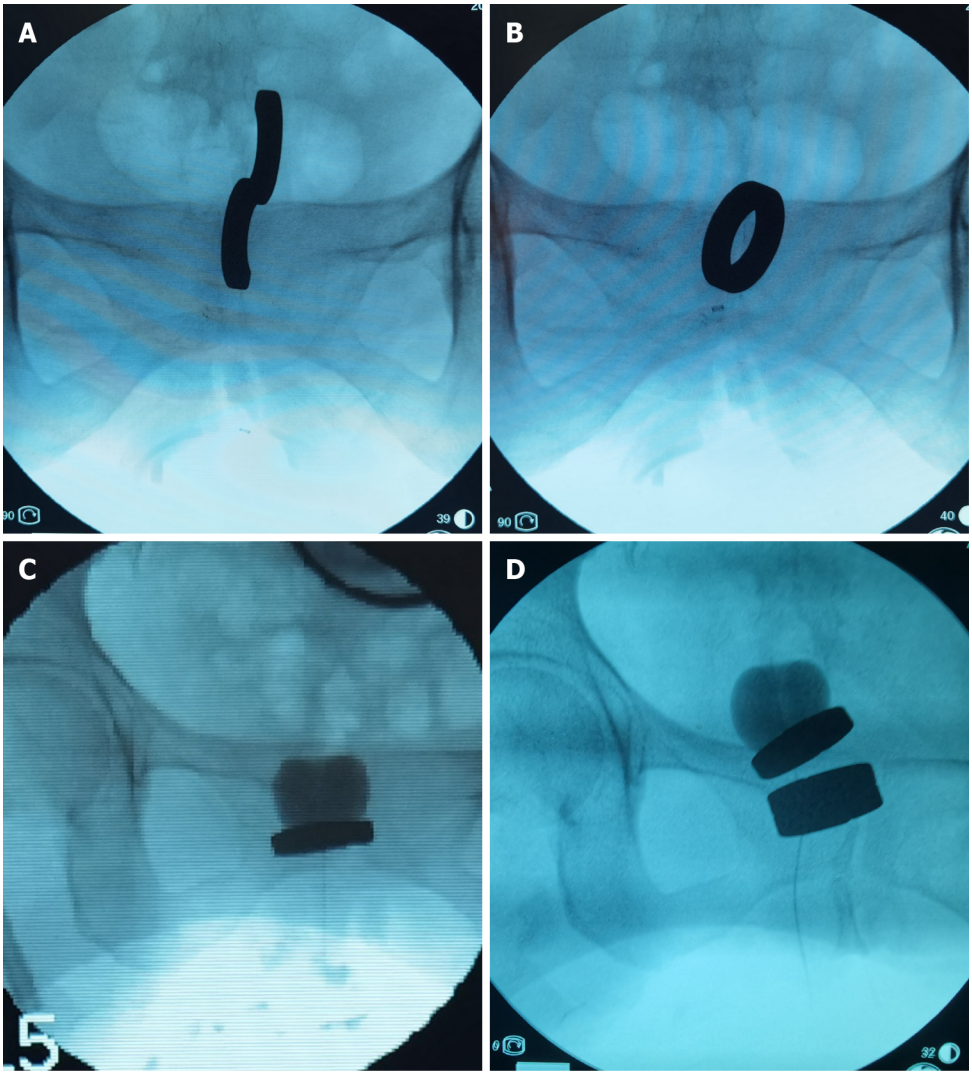

DOI: 10.3748/wjg.v30.i6.599

Figure 3 Surgical procedure. A: The S-shaped magnetic ring passes the narrow rectum; B: The S-shaped magnetic ring becomes O-shaped; C: The catheter assists in adjusting the magnet position; D: The daughter ring and the parent ring attract each other and compress the narrow section of the rectum.

gradually worsening, forcing the patient to rely only on a slag-free nutrient solution. As the patient refused other treatment options, she was offered the Y–Z DMR procedure. Thus, she became the first patient to benefit from the Y–Z DMR procedure.

In the previously reported cases of colorectal stenosis treated by the magnetic compression technique, all patients had undergone enterostomy. The resulting stoma provided an important access for placing magnets[30,31]. In the magnetic anastomosis of the digestive tract, the area of compression of the magnetic anastomosis ring is an important factor that determines the size of the final anastomosis. Therefore, to achieve the optimum magnet placement, clinicians tend to choose as large a magnetic ring as possible so as to obtain a larger anastomotic diameter. For those with a stoma, magnets can be easily inserted both through the anus and the stoma on either side of the rectum stenosis. In patients with rectal stenosis but without a stoma, conventional magnets cannot be inserted into the side of the rectal stenosis. Therefore, passing a large magnetic ring through the narrow section is a major research topic.

Inspired by the serpentine movement of snakes, we designed a Y–Z DMR with the following characteristics: First, it is composed of two semicircular magnetic rings. It forms an S-shaped structure when its one end is fixed and the other end is rotated by 180°. As a result, the cross-section of the magnet becomes significantly small, allowing the deformable magnetic ring to pass through the narrow section. Second, as the S-shaped magnetic ring adopts the serpentine movement, the whole S-shaped magnetic ring can be passed through the narrow section by constantly adjusting the direction of the magnetic ring. Third, the control wire was loaded on the end face of the semicircular magnetic ring and the S-shaped magnetic ring, which has reached the narrow section, can be deformed and reassembled into an O-shaped magnetic ring through wire pulling. The above three-point design is key to passing a large magnetic loop through a small channel.

Although we have treated only one patient at our clinic so far, our results show that it is possible to deform the Y-Z DMR from the S shape to the O shape. Satisfactory results were obtained at the 6-month follow-up. This is the first-generation Y–Z DMR. We believe that further optimization of the magnetic ring structure would increase the applications of the Y-Z DMR.

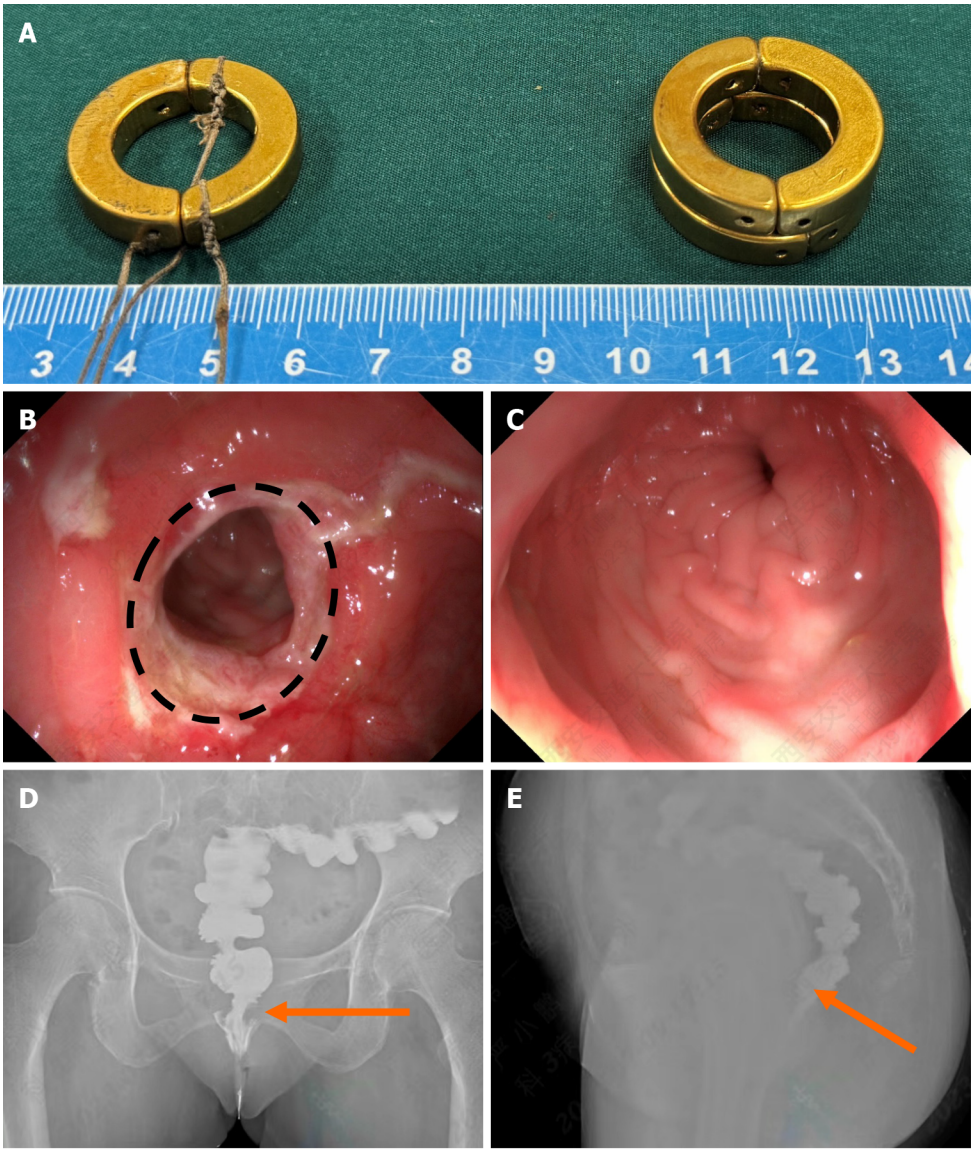

DOI: 10.3748/wjg.v30.i6.599

Figure 4 Postoperative anastomosis. A: Daughter and parent magnetic rings expelled from the body; B: Rectal anastomosis stoma; C: The colonoscope smoothly passes the stenosis; D: Anteroposterior colography; E: Lateral colography.

CONCLUSION

This study described the procedure and outcome of the first successful treatment of rectal stenosis using a Y–Z DMR through a unique anal access. The controllable deformation ability of the Y–Z DMR made this treatment strategy successful. We believe that our case report will provide more options to colorectal surgeons to treat rectal stenosis.

FOOTNOTES

Co-corresponding authors: Xiao-Peng Yan and Yi Lyu.

Author contributions: Lyu Y and Yan XP designed and coordinated the study; Yan XP and Zhang MM designed the deformable magnetic ring, Zhang MM, Sha HC, Qin YF, Yan XP performed the operation; Zhang MM, and Yan XP wrote the manuscript; Yan XP and Lyu Y conceived of the study and contributed to the study design, the interpretation of the results, and the critical revision of the manuscript; all authors read and approved the final manuscript. The reasons for designating Yan XP and Lyu Y as co-corresponding authors are as follows: Yan XP and Lyu Y have equal contributions in study design and making critical revisions to the manuscript. The two co-corresponding authors ensures effective communication and management of post-submission matters, ultimately enhancing the paper's quality and reliability. Yan XP and Lyu Y contributed efforts of equal substance throughout the research process. Therefore, Yan XP and Lyu Y are designated as co-corresponding authors in this manuscript.

Supported by Institutional Foundation of The First Affiliated Hospital of Xi'an Jiaotong University, No. 2022MS-07; and The Fundamental Research Funds for the Central Universities, No. xzy022023068.

Informed consent statement: Informed written consent was obtained from the patient for publication of this report and any accompanying images.

Conflict-of-interest statement: The authors declare that they have no conflict of interest.

CARE Checklist (2016) statement: The authors have read the CARE Checklist (2016), and the manuscript was prepared and revised according to the CARE Checklist (2016).

Country/Territory of origin: China

ORCID number: Miao-Miao Zhang 0000-0001-5679-7061; Huan-Chen Sha 0000-0002-8183-2591; Yi Lyu 0000-0003-3636-6664; Xiao-Peng Yan 0000-0002-0335-829X.

S-Editor: Qu XL
L-Editor: A
P-Editor: Yuan YY

REFERENCES

1 **Wang S**, Wan J, Li Z, Long C, Zhang R, Luo Y, Han Z, Yan J. Comparison of the Efficacy of Endoscopic Radial Incision and Cutting Procedure and Endoscopic Balloon Dilation for Benign Anastomotic Stricture After Low Anterior Resection Combined With Preventive Loop Ileostomy in Rectal Cancer. *Dis Colon Rectum* 2023; **66**: 1392-1401 [PMID: 37339319 DOI: 10.1097/DCR.0000000000002653]

2 **Clifford RE**, Fowler H, Manu N, Vimalachandran D. Management of benign anastomotic strictures following rectal resection: a systematic review. *Colorectal Dis* 2021; **23**: 3090-3100 [PMID: 34374203 DOI: 10.1111/codi.15865]

3 **Lamazza A**, Fiori E, Sterpetti AV, Schillaci A, Scoglio D, Lezoche E. Self-expandable metal stents in the treatment of benign anastomotic stricture after rectal resection for cancer. *Colorectal Dis* 2014; **16**: O150-O153 [PMID: 24206040 DOI: 10.1111/codi.12488]

4 **Lamazza A**, Fiori E, Schillaci A, Sterpetti AV, Lezoche E. Treatment of anastomotic stenosis and leakage after colorectal resection for cancer with self-expandable metal stents. *Am J Surg* 2014; **208**: 465-469 [PMID: 24560186 DOI: 10.1016/j.amjsurg.2013.09.032]

5 **Lee TG**, Yoon SM, Lee SJ. Endoscopic radial incision and cutting technique for treatment-naive stricture of colorectal anastomosis: Two case reports. *World J Gastrointest Surg* 2020; **12**: 460-467 [PMID: 33304448 DOI: 10.4240/wjgs.v12.i11.460]

6 **Imagami T**, Takayama S, Maeda Y, Hattori T, Matsui R, Sakamoto M, Kani H. Surgical Resection of Anastomotic Stenosis after Rectal Cancer Surgery Using a Circular Stapler and Colostomy with Double Orifice. *Case Rep Surg* 2019; **2019**: 2898691 [PMID: 31214375 DOI: 10.1155/2019/2898691]

7 **Sterlin A**, Evans L, Mahler S, Lindner A, Dickmann J, Heimann A, Sahlabadi M, Aribindi V, Harrison MR, Muensterer OJ. An experimental study on long term outcomes after magnetic esophageal compression anastomosis in piglets. *J Pediatr Surg* 2022; **57**: 34-40 [PMID: 34656308 DOI: 10.1016/j.jpedsurg.2021.09.032]

8 **Muensterer OJ**, Sterlin A, Oetzmann von Sochaczewski C, Lindner A, Heimann A, Balus A, Dickmann J, Nuber M, Patel VH, Manfredi MA, Jennings RW, Smithers CJ, Fauza DO, Harrison MR. An experimental study on magnetic esophageal compression anastomosis in piglets. *J Pediatr Surg* 2020; **55**: 425-432 [PMID: 31128845 DOI: 10.1016/j.jpedsurg.2019.04.029]

9 **Bruns NE**, Glenn IC, Craner DR, Schomisch SJ, Harrison MR, Ponsky TA. Magnetic compression anastomosis (magnamosis) in a porcine esophagus: Proof of concept for potential application in esophageal atresia. *J Pediatr Surg* 2019; **54**: 429-433 [PMID: 30309731 DOI: 10.1016/j.jpedsurg.2018.09.014]

10 **Gagner M**, Abuladze D, Koiava L, Buchwald JN, Van Sante N, Krinke T. First-in-Human Side-to-Side Magnetic Compression Duodeno-ileostomy with the Magnet Anastomosis System. *Obes Surg* 2023; **33**: 2282-2292 [PMID: 37393568 DOI: 10.1007/s11695-023-06708-x]

11 **Gagner M**, Cadiere GB, Sanchez-Pernaute A, Abuladze D, Krinke T, Buchwald JN, Van Sante N, Van Gossum M, Dziakova J, Koiava L, Odovic M, Poras M, Almutlaq L, Torres AJ. Side-to-side magnet anastomosis system duodeno-ileostomy with sleeve gastrectomy: early multi-center results. *Surg Endosc* 2023; **37**: 6452-6463 [PMID: 37217682 DOI: 10.1007/s00464-023-10134-6]

12 **Marchegiani F**, Noll E, Riva P, Kong SH, Saccomandi P, Vita G, Lindner V, Namer IJ, Marescaux J, Diemunsch P, Diana M. Effects of Warmed and Humidified CO(2) Surgical Site Insufflation in a Novel Experimental Model of Magnetic Compression Colonic Anastomosis. *Surg Innov* 2021; **28**: 7-17 [PMID: 33095686 DOI: 10.1177/1553350620967225]

13 **Wall J**, Diana M, Leroy J, Deruijter V, Gonzales KD, Lindner V, Harrison M, Marescaux J. MAGNAMOSIS IV: magnetic compression anastomosis for minimally invasive colorectal surgery. *Endoscopy* 2013; **45**: 643-648 [PMID: 23807805 DOI: 10.1055/s-0033-1344119]

14 **Klima U**, MacVaugh H 3rd, Bagaev E, Maringka M, Kirschner S, Beilner J, Haverich A. Magnetic Vascular Port in minimally invasive direct coronary artery bypass grafting. *Circulation* 2004; **110**: II55-II60 [PMID: 15364839 DOI: 10.1161/01.CIR.0000138391.77285.d9]

15 **Zhang M**, Ma J, An Y, Lyu Y, Yan X. Construction of an intrahepatic portosystemic shunt using the magnetic compression technique: preliminary experiments in a canine model. *Hepatobiliary Surg Nutr* 2022; **11**: 611-615 [PMID: 36016743 DOI: 10.21037/hbsn-22-209]

16 **Heitmann C**, Khan FN, Erdmann D, Olbrich KC, Adam Sharkawy A, Klitzman B. Vein graft anastomoses with magnets. *J Plast Reconstr Aesthet Surg* 2007; **60**: 1296-1301 [PMID: 17481977 DOI: 10.1016/j.bjps.2006.10.017]

17 **Uygun I**, Okur MH, Cimen H, Keles A, Yalcin O, Ozturk H, Otcu S. Magnetic compression gastrostomy in the rat. *Pediatr Surg Int* 2012; **28**: 529-532 [PMID: 22270732 DOI: 10.1007/s00383-012-3053-2]

18 **Uygun I**, Okur MH, Arayici Y, Keles A, Ozturk H, Otcu S. Magnetic compression ostomy for simple tube colostomy in rats--magnacolostomy. *Adv Clin Exp Med* 2012; **21**: 301-305 [PMID: 23214192]

19 **Uygun I**, Okur MH, Cimen H, Keles A, Yalcin O, Ozturk H, Otcu S. Magnetic compression ostomy as new cystostomy technique in the rat: magnacystostomy. *Urology* 2012; **79**: 738-742 [PMID: 22386431 DOI: 10.1016/j.urology.2011.11.048]

20 **Jang SI**, Cho JH, Lee DK. Magnetic Compression Anastomosis for the Treatment of Post-Transplant Biliary Stricture. *Clin Endosc* 2020; **53**: 266-275 [PMID: 32506893 DOI: 10.5946/ce.2020.095]

21 **Jang SI**, Lee KH, Joo SM, Park H, Choi JH, Lee DK. Maintenance of the fistulous tract after recanalization *via* magnetic compression anastomosis in completely obstructed benign biliary stricture. *Scand J Gastroenterol* 2018; **53**: 1393-1398 [PMID: 30351979 DOI: 10.1080/00365521.2018.1526968]

22 **Kubo M**, Wada H, Eguchi H, Gotoh K, Iwagami Y, Yamada D, Akita H, Asaoka T, Noda T, Kobayashi S, Nakamura M, Ono Y, Osuga K, Yamanouchi E, Doki Y, Mori M. Magnetic compression anastomosis for the complete dehiscence of hepaticojejunostomy in a patient after living-donor liver transplantation. *Surg Case Rep* 2018; **4**: 95 [PMID: 30112678 DOI: 10.1186/s40792-018-0504-6]

23 **Shlomovitz E**, Copping R, Swanstrom LL. Magnetic Compression Anastomosis for Recanalization of Complete Ureteric Occlusion after Radical Cystoprostatectomy. *J Vasc Interv Radiol* 2023; **34**: 1640-1641 [PMID: 37620060 DOI: 10.1016/j.jvir.2023.04.005]

24 **Holler AS**, König TT, Chen C, Harrison MR, Muensterer OJ. Esophageal Magnetic Compression Anastomosis in Esophageal Atresia Repair: A PRISMA-Compliant Systematic Review and Comparison with a Novel Approach. *Children (Basel)* 2022; **9** [PMID: 35892616 DOI: 10.3390/children9081113]

25 **Evans LL**, Chen CS, Muensterer OJ, Sahlabadi M, Lovvorn HN, Novotny NM, Upperman JS, Martinez JA, Bruzoni M, Dunn JCY, Harrison MR, Fuchs JR, Zamora IJ. The novel application of an emerging device for salvage of primary repair in high-risk complex esophageal atresia. *J Pediatr Surg* 2022; **57**: 810-818 [PMID: 35760639 DOI: 10.1016/j.jpedsurg.2022.05.018]

26 **Ödemiş B**, Başpınar B, Durak MB, Coşkun O, Torun S. Lumen reconstruction with magnetic compression anastomosis technique in a patient with complete esophageal stricture. *Acta Gastroenterol Belg* 2022; **85**: 393-395 [PMID: 35709784 DOI: 10.51821/85.2.8436]

27 **Zhang M**, He S, Sha H, Xue H, Lv Y, Yan X. A novel self-shaping magnetic compression anastomosis ring for treatment of colonic stenosis. *Endoscopy* 2023; **55**: E1132-E1134 [PMID: 37875150 DOI: 10.1055/a-2183-8942]

28 **Mascagni P**, Tringali A, Boškoski I, Bove V, Schepis T, Perri V, Costamagna G. Magnetic kissing for the endoscopic treatment of a complete iatrogenic stenosis of the hypopharynx. *Endoscopy* 2023; **55**: E499-E500 [PMID: 36894138 DOI: 10.1055/a-2029-6340]

29 **Zhang M**, Lyu X, Zhao G, An Y, Lyu Y, Yan X. Establishment of Yan-Zhang's staging of digestive tract magnetic compression anastomosis in a rat model. *Sci Rep* 2022; **12**: 12445 [PMID: 35859162 DOI: 10.1038/s41598-022-16794-z]

30 **Russell KW**, Rollins MD, Feola GP, Scaife ER. Magnamosis: a novel technique for the management of rectal atresia. *BMJ Case Rep* 2014; **2014** [PMID: 25096648 DOI: 10.1136/bcr-2013-201330]

31 **Kamada T**, Ohdaira H, Hoshimoto S, Narihiro S, Suzuki N, Marukuchi R, Takeuchi H, Yoshida M, Yamanouchi E, Suzuki Y. Magnetic compression anastomosis with atypical anastomosis for anastomotic stenosis of the sigmoid colon: a case report. *Surg Case Rep* 2020; **6**: 59 [PMID: 32291530 DOI: 10.1186/s40792-020-00826-9]

World Journal of Gastroenterology

Submit a Manuscript: https://www.f6publishing.com

World J Gastroenterol 2024 February 14; 30(6): 607-609

DOI: 10.3748/wjg.v30.i6.607

ISSN 1007-9327 (print) ISSN 2219-2840 (online)

LETTER TO THE EDITOR

Angiotensin-converting enzyme 2 alleviates liver fibrosis through the renin-angiotensin system

Bai-Wei Zhao, Ying-Jia Chen, Ruo-Peng Zhang, Yong-Ming Chen, Bo-Wen Huang

Specialty type: Gastroenterology and hepatology

Provenance and peer review: Unsolicited article; Externally peer reviewed.

Peer-review model: Single blind

Peer-review report's scientific quality classification

Grade A (Excellent): 0
Grade B (Very good): 0
Grade C (Good): C, C
Grade D (Fair): D
Grade E (Poor): 0

P-Reviewer: Buechler C, Germany; Ferraioli G, Italy

Received: October 31, 2023
Peer-review started: October 31, 2023
First decision: December 6, 2023
Revised: December 17, 2023
Accepted: January 15, 2024
Article in press: January 15, 2024
Published online: February 14, 2024

Bai-Wei Zhao, Ruo-Peng Zhang, Yong-Ming Chen, Bo-Wen Huang, Department of Gastric Surgery, Sun Yat-sen University Cancer Center, State Key Laboratory of Oncology in South China, Guangdong Provincial Clinical Research Center for Cancer, Guangzhou 510060, Guangdong Province, China

Ying-Jia Chen, Health Science Center, Peking University, Beijing 100191, China

Corresponding author: Bo-Wen Huang, MD, Professor, Department of Gastric Surgery, Sun Yat-sen University Cancer Center, State Key Laboratory of Oncology in South China, Guangdong Provincial Clinical Research Center for Cancer, No. 651 Dongfeng East Road, Yuexiu District, Guangzhou 510060, Guangdong Province, China. huangbw1@sysucc.org.cn

Abstract

The present letter to the editor is related to the study titled 'Angiotensin-converting enzyme 2 improves liver fibrosis in mice by regulating autophagy of hepatic stellate cells'. Angiotensin-converting enzyme 2 can alleviate liver fibrosis by regulating autophagy of hepatic stellate cells and affecting the renin-angiotensin system.

Key Words: Angiotensin-converting enzyme 2; Hepatic stellate cells; Liver fibrosis; Angiotensin II; Angiotensin 1-7; Renin-angiotensin system

Core Tip: This letter to the editor adds to the ongoing conversation regarding the involvement of angiotensin-converting enzyme 2 (ACE2) in liver fibrosis from the perspective of its effect on the renin-angiotensin system (RAS). The major highlight of this letter is the discussion of the role of ACE2 in regulating liver fibrosis through RAS beyond the pathway studied in the article titled 'Angiotensin-converting enzyme 2 improves liver fibrosis in mice by regulating autophagy of hepatic stellate cells'.

Citation: Zhao BW, Chen YJ, Zhang RP, Chen YM, Huang BW. Angiotensin-converting enzyme 2 alleviates liver fibrosis through the renin-angiotensin system. *World J Gastroenterol* 2024; 30(6): 607-609
URL: https://www.wjgnet.com/1007-9327/full/v30/i6/607.htm
DOI: https://dx.doi.org/10.3748/wjg.v30.i6.607

TO THE EDITOR

In the study of Wu *et al*[1], the authors concluded that the overexpression of angiotensin-converting enzyme 2 (ACE2) can regulate hepatic stellate cells (HSCs) autophagy by the adenosine monophosphate-activated protein kinase (AMPK)/mammalian target of rapamycin pathway to inhibit the activation of HSC and promote HSC apoptosis, thereby alleviating liver fibrosis and hepatic sinusoidal remodeling.

Hepatic fibrosis is caused by a sustained normal wound healing response, resulting in an abnormal persistence of the production and deposition of connective tissue[2]. Liver fibrogenesis and cirrhosis are usually accompanied by severe complications, such as portal hypertension, liver failure, and an increased risk of hepatocellular carcinoma[3].

HSCs play an essential role in the pathogenesis and development of hepatic fibrosis. In healthy livers, HSCs are situated in the perisinusoidal space, also known as the space of Disse, between hepatocytes and liver sinusoidal endothelial cells[4]. However, in chronic liver diseases, HSCs are stimulated by damaged hepatocytes and transform into a myofibroblastic phenotype[5]. Upon activation, HSCs exhibit increased α-smooth muscle actin expression[6]. At the same time, HSCs produce a large number of extracellular matrix (ECM) proteins, such as collagens I and III, as well as fibronectin[6]. Excess fibrous ECM proteins are deposited in the space of Disse of hepatic sinusoids, ultimately resulting in liver fibrosis[7]. Moreover, the contraction of HSCs increases the pressure on hepatic sinusoids. This can cause stenosis, thereby causing and exacerbating portal hypertension[8].

Liver fibrosis has high rates of morbidity and mortality throughout the world. However, there are still no effective prevention and therapy methods for liver fibrosis currently. The findings of Wu *et al*[1]. indicate new directions for improving hepatic sinusoidal remodeling and give a new theoretical foundation for the preventive and targeted treatment of hepatic fibrogenesis and portal hypertension. However, further research is needed to enable its clinical application.

In addition to the pathway expounded by Wu *et al*[1], ACE2 can affect liver fibrosis through the renin-angiotensin system (RAS). In order to induce overexpression of ACE2 in a mouse model of hepatic fibrogenesis, Wu *et al*[1] injected a liver-specific recombinant adeno-associated virus ACE2 vector (rAAV2/8-ACE2) into the mice[1]. Then, Wu *et al*[1] measured the serum levels of angiotensin (Ang) II and Ang 1-7 and found that the level of Ang II decreased while the level of Ang 1-7 increased[1]. Osterreicher *et al*[9] showed that ACE2, a critical negative regulator of the RAS, can degrade Ang II and form Ang 1-7, thereby limiting fibrosis. In chronic liver injury models, loss of ACE2 activity exacerbates liver fibrosis, while the administration of recombinant ACE2 shows therapeutic potential.

RAS is a significant endocrine system that regulates vascular tension, maintains blood pressure homeostasis, and keeps water and electrolyte balance[10]. In the classic RAS pathway, juxtaglomerular cells of renal afferent arterioles secrete renin, which can cleave angiotensinogen (AGT), a liver-derived precursor peptide, to produce Ang I, a decapeptide[9]. AGT is produced in large quantities in liver cells and is the primary source of circulating AGT in healthy conditions[11]. Therefore, decreasing the secretion of AGT may be an effective strategy for treating liver fibrosis.

One of the RAS axes involves an angiotensin-converting enzyme (ACE)[12]. Through ACE action, Ang I, a main effector peptide of the RAS, is hydrolyzed to form Ang II, an octapeptide additionally[9]. Kurikawa *et al*[13] showed that HSCs exhibit significantly enhanced proliferation and increased collagen synthesis following Ang II binding to its receptor, which plays a vital role in the aggravation of hepatic fibrosis. The serum and tissue levels of Ang II were elevated in ACE2 knockout mice[14]. Ang II type 1 receptor (AT1R), which can be expressed in activated HSCs, is the main effector mediating the effects of Ang II[12]. AT1R blockers can inhibit the proliferation of HSC and improve hepatic fibrosis[13]. Ang II activates AT1R, which causes Ras homolog gene family member A to activate Rho-kinase. This up-regulates the phosphorylation and contraction of the myosin light chain, which participates in developing hepatic fibrosis and portal hypertension[15]. Furthermore, ACE inhibitors can alleviate the progression of hepatic fibrosis[16].

Another axis of RAS is the hydrolysis of Ang II to Ang 1-7 mediated by ACE2[12]. Ang 1-7 is an active peptide and a vasodilator, exerting its effects through binding to the G-protein coupled receptor, Mas[10]. Mas is the main effector of Ang 1-7, conveying vasodilation, anti-proliferation, anti-inflammation, and anti-fibrosis effects. In different models of human diseases, activation of the ACE2/Ang 1-7/Mas axis inhibits inflammatory cell function and fibrogenesis[12]. Furthermore, Ang 1-7 can activate the production of nitric oxide and endothelial nitric oxide synthase in endothelial cells [10].

The pathway described in the study of Wu *et al*[1] is not entirely independent of the pathway associated with RAS. When the balance between the classical RAS arm (ACE/Ang II/AT1R) and the protective arm (ACE2/Ang 1-7/Mas receptor) is disrupted, the expression of ACE and AT1R is inhibited, and the expression of ACE2 and Mas is increased at the same time under the action of activated AMPK. Following the up-regulation of ACE2, the metabolism of Ang II to Ang 1-7 is increased; activated AMPK suppresses the classical RAS pathway and elevates the protective arm, maintaining the balance of RAS[17].

FOOTNOTES

Co-first authors: Bai-Wei Zhao and Ying-Jia Chen.

Author contributions: Zhao BW and Chen YJ share the first author; Huang BW and Chen YJ designed research; Zhao BW and Zhang RP performed research; Chen YJ and Chen YM wrote the letter; Huang BW and Zhao BW revised the letter.

Conflict-of-interest statement: All the authors report no relevant conflicts of interest for this article.

Country/Territory of origin: China

ORCID number: Bo-Wen Huang 0000-0003-4588-659X.

S-Editor: Li L
L-Editor: A
P-Editor: Li L

REFERENCES

1 **Wu Y**, Yin AH, Sun JT, Xu WH, Zhang CQ. Angiotensin-converting enzyme 2 improves liver fibrosis in mice by regulating autophagy of hepatic stellate cells. *World J Gastroenterol* 2023; **29**: 4975-4990 [PMID: 37732000 DOI: 10.3748/wjg.v29.i33.4975]
2 **Schuppan D**, Afdhal NH. Liver cirrhosis. *Lancet* 2008; **371**: 838-851 [PMID: 18328931 DOI: 10.1016/S0140-6736(08)60383-9]
3 **Iredale JP**. Models of liver fibrosis: exploring the dynamic nature of inflammation and repair in a solid organ. *J Clin Invest* 2007; **117**: 539-548 [PMID: 17332881 DOI: 10.1172/JCI30542]
4 **Deleve LD**, Wang X, Guo Y. Sinusoidal endothelial cells prevent rat stellate cell activation and promote reversion to quiescence. *Hepatology* 2008; **48**: 920-930 [PMID: 18613151 DOI: 10.1002/hep.22351]
5 **Tsuchida T**, Friedman SL. Mechanisms of hepatic stellate cell activation. *Nat Rev Gastroenterol Hepatol* 2017; **14**: 397-411 [PMID: 28487545 DOI: 10.1038/nrgastro.2017.38]
6 **Sui M**, Jiang X, Chen J, Yang H, Zhu Y. Magnesium isoglycyrrhizinate ameliorates liver fibrosis and hepatic stellate cell activation by regulating ferroptosis signaling pathway. *Biomed Pharmacother* 2018; **106**: 125-133 [PMID: 29957462 DOI: 10.1016/j.biopha.2018.06.060]
7 **Dewidar B**, Meyer C, Dooley S, Meindl-Beinker AN. TGF-β in Hepatic Stellate Cell Activation and Liver Fibrogenesis-Updated 2019. *Cells* 2019; **8** [PMID: 31718044 DOI: 10.3390/cells8111419]
8 **Iwakiri Y**, Trebicka J. Portal hypertension in cirrhosis: Pathophysiological mechanisms and therapy. *JHEP Rep* 2021; **3**: 100316 [PMID: 34337369 DOI: 10.1016/j.jhepr.2021.100316]
9 **Osterreicher CH**, Taura K, De Minicis S, Seki E, Penz-Osterreicher M, Kodama Y, Kluwe J, Schuster M, Oudit GY, Penninger JM, Brenner DA. Angiotensin-converting-enzyme 2 inhibits liver fibrosis in mice. *Hepatology* 2009; **50**: 929-938 [PMID: 19650157 DOI: 10.1002/hep.23104]
10 **Iwakiri Y**, Shah V, Rockey DC. Vascular pathobiology in chronic liver disease and cirrhosis - current status and future directions. *J Hepatol* 2014; **61**: 912-924 [PMID: 24911462 DOI: 10.1016/j.jhep.2014.05.047]
11 **Paizis G**, Cooper ME, Schembri JM, Tikellis C, Burrell LM, Angus PW. Up-regulation of components of the renin-angiotensin system in the bile duct-ligated rat liver. *Gastroenterology* 2002; **123**: 1667-1676 [PMID: 12404241 DOI: 10.1053/gast.2002.36561]
12 **Simões e Silva AC**, Silveira KD, Ferreira AJ, Teixeira MM. ACE2, angiotensin-(1-7) and Mas receptor axis in inflammation and fibrosis. *Br J Pharmacol* 2013; **169**: 477-492 [PMID: 23488800 DOI: 10.1111/bph.12159]
13 **Kurikawa N**, Suga M, Kuroda S, Yamada K, Ishikawa H. An angiotensin II type 1 receptor antagonist, olmesartan medoxomil, improves experimental liver fibrosis by suppression of proliferation and collagen synthesis in activated hepatic stellate cells. *Br J Pharmacol* 2003; **139**: 1085-1094 [PMID: 12871826 DOI: 10.1038/sj.bjp.0705339]
14 **Crackower MA**, Sarao R, Oudit GY, Yagil C, Kozieradzki I, Scanga SE, Oliveira-dos-Santos AJ, da Costa J, Zhang L, Pei Y, Scholey J, Ferrario CM, Manoukian AS, Chappell MC, Backx PH, Yagil Y, Penninger JM. Angiotensin-converting enzyme 2 is an essential regulator of heart function. *Nature* 2002; **417**: 822-828 [PMID: 12075344 DOI: 10.1038/nature00786]
15 **Trebicka J**, Hennenberg M, Laleman W, Shelest N, Biecker E, Schepke M, Nevens F, Sauerbruch T, Heller J. Atorvastatin lowers portal pressure in cirrhotic rats by inhibition of RhoA/Rho-kinase and activation of endothelial nitric oxide synthase. *Hepatology* 2007; **46**: 242-253 [PMID: 17596891 DOI: 10.1002/hep.21673]
16 **Jonsson JR**, Clouston AD, Ando Y, Kelemen LI, Horn MJ, Adamson MD, Purdie DM, Powell EE. Angiotensin-converting enzyme inhibition attenuates the progression of rat hepatic fibrosis. *Gastroenterology* 2001; **121**: 148-155 [PMID: 11438504 DOI: 10.1053/gast.2001.25480]
17 **Liu J**, Li X, Lu Q, Ren D, Sun X, Rousselle T, Li J, Leng J. AMPK: a balancer of the renin-angiotensin system. *Biosci Rep* 2019; **39** [PMID: 31413168 DOI: 10.1042/BSR20181994]

World Journal of Gastroenterology

Submit a Manuscript: https://www.f6publishing.com

World J Gastroenterol 2024 February 14; 30(6): 610-613

DOI: 10.3748/wjg.v30.i6.610

ISSN 1007-9327 (print) ISSN 2219-2840 (online)

LETTER TO THE EDITOR

Endoscopic intramural cystogastrostomy for treatment of peripancreatic fluid collection: A viewpoint from a surgeon

Chen-Guo Ker

Specialty type: Gastroenterology and hepatology

Provenance and peer review: Invited article; Externally peer reviewed.

Peer-review model: Single blind

Peer-review report's scientific quality classification

Grade A (Excellent): 0
Grade B (Very good): B, B
Grade C (Good): C, C
Grade D (Fair): 0
Grade E (Poor): 0

P-Reviewer: Dedemadi G, Greece; Fujino Y, Japan; Shi RH, China

Received: October 31, 2023
Peer-review started: October 31, 2023
First decision: December 4, 2023
Revised: December 8, 2023
Accepted: January 16, 2024
Article in press: January 16, 2024
Published online: February 14, 2024

Chen-Guo Ker, Department of General Surgery, E-Da Hospital, I-Shou University, Kaohsiung 824, Taiwan

Corresponding author: Chen-Guo Ker, FACS, MD, PhD, Professor of Surgery, Department of General Surgery, E-Da Hospital, I-Shou University, No. 1 Yi-Da Rd, Yanchao District, Kaohsiung 824, Taiwan. ed112739@edah.org.tw

Abstract

Percutaneous or endoscopic drainage is the initial choice for the treatment of peripancreatic fluid collection in symptomatic patients. Endoscopic transgastric fenestration (ETGF) was first reported for the management of pancreatic pseudocysts of 20 patients in 2008. From a surgeon's viewpoint, ETGF is a similar procedure to cystogastrostomy in that they both produce a wide outlet orifice for the drainage of fluid and necrotic debris. ETGF can be performed at least 4 wk after the initial onset of acute pancreatitis and it has a high priority over the surgical approach. However, the surgical approach usually has a better success rate because surgical cystogastrostomy has a wider outlet (> 6 cm *vs* 2 cm) than ETGF. However, percutaneous or endoscopic drainage, ETGF, and surgical approach offer various treatment options for peripancreatic fluid collection patients based on their conditions.

Key Words: Pancreatitis; Pancreatic pseudocyst; Endoscopic cystogastrostomy; Surgical cystogastrostomy; Peripancreatic fluid collection; Fenestration for pancreatic cyst

Core Tip: Endoscopic transgastric fenestration (ETGF) actually shares the same indications and procedures as surgical cystogastrostomy for the management of pancreatic pseudocysts. From a surgeon's viewpoint, both ETGF and surgical cystogastrostomy are used for producing a wide outlet orifice for the drainage. Endoscopic ultrasound-guided drainage and necrosectomy or ETGF has a high priority over the surgical approach. However, the surgical approach usually has a better success rate because surgical cystogastrostomy has a wider outlet than ETGF.

Citation: Ker CG. Endoscopic intramural cystogastrostomy for treatment of peripancreatic fluid collection: A viewpoint from a surgeon. *World J Gastroenterol* 2024; 30(6): 610-613
URL: https://www.wjgnet.com/1007-9327/full/v30/i6/610.htm
DOI: https://dx.doi.org/10.3748/wjg.v30.i6.610

TO THE EDITOR

A comment was raised after reading the article titled "Endoscopic transgastric fenestration *vs* percutaneous drainage for management of (peri) pancreatic fluid collections adjacent to gastric wall (with video)" by Zhang *et al*[1]. The clinical consequences of local complications in the natural course of acute pancreatitis are acute peripancreatic fluid collection (PPFC), pancreatic pseudocyst (PPC), acute necrotic collection (ANC), and walled-off necrosis (WON)[2,3]. Acute PPFC tends to be poorly walled-off and can leak into the retroperitoneum, peritoneal cavity, or a third space. Therefore, early interventions for these local complications are not recommended according to Japanese or American guidelines[4,5]. If percutaneous or endoscopic interventions for these local complications are necessary, it is necessary to wait until well-encapsulated formation, such as PPC or WON, is achieved. This condition usually occurs more than 4 wk after the onset of interstitial edematous pancreatitis to mature[3].

Percutaneous drainage (PD) or the endoscopic approach is the initial choice for the treatment of symptomatic patients [6]. However, most cystic spaces contain solid debris, which can occlude the tube, leading to impaired drainage. Hence, percutaneous or transmural drainage alone is often inadequate, and additional endoscopic or surgical necrosectomy is frequently required[7-10]. Surgical drainage is reserved only when PD is not successful[11]. Bleeding during management with endoscopic necrosectomy for ANC or WON may occur and result in catastrophic complications. Therefore, it is better to perform this procedure at referral centers with surgical backup[5].

Zhang *et al*[1] compared endoscopic transgastric fenestration (ETGF) with PD for the management of PPFC, and Liu *et al*[12] conducted the first ETGF in 2015. Actually, Varadarajulu *et al*[7] reported endoscopic ultrasound (EUS)-guided cystogastrostomy (same procedure as ETGF) for the management of PPS of 20 patients in 2008. From a surgeon's viewpoint, ETGF performed by an endoscopist is a similar procedure to cystogastrostomy performed by a surgeon, and both are used for producing a wide outlet orifice for the drainage of fluid and necrotic debris between the cyst and stomach. Therefore, ETGF can be performed only under the condition of stringent adhesion between the posterior gastric and cystic walls. Additionally, ETGF has the same indications as surgical cystogastrostomy. Technically, the operator should first use EUS guidance to demonstrate presumably a resection line on the gastric wall at the site of maximal prominence of the PPC into the stomach to select the thinnest wall, thus minimizing adverse events.

As a novel development, therapeutic endoscopy can extend the dissection skills to perform ETGF to drain and clean the PPFC with well encapsulation where possible. What is already known about ETGF for PPC or WON is accepted as a minimally invasive alternative to the surgical approach. EUS guidance reduces the risk of perforation and hemorrhage. The probability of post-procedure complications and outcomes differs among the various techniques (Table 1). Varadarajulu *et al*[7] conducted a retrospective study to compare patients with uncomplicated PPC managed by surgical or EUS-guided cystogastrostomy. The results showed no significant differences in treatment success rates, complications, or re-interventions. Furthermore, costs were lower, and the post-procedure length of hospital stay was shorter for EUS-guided cystogastrostomy[7].

Table 1 Comparison of treatment procedures for pancreatic pseudocyst and walled-off necrosis

Procedure	Percutaneous cystic drainage	EUS-guided drainage with/without necrosectomy	ETGF[1] with/without necrosectomy	Surgical cystogastrostomy[2]
Variable				
Technique difficulty	Less	Less	High	High
Risk	Less	Less	Moderate	High
Re-insertion	Yes	Yes	-	-
Complications	Less	Less	Moderate	Less
Healing course	Long	Long	Short	Short
Cost	Less	Moderate	Moderate	High
Ref.	Johnson *et al*[11]; Akshintala *et al*[6]	Seicean *et al*[8]; McGuire *et al*[10]	Varadarajulu *et al*, 2008[7]; Suggs *et al*[14]; Liu *et al*[12]	Varadarajulu *et al*[7]; Suggs *et al*[14]

[1]ETGF: Similar to the surgical procedure (cystogastrostomy).

[2]Cystogastrostomy performed using a traditional or laparoscopic approach.
ETGF: Endoscopic transgastric fenestration; EUS: Endoscopic ultrasound.

Generally, EUS-guided drainage and necrosectomy or ETGF has a high priority over the surgical approach. However, the surgical approach usually has a better success rate because surgical cystogastrostomy has a wider outlet (> 6 cm *vs* 2 cm) than ETGF[13,14]. Either ETGF or operative cystogastrostomy is indicated in cases where: (1) The cystic wall is well matured; and (2) the cyst is large enough to have a severe adhesion area with the gastric posterior wall instead of the early phase of PPFC without being walled-off. However, PD, endoscopic drainage, ETGF, and surgical approach offer various treatment options that can be tailored to the needs of individual patients with PPFC and the facilities of institutions.

FOOTNOTES

Author contributions: Ker CG performed literature search and evaluation, and manuscript preparation.

Conflict-of-interest statement: The author declares no conflict of interest for this article.

Country/Territory of origin: Taiwan

ORCID number: Chen-Guo Ker 0000-0003-4683-9365.

S-Editor: Qu XL
L-Editor: Wang TQ
P-Editor: Qu XL

REFERENCES

1 **Zhang HM**, Ke HT, Ahmed MR, Li YJ, Nabi G, Li MH, Zhang JY, Liu D, Zhao LX, Liu BR. Endoscopic transgastric fenestration *versus* percutaneous drainage for management of (peri)pancreatic fluid collections adjacent to gastric wall (with video). *World J Gastroenterol* 2023; **29**: 5557-5565 [PMID: 37970477 DOI: 10.3748/wjg.v29.i40.5557]

2 **Banks PA**, Bollen TL, Dervenis C, Gooszen HG, Johnson CD, Sarr MG, Tsiotos GG, Vege SS; Acute Pancreatitis Classification Working Group. Classification of acute pancreatitis--2012: revision of the Atlanta classification and definitions by international consensus. *Gut* 2013; **62**: 102-111 [PMID: 23100216 DOI: 10.1136/gutjnl-2012-302779]

3 **Zerem E**, Kurtcehajic A, Kunosić S, Zerem Malkočević D, Zerem O. Current trends in acute pancreatitis: Diagnostic and therapeutic challenges. *World J Gastroenterol* 2023; **29**: 2747-2763 [PMID: 37274068 DOI: 10.3748/wjg.v29.i18.2747]

4 **Yokoe M**, Takada T, Mayumi T, Yoshida M, Isaji S, Wada K, Itoi T, Sata N, Gabata T, Igarashi H, Kataoka K, Hirota M, Kadoya M, Kitamura N, Kimura Y, Kiriyama S, Shirai K, Hattori T, Takeda K, Takeyama Y, Sekimoto M, Shikata S, Arata S, Hirata K. Japanese guidelines for the management of acute pancreatitis: Japanese Guidelines 2015. *J Hepatobiliary Pancreat Sci* 2015; **22**: 405-432 [PMID: 25973947 DOI: 10.1002/jhbp.259]

5 **Baron TH**, DiMaio CJ, Wang AY, Morgan KA. American Gastroenterological Association Clinical Practice Update: Management of Pancreatic Necrosis. *Gastroenterology* 2020; **158**: 67-75.e1 [PMID: 31479658 DOI: 10.1053/j.gastro.2019.07.064]

6 **Akshintala VS**, Saxena P, Zaheer A, Rana U, Hutfless SM, Lennon AM, Canto MI, Kalloo AN, Khashab MA, Singh VK. A comparative evaluation of outcomes of endoscopic *versus* percutaneous drainage for symptomatic pancreatic pseudocysts. *Gastrointest Endosc* 2014; **79**: 921-8; quiz 983.e2, 983.e5 [PMID: 24315454 DOI: 10.1016/j.gie.2013.10.032]

7 **Varadarajulu S**, Lopes TL, Wilcox CM, Drelichman ER, Kilgore ML, Christein JD. EUS *versus* surgical cyst-gastrostomy for management of pancreatic pseudocysts. *Gastrointest Endosc* 2008; **68**: 649-655 [PMID: 18547566 DOI: 10.1016/j.gie.2008.02.057]

8 **Seicean A**, Pojoga C, Rednic V, Hagiu C, Seicean R. Endoscopic ultrasound drainage of pancreatic fluid collections: do we know enough about the best approach? *Therap Adv Gastroenterol* 2023; **16**: 17562848231180047 [PMID: 37485492 DOI: 10.1177/17562848231180047]

9 **Working Group IAP/APA Acute Pancreatitis Guidelines**. IAP/APA evidence-based guidelines for the management of acute pancreatitis. *Pancreatology* 2013; **13**: e1-15 [PMID: 24054878 DOI: 10.1016/j.pan.2013.07.063]

10 **McGuire SP**, Maatman TK, Zyromski NJ. Transgastric pancreatic necrosectomy: Tricks of the trade. *Surg Open Sci* 2023; **14**: 1-4 [PMID: 37599671 DOI: 10.1016/j.sopen.2023.06.003]

11 **Johnson MD**, Walsh RM, Henderson JM, Brown N, Ponsky J, Dumot J, Zuccaro G, Vargo J. Surgical *versus* nonsurgical management of pancreatic pseudocysts. *J Clin Gastroenterol* 2009; **43**: 586-590 [PMID: 19077728 DOI: 10.1097/MCG.0b013e31817440be]

12 **Liu BR**, Song JT, Zhang XY. Video of the Month: Emergency Endoscopic Fenestration for Treatment of a Recurrence Pancreatic Pseudocyst. *Am J Gastroenterol* 2015; **110**: 644 [PMID: 25942297 DOI: 10.1038/ajg.2015.13]

13 **van Brunschot S**, van Grinsven J, Voermans RP, Bakker OJ, Besselink MG, Boermeester MA, Bollen TL, Bosscha K, Bouwense SA, Bruno

MJ, Cappendijk VC, Consten EC, Dejong CH, Dijkgraaf MG, van Eijck CH, Erkelens GW, van Goor H, Hadithi M, Haveman JW, Hofker SH, Jansen JJ, Laméris JS, van Lienden KP, Manusama ER, Meijssen MA, Mulder CJ, Nieuwenhuis VB, Poley JW, de Ridder RJ, Rosman C, Schaapherder AF, Scheepers JJ, Schoon EJ, Seerden T, Spanier BW, Straathof JW, Timmer R, Venneman NG, Vleggaar FP, Witteman BJ, Gooszen HG, van Santvoort HC, Fockens P; Dutch Pancreatitis Study Group. Transluminal endoscopic step-up approach *versus* minimally invasive surgical step-up approach in patients with infected necrotising pancreatitis (TENSION trial): design and rationale of a randomised controlled multicenter trial [ISRCTN09186711]. *BMC Gastroenterol* 2013; **13**: 161 [PMID: 24274589 DOI: 10.1186/1471-230X-13-161]

14 **Suggs P**, NeCamp T, Carr JA. A Comparison of Endoscopic Versus Surgical Creation of a Cystogastrostomy to Drain Pancreatic Pseudocysts and Walled-Off Pancreatic Necrosis in 5500 Patients. *Ann Surg Open* 2020; **1**: e024 [PMID: 37637446 DOI: 10.1097/AS9.0000000000000024]

Published by **Baishideng Publishing Group Inc**
7041 Koll Center Parkway, Suite 160, Pleasanton, CA 94566, USA
Telephone: +1-925-3991568
E-mail: office@baishideng.com
Help Desk: https://www.f6publishing.com/helpdesk
https://www.wjgnet.com